



BIBLIOTHÈQUE

CÉGEP DE L'ABITIBI-TÉMISCAMINGUE
UNIVERSITÉ DU QUÉBEC EN ABITIBI-TÉMISCAMINGUE

Mise en garde

La bibliothèque du Cégep de l'Abitibi-Témiscamingue et de l'Université du Québec en Abitibi-Témiscamingue (UQAT) a obtenu l'autorisation de l'auteur de ce document afin de diffuser, dans un but non lucratif, une copie de son œuvre dans [Depositum](#), site d'archives numériques, gratuit et accessible à tous. L'auteur conserve néanmoins ses droits de propriété intellectuelle, dont son droit d'auteur, sur cette œuvre.

Warning

The library of the Cégep de l'Abitibi-Témiscamingue and the Université du Québec en Abitibi-Témiscamingue (UQAT) obtained the permission of the author to use a copy of this document for nonprofit purposes in order to put it in the open archives [Depositum](#), which is free and accessible to all. The author retains ownership of the copyright on this document.

UNIVERSITÉ DU QUÉBEC EN ABITIBI-TÉMISCAMINGUE

RECONSTITUTION DES DÉBITS ET DES HAUTS NIVEAUX D'EAU POUR LA
RÉGION DES PLAINES DE L'ABITIBI DEPUIS LA FIN DU PETIT ÂGE
GLACIAIRE ET PRÉVISIONS SUITE AUX CHANGEMENTS CLIMATIQUES

THÈSE

PRÉSENTÉE

COMME EXIGENCE PARTIELLE

AU DOCTORAT EN SCIENCES DE L'ENVIRONNEMENT

PAR

ALEXANDRE FLORENT NOLIN

OCTOBRE 2022

REMERCIEMENTS

Cette thèse s'est écrite entre les notes de ma guitare et les intégrales d'Eric Clapton, Steve Winwood, J.J. Cale, B.B. King, John Mayer, et d'autres bluesmans qui je crois m'auront permis de rester à flot, de trouver l'inspiration dont j'avais besoin pour écrire mes histoires et traverser le Doctorat :

« Give me my guitar, I'm going to go far » J.J. Cale.

*

**

L'accomplissement d'une thèse est souvent perçu comme un travail solitaire, en regardant derrière moi aujourd'hui je remercie les personnes rencontrées sur mon chemin sans qui mes recherches n'auraient pas été les mêmes. Je remercie mon directeur Yves Bergeron, autant pour ses conseils avisés, son soutien constant, que pour nos discussions de pêche autour de la machine à café de la station. Merci à mes directeurs de m'avoir permis des expériences inoubliables qu'auront été l'échange au Laboratory of Tree-Ring Research (LTRR) de Tucson pour le cours de Dave Meko, ou le AGU San Francisco. Sans quoi je n'aurais pas eu la chance de rencontrer mes amis Jan Altman, Lara Klippel, Tom De Mil, Bieke Verhelst et la petite Alma, Axel Rodriguez, tous réunis autour de la dendro, et bien sûr, d'une bonne bière fraîche; mais aussi d'échanger avec toutes les autres fabuleuses personnes qui m'auront accueilli au LTRR.

Je remercie mon directeur Jacques C. Tardif ainsi que France Conciatori, qui vont de pair, et m'ont appris les rudiments et la rigueur de la dendrochronologie. France, merci pour ta patience et tes enseignements, les critères élaborés que tu appliques en dendrochronologie sont aujourd'hui devenus mes standards. Jacques, malgré la distance, ta disponibilité et ta patience, ton pragmatisme et ta philosophie des sciences et de la vie auront forgé le jeune chercheur qui écrit ces mots. Je n'oublierais pas nos jams de guitare, les journées de terrains, les bons moments avec France passés sous l'hiver de Winnipeg ou sous le soleil de l'Arizona. ¡Foto grupo!

J'aimerais également remercier le soutien de mon comité de projet: Etienne Boucher, Marie-Amélie Boucher, et Martin Girardin; et de mon comité de financement: David Huard, Jacinthe Clavet-Gaumont, et Kurt Kornelsen pour leurs conseils avisés et leur disponibilité, ainsi que les membres du comité examinateur: Philippe Gachon, Fabio Gennaretti et Scott St. George pour leurs révisions approfondies, leurs discussions constructives et le regard neuf apporté sur ce travail.

À mes collègues de l'Institut de Recherche sur les Forêts aujourd'hui devenus grands Mohammed Henneb, Benjamin Marquis, Mélissande Nagati, et ceux en devenir, Nils Ambec, Nathand Chabaud, Mariano Feldman, Marc-Frédéric Indorf, Marion Noualhaguet, Maxence Soubeyrand (Marine et petit Malo), Marianne Vogel: nos discussions de comptoir, nos festifs repas d'expatriés, nos virées en canot, et nos campings nordiques imprévisibles resteront dans ma mémoire.

Deux personnes sans qui bien des choses n'auraient pas pu rester à flot, à commencer par ma chaloupe, Danielle Charron et Raynald Julien de la Forêt d'Enseignement et de Recherche du Lac Duparquet (FERLD). Merci pour votre soutien sans faille et pour avoir partagé vos connaissances des expéditions et du travail de terrain. Mes montagnes d'échantillons restées à la station sont un peu les vôtres. Je remercie également

l'inestimable Marie-Robin Myler de la FERLD. Danièle Laporte et Marie-Hélène Longpré merci pour votre gaieté quotidienne et pour m'avoir guidé dans le dédale des procédures académiques que vous seules connaissez par cœur ! Merci à Mélanie Desrochers pour son aide avec les bases de données géostatistiques et Lidar.

Mes aides de terrain vaillants à commencer par Stéphane Hébert (2017) et Isabelle Gareau (2018), un grand merci pour votre patience avec mon caractère et l'excellent travail que vous avez mené parfois à bout de souffle pendant nos longues journées de terrain ou au laboratoire. Je remercie également l'appui d'Annick Antaya, Marion Cartier, Cyrielle Ducrot, Chloé Lavelle, et Ralitsa Mincheva.

Les analyses au Dendroecology Laboratory de l'Université de Winnipeg ont été assistées par Johanna M. Robson, Hollie Swart et Dominique Levin, merci à vous trois pour le temps passé sur WinCell et pour nos échanges. Johanna tu auras été ma guide touristique de Winnipeg, et une vraie prof d'anglais. Je n'oublierai pas les moments passés avec ta famille à Thanksgiving et votre gentillesse.

Mes remerciements les plus personnels seront pour mes proches (Julien, Graziella & petite Lya ; Jérôme, Kimberley & petite Noémie) et ma famille (ma maman Eliane, ma sœur Florine sans oublier Ficelle & Jones!), qui, sans forcément comprendre mes choix ou mes activités académiques, m'auront toujours soutenu et porté jusque-là. Enfin, une pensée toute particulière pour Jacques & Andrée et Paul & Madeleine Lhermigny qui n'auront pas su tout ce que j'ai vécu et accompli ici, mais sans qui rien de tout ça n'aurait été possible. Merci pour tout.

La meilleure étant pour la fin, une pensée particulière pour Manon, ma compagne de vie, qui partage ma passion pour la forêt et les petites choses qui y vivent. Merci à toutes et à tous.

AVANT-PROPOS

Cette thèse de Doctorat est présentée par articles et sous forme de cinq chapitres. Le projet de thèse initial ayant évolué au fil du temps, le chapitre premier a été scindé en deux articles. Selon l'avancement de mes recherches, les articles sont soit déjà publiés, soit en cours de soumission dans des journaux scientifiques avec comité de lecture, et leur forme peut varier selon les journaux visés. Les données utilisées dans chacun des chapitres sont issues d'un large échantillonnage de terrain effectué dans le nord-est de l'Ontario et le nord-ouest du Québec, jusqu'au nord du 50^e parallèle, et pour lequel plus de 1 200 échantillons dendrochronologiques de frêne noir (*Fraxinus nigra* Marsh.) riverains des cours d'eau et des lacs, et plus de 1 800 de pin gris (*Pinus banksiana* Lamb.) des sables et caps rocheux, ont été collectés. Bien que mon épopée de terrain en chaloupe sur les eaux abitibiennes puisse faire l'objet d'un ouvrage aussi conséquent que cette thèse, ces aventures mémorables resteront à la discrétion de leurs joyeux protagonistes ! Les chronologies finales ainsi que les résultats de chacun des chapitres sont disponibles sur une base de données scientifiques en ligne (data.mendeley.com). Les lecteurs trouveront à la fin de chaque chapitre les informations pour télécharger et comprendre les données. Puisque chaque article doit se suffire à lui-même, certaines parties, notamment introductives ou méthodologiques, peuvent apparaître redondantes au lecteur entre les chapitres.

Les cinq chapitres présentés sont le fruit d'une étroite collaboration entre chacun des coauteurs y ayant participé. Je figure en premier auteur sur chacun d'eux ayant été le principal responsable des études, de la collecte de données, de leur analyse, et de la rédaction des articles. Les membres de l'équipe de recherche qui m'ont suivi tout au

long de cette thèse sont présents comme co-auteurs sur chacun de mes travaux, mon directeur Yves Bergeron, et mon co-directeur Jacques Clément Tardif, ainsi que la professionnelle de recherche France Conciatori. Le chapitre I a été réalisé en collaboration avec David Matthew Meko du Laboratory of Tree-Ring Research de l'Université d'Arizona qui a fourni de précieux conseils statistiques et une expertise incomparable en dendrohydrologie. Les chapitres IV et V ont été réalisés avec la collaboration de Martin Philippe Girardin et de Xiao Jing Guo du Service Canadien des Forêts (Ressources Naturelles Canada) qui ont fourni leur large expertise en modélisation statistique, écologie forestière et dynamique climatique. Finalement, Marie-Amélie Boucher de l'Université de Sherbrooke, Jan Adamoswki et Rahim Barzegar de l'Université McGill ont apporté leur expertise des modélisations hydrologiques et des analyses de tendances dans les séries temporelles pour le chapitre V qui est en préparation. Les chapitres I, II, III ont été réalisés en collaboration étroite avec Susanne Kames qui a apporté sa connaissance étendue des cernes de crues du Lac Duparquet et de la langue anglaise. Le chapitre III a été produit à l'occasion d'un numéro spécial du journal *Frontiers in Plant Science* intitulée '*Quantitative wood anatomy to explore tree responses to global change*', pour laquelle mes travaux de recherche étaient tout désignés.

Chapitre I. Nolin, A.F., Tardif, J.C., Conciatori, F., Kames, S., Meko, D.M., & Bergeron, Y. (2021). Multi-century tree-ring anatomical evidence reveals increasing frequency and magnitude of spring discharge and floods in eastern boreal Canada. *Global and Planetary Change*, 199, 103444. <https://doi.org/10.1016/j.gloplacha.2021.103444>

Chapitre II. Nolin, A.F., Tardif, J.C., Conciatori, F., & Bergeron, Y. (2021). Spatial coherency of the spring flood signal among major river basins of eastern boreal Canada inferred from flood rings. *Journal of Hydrology*, 596, 126084. <https://doi.org/10.1016/j.jhydrol.2021.126084>

Chapitre III. Nolin A.F., Tardif J.C., Conciatori F., Bergeron Y. (2021). Flood ring production modulated by river regulation in eastern boreal Canada. *Frontiers in Plant Science*. 12: 757280, <https://doi.org/10.3389/fpls.2021.757280>

Chapitre IV. Nolin, A.F., Girardin, M.P., Tardif, J.C., Guo, X.J., Conciatori, F., & Bergeron, Y. (2022). A 247-years tree-ring reconstruction of spring temperature and relationship to spring flooding in eastern boreal Canada. *International Journal of Climatology*. 1-20 <https://doi.org/10.1002/joc.7608>

Chapitre V. Nolin, A.F., Girardin, M.P, Adamowski, J.F., Barzegar, R., Boucher, M.-A., Tardif, J.C., & Bergeron, Y. (subm.). A 330-year perspective (1771-2100) on historical and projected trends and variability of spring discharges in the Upper Harricana River, eastern boreal Canada. *Journal of hydrology – Regional studies*.

TABLE DES MATIÈRES

AVANT-PROPOS	vii
LISTE DES FIGURES.....	xvii
LISTE DES TABLEAUX.....	xxvii
Résumé.....	xxxiii
INTRODUCTION GÉNÉRALE	1
0.1 Contexte.....	1
0.2 Changements hydroclimatiques.....	2
0.3 Approche dendrohydrologique	4
0.4 Particularité des feuillus à zone poreuse pour l'étude et la reconstitution des inondations	6
0.5 Objectifs de la thèse.....	10
CHAPITRE I MULTI-CENTURY TREE-RING ANATOMICAL EVIDENCE REVEALS INCREASING FREQUENCY AND MAGNITUDE OF SPRING DISCHARGE AND FLOODS IN EASTERN BOREAL CANADA	13
1.1 Abstract.....	14
1.2 Résumé	15
1.3 Introduction.....	16
1.4 Materials and methods.....	21
1.4.1 Study area	21
1.4.2 Sample collection, measurement and crossdating	23
1.4.3 Chronology development.....	26
1.4.4 Reconstruction of spring discharge	27
1.4.5 Model performance.....	28
1.4.6 Climate and large-scale atmospheric circulations relationships to spring flooding.....	28

1.5	Results	32
1.5.1	Predictor chronology characteristics	32
1.5.2	Reconstruction of Harricana River spring discharge	35
1.5.3	Extreme low and high discharge	38
1.5.4	Temporal stability in the spring flood reconstruction	39
1.5.5	Reconstructed spring discharge, climate, ice-breakup and large-scale atmospheric circulation indices	41
1.5.6	Spatial agreement between REC1 and hydrological data and dendrohydrological reconstructions at the regional level	44
1.6	Discussion	47
1.6.1	Strength of the Harricana spring discharge reconstruction	47
1.6.2	Spatial coherency of spring discharge and flooding	48
1.6.3	Spring discharge, flooding and climatic changes	52
1.7	Conclusion	55
1.8	Acknowledgments	56
1.9	Data availability	57
1.10	Supplementary Materials	58
CHAPITRE II SPATIAL COHERENCY OF THE SPRING FLOOD SIGNAL AMONG MAJOR RIVER BASINS OF EASTERN BOREAL CANADA INFERED FROM FLOOD RINGS		63
2.1	Abstract	64
2.2	Résumé	65
2.3	Introduction	66
2.4	Material and methods	69
2.4.1	Study area	69
2.4.2	Sampling	71
2.4.3	Tree-ring data	73
2.4.4	Hydrological data	75
2.4.5	Statistical analyses	76
2.5	Results	78
2.5.1	Flood ring coherency across river basins	78
2.5.2	Continuous earlywood vessel chronologies	86
2.6	Discussion	95
2.6.1	Spatial coherency among spring flood proxy from natural rivers	95

2.6.2	Comparison of spring flood proxies among natural rivers, regulated rivers, and unflooded control sites.....	94
2.6.3	Adequacy between spring flood proxies, advantages and limitations.....	99
2.7	Conclusion.....	101
2.8	Acknowledgments.....	102
2.9	Data availability.....	102
2.10	Supplementary Materials.....	104
	CHAPITRE III FLOOD-RING PRODUCTION MODULATED BY RIVER REGULATION IN EASTERN BOREAL CANADA.....	109
3.1	Abstract.....	110
3.2	Résumé.....	111
3.3	Introduction.....	112
3.4	Material and methods.....	116
3.4.1	Study area.....	116
3.4.2	Tree-ring data.....	122
3.4.3	Statistical analysis and independent data.....	123
3.5	Results and discussion.....	125
3.5.1	Impact of regulation on stand structure.....	125
3.5.2	Flood-ring relative frequencies (pre-dam period).....	129
3.5.3	Flood-ring relative frequencies (post-dam period).....	130
3.5.4	Ring-width chronologies.....	135
3.6	Conclusion.....	140
3.7	Data availability statement.....	141
3.8	Acknowledgments.....	142
3.9	Supplementary Materials.....	143
	CHAPITRE IV A 247-YEARS TREE-RING RECONSTRUCTION OF SPRING TEMPERATURE AND RELATION TO SPRING FLOODING IN EASTERN BOREAL CANADA.....	145
4.1	Graphical abstract.....	146
4.2	Abstract.....	147
4.3	Résumé.....	148
4.4	Introduction.....	149

4.5	Material and methods.....	154
4.5.1	Study Area.....	155
4.5.2	Tree-ring data.....	157
4.5.3	Climate data.....	157
4.5.4	Reconstruction of temperatures.....	160
4.6	Results.....	162
4.6.1	Reconstruction of spring temperatures.....	162
4.6.2	Relationship to spring flooding.....	170
4.7	Discussion.....	173
4.8	Conclusion.....	179
4.9	Data Availability statement.....	180
4.10	Acknowledgments.....	180
4.11	Supplementary Materials.....	181
4.11.1	Construction of tree-ring chronologies.....	181
4.11.2	Strength of tree-ring chronologies.....	183
4.11.3	Sensitivity of tree-ring chronologies to temperature.....	183
CHAPITRE V OBSERVED AND PROJECTED TRENDS IN SPRING FLOOD DISCHARGES FOR THE UPPER HARRICANA RIVER, EASTERN BOREAL CANADA.....		193
5.1	Abstract.....	194
5.2	Résumé.....	195
5.3	Introduction.....	196
5.4	Material and Methods.....	199
5.4.1	Study area.....	199
5.4.2	Hydroclimatic data.....	201
5.4.3	Climate projections and scenarios.....	202
5.4.4	Snowfall and rainfall amounts.....	202
5.4.5	Potential evaporation.....	204
5.4.6	Machine Learning model.....	205
5.4.7	Independent hydrological simulations using a 10-GCM ensemble.....	208
5.4.8	Hydroclimatic trend analysis.....	208
5.5	Results.....	210
5.5.1	Machine Learning model conception and evaluation.....	210
5.5.2	Historical trends in discharge and climate.....	215

5.5.3	Projected impacts of climate change on the mean A15J30 discharge	221
5.5.4	Projected impacts of climate change on the low and high values and frequency of high mean A15J30 discharge	221
5.5.5	Projected climate change trends by 2100	222
5.5.6	Assessment of the projected climate changes leading to increased high mean A15J30 discharge.....	225
5.6	Discussion.....	230
5.6.1	Observed hydroclimatic changes affecting the mean A15J30 discharge	230
5.6.2	Projected hydroclimatic changes affecting the mean A15J30 discharge by 2100.....	232
5.6.3	Uncertainties in climate change results	233
5.7	Conclusion	235
5.8	Acknowledgements.....	236
5.9	Supplementary Materials	237
5.9.1	Adaptation of climate indexes for the Upper Harricana River watershed	237
CHAPITRE VI CONCLUSION GÉNÉRALE		245
6.1	Variabilité printanière des débits moyens et des températures moyennes reconstituées depuis la fin du Petit Âge Glaciaire	246
6.2	Contrôles climatiques à large échelle et cohérence régionale des hauts débits moyens printaniers	248
6.3	Trajectoires hydroclimatiques prévisionnelles pour les débits moyens printaniers de la rivière Harricana	249
6.4	Avantages, limites et perspectives de l'utilisation des cernes de crues comme indicateur des débits printaniers boréaux.....	250
6.5	Perspectives méthodologiques pour la caractérisation et la mesure des cernes de crues	253
6.6	Perspectives de recherche et mot final.....	254
RÉFÉRENCES.....		259

LISTE DES FIGURES

Figure	Page
0.1 Micrographie électronique à balayage (MEB) du bois d'un <i>Fraxinus excelsior</i> en plan transversal (TS) et longitudinal tangentiel (TLS) montrant les éléments de vaisseaux (EV) et les vaisseaux (V). Les éléments de vaisseaux s'empilent un à un pour former les vaisseaux, organes tubulaires creux allongés verticalement dans l'axe de la tige et transportant la sève. Photo MEB © SciencePhotoLibrary Limited, 2022, England.	6
0.2 Représentation matricielle du débit journalier de la rivière Harricana à Amos (04NA001-2) de 1914 à 2022. Les données manquantes sont figurées en blanc.	8
0.3 Représentation matricielle de la durée des hauts débits printaniers de la rivière Harricana à Amos (04NA001-2) de 1914 à 2022, exprimé en nombre maximum de jours consécutifs par an où le débit est supérieur à une lecture de jauge spécifiée pendant l'intervalle du 1er janvier au 31 Juillet (211 jours)	9
0.4 Frênaies noires alluviales du Lac Duparquet. a) Frênaie #42, début Septembre 2017 (date inconnue). Les contreforts proéminents de ces arbres révèlent le caractère périodique et prolongé des inondations printanières (Varnell 1998; Tiner, 2016). La végétation au sol est dominée par la fougère Onoclée sensible (<i>Onoclea sensibilis</i> L.), elle-même indicatrice des plaines alluviales basses aux inondations printanières prolongées (Tardif et Bergeron, 1992). Annick Antaya - "Madame Grand Pic", sur la photo. b) Frênaie #42, 24 Mai 2018. Les arbres sont inondés par plus de 50cm d'eau, nous circulons en chaloupe entre les frênes. c) Frênaie #103-Mouilleuse, 2 Juillet 2019. Le haut niveau d'eau de la crue printanière persiste jusqu'en début d'été. d) Frênaie #103-Mouilleuse, 3 Juillet 2019. Les lignes de jaunes sont des laisses de pollen et indiquent le niveau maximal et les phases de décrue de l'inondation printanière de 2019.	11

- 1.1 Map of the study area. Geographic location of the study area at the border between Ontario (ON) and Québec (QC), in Canada (left panel upper inset). Lake Duparquet (red circle in left panel) is located at the head of the Abitibi River basin. Discharge record reconstructed is at Harricana River (black squares No. 4 & 5) on the upper reach of the Harricana River basin. Other hydrological stations are listed by their numbers in Table 1.1 The upper right inset shows locations of riparian *Fraxinus nigra* sampling sites at Lake Duparquet (white dots).22
- 1.2 Chronology characteristics. A) Tree-ring anatomical and width chronologies developed for Lake Duparquet. Abbreviations of chronologies are listed in Table 1.2. The grey shade indicates the two-standard-error confidence intervals. B) 40-year running windows of subsample signal strength (SSS, green) and mean inter-series correlation (Rbar, blue). C) Yearly sample size for ring-width and anatomical chronologies expressed as number of trees per year.33
- 1.3 Comparison between observed and reconstructed discharge. A) Instrumental (blue) and reconstructed Harricana River spring discharge for the two models REC1 (black) and REC2 (grey) for the 1915–2016 calibration period. Horizontal lines mark the mean (solid) and ± 1.5 sd (dashed) of the instrumental Harricana spring discharge. High (black triangles) and low (white triangles) discharge years exceed the threshold ± 1.5 sd. B) The four K-Means clusters of daily instrumental Harricana spring discharge from April 15 to June 30 and from 1915 to 2020. Shaded areas indicate standard deviation within each cluster. The number in parenthesis represents the number of years in each cluster.37
- 1.4 Reconstruction characteristics. A) Reconstruction of Harricana River spring discharge (April 15 to June 30) from 1771 to 2016. Decadal variations are highlighted by a 10-year smoothing spline (red curve) and confidence intervals correspond to the standard deviation envelope (sd = 20.49 m³/s; grey shade). High (red dots) and low (blue dots) discharge years exceed the threshold of the mean ± 1.5 sd. Horizontal line at 120.60 m³/s marks the mean for the 1771 to 2016 period. B) Decomposition of REC1 into Morlet 6th power in continuous wavelet transformation. The black lines encircle areas were p -value < 0.05, tested against white noise background as lag-1 autocorrelation in REC1 was not significant. The white shaded area indicates the cone of influence where wavelets are stretched beyond the range of

reconstructed data and may be altered by edge-effects. Variance magnitude range for blue (low) to red (high).....	40
1.5 Climate signals. A) Spatial correlations maps ($p < 0.10$) between REC1 and April and May (1966–2016) NOAA Rutgers snow cover. The black square indicates Lake Duparquet location. B) Bootstrapped correlation coefficients between REC1 and monthly maximum, mean, minimum temperature (maxT, meanT, minT) and total precipitation (Ptot; 1901–2016 CRU TS 4.03). C) Bootstrapped correlation coefficients between REC1 and large-scale atmospheric circulation indices for the common period 1880–2016. Correlation coefficients in A, B and C panels range from red (positive correlation) to blue (negative correlation). Asterisks in B and C panels indicate p -value < 0.1 (*), < 0.05 (**), and < 0.01 (***).....	43
1.6 Comparison of ice-scar chronologies and reconstructed spring discharge from Northern Québec. Chronologies are presented in order of decreasing correlation with (A) Harricana River reconstructed spring discharge (REC1)	46
2.1 Map of the study area. Location of the study area within North America (upper inset). The tree-ring sampling sites (red triangles) and hydrometric stations (blue squares) are indicated as well as the four major river basins under study. The abbreviations refer to those listed in Table 2.1, Lake Duparquet is coded ‘DPL’	70
2.2 Segmented earlywood vessels in <i>Fraxinus nigra</i> tree rings. Vessels appear black as the result of the digitalization process. The years are given with the classification of flood rings: F0 = null, F1 = weakly defined flood ring and F2 = well-defined flood ring. Notice the difference in the strength of the flood rings between Little Abitibi Lake (left) and Lake Duparquet (right) for the year 1960.....	74
2.3 Flood-ring chronologies among hydrological regimes. Comparison between (A) the reconstructed Harricana River discharge flood-ring relative chronologies from <i>Fraxinus nigra</i> trees from (B) Lake Duparquet (DPL), (C) pooled natural rivers (PSL, HAR, LAL), (D) regulated rivers (ABL, DFR, FHL, MGR), and (E) unflooded control sites (CTL1, CTL2). Grey and black histograms are respectively F1 and F2 flood-ring relative frequencies. The background solid black lines indicate the number of trees per year. The dashed horizontal lines indicate the three thresholds used to extract the highest F12 values from the three hydrological regimes, and respectively F12	

- $\geq 75\%$ for Lake Duparquet, $F12 \geq 50\%$ for natural rivers and $F12 \geq 10\%$ for regulated rivers. The 18 years with the highest reconstructed spring discharge for the Harricana River and over the last 250 years are represented by grey dots on the upper A curve and extending as blue bars. Those 18 years were defined using a threshold corresponding to the mean + 1.5 SD (threshold value = $151.3 \text{ m}^3/\text{s}$; Nolin et al., 2021a).81
- 2.4 Box plot of the dispersion of Spearman's rank correlation coefficients between flood-ring series per tree and the reconstruction of the Harricana River spring discharge. Correlations are pooled by river hydrological regime (natural, regulated and unflooded control; separated by dotted lines and respectively from top to bottom) and by increasing distance from sites to Lake Duparquet. Site abbreviations are defined in Table 2.1. The left and right-most edges of the rectangles indicate the interquartile range between the 25th and 75th percentiles and the dots indicate outliers outside the 10th and 90th percentiles. The center line of the graph indicates the median, and the diamond indicates the mean.83
- 2.5 Comparison between continuous earlywood vessel chronologies and their continuous wavelet transform among river basins. A) Chronologies of mean earlywood vessel cross-sectional (MVA). B) Chronologies of number of earlywood vessels (N). Left panel is the comparison between chronologies from Lake Duparquet and from the four river basins. The vertical blue bars indicate the 18 years with the highest reconstructed spring discharge for the Harricana River and over the last 250 years. Those 18 years were defined using a threshold corresponding to the mean + 1.5 SD (threshold value = $151.3 \text{ m}^3/\text{s}$; Nolin et al., 2021a). Right panel is the decomposition of mean standardized chronologies into Morlet 6th power in continuous wavelet transform. The color bar gives the range of variance intensity from low (blue) to high (red) and black lines encircle significant high variance tested against a white noise background at a p -value < 0.05 . The cone of influence is figured in white and delimit areas where wavelets are altered by edge-effect. For both A) and B) right and left panels, chronologies are as follow: 1) Lake Duparquet, 1771–2016, $n = 43$; 2) Harricana River basin, site HAR, 1783–2016, $n = 2$; 3) upper Ottawa River basin, site PSL, 1814–2016, $n = 1$; 4) Abitibi River, site LAL, 1840–2016, $n = 2$ and 5) Mattagami River, site MGR, 1922–2016, $n = 1$. The Lake Duparquet, Harricana, Abitibi and upper Ottawa River chronologies were developed from trees growing with natural discharge, while the Mattagami River basin index is from a site where the river is regulated by a dam.89

- 3.1 Map of the study area. Geographic location of the Driftwood River at the border between Ontario and Québec in Canada (upper right inset) and within the Abitibi River basin (lower right inset). Locations of the *Fraxinus nigra* sampling sites along the Driftwood River are coded as follows: MOL - Moose Lake; DFR - Driftwood River; RPR - Rapid River. 119
- 3.2 The old and the new on Driftwood River at Monteith. First log dam (a, b) and second concrete dam (c) in the years of their construction as compared to today structure (d). Historical photos b) and c) by Mrs. C. Clifford were published in an unknown local newspaper on May 6, 1953. All historical photos retrieved from the digitalized archives of the Monteith Women Institute Tweedsmuir Community History, a courtesy of the Federated Women’s Institutes of Ontario (FWIO; <https://collections.fwio.on.ca>). Photo in August 2021 by AFN. 120
- 3.3 Comparison of the daily water level of the Driftwood River downstream of the Monteith dam (2006–2020) with the daily water levels of the unregulated Porcupine River at Hoyle (~50km west; 2007–2019) and the daily discharge of the unregulated Harricana River at Amos (~200km east; 2006–2020). Daily data for the year 2007 are incomplete at the Porcupine River gauge station. Data were extracted from the historical hydrological station data of the Water Survey Canada. The years of maximum discharge or water level found during the 2006–2020 period and in the three rivers are highlighted in color. The light blue line represents the year 2019 (maximum discharge in the Harricana River), the dark blue line represents the year 2013 (maximum water level found in the Porcupine River), and the orange line represents the year 2007 (maximum level found in the Driftwood River). Dashed line in the upper panel depict the operating level (260.36m) of the Monteith dam. 121
- 3.4 Flood-ring chronologies for each of the five sites and organized by distance classes to the shoreline (0–10m and 10–100m) and for the naturally flowing Harricana River. Trees close to the shoreline (0–10m) are shown with positive bars and trees from the floodplain (10–100m) with negative bars. Grey and black histograms are respectively F1 and F2 flood-ring relative frequencies, and the black solid line in the background indicates temporal replication among the trees sampled per year. Vertical red dashed lines indicate dates of construction of the first and second Monteith dam. Blue vertical bars indicate the years with the highest reconstructed spring discharge for the Harricana River (threshold value = 151.3 m³/s; Nolin et al., 2021ab). 129

- 3.5 Standardized tree-ring width series (pale blue line) and mean site chronologies (dark black lines), and comparison of mean site chronologies among the five sites. Vertical red dashed lines indicate dates of construction of the first and second Monteith dam. The red curves are 10-year spline functions and depict decadal variations in the mean radial tree growth at each site..... 138
- 3.6 Bootstrapped moving Pearson correlations between individual site ring-width chronologies a) Harricana River spring (April 15 to June 30; 1869–2017) discharge, and b) the CRU TS 4.04 mean spring precipitation (MAR-APR-MAY-JUN; 1901–2017). The mean spring discharge of the Harricana River used in this analysis is constructed from the reconstructed (1869–1914) and instrumental (1915–2017) series. Pearson correlation coefficients were calculated by 40-year moving windows lagged backward by 5 years and range from red (positive correlation) to blue (negative correlation). Grey color indicates no data. Asterisks in a) and b) panels indicate p -value < 0.1 (*), < 0.05 (**), and < 0.01 (***). Vertical red dashed lines indicate dates of construction of the first and second Monteith dam 139
- 4.1 Map of the study area. *Pinus banksiana* (black triangles) and *Fraxinus nigra* (green triangle) sampling sites at the border between Ontario and Québec. River basin extents are provided for base map, and site codes are listed in Table 4.1. 156
- 4.2 Characteristics of the composite temperature reconstruction. (a) Reconstruction of spring (March to May) temperature from 1770 to 2016 with two-standard-error confidence interval (grey) and decadal variation highlighted by a 10-year smoothing spline (black). Observed temperature data is illustrated by the dashed red line. A horizontal line delineates the reconstructed temperature mean at 0.41°C. (b) Sample depth of *Fraxinus nigra* (FRNI, dark grey) and *Pinus banksiana* (PIBA, light grey). (c) Adjusted multiple correlation coefficient (AdjR^2) for each model periods and for the calibration (green), verification (blue) and full model (black) equations. 166
- 4.3 Comparison from 1770 to 2016 between (a) reconstructed mean spring air temperature and (b) Berkeley mean spring air temperature. Warm and cold phases are illustrated respectively by red and blue areas and supported by a 10-yr spline highlighting the decadal variability. Note that the two series are presented with a different y-axis range. Vertical dashed lines indicate the

- three periods (1770–1875, 1875–1940, 1940–2016) distinguished in the reconstruction. (c) Scatterplot of the two time-series showing the dispersion of their respective values (blue circles). Years highlighted by red circles indicate the ones with the highest discharge values in the reconstructed spring mean discharge of the Harricana River since 1770 (discharge higher than 151.3 m³/s; Nolin et al., 2021a)..... 167
- 4.4 Spatial correlation maps ($p < 0.1$) between reconstructed spring mean air temperature and March to May (a) Berkeley average temperature anomalies (1770–2016), (b) NOAA Rutgers snow cover (1967–2016) and (c) GRUN runoff (1902–2014). Correlation coefficients range from positive (red) to negative (blue). Spatial correlations were done using the KNMI Climate Explorer engine (<https://climexp.knmi.nl>; Trouet and Van Oldenborgh, 2013). Green square symbol indicates the study area. 168
- 4.5 Spatial correlation maps ($p < 0.1$) between reconstructed mean spring air temperature and (a) Berkeley spring average temperature anomalies, and (b) 20th Century Reanalysis average spring temperature. Correlations are given for 50-years moving windows lagged backward by 25 years and were done using the KNMI Climate Explorer engine (<https://climexp.knmi.nl>; Trouet and Van Oldenborgh, 2013). Green square symbol indicates the study area. . 169
- 5.1 Map of the study area. Location of the study area within North America at the border between Ontario and Québec, Canada (right panel upper inset). Harricana River basin is flowing north to James Bay in the Hudson Sea (right panel). The study area encompasses the Upper Harricana watershed (left panel), located on the upper reach of the Harricana River and delimited by the Amos hydrometric station (red dot). 200
- 5.2 Associations between mean April 15 to June 30 discharge and selected climate variables over the 1915–2020 period. a) monthly and seasonal variables as detailed in Table 5.S1. b) climate variables aggregated according to different time periods as detailed in Table 5.S1. Note that the X axes are different between a) and b) panels. Pearson correlation coefficients range from red (positive correlation) to blue (negative correlation). Asterisks indicate p -value < 0.01 (*), < 0.05 (**) and < 0.001 (***). 212
- 5.3 Boruta – Random Forest (BRF) selection of the climate predictors of the mean April 15 to June 30 Upper Harricana River discharge. The BRF selection results are presented for (a) the complete climate dataset, and (b) the climate variables excluding the SWE data, both over the period 1915–

2020. Both a) and b) panels are box plots of the z-scores (Importance, Y-axes) ranking the variables (X-axes) according to their contribution to the model over 1,000 iterations, and compared to the that of the shadow variables. Blue box plots are minimal, mean, and maximum importance of a shadow variable. Red and green box plots are importance of respectively rejected (non-significant contribution compared to that of the shadow variables) and confirmed ($p < 0.05$) variables. The top insert (beige background) in (a) and (b) presents the full selection of the BRF and then the details of the ranking for the selected variables (white background). The stepwise multiple linear regression performed among the variables indicated important by the BRF in panels a) and b) selected the variables highlighted with a red background on each X-axis.213
- 5.4 Comparison between observed (grey) and estimated (blue) Harricana River mean April 15 to June 30 discharge over the calibration period (1915–2020). Dashed line highlights the mean of the observed discharge at 121.01 m³/s.....215
- 5.5 Comparison over 10-years windows between historical (blue), observed (green), and projected mean discharges from April 15 to June 30 (A15J30) of the Upper Harricana River. Projected discharges are those simulated by the machine learning model (ML, grey) and those from the Hydroclimatic Atlas of Southern Québec 2022 (DEH22). a) Frequency of mean A15J30 discharges higher than 151.3m³/s and represented by the median (solid dots) and maximum (empty dots) values produced by 10-GCMs ensemble. b) Mean A15J30 discharge. Historical discharges are represented by crossbars where the median value is a thick black line, the interval containing 80% of the values is a solid color, and the minimum to maximum range of values is a shading color. Projected discharges under the RCP4.5 and RCP8.5 scenarios are represented by lines of minimum, 80% lower bound, median, 80% upper bound and maximum values produced among the 10-GCMs ensemble and for ML (grey triangles) and DEH22 (orange circles) projections respectively. Horizontal dashed line indicates the median of the observed discharge for 1971–2000 period at 121.03m³/s.....217
- 5.6 0.10 (green) and 0.90 (red) quantiles regressions calculated on the hydrological models' outputs (ML and DEH22) produced by each of the 10 GCMs and under the two climate scenarios (RCP4.5 and RCP8.5). Significant ($p < 0.05$) quantiles regressions are indicated with “***”, respectively for the 0.10 (green) and 0.90 quantiles (red). Horizontal dashed lines indicate 151.3m³/s.....224

- 5.7 Comparison of the decadal frequencies of high floods (mean A15J30 discharge above $151.3 \text{ m}^3/\text{s}$) among the 10-GCM ensemble. Hydrological simulations are those by the machine learning model (grey triangle) and the Hydroclimatic Atlas of Southern Québec 2022 (DEH22, orange dots). Horizontal dashed line is 2 high floods per decade and can be used to compare graphs among others..... 227
- 5.8 Comparison between the highest projected A15J30 mean discharge (2021–2100) and the extreme values projected in various climate predictors for (a) RCP4.5 and (b) RCP8.5 climate scenarios and each of the 10 GCM climate model. Each climate serie has been scale to z-score for comparison purposes. Extremes values in climate predictors were defined as below the 0.5 quantile of above the 0.95 quantile. High A15J30 mean discharge were defined as above the $151.3 \text{ m}^3/\text{s}$ threshold (depicted as the upper dashed line). Discharge projections are depicted for the ML model (blue lines) and the DEH2022 model (grey lines). Climate predictors are figured with various shapes as explained in the upper graphic legend, and coded as in Table 5.S1. For vizualisation purposes, IBU and ISL values have been set negative..... 229

LISTE DES TABLEAUX

Tableau	Page
1.1 Hydrological stations from the Water Survey of Canada (WSC). The numbers (No.) refer to Figure 1.1 and the distance is relative to Lake Duparquet. Note that the two Harricana River stations (No. 4 & 5) were combined into one for calibration purposes as there were no value differences in the overlapping period and in drainage area.	30
1.2 Descriptive statistics of the 12 anatomical and ring-width chronologies derived from 43 <i>Fraxinus nigra</i> trees sampled at Lake Duparquet.	34
1.3 Statistics for the split-sampling calibration and verification procedure, and the full period reconstruction. Models REC1 and REC2 are presented together.....	36
1.4 Pearson correlation coefficients between reconstructed Harricana River spring discharge from April 15 to June 30 (REC1) and mean instrumental discharge from April 15 to June 30 at nine hydrometric stations surrounding Harricana River and Lake Duparquet. The table is ordered by distance to Lake Duparquet (top to bottom). Each correlation in bold corresponds to p -value < 0.001. Note that the periods and number of years differ between hydrometric stations.	45
2.1 Number of <i>Fraxinus nigra</i> trees sampled, and cores collected per site. Sites are classified by hydrological regime. The field “Period” indicates the maximum period covered by the flood-ring and continuous series of earlywood vessel chronologies. The distance provided are in reference to Lake Duparquet’s location. Among the regulated river sites, the ABL, DFR and FHL sites are located upstream of the dams while the MGR site is located between two dams.	72

- 2.2 Spearman’s rank correlation coefficients (ρ) and p -values (p) between the flood-ring chronologies at each site and the reconstructed Harricana River spring discharge. F1 and F2 represent weakly and well-defined flood rings and F12 is the sum of their relative frequencies. Bold characters denote p -values < 0.05 79
- 2.3 Spearman’s rank correlation coefficients (ρ) and p -values (p) between flood-ring chronologies from Lake Duparquet (DPL), natural rivers (NAT), regulated rivers (REG) and unflooded control sites (CTL) and 10 instrumental records of April 15 to June 30 mean discharge across the study area. The field “Id” is the Canadian federal hydrometric station identification number. F1 and F2 represent weakly and well-defined flood rings and F12 is the sum of the relative frequencies F1 and F2. The table is ordered by increasing distance between hydrometric station and Lake Duparquet (left to right) to visualize spatial coherency in the correlation structure. Bold characters denote p -values < 0.05 81
- 2.4 Pearson’s correlations (r) and p -values (p) between continuous earlywood vessels chronologies from the naturally flowing Lake Duparquet ($n = 43$), Harricana River (site HAR, $n = 2$), Abitibi River (site LAR, $n = 2$), upper Ottawa River (site PSL, $n = 1$) and the regulated Mattagami River (site MGR, $n = 1$). Chronologies abbreviation are as follows: (MVA) mean cross-sectional lumen area of earlywood vessels, (N) number of earlywood vessels. Pearson’s correlation coefficients are given for the common period 1922–2016 and bold characters denote p -values < 0.05 87
- 2.5 Pearson’s correlation coefficients (r) and p -values (p) between chronologies of mean lumen cross-sectional area (MVA) and number (N) of earlywood vessels, from four river basins and 10 instrumental records of April 15 to June 30 mean discharge across the study area. The field “Id” is the Canadian federal hydrometric station identification number. The table is ordered by increasing distance between hydrometric stations and Lake Duparquet (left to right) to visualize spatial coherency in the correlation structure. Bold characters denote p -values < 0.05 88
- 3.1 Location of sampling sites. Data are ordered by increasing distance to the dam from top to bottom. Period is the length of flood-ring records..... 118

- 3.2 Characteristics of *Fraxinus nigra* stands. Mean values and standard deviation by site indicating (1) stem diameters at breast height, (2) maximum tree age, and (3) their position in the floodplain relative to the shoreline. Data are ordered by increasing distance to the dam from top to bottom. 127
- 3.3 Comparison of F12 flood-ring relative frequencies with instrumental and reconstructed mean spring (April 15 to June 30) discharge of the naturally flowing Harricana River and by distance to shoreline (0–10m and 10–100m). Spearman correlation coefficients (ρ) are given after calculating 10,000 bootstrap iterations. Bold characters denote significant ρ coefficients at $p < 0.05$. Spearman coefficients were calculated for four periods (1) the pre-dam period before the first log dam (1850–1917), (2) after the first log dam (1918–2016); (3) in between the first log dam and the second concrete dam (1918–1952); and (4) after the second concrete dam (1953–2016). (*) Note that for the pre-dam period, the number of years varies among sites and distance classes with DFR 2 (1879–1917), MOL 1 (1898–1917), MOL 2 (1852–1917; Fig. 3.4; Table 3.1). The pre-dam period has been calculated with the reconstructed Harricana River discharge, the other periods with the instrumental Harricana River discharge. nd: no data. 131
- 4.1 Tree-ring chronologies provenance. Species are *Pinus banksiana* (PIBA) and *Fraxinus nigra* (FRNI). Code refers to Figure 4.1. (Period is the period after truncation to $n > 3$ samples to account for post-fire regeneration gaps in each site chronologies). 158
- 4.2 Comparison of reconstructed mean spring (March to May) temperature minimums and of reconstructed and instrumental mean spring (April 15 to June 30) discharge maximums. Values are compared by decade and for the last 247 years. ‘REC discharge’ is the reconstructed mean spring discharge of the Harricana River (1771–2016) and is taken from Nolin et al. (2021a). ‘HAR discharge’ is the instrumental mean Harricana River spring discharge (1915–2020). Both mean spring discharges are average from April 15 to June 30 daily discharge data, while temperature reconstruction is average March to May. Years in bold highlight the years that are part of the highest mean spring discharge years since 1771. Grey cells highlight the years for which, per decade, the minimum spring temperature corresponds to the maximum spring discharge. The first (1771–1779) and last (2010–2016) periods used for comparisons are not complete decades. 172

- 5.1 Climate simulations (r1i1p1) from CMIP5 ensemble used in this study. This set of 10 standard scenarios (cb-oura-1.0) was produced by Ouranos to cover the range of expected changes in daily temperature and precipitation in the province of Québec.....203
- 5.2 (a) Annual Stepwise selection statistics for the full period calibration (1915–2020). (b) Annual Regression statistics for the split-sampling calibration and verification procedure, and the full period calibration.213
- 5.3 Hydrological (observed data) and meteorological (BioSIM data) trends in the Upper Harricana River watershed from 1915 to 2020. Only significant ($p < 0.05$) trends are not shown. Sen’s slopes are expressed as 105-year change in the original data units. Percent change is relative to the 1916–1925 (10-year) average which is assumed to be representative of the beginning of the trend line. To account for the spring flood generating mechanisms, hydrological years from previous July to current June have been considered. Months in lowercase letters are those of the previous year (*e.g.*, 1915) and months in capital letters are those of the current year (*e.g.*, 1916). Variables abbreviations are listed in Table 5.S1.....218
- 5.4 Scenario (a) RCP4.5 and (b) RCP8.5. Projected hydroclimatic trends in the Upper Harricana River watershed from 1971 to 2100 and calculated using the median of the 10-GCM ensemble. Non-significant ($p < 0.05$) trends are not shown. Sen’s slopes are expressed as 130-year change in the original data units. Percent change is relative to the 1971–1980 (10-year) average which is assumed to be representative of the beginning of the trend line. Value below the trend is the inter-GCMs agreement and expresses the number of positive trend / negative trend / non-significant change found among the ten GCMs when calculating the Sen’s slope for each of GCM projection separately. Variables abbreviations are listed in Table 5.S1.219

RÉSUMÉ

Depuis la fin du Petit Âge Glaciaire (1850–1870 CE) la région des Plaines de l’Abitibi, située dans l’est du Canada boréal, subit une augmentation de la fréquence et de la sévérité des inondations de dégel printanier. Les projections climatiques prévoient un renforcement de la fréquence et de la sévérité de ces inondations, pour lesquelles les facteurs et forçages climatiques sont peu connus. Pour cette région productrice d’hydroélectricité, l’estimation des impacts potentiels des changements climatiques sur le régime hydrologique des rivières constitue une priorité. Le manque de données hydrologiques et climatiques instrumentales rend l’étude des indicateurs paléo-environnementaux nécessaires pour identifier les tendances historiques et les trajectoires hydroclimatiques à long terme.

Des études antérieures au Lac Duparquet indiquent que les éléments de vaisseaux (nombre et surface) dans le bois initial de cernes de croissance de frênes noirs (*Fraxinus nigra* Marsh.) peuvent être utilisés comme indicateurs des crues printanières. Ce lac est inondé annuellement par des crues lors de la phase de dégel printanier qui peuvent s’étaler jusqu’au début du mois de juillet et qui affectent la formation et le développement des éléments de vaisseaux des frênes noirs.

Les objectifs de cette thèse de Doctorat sont (1) de reconstituer et étudier la variabilité historique des inondations printanières par l’étude des cernes de crues localement puis régionalement, pour déterminer les patrons de cohérence spatiale sur la région des Plaines de l’Abitibi entre le déclenchement des inondations et leurs forçages climatiques ; (2) de reconstituer et étudier les mécanismes climatiques à l’origine du déclenchement des crues printanières historiques ; (3) et d’identifier les tendances climatiques à long terme de l’écoulement régional pour anticiper les changements des crues printanières et leurs facteurs météorologiques déterminant sous différents scénarios de changements climatiques.

Le premier chapitre de cette thèse utilise l’analyse quantitative de l’anatomie des cernes de frênes noirs périodiquement inondés au Lac Duparquet pour reconstituer la variabilité historique des débits printaniers de la Rivière Harricana. Les résultats indiquent que l’intensité et la fréquence des hauts débits moyens printaniers

reconstitués depuis 1771 ont augmenté depuis la fin du Petit Âge Glaciaire, et particulièrement depuis 1950, ce qui rejoint d'autres paléo-enregistrements du Québec subarctique. Ces changements sont associés, en autres, à l'épaisseur des couverts de neige à l'échelle du centre-est du Canada et à des changements probables des circulations atmosphériques à large échelle. Les plus hauts débits moyens printaniers de la seconde moitié du 20^e siècle ont été déclenchés par des hivers froids accumulant des couverts neigeux persistants tard au printemps et dont la fonte a été activée en même temps que des pluies intenses. Ces conditions climatiques étaient notamment associées aux phases négatives de l'indice NINO3.4 - Oscillation Australe (La Niña).

Le second chapitre analyse les cernes de crues de frênes noirs répartis dans dix plaines inondables de quatre grands bassins versants (Mattagami, Abitibi, Harricana, Outaouais Amont), et caractérisés par des rivières naturelles et régulées, et des sites témoins non inondés. A cette échelle régionale, l'analyse semi-quantitative des cernes de crues indique que le signal hydrologique reconstitué pour la rivière Harricana est commun aux rivières naturelles des plaines de l'Abitibi sur les dernières 250 années. Dans les rivières régulées, les arbres semblent avoir enregistré la dynamique naturelle de la rivière avant la création des barrages, puis les manœuvres de gestion des barrages et les crues de printemps dépassant leur capacité.

Le troisième chapitre analyse l'effet de la régulation de la Driftwood River, en Ontario sur la production de cernes de crues des frênes noirs riverains. La mise en place du barrage a été enregistrée par les cernes de crues. Avant la construction du barrage, des fréquences relatives élevées de cernes de crues bien définis ont été enregistrées pendant les années de crue connues. Après la construction du barrage, les cernes de crues étaient moins distincts, certains correspondant à des années de crues connues et d'autres reflétant probablement la gestion du barrage. Par rapport au site en aval du barrage, ceux en amont ont enregistré plus de cernes de crues dans la période post-barrage. Les résultats ont aussi démontré qu'il était possible de distinguer le signal d'inondation du signal de gestion du barrage en échantillonnant des arbres dans de multiples peuplements riverains (amont et aval du barrage) et à des distances proches et éloignées de la berge.

Le quatrième chapitre démontre l'utilisation des cernes de crues de frêne noir (un site) et des largeurs de bois final de pin gris (*Pinus banksiana* Lamb.; dix sites) comme indicateurs pour la reconstitution des températures printanières. De 1770 à 2016, la reconstitution indique que la variabilité interannuelle des températures moyennes printanières s'est accélérée depuis la fin du Petit Âge Glaciaire et que la fréquence et la sévérité des printemps chauds ont particulièrement augmenté depuis 1940. Ces nouvelles données rejoignent les résultats du chapitre I et démontrent une nouvelle fois

que les crues historiques majeures étaient associées à des printemps tardifs et froids avec un couvert neigeux important durant cette période. Cependant, dans les 40 dernières années des températures moyennes plus chaudes à la fin du printemps, semblent contribuer à avancer la date de la crue printanière et à probablement favoriser la contribution de la pluie au lieu de la neige dans les processus d'inondations printanières.

Le cinquième chapitre prolonge la perspective historique apportée par les chapitres précédents en analysant les tendances observées dans les enregistrements hydroclimatiques puis en projetant les trajectoires potentielles à l'aide de simulations de modèles climatiques afin d'anticiper les changements du débit moyen printanier de la Rivière Harricana sous deux scénarios de changements climatiques (RCP4.5 et RCP8.5). Les analyses de tendances pour le 20^e siècle démontrent que le réchauffement des températures moyennes hivernales et printanières contribue à diminuer la quantité de neige accumulée et son équivalent en eau, au contraire de la pluie qui a augmenté à la fois en quantité et en intensité, avec également plus de pluies sur neige. Le dégel des rivières au printemps semble aussi être devenu plus hâtif, ce qui soutient les résultats de la reconstitution des températures. Par rapport au débit reconstitué du Petit Âge Glaciaire et aux observations du 20^e siècle et du début 21^e siècle, les trajectoires hydroclimatiques projetées par huit modèles GCM (modèle climatique à échelle planétaire) sur dix suggèrent peu de changements d'ici la fin du 21^e siècle. Notamment, les projections indiquent une nette compensation de la fonte des neiges par les pluies dans les débits, et ce sous les deux scénarios climatiques utilisés (RCP4.5 et RCP8.5). Les deux autres modèles GCM de l'ensemble climatique projettent des conditions similaires à celles ayant entraîné les inondations printanières majeures du 20^e siècle et prévoient une augmentation de leur sévérité et de leur fréquence d'ici 2100.

Finalement, cette thèse contribue à l'avancement des connaissances et de la compréhension du climat et des débits printaniers régionaux durant et après le Petit-Âge Glaciaire et apporte une base pour la compréhension à plus large échelle des conditions climatiques qui engendrent des hauts débits printaniers dans l'est du Canada boréal. Les différents chapitres sont aussi un apport théorique et méthodologique important pour l'échantillonnage et l'analyse des cernes de crues pour les reconstitutions dendrohydrologiques en milieu boréal, ainsi que pour l'utilisation d'indicateurs du climat printanier, qui restent encore peu représentés en dendroclimatologie.

Mots-clés : dendrochronologie, hydrologie, *Fraxinus nigra*, *Pinus banksiana*, Rivière Harricana, Lac Duparquet, inondation printanière, est du Canada boréal, Plaines de l'Abitibi

INTRODUCTION GÉNÉRALE

0.1 Contexte

L'hydrologie des rivières de l'est du Canada boréal est caractérisée par un régime nivopluvial à forte saisonnalité des écoulements (Ashmore et Church, 2001; Moore et al., 2017). Sous l'effet combiné de la fonte du couvert nival et la pluie sur neige lors de la phase de dégel au printemps, le faible débit hivernal qui s'écoule sous la glace passe rapidement à un débit de crue printanière, fracturant l'emprise des glaces. Le niveau d'eau que peuvent atteindre les crues printanières et les dégâts que peuvent causer les embâcles de glace emportés par le courant constituent un risque naturel majeur (Buttle et al., 2016; Peters et al., 2016). Ces crues peuvent aussi menacer la sécurité des barrages hydroélectriques implantés dans le nord du Québec et de l'Ontario, desquels dépend plus de 70% de la production énergétique du Canada (Boucher et Leconte, 2013; Winsemius et al., 2016; Cherry et al., 2017). En parallèle des changements climatiques observés depuis la deuxième moitié du 20^e siècle, les inondations deviennent de plus en plus fréquentes à travers le monde (Berghuijs et al., 2017; Kundzewicz et al., 2019) et particulièrement au Canada (Burn et al., 2016; Burn et Whitfield, 2016; Buttle et al., 2016; Burn et al., 2016; Burn et Whitfield, 2018; Bush et Lemmen, 2019). Les changements climatiques sont le résultat de causes naturelles et anthropiques qui affectent, notamment, la concentration en gaz à effet de serre de l'atmosphère (IPCC, 2014, 2021). Il apparaît donc prioritaire de comprendre les changements hydroclimatiques récents et de les comparer à la variabilité historique naturelle pour

anticiper leurs conséquences potentielles sur l'hydrologie des crues printanières au Canada.

0.2 Changements hydroclimatiques

Le réchauffement de la température moyenne annuelle (+2,3°C) et l'intensification des précipitations totales annuelles (+30% à +40%) du nord canadien (Nord de 60°N) depuis 1950 sont plus importants que dans l'ensemble du Canada (+1.7°C, +20%; Zhang et al., 2000; Zhang et al., 2001b; Vincent et al., 2015; Bush et Lemmen, 2019; Aýgun et al., 2019). Le réchauffement le plus important est observé en hiver et les projections climatiques suggèrent un réchauffement (+2 à +6°C depuis 1950) environ deux fois plus conséquent que la température moyenne mondiale tous scénarios d'émissions de gaz à effet de serre confondus (IPCC, 2014, 2021; Bush and Lemmen, 2019). Le régime des rivières boréales est déjà particulièrement affecté par le réchauffement observé des températures (Whitfield et Cannon 2000; Ashmore et Church, 2001; Javelle et al. 2003; Buttle et al., 2016; Burn et al., 2016; Burn et Whitfield, 2016; Aýgün et al. 2019) avec notamment des crues de dégel printanier plus précoces (revues par Prowse et Bonsal, 2004; Prowse et al., 2007; Aýgun et al., 2019; Bush et Lemmen, 2019) soutenues par un débit hivernal plus élevé (Whitfield et Cannon, 2000; Zhang et al., 2001a; Déry et al., 2009; Vincent et al., 2015). En hiver, l'augmentation observée des précipitations (+50% ; Bush and Lemmen, 2019) et particulièrement des pluies par rapport à la neige (Yagouti et al., 2008; Brown, 2010; Mudryk et al., 2018; Aýgun et al., 2019; Mudryk et al., 2020) soutenue par de plus fréquents gel-dégel, libèrent une plus grande partie de l'eau stockée dans les couverts neigeux (Mudryk et al., 2018; Aýgun et al., 2019; Mudryk et al., 2020). Pourtant, dans l'est du Canada boréal, les enregistrements hydrologiques démontrent de manière consistante que la fréquence et la sévérité des crues printanières ont augmenté durant le 20^e et 21^e siècle (Déry et al., 2011; Burn et al., 2016; Buttle et al., 2016; Burn et Whitfield, 2018; Gaur et al., 2018; Bush et

Lemmen, 2019). Les crues de la dernière décennie (2010–2020) sont sans précédent à l'échelle des enregistrements hydrologiques du 20^e siècle (Burn et Whitfield, 2016; Gaur et al., 2018). Les enregistrements paléohydrologiques démontrent aussi une augmentation significative du niveau des lacs et de l'activité des glaces depuis 1850¹ dans la région du Lac Duparquet (Tardif et Bergeron, 1997b) et dans le Québec subarctique (Bégin, 2000; Bégin, 2001; Lemay et Bégin, 2008; Boucher et al., 2011; Lemay et Bégin, 2012; Nicault et al., 2014; Nasri et al., 2020).

Avec le réchauffement projeté, la diminution des couverts neigeux et l'augmentation des précipitations totales (Guay et al., 2015; Mudryk et al., 2018), les projections pour le nord-est du Canada boréal suggèrent une augmentation des débits maximaux et moyens d'automne et d'hiver, et des débits maximaux de printemps plus précoces (*Québec* : Huziy et al., 2013; Guay et al., 2015; MELCC, 2018; *Sud Ontario*: Cunderlik et Simonovic, 2005; Grillakis et al., 2011; *affluents du Lac St. Jean*: Dibike et Coulibaly, 2005; Minville et al., 2008; Minville et al., 2009; Minville et al., 2010; *affluents du St. Laurent*: Roy et al., 2001; Quilbé et al., 2008; Boyer et al., 2010; Riboust & Brissette, 2015). Pour le Québec, une augmentation des fréquences de retour des débits de forte sévérité est projetée d'ici à 2050 à 2070, avec les plus fortes augmentations projetées pour les rivières du nord du 60°N (Frigon et al., 2010; Huziy et al., 2013; Clavet-Gaumont et al., 2013a, 2013b, 2017; MELCC, 2018). D'une manière générale

¹ En Amérique du Nord, la période 1850–1870 correspond à la fin du Petit Âge Glaciaire, intervalle climatique caractérisé du 16^e au 19^e siècles par la persistance de phases climatiques multidécennales froides centrées sur les années 1650, 1770 et 1850 (Matthews et Briffa, 2005; Viau et Gajewski, 2009). Le climat du nord Canadien de la fin du 19^e siècle a été caractérisé par des fluctuations importantes des températures et des précipitations en réponse à un changement de régime dans les circulations des masses d'air à l'échelle terrestre. Notamment, en réponse à une migration du front polaire arctique vers le nord (position moyenne pendant le Petit Âge Glaciaire : 48°N ; position moyenne en 1875 : nord du 50°N) les masses d'air chaud en provenance de l'océan Pacifique équatorial ont pénétrés plus au Nord du Canada (Hofgaard et al., 1999 ; Bonsal, 2006) affectant la variabilité et les extrêmes hydroclimatiques à large échelle (Kundzewicz et al., 2019).

cependant, comment les changements hydroclimatiques affecteront la fréquence et la sévérité des crues printanières reste incertain à l'échelle du nord-est canadien (Gaur et al., 2018; Bush et Lemmen, 2019). La modélisation des facteurs hydroclimatiques impliqués dans leur déclenchement reste complexe, et la qualité des enregistrements climatiques et hydrologiques reste limitante (Dibike et Coulibaly, 2005; Quilbé et al., 2008; Huziy et al., 2013; Clavet-Gaumont et al., 2017). Particulièrement dans l'est du Canada boréal, l'analyse de la variabilité hydrologique naturelle historique est contrainte par la faible couverture spatiale et temporelle des enregistrements hydroclimatiques (Boucher et al., 2011; Mortsch et al., 2015; Pellerin et al., 2019).

Cette thèse précise le portrait global des changements observés et des trajectoires hydroclimatiques prévisionnelles pour le nord-est du Canada boréal en s'appuyant sur une reconstitution de la variabilité hydroclimatique passée des crues printanières, c'est-à-dire avant la période où les enregistrements climatiques et hydrologiques sont disponibles. Reconstituer les débits et les climats historiques peut non seulement permettre d'allonger la fenêtre de données disponibles pour appuyer la calibration des modèles statistiques mais également de préciser l'analyse des périodes de retour des inondations printanières extrêmes. Comparer les évolutions hydroclimatiques récentes avec des variations analogues ayant eu lieu dans le passé aiderait aussi à mieux comprendre le rôle relatif des facteurs climatiques impliqués dans le déclenchement des inondations de printemps, et améliorerait notre compréhension des changements observés et prévisionnels.

0.3 Approche dendrohydrologique

En paléoclimatologie, parmi les indicateurs étudiés, les cernes de croissance d'arbres fournissent de l'information paléohydrologique à une résolution annuelle en raison de l'interconnexion entre climat, hydrologie et croissance radiale (Fritts, 1976;

Schweingruber, 1996). Hormis les archives manuscrites, les cernes de croissance des arbres peuvent fournir des données avec une résolution annuelle continue et sur de longues périodes. Les mesures de largeurs de cernes de croissance provenant d'arbres à longue durée de vie et poussant dans des conditions environnementales sensibles aux stress hydriques sont traditionnellement utilisées pour reconstituer les débits historiques, et particulièrement les bas débits (synthèse par Loáiciga et al., 1993; Boucher et al., 2010; Meko et Woodhouse, 2011; Meko et al., 2012; Ballesteros-Cánovas, et al., 2015; Tardif et al., 2021b). Dans les environnements boréaux, où l'eau n'est pas un facteur limitant la croissance des arbres, les largeurs et la densité des cernes de croissance, ou les isotopes stables sont aussi utilisés pour des reconstitutions hydrologiques (Boucher et al., 2011, Nicault et al., 2014, Agafonov et al., 2016; Nasri et al., 2020, Meko et al., 2020). Les relations entre cernes de croissance et débit dans les environnements boréaux peuvent, en effet, être parfois de faible intensité (Tardif et al., 1998; Kames, 2009; Kames et al., 2016). Les arbres poussant dans les plaines inondables peuvent aussi permettre de dater les phases d'érosion (départ sédimentaire) ou d'aggradation (apport sédimentaire), les variations de niveaux des lacs, et les crues de débris, ou les crues glacielles (synthèse par Schweingruber, 1996; Boucher et al., 2010; Ballesteros-Cánovas et al., 2015; Wilhelm et al., 2018). Hormis les mesures de largeurs de cernes, les mesures anatomiques des éléments de vaisseaux (Fig. 0.1) enregistrent des signaux climatiques ou environnementaux prévalant pendant la croissance des arbres et avec une résolution annuelle à sub-annuelle, et particulièrement les stress hydriques (García-González et Eckstein, 2003; Fonti et García-González, 2004; Tardif et Conciatori, 2006b; Fonti et García-González 2008; Fonti et al., 2009; Fonti et al., 2010; González-González et al., 2015, et synthèse par García-González et al., 2016).

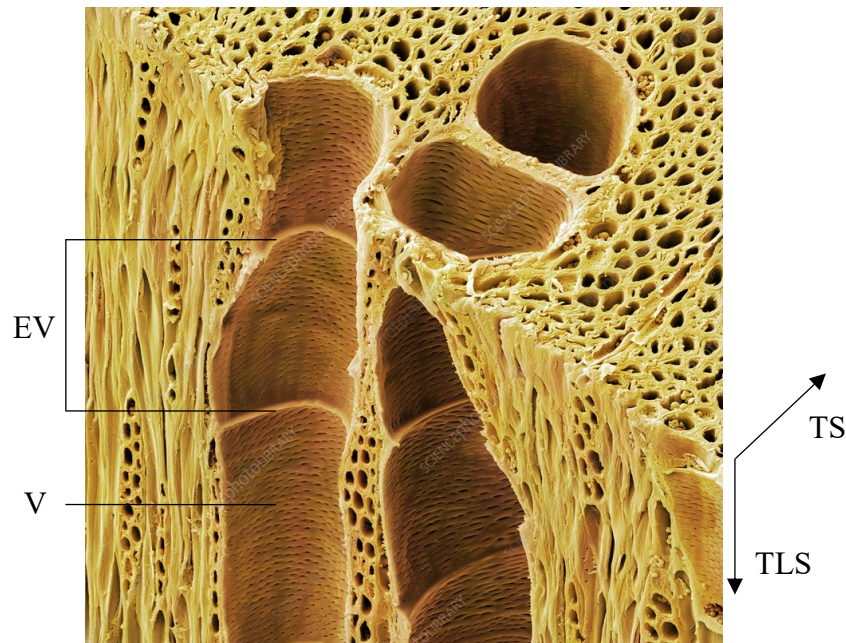


Figure 0.1 Micrographie électronique à balayage (MEB) du bois d'un *Fraxinus excelsior* en plan transversal (TS) et longitudinal tangentiel (TLS) montrant les éléments de vaisseaux (EV) et les vaisseaux (V). Les éléments de vaisseaux s'empilent un à un pour former les vaisseaux, organes tubulaires creux allongés verticalement dans l'axe de la tige et transportant la sève. Photo MEB © SciencePhotoLibrary Limited, 2022, England.

0.4 Particularité des feuillus à zone poreuse pour l'étude et la reconstitution des inondations

Les feuillus à zone poreuse (*e.g.*, genres *Castanea*, *Fraxinus*, *Quercus*, et *Ulmus*) sont utilisés de longue date en dendrohydrologie (Sigafos, 1964; Yanosky, 1983; Yanosky 1984) en raison de leur physiologie vulnérable au stress hydrique et de leur phénologie particulièrement hâtive (Tyree et Zimmerman, 2003). En réponse aux inondations, les feuillus à zone poreuse produisent des vaisseaux du bois initial plus petits et/ou plus nombreux que dans une année de croissance régulière, nommés 'cernes de crues' (Astrade et Bégin, 1997; St. George et Nielsen, 2000; Tardif et al., 2010). L'ensemble

des mécanismes à l'origine de la formation des cernes de crues restent incertains, mais les études physiologiques convergent vers un effet cumulé du manque d'oxygène et de l'accumulation anormale de composés issus du métabolisme des arbres notamment l'éthylène (Kozłowski, 1984; Jackson, 1985; Yamamoto, 1995; Kowłowski, 1997; Junghans et al., 2004). Leur formation semble dépendante de la tolérance des feuillus à zone poreuse aux inondations, de leur génotype, leur âge, des propriétés physico-chimiques de l'eau ou encore de la durée des inondations (Kozłowski, 1984; Kowłowski, 1997; Glenz et al., 2006). St. George et al. (2002) ont démontré que la durée d'inondation avait une plus grande influence que le débit maximal sur la taille des vaisseaux du bois initial chez *Quercus macrocarpa*. Les expériences d'inondation de *Quercus robur* démontrent également que leur formation est indépendante de l'âge des arbres (Sass-Klaasen et al., 2010; Copini et al., 2016). Plusieurs autres facteurs pourraient aussi être susceptibles d'amplifier ou d'atténuer la formation des cernes de crues, comme le phasage de la crue par rapport au début ou à la fin de la formation du cerne de croissance, ou encore le temps écoulé depuis la dernière crue (Glenz et al., 2006; Copini et al., 2016). Les cernes de crues ont déjà permis de reconstituer la variabilité historique des débits (notamment, chez *Quercus robur* L. en France, Astrade et Begin, 1997 ; et *Quercus macrocarpa* Michx. au Manitoba, Canada, St. George et Nielsen, 2000; St. George et al., 2002; St. George et Nielsen, 2003; Wertz et al., 2013) ou de dater des inondations historiques majeures (notamment St. George et Nielsen, 2002, St. George et Nielsen, 2003, Tardif et al., 2010; Wertz et al., 2013, Therrell et Bialecki, 2015, Kames et al., 2016; Meko et Therrell, 2020). Au Lac Duparquet, des chronologies continues d'éléments de vaisseaux de frênes noirs (*Fraxinus nigra* Marsh.) périodiquement inondés par les crues printanières (Fig. 0.2) ont aussi permis de quantifier les associations entre la variabilité des débits printaniers de la rivière Harricana (Fig. 0.2; Fig. 0.3; Fig. 1.1) et la variabilité anatomique des vaisseaux (Kames, 2009; Tardif et al., 2010; Kames et al., 2016).

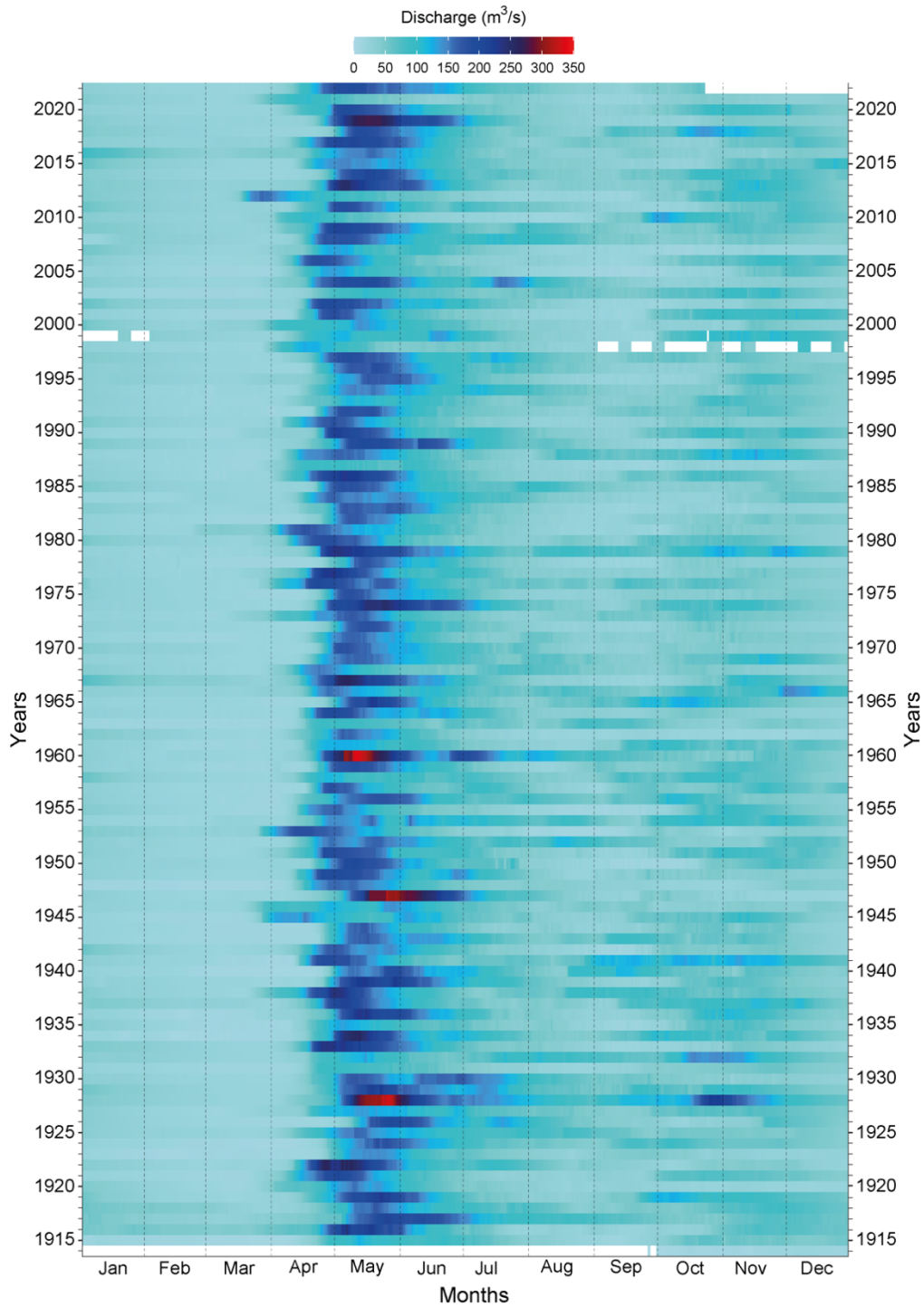


Figure 0.2 Représentation matricielle du débit journalier de la rivière Harricana à Amos (04NA001-2) de 1914 à 2022. Les données manquantes sont figurées en blanc.

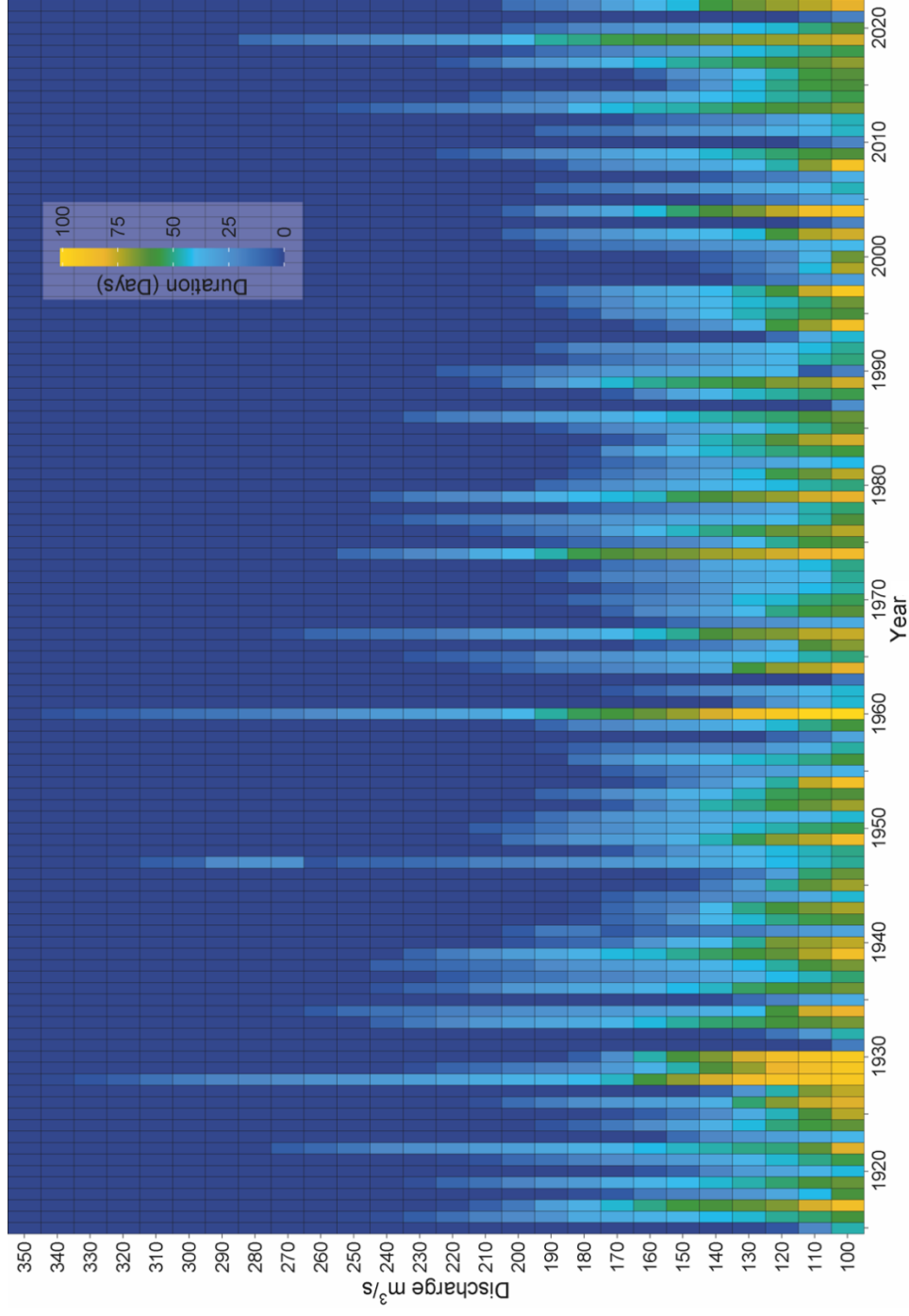


Figure 0.3 Représentation matricielle de la durée des hauts débits printaniers de la rivière Harricana à Amos (04NA001-2) de 1914 à 2022, exprimé en nombre maximum de jours consécutifs par an où le débit est supérieur à une lecture de jauge spécifiée pendant l'intervalle du 1er janvier au 31 Juillet (211 jours).

0.5 Objectifs de la thèse

L'objectif principal de cette thèse est de caractériser la variabilité historique des débits printaniers, puis de calculer les trajectoires hydroclimatiques potentielles pour la région des Plaines de l'Abitibi sous différents scénarios de changements climatiques. Le premier volet (chapitres I, II, III) s'attache a) à reconstituer la variabilité historique des hauts débits printaniers de la rivière Harricana depuis la fin du Petit Âge Glaciaire par l'étude de cernes de crues et à analyser les mécanismes climatiques à l'origine des hauts débits de printemps et leurs relations avec les principaux indices de circulations atmosphériques affectant le climat de l'Amérique du nord ; b) à étudier la temporalité et la cohérence spatiale régionale des hauts débits printaniers dans les bassins versants des rivières Mattagami, Abitibi, Harricana, Outaouais amont, et entre contextes hydrologiques naturels, régulés par barrage, et contrôles non inondés ; c) à déterminer comment la régulation des débits printaniers par un barrage affecte la production de cernes de crues (variabilité des éléments de vaisseaux du bois initial) et la largeur des cernes de croissance des frênes noirs riverains selon les contextes hydrologiques. Le deuxième volet (chapitre IV) s'attache à reconstituer la variabilité historique des températures printanières régionales et à analyser les relations entre les hauts débits printaniers reconstitués pour la rivière Harricana et l'évolution des températures printanières depuis la fin du Petit Âge Glaciaire. Enfin, le troisième volet (chapitre V) étudie des trajectoires potentielles futures des hauts débits de dégel printanier de la Rivière Harricana, analyse les tendances à long terme dans les variables climatiques et leur contribution relative aux hauts débits printaniers, et compare les tendances futures estimées par rapport à la perspective historique à long terme détaillée dans les précédents chapitres (et particulièrement les reconstitutions des débits de printemps de la Rivière Harricana – chapitre I; et des températures printanières régionales – chapitre IV). Cette thèse conclut sur l'apport des reconstitutions dendrohydrologiques à la

compréhension de la dynamique hydroclimatique régionale et aux prévisions hydrologiques futures, ainsi que des travaux à poursuivre pour l'applicabilité de la méthode des cernes de crues à la reconstitution à grande échelle des inondations au Canada boréal.



Figure 0.4 Frênaies noires alluviales du Lac Duparquet. a) Frênaie #42, début septembre 2017 (date inconnue). Les contreforts proéminents de ces arbres révèlent le caractère périodique et prolongé des inondations printanières (Varnell 1998 ; Tiner, 2016). La végétation au sol est dominée par la fougère *Onoclea sensibilis* L.), elle-même indicatrice des plaines alluviales basses aux inondations printanières prolongées (Tardif et Bergeron, 1992). Annick Antaya - “Madame Grand Pic”, sur la photo. b) Frênaie #42, 24 mai 2018. Les arbres sont inondés par plus de 50cm d'eau, nous circulons en chaloupe entre les frênes. c) Frênaie #103-Mouilleuse, 2 juillet 2019. Le haut niveau d'eau de la crue printanière persiste jusqu'en début d'été. d) Frênaie #103-Mouilleuse, 3 juillet 2019. Les lignes de jaunes sont des laisses de pollen et indiquent le niveau maximal et les phases de décrue de l'inondation printanière de 2019.

CHAPITRE I

MULTI-CENTURY TREE-RING ANATOMICAL EVIDENCE REVEALS INCREASING FREQUENCY AND MAGNITUDE OF SPRING DISCHARGE AND FLOODS IN EASTERN BOREAL CANADA

Alexandre F. Nolin, Jacques C. Tardif, France Conciatori, Susanne Kames, David. M.
Meko, Yves Bergeron

Publié dans *Global and Planetary Change*

Février 2021

1.1 Abstract

In eastern boreal Canada, variability in river discharge is poorly understood at the multi-century scale due to short instrumental records. In recent decades, increased magnitude and frequency of spring floods have raised concerns about the potential effects of climate change on flood risk. Unlike tree-ring width, flood rings have a demonstrated dendrochronological utility for reconstructing high discharge in boreal environments. In this study, twelve chronologies of earlywood vessel cross-sectional area (a new hydrological proxy) and ring width were developed from riparian *Fraxinus nigra* trees periodically flooded in spring. These chronologies were used as predictors of Harricana River spring discharge, which was reconstructed for the period 1771–2016. The reconstruction captured 69% of the variance over a 102-year calibration period. The reconstruction indicates that the magnitude and frequency of spring high discharge has increased since the end of the Little Ice Age (1850–1870 CE) and since 1950. The change from a multi-decadal frequency in the late 19th century to a decadal and then interannual frequency in the late 20th century is associated with an increase in snow cover over much of central-eastern Canada. The association between the reconstructed spring discharge and spring atmospheric circulation indices NINO3.4, AMO, NAO may also have changed in these periods and further work is needed to assess the stability of these associations. The correlation between reconstructed and instrumental spring discharge at the regional scale, as well as the shared features in reconstructed discharge and other paleorecords from subarctic Québec suggest a common hydrological signal across the study area and for the early 20th to 21st centuries. The unprecedentedly low and high spring discharge in recent decades compared to the historical natural variability of the last 250 years also suggests that the increase in flood frequency and magnitude originates from climate change.

Keywords : climate change, atmospheric circulation, dendrohydrology, earlywood vessels, *Fraxinus nigra*, Lake Duparquet

1.2 Résumé [Ajout à l'article original]

Dans l'est du Canada boréal, la variabilité du débit des derniers siècles est peu connue en raison du manque d'enregistrements hydrologiques. Au cours des dernières décennies, l'augmentation de l'intensité et de la fréquence des crues printanières ont suscité des inquiétudes quant aux effets potentiels des changements climatiques sur le risque inondation. Contrairement à la largeur totale des cernes de croissance des arbres, les cernes de crues se sont avérés particulièrement efficaces en dendrochronologie pour reconstituer les hauts débits. Dans cette étude, douze chronologies (de paramètres anatomiques de vaisseaux du bois initial, et de largeur des cernes de croissance) ont été développées à partir de frênes noirs riverains et périodiquement inondés au printemps. Ces chronologies ont été utilisées comme prédicteurs du débit moyen printanier de la rivière Harricana, qui a été reconstitué de 1771 à 2016. La reconstitution a capturé 69% de la variance sur une période de calibration de 102 ans. La reconstitution indique que l'intensité et la fréquence des hauts débits printaniers ont augmentés depuis la fin du Petit Âge Glaciaire (1850–1870 CE) et particulièrement depuis 1950. Le passage d'une fréquence pluri-décennale à la fin du 19^e siècle à une fréquence décennale, puis interannuelle à la fin du 20^e siècle est associé à une augmentation du couvert neigeux sur une grande partie du centre-est du Canada. L'association entre le débit printanier reconstitué et les indices de circulation atmosphérique printaniers NINO3.4, AMO, NAO pourrait également avoir changée au cours de ces périodes, et des recherches supplémentaires sont nécessaires pour évaluer la stabilité de ces associations. La corrélation entre les débits moyens printaniers reconstitués et instrumentaux à l'échelle régionale, ainsi que les caractéristiques communes des débits reconstitués et d'autres paléo-enregistrements du Québec subarctique, suggèrent un signal hydrologique commun dans toute la zone d'étude pour le début du 20^e et du 21^e siècle. Les débits printaniers exceptionnellement haut et bas des dernières décennies comparés à la variabilité historique des 250 dernières années suggèrent que l'augmentation récente de la fréquence et l'intensité des inondations est due au changement climatique.

Mots-clés : changement climatique, circulation atmosphérique, dendrohydrologie, vaisseaux du bois initial, *Fraxinus nigra*, Lac Duparquet

1.3 Introduction

Climate extremes and exceptional floods are becoming more frequent worldwide (Berghuijs et al., 2017; Kundzewicz et al., 2019) and particularly in Canada (Burn et al., 2016; Buttle et al., 2016; Burn & Whitfield, 2016, 2018; Bush & Lemmen, 2019). Over the last decade (2010–2020), flooding has emerged as the costliest natural disaster in Canada with insurance payouts exceeding one billion Canadian dollars per year (IBC, 2020). The 2019 floods in Ontario (McNeil, 2019) and Québec (ECCC, 2020) surpassed the 2017 flood level considered, at the time, as the 100-year flood in the Ottawa River basin (Turcotte et al., 2019; ECCC, 2020). Given that most Canadian communities are located close to water bodies, and given the reliance on hydropower in the country, there is an urgent need to plan for future resilience of water and flood security management to climate change (Winsemius et al., 2016; Cherry et al., 2017).

In Canada, observed global warming and projections from greenhouse gases emission scenarios indicate a rate of warming about twice as fast as that projected for the rest of the Northern Hemisphere (Vincent et al., 2018; Bush & Lemmen, 2019). The majority of floods in Canada are generated by either intense rainfall, snowmelt or ice melt (Buttle et al., 2016; Burn et al., 2016; Burn & Whitfield, 2018). In northern Canadian watersheds where discharge is determined by the accumulation and melting of snow and ice, flooding results from a complex combination of excess rain and snow, rain-on-snow events or ice jams and the magnitude of temperature jump from winter to spring (Javelle et al., 2003; Aygün et al., 2019). However, so far, no consistent trend in mean or extreme annual precipitation or in annual discharge has been observed for Canada as a whole (Aygün et al., 2019). In northern Canada, and particularly in winter, an increase in annual precipitation relative to snowfall, was observed (Vincent et al., 2018). Seasonal snow cover is also projected to decrease during the 21st century with a later snow onset and an earlier spring snowmelt (Bush & Lemmen, 2019). This trend

is visible in the ice freeze-up and break-up records for south-central Ontario, where a longer ice-free period has been observed since the 1900s related to the seasonal temperature warming (Fu & Yao, 2015). Analysis of Canada-wide instrumental discharge data indicates that the timing and magnitude of seasonal maxima has shifted toward higher winter discharge and earlier spring snowmelt since 1950 (Mortsch et al., 2015). This is consistent with the observed change in the seasonality of river input to the Hudson Bay between 1968 and 2008; with an increase in winter discharge, a decrease in summer discharge, and an increase in maximum annual discharge being observed since the mid-1980s (Déry et al., 2011).

From a climate change perspective, i) a decrease in snow accumulation would lead to a reduction in the magnitude of snowmelt flooding, whereas ii) an increase in extreme precipitation events would lead to an increase in rain associated to flooding. Hydrological simulations using outputs from regional climate models for northern Québec and Ontario (Guay et al., 2015; Wang et al., 2015; Clavet-Gaumont et al., 2017) suggest that by 2050 rain and snow amounts will contribute more to discharge in the winter and fall months and less to discharge in the summer months than during the 20th century. Increases in the magnitude of hydrological extremes are also expected but it remains uncertain how the projected change in climate will affect flood frequency and magnitude (Gaur et al., 2018). Gaur et al (2019) showed from simulations that under various climate change scenarios about 40 to 60 of the 100 most populous Canadian cities are expected to experience increasingly frequent flooding by 2100, particularly in coastal areas, southern Ontario and northern Canada. For example, in Toronto, the return period of the historic 100-year flood would be reduced to a return period of 22 to 30 years under a minimum climate change scenario (RCP2.6).

The uncertainties in projecting future hydroclimatic trajectories limit flood risk estimations currently based on instrumental records of natural discharge (Mortsch et

al., 2015; Buttle et al., 2016). Unfortunately, because of technical and economical limitations, the hydrological records in northern Canada are of short length and highly dispersed in space (Koshida et al., 2015; Pellerin, 2019). Also, because most Canadian hydropower capacity is located in the North (Cherry et al., 2017), the influence of dams on lakes and rivers complicate the analysis of climate change impacts using these short instrumental records (Ljungqvist et al., 2016). It is thus particularly important to extend the existing discharge data spatially and temporally in these regions. Simulations from the north of Finland have shown that more frequent freeze-thaw episodes and ice-flooding in winter or spring could threaten the integrity of hydroelectric facilities or force them to divert floodwaters more often to spillways instead of generating power (Gebre et al., 2014). To improve planning for the economic and social impacts of future climate change, it is essential to understand whether recent changes in discharge and flooding in eastern boreal Canada are part of the historical natural variability or whether they are unprecedented and associated with recent climate change.

Paleoindicators can provide proxy data to complement short instrumental discharge records and help place them in a historical perspective (Saint-Laurent, 2004; Baker, 2008; Meko & Woodhouse, 2011; Ballesteros-Cánovas et al., 2015; Wilhelm et al., 2019). Among the paleoflood indicators, tree rings can be considered an excellent hydrological proxy due to the interconnection among climate, hydrology and tree growth, and tree-ring chronologies are annually resolved and continuous series (Meko & Woodhouse, 2011; Meko et al., 2012). In semi-arid environments, where water deficit is a major factor limiting tree growth, ring-width chronologies have been successfully used to reconstruct past discharge and especially low discharge (Meko et al., 2001; Woodhouse et al., 2006; Biondi & Meko, 2019; Martínez-Sifuentes et al., 2020). In contrast, in boreal environments where water is not as limiting to tree growth, the relationship between tree-ring width and discharge may not be as clear (Tardif et al., 1998; Kames et al., 2016). Ring-width chronologies integrate many environmental

factors and extracting a specific flood signal can be complex or difficult (Boucher et al., 2011; Agafonov et al., 2016). In addition, if spring thaw occurs before the start of the growing season, ring-width chronologies may not register variations related to high spring water levels. In a northern Québec reservoir, Nicault et al. (2014) showed that spring discharge was difficult to reconstruct using a combination of ring widths, earlywood density and stable isotope chronologies mainly because flooding occurred during the period of tree dormancy. The authors had better results when including ice-scar frequency in their reconstruction. Indeed, spring flooding in Northern Québec has been reconstructed mostly by studying the physical injuries (scars) left on shoreline trees by the abrasion of floating ice and debris during spring break-up (Tardif & Bergeron, 1997b; Bégin, 2001; Lemay & Bégin, 2008; Boucher et al., 2011; Nicault et al., 2014).

The study of the anatomy of growth rings in trees directly exposed to seasonal floods can provide quantitative and continuous predictors of seasonal discharge in boreal regions. Anatomical changes in earlywood vessels associated with the physiological response to anoxia during persistent flooding (hereafter referred as flood rings) have been noted in riparian ring-porous trees (*Fraxinus* sp., *Quercus* sp.) following major flood years (Astrade & Bégin, 1997; St. George & Nielsen, 2000; Tardif et al., 2010; Kames et al., 2016; Nolin et al., 2021b). Recent works (Meko et al., 2020; Dickson, 2020) indicate that in riparian diffuse-porous trees (*Salix* sp., *Populus* sp.) flooding also lead to the development of tree-ring anomalies (anatomical irregularities). Flood rings have also been experimentally reproduced and been shown to form when ring-porous trees are flooded during the period of earlywood vessels formation (Copini et al., 2016; Tardif unpublished data). Flood rings are characterized by either an increase in earlywood vessel number and/or a reduction in earlywood vessel cross-sectionnal areas according to species (St. George & Nielsen, 2000; Copini et al., 2016; Kames et al., 2016; Nolin et al., 2021b). The timing and duration of flooding relative to the period

of earlywood vessel formation and sample location along the tree stem are factors that influence flood-ring formation (St. George et al., 2002; Copini et al., 2016).

Flood rings have been successfully used to detect major floods (St. George & Nielsen, 2003; Wertz et al., 2013; Therrell & Bialecki, 2015; Meko & Therrell, 2020; Nolin et al., 2021b) but few studies have used continuous year-to-year measurements of earlywood vessels to study hydroclimate variability (Tardif et al., 2010; Kames et al., 2016). Recently, Meko & Therrell (2020), in addition to visual identification of flood rings, measured the width of the first row of earlywood vessels in ring-porous overcup oak (*Quercus lyrata* Walt.). This work allowed effective reconstruction of spring floods in the White River, Mississippi. López et al. (2014) reconstructed summer and annual discharge of the Atrato River, Columbia, from the number of vessels in the annual tree ring in the diffuse-porous *Prioria copaifera*. The authors found that in the equatorial forest, the number of vessels in the annual ring tends to be higher and the total ring width greater in flood years than in dry years. On the other hand, Kames et al. (2016) demonstrated that in the boreal forest of Lake Duparquet, earlywood vessel chronologies from ring-porous black ash (*Fraxinus nigra* Marsh.) were more effective than ring width in capturing the variability of low and high spring discharge. These results support the utility of developing long earlywood vessel chronologies from floodplain trees as proxy records of river discharge and flooding. Tree-ring anatomical sequences from trees growing directly on floodplains may also allow reconstruction of the full range of spring discharge variability in boreal environments.

The objectives of this study are twofold. First is the multi-century reconstruction of annually resolved spring discharge from hydrological proxies: ring width and cross-sectional area of earlywood vessels from *F. nigra* trees growing on the floodplain of Lake Duparquet. Second is investigation of the temporal stability of the reconstruction

and determination of the main climatic and large-scale atmospheric circulations drivers associated with multi-century spring discharge variability.

1.4 Materials and methods

1.4.1 Study area

The study was conducted on Lake Duparquet (48°28' N, 79°16' W; Fig. 1.1) located in the Clay Belt of both Northern Ontario and Québec (Daubois et al., 2015). Lake Duparquet forms a 50 km² waterbody draining north into the James Bay through the Abitibi River (Tardif & Bergeron, 1997b). The rivers feeding Lake Duparquet are not regulated by dams, making it a unique site for the study of long-term flood dynamics in a watershed in which hydroelectric dams have been present downstream since the 1910s (CEHQ, 2019; Hydro-Québec, 2019). The closest dam to Lake Duparquet is located 140 km downstream (Iroquois Falls dam, built in 1914) and regulates Lake Abitibi (OMNRF, 2019; OPG, 2019). A natural steep rapids 5 km downstream of Lake Duparquet (Rapide Danseur) prevents any effect of downstream dams or regulation on the lake level.

Lake Duparquet is situated at the southern fringe of the boreal ecozone where forests can be characterized by an association of balsam fir (*Abies balsamea* (L.) Mill.), black spruce (*Picea mariana* (Mill.) BSP), paper birch (*Betula papyrifera* Marsh.), white spruce (*Picea glauca* (Moench) Voss) and trembling aspen (*Populus tremuloides* Michx.) (Denneler et al., 1999). *Fraxinus nigra* can be found in waterlogged areas and riparian forests in pure stands (Tardif & Bergeron, 1997a) or in association with eastern white-cedar (*Thuja occidentalis* L.) and occasionally balsam poplar (*Populus balsamifera* L.) (Tardif & Bergeron, 1992; Denneler et al., 1999; Tardif & Bergeron, 1999).

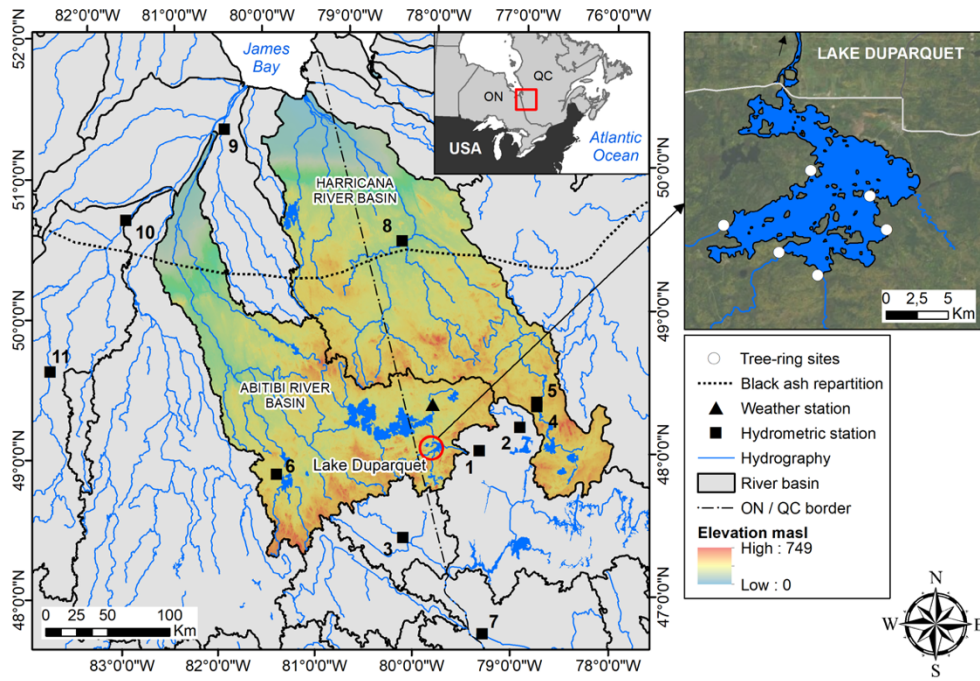


Figure 1.1 Map of the study area. Geographic location of the study area at the border between Ontario (ON) and Québec (QC), in Canada (left panel upper inset). Lake Duparquet (red circle in left panel) is located at the head of the Abitibi River basin. Discharge record reconstructed is at Harricana River (black squares No. 4 & 5) on the upper reach of the Harricana River basin. Other hydrological stations are listed by their numbers in Table 1.1. The upper right inset shows locations of riparian *Fraxinus nigra* sampling sites at Lake Duparquet (white dots).

The soils of the region are dominated by deposits from the Quaternary Ojibway Lake and by glacial till that transitions into peatlands northward (Daubois et al., 2015). The very flat and clayey banks of Lake Duparquet are flooded each spring for a period ranging from a few days to months and are largely colonized by *F. nigra*. The species can reach an age of 250 years in these forests (Tardif & Bergeron, 1999).

Lake Duparquet area has a sub-boreal climate with a mean annual air temperature of 0.7°C, mean annual precipitation of 890 mm and mean annual snowfall of 250 mm for the period 1971–2000, as indicated by data from La Sarre weather station data (48°48' N, 79°11' W ; Fig. 1.1) obtained from Canadian Climate Normals, http://climate.weather.gc.ca/climate_normals). Precipitation peaks occur in spring and fall, and persistent winter snowpack is common until the month of May (Fig. 1.S1). Lake Duparquet is not equipped with a hydrometric station, but its hydrology is comparable to that recorded on the Harricana River (48°34' N, 78°07' W; Fig. 1.1) located 85 km to the east (Tardif et al., 2010; Kames et al., 2016). Both show a boreal regime driven by mixed snow and rain processes. At the end of the ice season, the winter snowpack melts and rapidly transforms the low winter discharge into a spring freshet peak. The spring breakup flood usually occurs in May and its average contribution to annual discharge ranges from 11 to 30% for the period 1915–2020 (Water Survey of Canada, <https://wateroffice.ec.gc.ca>; Fig. 1.S1). Spring recession magnitude and summer precipitation generally contribute to high summer discharge. In the fall, small floods may be triggered by episodes of intense rainfall, prior to a return of river ice and accumulation of snow in winter.

1.4.2 Sample collection, measurement and crossdating

In summer 2017 and 2018, 125 increment core samples from 65 trees were collected from *F. nigra* sites exposed to periodical flooding on Lake Duparquet. Cores were collected from living trees using a 5mm increment borer and discs were collected from old logs or fallen trees. This sampling aimed to update existing *F. nigra* anatomical and ring-width chronologies from Lake Duparquet (Tardif & Bergeron, 1993; Kames et al., 2016; Tardif et al., 2016). Because flood rings were reported to occur below the water level at the onset of earlywood formation (St. George et al., 2002; Copini et al., 2016) samples were collected as close as possible to the ground. Wood samples were prepared according to standard dendrochronological techniques (Phipps, 1985; Cook &

Kairiukstis, 1990) and were sanded on a series of progressively finer grit up to P600 grade. After cleaning with pressurized air, the sample surfaces were rubbed with white chalk to increase the contrast between the vessels and the other cell types (Tardif & Conciatori, 2006b; Kames et al., 2016). Tree rings were visually crossdated using the pointer-years developed for *F. nigra* on Lake Duparquet (Tardif & Bergeron, 1993; Kames et al., 2016) and the list method (Phipps, 1985).

Given that *F. nigra* trees seldom reach many centuries in age (Tardif & Bergeron 1999), the oldest and best well-preserved wood samples from Tardif & Bergeron (1993) (11 cores from 9 trees) and from those collected in 2017 (13 cores from 13 trees) were selected for image analysis and anatomical measures. Given our objective to reconstruct discharge at the multi-century scale, the oldest samples showing clear tree rings with no rot or missing sections were selected after inspection under a stereomicroscope. The pre-existing anatomical series from Kames et al. (2016) (40 cores from 20 trees) and Tardif et al. (2016) (4 cores from 4 trees) were also used. Anatomical measurements were produced from high-resolution pictures using procedures similar to those described in Tardif and Conciatori (2006b) and Kames et al. (2016). The prepared surfaces were scanned by a digital camera (Nikon DS-Fi1) mounted on a stereomicroscope (Nikon SMZ1000) to obtain standardized images (TIFF format, 20x magnification, 1,600 x 1,200 dpi) of the tree rings. Pictures were then processed with the Canny (1986) edge detection algorithm with ImageJ2X (Rueden et al., 2017) to automatically delineate the vessel shapes. Each output image was then manually corrected using a graphics tablet to verify and improve vessel identification. Incomplete areas of lumen at the edges of cores or images were excluded from the analysis. Once each vessel shape was clearly delineated, the boundary between early and latewood was qualitatively identified as the interruption of the largest vessels (Tardif & Conciatori, 2006b; Kames et al., 2016). Each ring was analyzed with WinCell Pro v2018c (Régent instrument, 2018) on vessels with a cross-

sectional area greater than 3,000 μm^2 (Tardif, unpublished data). For each tree-ring sample, 12 continuous variables were measured, including 8 anatomical variables and 4 ring-width variables.

Anatomical variables were mean (MVA) and total vessel lumen cross-sectional area (TVA) within the earlywood, number of vessels (N), mean vessel area of the 25% largest (L25) and smallest vessels (S25), porosity within the earlywood (pE) (defined as $\frac{TVA}{A}$, with A the earlywood area), density of vessels in the earlywood (dE) (defined as $\frac{N}{A}$), and hydraulic diameter (Dh) (defined as $\left(\frac{\sum D_i^4}{N}\right)^{\frac{1}{4}}$ with D_i equivalent circle diameter (in meter) expressed as $\sum_{i=1}^n D_i = 2\sqrt{\frac{A}{\pi}}$ from the Hagen-Poiseuille law (Tyree & Zimmermann, 2003). Hydraulic diameter is a more physiologically-based expression of water transport in trees than vessel conductance area (Scholz et al., 2013), whereas the S25 and L25 chronologies separate the signals that may be carried by different classes of vessels size (García-González & Fonti, 2006).

Ring-width variables were the total ring width (RW), earlywood width (EW), and latewood width (LW) (defined as RW-EW), and the proportion of earlywood within the total ring-width (EW%RW) (defined as $\frac{EW}{RW}$). The EW was measured with WinCell as it was more appropriate for suppressed years, but the RW was measured with CooRecorder (Larsson, 2003b), and LW resulted from their difference.

Because the anatomical measurements of tree-ring series (L25, S25, MVA, TVA, pE, N, dE and Dh) were designed to extend the existing chronologies (Kames et al., 2016; Tardif et al., 2016) back in time and considering that image analyses are time-consuming, the measurements did not include years after 1950 for 9 series. Tree-ring

width measurements (EW, LW, RW, EW%RW), however, were conducted over the entire period of time available.

1.4.3 Chronology development

The quality of crossdating and measurement of each of the ring-width series (43 trees x 12 variables) was inspected in CDendro (Larsson, 2003a) and COFECHA (Holmes, 1983) prior to analysis. Series detrending and chronology development were computed using the ‘dplR’ package (Bunn, 2008) in R environment (R Core Team, 2020). Some 302 missing values (representing 0.43% of the total measurements) related to rotten parts in the oldest samples were interpolated using the spline filling function in ‘dplR’ package. Once the series were completed and quality-checked, a detrending was performed to remove low-frequency age-related or stand-related dynamics and to retain mainly high-frequency variations (Cook & Kairiukstis, 1990). Individual tree-ring series were divided by a cubic smoothing spline function with a 50% frequency response at 60 years (Kames et al., 2016). The spline function rigidity was set at 30 years for 0.19% (41/516) of the series i.e.; when adverse effects at the start or at the end of the series (extremely high values) were observed. Series with significant autocorrelation were prewhitened using a best-fit autoregressive model (Cook & Kairiukstis, 1990) to produce residual chronologies. When autocorrelation was found to be non-significant, the standard chronology was preferred (Kames et al., 2016). Finally, to lower the influence of outliers, detrended series for individual cores were averaged into site chronologies using a bi-weight robust mean (Cook & Kairiukstis, 1990). Temporal coherence among series was assessed with the inter-series correlation coefficient (R_{bar}), and adequacy of sample size was assessed with the subsample signal strength (SSS; Wigley et al., 1984; Cook et al., 1999). The R_{bar} statistic expresses the mean correlation between all possible pairs of the individual tree-ring series, while the

SSS reflects the loss of common variance between the series due to the decrease in sample size back in time (Wigley et al., 1984; Cook et al., 1999).

1.4.4 Reconstruction of spring discharge

Based on Kames et al. (2016), linear regressions were computed between discharge variables (predictand) and tree-ring chronologies (predictors) in exploratory analyses. For the common period 1915–2016, the best linear correlation between the Lake Duparquet MVA chronology and the Harricana River discharge was found with the mean discharge from April 15 to June 30 ($r = -0.79$, $p < 0.001$), which was therefore chosen as the variable to be reconstructed (hereafter, Harricana spring discharge).

Two stepwise multiple linear regression models were developed to reconstruct Harricana spring discharge using the R package "Olsrr" (Hebbali, 2020). In the first model (REC1) the 12 predictor chronologies were transformed using principal components analysis (PCA) to overcome multicollinearity issues among predictors (Hidalgo et al., 2000; Woodhouse et al., 2006). PCA was performed on a correlation matrix with the R base environment for a 1771 to 2016 common period, and the number of statistically significant principal components (PC) to be used as predictors of discharge was selected by a broken stick model (Legendre & Legendre, 2012). To account for autocorrelation in tree-ring time series, because tree growth is influenced by climate conditions prevailing during the current and the previous growing season, lagged PC (-1, 0, +1 year) were introduced in regression series (Cook & Kairiukstis, 1990; Meko & Graybill, 1995). The second model (REC2) consisted of the 8 anatomical and 4 ring-width chronologies and their lags (-1, 0, +1) without PCA transformation.

1.4.5 Model performance

Model assumptions were checked with a standard analysis of residuals, and the final models were validated using a split-sample procedure (Snee, 1977; Cook & Kariukstis, 1990). This cross-validation technique consists of dividing the period of overlap between instrumental discharge data and tree-ring chronologies into two sets of half-calibration and verification of equal length. A first half (1915–1965) was used to calibrate the model, and the second half (1966–2016) was used to verify the model. This procedure was then inverted (1966–2016 for calibration, 1915–1965 for verification). The overall performance of the models was estimated using the adjusted explained variance ($\text{adj}R^2$) from calibration, as well as the reduction of error statistic (RE; Briffa et al., 1988) and the coefficient of efficiency (CE; Cook & Kariukstis, 1990) from validation. Agreement between the reconstructed estimates and instrumental data was estimated with the conventional statistics of root-mean-square error and mean-absolute error (RMSE, MAE; Cook et al., 1999) and the sign test and product-mean test (PMT) calculated on z-scores (Cook & Kariukstis, 1990). These statistics provide information on the ability of the models to reconstruct the discharge not used in model fitting. In addition, the daily hydrographs of the Harricana spring discharge (April 15 to June 30, calculated for 1915–2020) were submitted to a K-Means clustering analysis (Legendre & Legendre, 2012) to further assess the model performance in reconstructing extreme low and high discharge associated with individual clusters.

1.4.6 Climate and large-scale atmospheric circulations relationships to spring flooding

To assess the degree of association between the reconstructed spring discharge and current climatic data, hydrological data, large-scale atmospheric circulation indices and existing hydrological reconstructions from subarctic Québec, simple and bootstrapped Pearson correlations were calculated. The stationary bootstrapped correction avoids bias in variance from multiple spatial and temporal resolutions between autocorrelated dataset (Efron, 1979). This was calculated with the R package ‘treeclim’ (Zang & Biondi, 2015). Various datasets were obtained to conduct these analyses. Monthly climate data were extracted from a 0.5 x 0.5° landmask corresponding to Lake Duparquet (48.00°N, -79.50°E ; 48.50N°, -79.00°E) using the KNMI Climate Explorer (<https://climexp.knmi.nl>; Trouet & Van Oldenborgh, 2013). Monthly gridded temperature and precipitation were obtained from 1901–2016 CRU TS 4.03 (Harris et al., 2020) and monthly snow-cover extent were obtained from 1966–2016 NOAA/NCDC Rutgers Snow cover at a 1 x 1° resolution (Estilow et al., 2015). Correlations were also conducted with Lake Duparquet’s observational ice-breakup dates from 1960 to 2016 (Mongrain, 2014; pers. comm. 2017) and reconstructed water levels from maximum ice-scar height associated with spring ice-breakup (Tardif & Bergeron, 1997b). Existing hydrological reconstructions from subarctic Québec were also used. Correlation coefficient between the ice-scar chronologies from Bégin (2001), Lemay & Bégin (2008) and Boucher et al. (2011) as well as the May, Spring (March - April - May) and annual discharge reconstructions respectively from Boucher et al., (2011), Nicault et al. (2014) and Nasri et al. (2020) were compared with the Harricana River spring discharge reconstruction using 40-year moving windows lagged by 21 years to assess temporal stability. Finally, we used discharge data from not only the Harricana River itself, but from nine unregulated hydrometric stations (Table 1.1; Water Survey of Canada, <https://wateroffice.ec.gc.ca>) with at least 25 years of records and located within a radius of 300 km of Lake Duparquet.

Table 1.1 Hydrological stations from the Water Survey of Canada (WSC). The numbers (No.) refer to Figure 1.1 and the distance is relative to Lake Duparquet. Note that the two Harricana River stations (No. 4 & 5) were combined into one for calibration purposes as there were no value differences in the overlapping period and in drainage area.

No.	Station Name	Federal Id	Distance (km)	Latitude / Longitude	Drainage Area (km ²)	Period
1	downstream Kinojévis River	02JB013	30	48°22' N ; 78°51' W	2,590	1971–2016
2	upstream Kinojévis River	02JB003	70	48°27' N ; 78°21' W	1,680	1937–1965
3	Blanche River	02JC008	80	47°53' N ; 79°52' W	1,780	1968–2016
4	Harricana River (old gauge)	04NA002	85	48°34' N ; 78°07' W	3,680	1915–1933
5	Harricana River (new gauge)	04NA001	85	48°36' N ; 78°06' W	3,680	1933–2019
6	Porcupine River	04MD004	130	48°33' N ; 81°03' W	408	1977–2015
7	Kipawa River	02JE015	155	47°04' N ; 79°18' W	5,980	1962–2011
8	Turgeon River	04NB001	170	49°59' N ; 79°05' W	11,200	1969–1999
9	North French River	04MF001	310	51°04' N ; 80°46' W	6,680	1967–2016
10	downstream Missinaibi River	04LM001	310	50°35' N ; 82°05' W	22,900	1973–2016
11	upstream Missinaibi River	04LJ001	320	49°36' N ; 83°16' W	8,570	1920–2016

The impacts of several large-scale ocean-atmosphere circulation features on the variability of hydroclimate and extreme events have been documented in different parts of the world (Bush & Lemmen, 2019). For example, across North America and Canada, flooding and river ice phenology have shown to be influenced by sea surface temperature anomalies in the equatorial Pacific, i.e. phases of the El-Niño Southern Oscillation (Bonsal et al., 2006; Kundzewicz et al., 2019). To further assess how large-scale atmospheric circulation indices correlated to spatial and temporal variations in reconstructed spring discharge, we included in these analyses the Atlantic Multidecadal Oscillation (AMO) from 1856 to 2016, the Arctic Oscillation (AO) from 1871–2011, the North-Atlantic Oscillation (NAO) from 1821 to 2016 and the reconstructed NAO (RNAO) from 1770–2001 downloaded from https://www.psl.noaa.gov/gcos_wgsp/Timeseries/. The El-Niño Southern Oscillation (NINO3.4) index for 1854–2016, and the Pacific Decadal Oscillation (PDO ERSSTv5) index for 1880–2016 were also downloaded from KNMI Climate Explorer (Trouet & Van Oldenborgh, 2013).

The continuous wavelet transformation (CWT) was used to decompose the variance in the spring discharge reconstruction in low and high frequencies (Torrence & Compo, 1998). The temporal variability of the reconstructions was evaluated by transforming the time series into CWT on a $\omega_0 = 6$ Morlet power spectrum base with the "WaveletComp" package in R (Roesch & Schmidbauer, 2018). In this way the Morlet wavelet scale is comparable to the Fourier period (Torrence & Compo, 1998).

1.5 Results

1.5.1 Predictor chronology characteristics

The 12 anatomical and ring-width chronologies developed for Lake Duparquet cover 1770 to 2016 (246 years) and have an average sample length of 120 years (Fig. 1.2). Crossdated tree-ring series were strongly temporally coherent within the two common periods 1855–1950 and 1940–2005 (Table 1.2). The number of series in site chronologies exceeds 10 from 1820 to 2016, and both 40-year running windows of SSS and Rbar demonstrated the stability of the common signal through this period ($SSS \geq 0.85$, $Rbar \geq 0.20$; Fig. 1.2). The MVA and L25 chronologies showed a higher SSS than the N, pE, and TVA chronologies and an even higher SSS than the rest of the chronologies over the first 50 years (1770 to 1820; Fig. 1.2b). To further test the stability of the common earlywood vessel signal, we recomputed successively the MVA chronology using the 5, 10, 20 and 30 longest series. For $n = 5$ series, the SSS was maintained above 0.70 for the complete 1770–2016 period (results not shown) indicating the potential to provide high-resolution reconstruction when using the 43 series available.

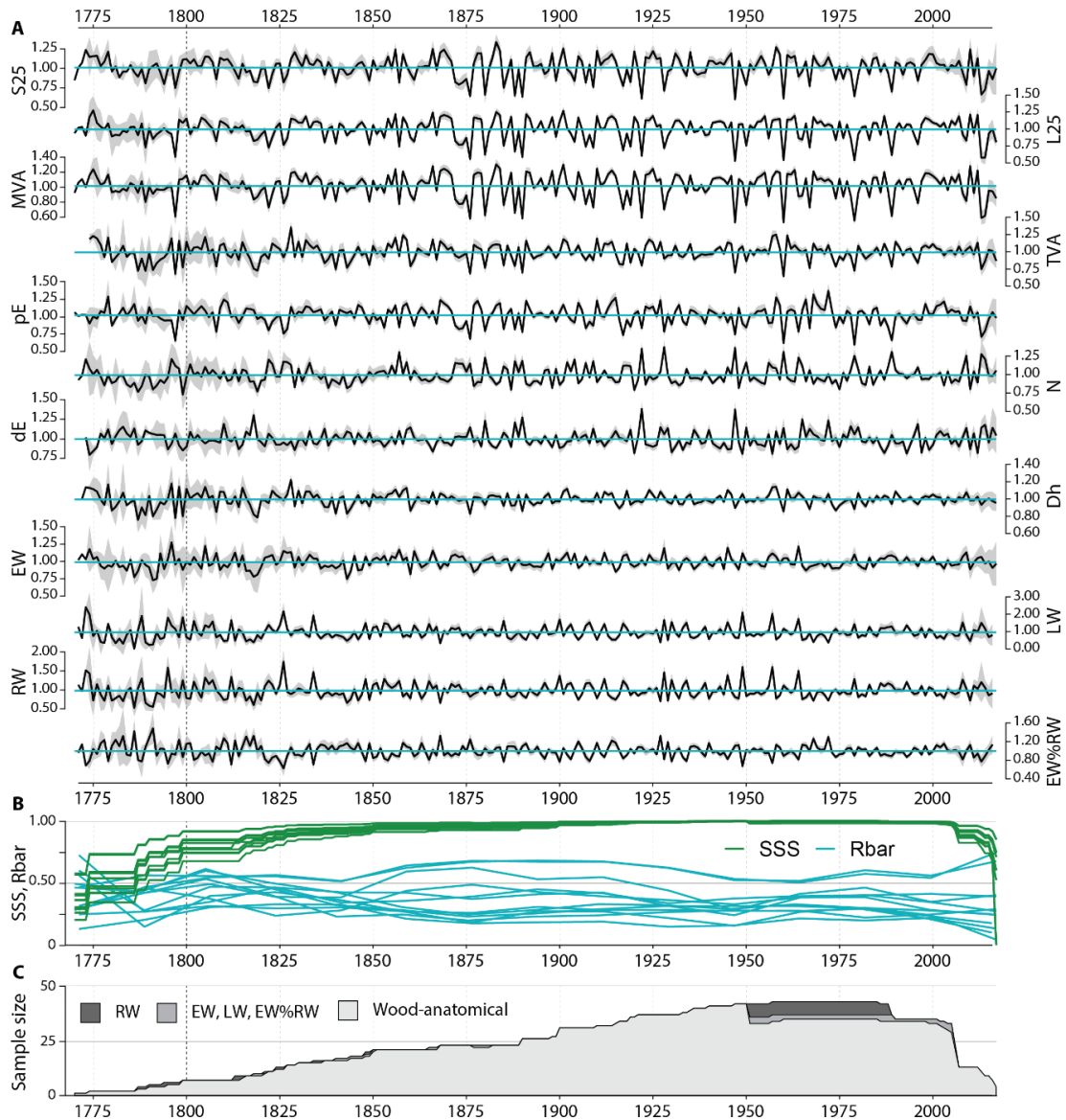


Figure 1.2 Chronology characteristics. A) Tree-ring anatomical and width chronologies developed for Lake Duparquet. Abbreviations of chronologies are listed in Table 1.2. The grey shade indicates the two-standard-error confidence intervals. B) 40-year running windows of subsample signal strength (SSS, green) and mean inter-series correlation (Rbar, blue). C) Yearly sample size for ring-width and anatomical chronologies expressed as number of trees per year.

Table 1.2 Descriptive statistics of the 12 anatomical and ring-width chronologies derived from 43 *Fraxinus nigra* trees sampled at Lake Duparquet.

Chronologies ^a Type ^b	1 st Common period 1855–1950		2 nd Common period 1940–2005	
	Variance explained by the first eigenvector (%)	Rbar ^c N° of series	Variance explained by the first eigenvector (%)	Rbar ^c N° of series
L25	70.83	0.64	70.54	0.57
S25	48.21	0.43	38.45	0.33
MVA	72.03	0.65	70.44	0.57
TVA	44.25	0.39	44.32	0.36
pE	59.52	0.54	44.94	0.38
N	48.50	0.40	49.14	0.41
dE	41.70	0.32	34.04	0.27
Dh	30.70	0.25	33.04	0.26
EW	25.77	0.20	28.03	0.22
LW	35.86	0.29	36.53	0.28
RW	37.69	0.31	38.40	0.30
EW%RW	30.76	0.25	32.25	0.25

a Abbreviations of chronologies are as follows: (L25 and S25) mean lumen cross-sectional area of the 25% largest (L) and smallest (S) earlywood vessels, (MVA) mean and (TVA) total earlywood vessel lumen cross-sectional area, (pE) porosity within the earlywood, (N) number of earlywood vessels, (dE) density of earlywood vessels, (Dh) hydraulic diameter, (EW) earlywood width, (LW) latewood width, (RW) total ring width, (EW%RW) proportion of earlywood within the total ring width. **b** Depending on autocorrelation significance, standard (S) or residual (R) chronologies were selected for analysis. **c** Inter-tree correlation coefficient (Rbar) computed for the two common periods.

1.5.2 Reconstruction of Harricana River spring discharge

Transfer functions were successfully derived for reconstructions REC1 and REC2 (Table 1.3). In REC1, stepwise regression selected the first (PC1, $R^2 = 63.87$), and the second principal component PC2 t+1 ($\Delta R^2 = 2.98$) and PC2 t-1 ($\Delta R^2 = 1.65$) as the best set of predictors. PC1 is driven by variables related to vessel size and number, while PC2 is driven mainly by ring-width (result not shown). Three predictors were also selected for REC2; MVA chronology ($R^2 = 61.92$), LW t+1 ($\Delta R^2 = 4.42$), and EW t-1 ($\Delta R^2 = 1.42$). In the two models, mean earlywood vessel area and number (PC1 in REC1, and MVA in REC2) account for the majority of the explained variance of Harricana spring discharge over the calibration period. The coherency between observed and reconstructed discharge was strong (Fig. 1.S2) and statistics were similar for the two models, whose determination coefficients (R^2) differ only slightly: 68.5% for REC1 and 67.8% for REC2 (Table 1.3).

In both models, the cross calibration-verification exercises for the two periods (1915–1965 and 1966–2016) indicated considerable predictive skill (Table 1.3; Fig. 1.3a) and approximately normally distributed residuals. The range of reconstructed discharge (73 to 184 m³/s) remains within that of the observed values (63 to 196 m³/s) and the reconstruction errors expressed in the units of observed discharge (MAE) are small and similar for both models (12.0 m³/s). The verification statistics RE and CE are strongly positive suggesting that low and high frequencies were very well reproduced by the two reconstructions (Table 1.3). The year-to-year direction and amplitude in discharge are also well reproduced (Fig. 1.3a), as indicated by the significant sign tests and product-mean test (PMT; Table 1.3).

Table 1.3 Statistics for the split-sampling calibration and verification procedure, and the full period reconstruction. Models REC1 and REC2 are presented together.

Calibration	MODEL REC1: PCA reduced series			MODEL REC2: non-reduced series		
	1915–2016	1915–1965	1966–2016	1915–2016	1915–1965	1966–2016
R ²	0.685	0.748	0.670	0.678	0.752	0.647
Adjusted R ²	0.675	0.732	0.649	0.668	0.736	0.624
Standard Error (SE) of the estimate	15.060	14.490	14.820	15.240	14.370	15.320
F-statistic	71.040	46.400	31.750	68.648	47.421	28.677
<i>p</i> -value	<0.001	<0.001	<0.001	<0.001	<0.001	<0.001
Verification	/	1966–2016	1915–1965	/	1966–2016	1915–1965
Pearson correlation coefficient <i>r</i>	0.828	0.817	0.788	0.823	0.827	0.782
<i>p</i> -value	<0.001	<0.001	<0.001	<0.001	<0.001	<0.001
Root Mean Squared Error (RMSE)	14.761	16.379	17.569	14.935	13.795	14.710
Mean Absolute Error (MAE) in m ³ /s	11.936	13.083	14.023	12.012	14.152	16.251
Reduction of Error (RE)	0.685	0.569	0.602	0.678	0.538	0.477
Coefficient of Efficiency (CE)	/	0.562	0.597	/	0.531	0.471
Product-mean test (PMT) (<i>on z-scores</i>)	5.331	3.942	3.143	5.396	3.725	3.417
Sign tests (<i>on z-scores</i>)						
Agreements	86	41	45	82	42	44
Disagreements	16	10	6	20	9	7

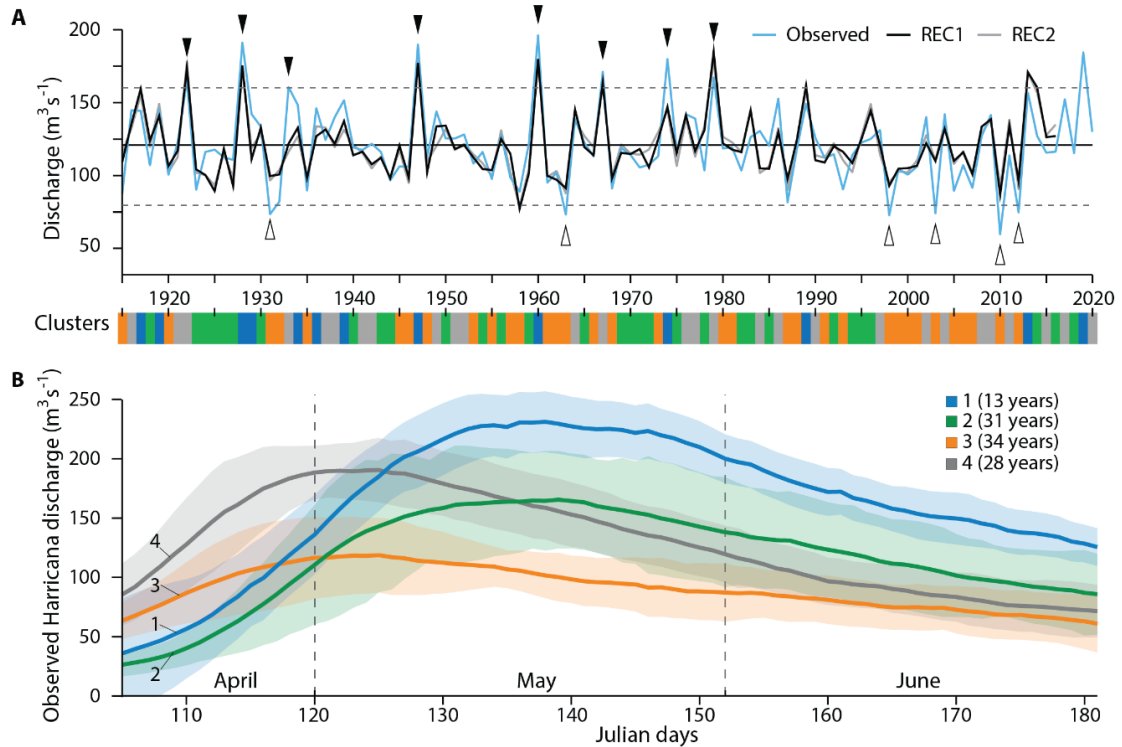


Figure 1.3 Comparison between observed and reconstructed discharge. A) Instrumental (blue) and reconstructed Harricana River spring discharge for the two models REC1 (black) and REC2 (grey) for the 1915–2016 calibration period. Horizontal lines mark the mean (solid) and ± 1.5 sd (dashed) of the instrumental Harricana spring discharge. High (black triangles) and low (white triangles) discharge years exceed the threshold ± 1.5 sd. B) The four K-Means clusters of daily instrumental Harricana spring discharge from April 15 to June 30 and from 1915 to 2020. Shaded areas indicate standard deviation within each cluster. The number in parenthesis represents the number of years in each cluster.

The strength of the common signal and the temporal stability of the reconstructions during the period of juvenile growth were assessed by recalculating the models using the first 50 years of each tree-ring width and anatomical series. Since sample replication decreases over time and the growth rate is maximal in young trees, the noise in these parts of chronology may be considered maximal. REC1 from a model limited to the first 50 years of the series spans 1770–2004 and is strongly associated with REC1 from the full data ($r = 0.884$, $p < 0.001$, $n = 231$). The restricted REC1 model performs well, with statistics $\text{adj}R^2 = 49.3$, $F = 44.20$ and $\text{MAE} = 14.98 \text{ m}^3/\text{s}$ comparable to those of the full REC1 model. Similar stability was observed for the REC2 model (result not shown). Given the similarities between both models ($r = 0.96$, $p < 0.001$, $n = 246$), the REC1 based on the full data was used for the remaining analyses.

1.5.3 Extreme low and high discharge

To assess whether reconstruction (REC1) accuracy differs in years of high vs low spring discharge (Fig. 1.3a), thresholds at the mean ± 1.5 sd were calculated from the instrumental Harricana spring discharge, 1915–2016 (high value = $159.8 \text{ m}^3/\text{s}$, low value = $80.3 \text{ m}^3/\text{s}$). Over the calibration period, high discharge years were 1922, 1928, 1933, 1947, 1960, 1967, 1974 and 1979 (2019 also but outside the calibration period). Low discharge years were 1931, 1963, 1998, 2003, 2010 and 2012 with the four lowest discharge values from 1915 to 2016 recorded after 1998 (Fig. 1.3a). For the eight highest and six lowest discharge years, the MAE of the reconstruction were comparable, being respectively $18.7 \text{ m}^3/\text{s} \pm 11.3$ and $23.8 \text{ m}^3/\text{s} \pm 6.4$.

The reconstruction's ability to capture the variability of the Harricana River flood regimes was determined by calculating a K-Means clustering of the daily Harricana River hydrograph from April 15 to June 30 for years 1915–2020 to identify conditions leading to low and high spring discharge (Fig. 1.3b). Four clusters were identified: 1) late break-up with maximum spring discharge, 2) late break-up with low spring

discharge, 3) early break-up with minimum spring discharge and 4) early break-up with intermediate spring discharge (Fig. 1.3b). The eight highest discharge years identified in the calibration data (Fig. 1.3a) were evenly distributed between cluster 1 ($n = 4$) and 4 ($n = 4$), and the six lowest discharge years corresponded to cluster 3. Interestingly, the clusters associated with early break-up with minimum to intermediate discharge (cluster 4 and mainly cluster 3) have dominated since about 1998 to 2012. Comparison of the mean errors (instrumental discharge minus REC1 values) and standard deviation corresponding to each cluster indicates that clusters 1 and 4 are slightly underestimated and cluster 3 is slightly overestimated in REC1 model (cluster 1: 9.97 ± 16.27 , cluster 2: -1.74 ± 13.92 , cluster 3: -9.60 ± 11.52 , cluster 4: 7.27 ± 13.96). This suggests that REC1 is robust in reconstructing both the timing and magnitude of spring discharge and performs equally well for both low and high discharge. It should be reemphasized that the difference between low and high extremes may have intensified in the last 20 years of the reconstruction (1997–2016) with more frequent low and intermediate levels (cluster 3 = 10/20 years and cluster 4 = 7/20 years; Fig. 1.3b). During this period, the low discharge years were less well captured by the reconstruction model (Fig. 1.3a).

1.5.4 Temporal stability in the spring flood reconstruction

Three distinct periods can be observed in REC1 as highlighted by both the 10-year smoothing spline (Fig. 1.4a) and the CWT analysis (Fig. 1.4b). A first period from about 1771 to 1850 shows a low-frequency multi-decadal variability (Fig. 1.4a) and a wavelet power spectrum with a persistent and significant high variance close to a periodicity of 32 years (Fig. 1.4b). A second period is observed from ~1850 to 1950 and shows a decadal variability at low frequency (Fig. 1.4a) in which the variance is high and significant near a periodicity of 16 years but mixed with smaller patches with periodicities of 4 to 8 years (Fig. 1.4a).

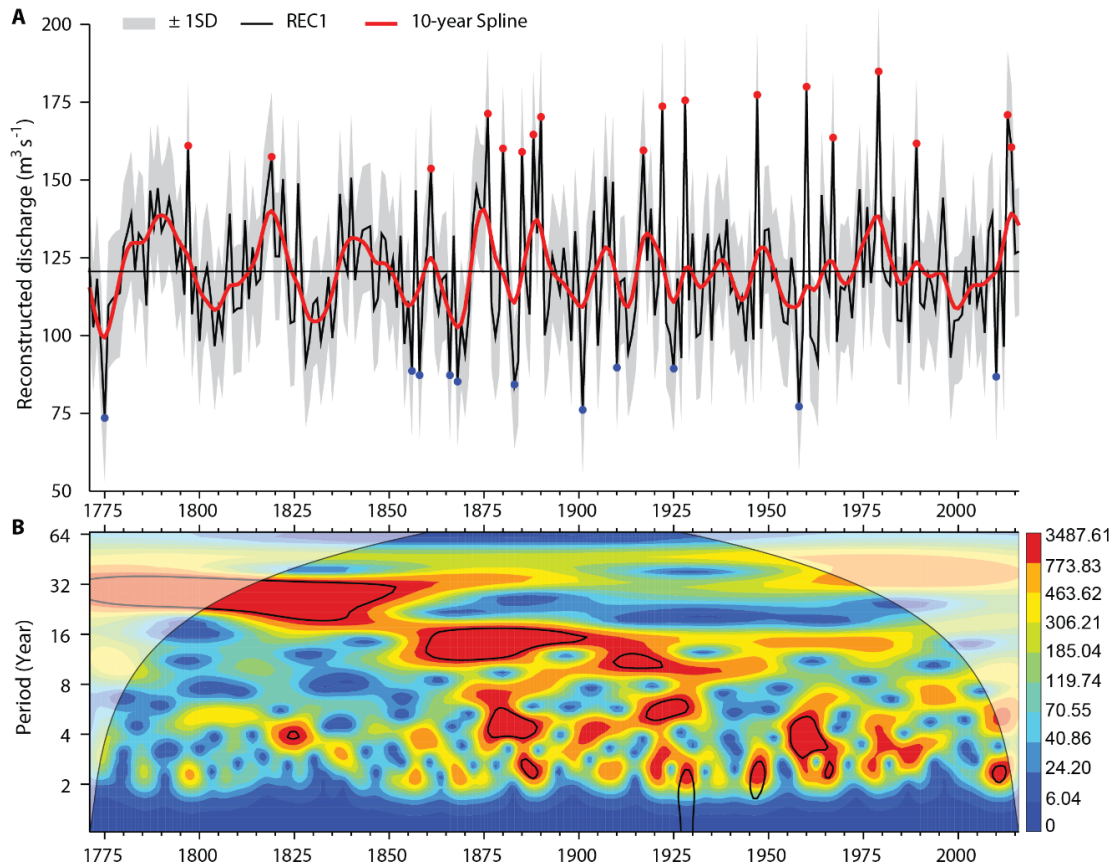


Figure 1.4 Reconstruction characteristics. A) Reconstruction of Harricana River spring discharge (April 15 to June 30) from 1771 to 2016. Decadal variations are highlighted by a 10-year smoothing spline (red curve) and confidence intervals correspond to the standard deviation envelope ($sd = 20.49 \text{ m}^3/\text{s}$; grey shade). High (red dots) and low (blue dots) discharge years exceed the threshold of the mean $\pm 1.5 \text{ sd}$. Horizontal line at $120.60 \text{ m}^3/\text{s}$ marks the mean for the 1771 to 2016 period. B) Decomposition of REC1 into Morlet 6th power in continuous wavelet transformation. The black lines encircle areas where p -value < 0.05 , tested against white noise background as lag-1 autocorrelation in REC1 was not significant. The white shaded area indicates the cone of influence where wavelets are stretched beyond the range of reconstructed data and may be altered by edge-effects. Variance magnitude range for blue (low) to red (high).

A third period from ~1950 to 2016, shows a low-frequency variability that may return to multi-decadal frequencies (Fig. 1.4a), with however significant high variance patches between 2 and 4-year periodicity bands (Fig. 1.4b). The evolution of spring discharge periodicity between these three periods suggest a change in the recent variability toward a higher frequency of high spring discharge after the Little Ice Age (1850–1870 CE; Matthews & Briffa, 2005; Fig. 1.4). The majority of high discharge years were recorded after the end of Little Ice Age and the highest discharge after 1950 (1960 and 1979). The majority of the low discharge were also recorded between 1850 and 1950, but the extreme minima were in 1775, 1901 and 1958 (Fig. 1.4). It should be remembered however, that the last low discharge events (1996–2016) were less well captured by REC1 model.

Using a linear regression of the 30 highest and 30 lowest values from REC1 over the period 1771–2016, the increase in spring maximum discharge can be quantified as 1 m³/s per decade ($R^2 = 0.334$, $p < 0.001$; Fig. 1.S3). No linear trends were revealed in mean and in the 30 lowest values from REC1 spring discharge: the R^2 coefficients are close to zero (Fig. 1.S3). In addition, the mean discharge calculated over the three periods identified in the CWT (1771–1850; 1850–1950; 1950–2016) remained very stable (sd = 0.82 m³/s). However, using a linear regression of the 10 lowest values from Harricana River instrumental spring discharge from 1915 to 2016, a trend toward a decrease in spring minimum discharge is revealed ($R^2 = 0.363$, $p < 0.001$; results not shown).

1.5.5 Reconstructed spring discharge, climate, ice-breakup and large-scale atmospheric circulation indices

REC1 spring discharge was significantly correlated with climate conditions leading to maximum spring discharge (Fig. 1.5). Field correlations indicated a strong and positive association between spring discharge and April and May snow cover across much of

central/eastern north Canada with most significant contour encompassing the study area, most of Ontario and eastern Manitoba (Fig. 1.5a). Low temperature and abundant precipitation in the previous December, during ice freeze-up, were positively and significantly associated to spring discharge (Fig. 1.5b). Similarly, both temperature and precipitation in spring (March and April) were respectively negatively and positively associated with spring discharge (Fig. 1.5b). Maximum spring discharge thus tended to occur during years with an early, cold winter, late spring and thick winter snowpack. Interestingly both reconstructed and instrumental spring discharge were also significantly and positively associated with observed ice-breakup dates for Lake Duparquet over the period 1968–2016 (REC1: $r = 0.493$, $p < 0.001$; Harricana instrumental: $r = 0.346$, $p < 0.001$), indicating that in the latest portion of the 20th century, maximum flooding tended to occur in years with a late ice-breakup.

Correlations of reconstructed discharge (REC1) with large-scale atmospheric circulation indices for the common period 1880–2016 revealed seasonal negative and positive associations (Fig. 1.5c). Discharge was significantly negatively correlated with January to May NINO3.4 and March to May AMO. For both indices, correlation was strongest in April (April NINO3.4, $r = -0.20$; April AMO, $r = -0.22$; $p < 0.001$). Significant positive associations also occurred in summer with June AO ($r = 0.16$, $p < 0.05$) and May to July NAO, with the highest NAO correlation in July (July NAO, $r = 0.30$, $p < 0.001$). The association was not significant with PDO in spring or summer PDO but was significant in previous September ($r = -0.14$, $p < 0.05$).

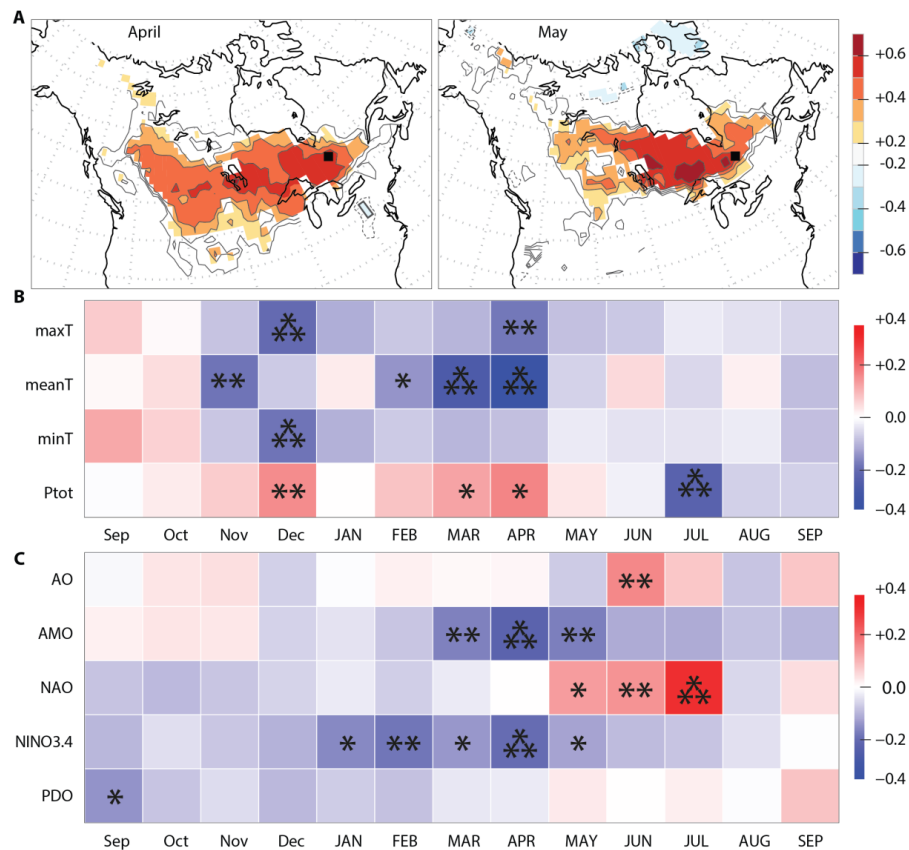


Figure 1.5 Climate signals. A) Spatial correlations maps ($p < 0.10$) between REC1 and April and May (1966–2016) NOAA Rutgers snow cover. The black square indicates Lake Duparquet location. B) Bootstrapped correlation coefficients between REC1 and monthly maximum, mean, minimum temperature (maxT, meanT, minT) and total precipitation (Ptot; 1901–2016 CRU TS 4.03). C) Bootstrapped correlation coefficients between REC1 and large-scale atmospheric circulation indices for the common period 1880–2016. Correlation coefficients in A, B and C panels range from red (positive correlation) to blue (negative correlation). Asterisks in B and C panels indicate p -value < 0.1 (*), < 0.05 (**) and < 0.01 (**).

1.5.6 Spatial agreement between REC1 and hydrological data and dendrohydrological reconstructions at the regional level

REC1 spring discharge is strongly coherent with regional hydrological gauge data over the second half of the 20th century (Table 1.4). Correlations with REC1 tended to decrease with distance from Lake Duparquet. The highest correlation was observed with the ‘upstream Kinojévis River’ gauge ($r = 0.92$, $p < 0.001$, $n = 29$) and the lowest correlation with the ‘Northern French River’ ($r = 0.52$, $p < 0.001$, $n = 50$), representative respectively of the closest and the farthest from the hydrological stations (Table 1.4).

Reconstructed spring discharge of the Harricana River shares features with other hydrological reconstructions from tree-rings and ice-scar chronologies developed for boreal and subarctic Québec (Fig. 1.6). REC1 was positively and significantly correlated with the ice-scar chronology developed for Lake Duparquet for the period 1850 to 1989 ($r = 0.434$; $p < 0.001$) and in each of the 40-year moving windows lagged by 21 years over that period (Fig. 1.6). This suggests that ice scars were more numerous during years of high reconstructed spring discharge. Correlations of REC1 with other proxies in a 40-year moving window were less temporally coherent but reveal several positive associations since the 20th century. The ice-scar chronologies from Corvette Lake, Lake Bienville and the reconstruction of the May discharge of the Caniapiscou Reservoir were positively correlated with REC1, but the p -value exceeds 0.05 (Fig. 1.6).

The ice-scar chronologies showed a gradient of intensification of spring ice scarring activity over time, with visible changes in magnitude around the 1870s and 1930s (Fig. 1.6). The ice-scar chronology from Lake Duparquet and the discharge reconstructions from Caniapiscou Reservoir (May, spring and annual) also share the periods of low discharge (1825) and high discharge (1875, 1970) but not the persistent drought period

of the early 1900s, illustrated mainly in the reconstructed spring discharge of the Caniapiscou Reservoir (Fig. 1.6). Moving correlation windows (40 years) also show a change in sign of associations between REC1 and the rest of subarctic Québec over time. The correlations were predominantly negative until 1850 and changed to predominantly positive correlations in 1990, with the exception of Lake Montausier.

Table 1.4 Pearson correlation coefficients between reconstructed Harricana River spring discharge from April 15 to June 30 (REC1) and mean instrumental discharge from April 15 to June 30 at nine hydrometric stations surrounding Harricana River and Lake Duparquet. The table is ordered by distance to Lake Duparquet (top to bottom). Each correlation in bold corresponds to p -value < 0.001 . Note that the periods and number of years differ between hydrometric stations.

No	Station	Id	Period	N years	Distance (km)	REC1
1	downstream Kinojévis River	02JB013	1971–2016	46	30	0.86
2	upstream Kinojévis River	02JB003	1937–1965	29	70	0.91
3	Blanche River	02JC008	1968–2016	49	80	0.76
4,5	Harricana River	04NA001–2	1915–2016	102	85	0.82
6	Porcupine River	04MD004	1977–2015	26	130	0.80
7	Kipawa River	02JE015	1962–2011	39	155	0.56
8	Turgeon River	04NB001	1969–1999	27	170	0.74
9	North French River	04MF001	1967–2016	50	310	0.52
10	downstream Missinaibi River	04LM001	1973–2016	43	310	0.69
11	upstream Missinaibi River	04LJ001	1920–2016	97	320	0.57

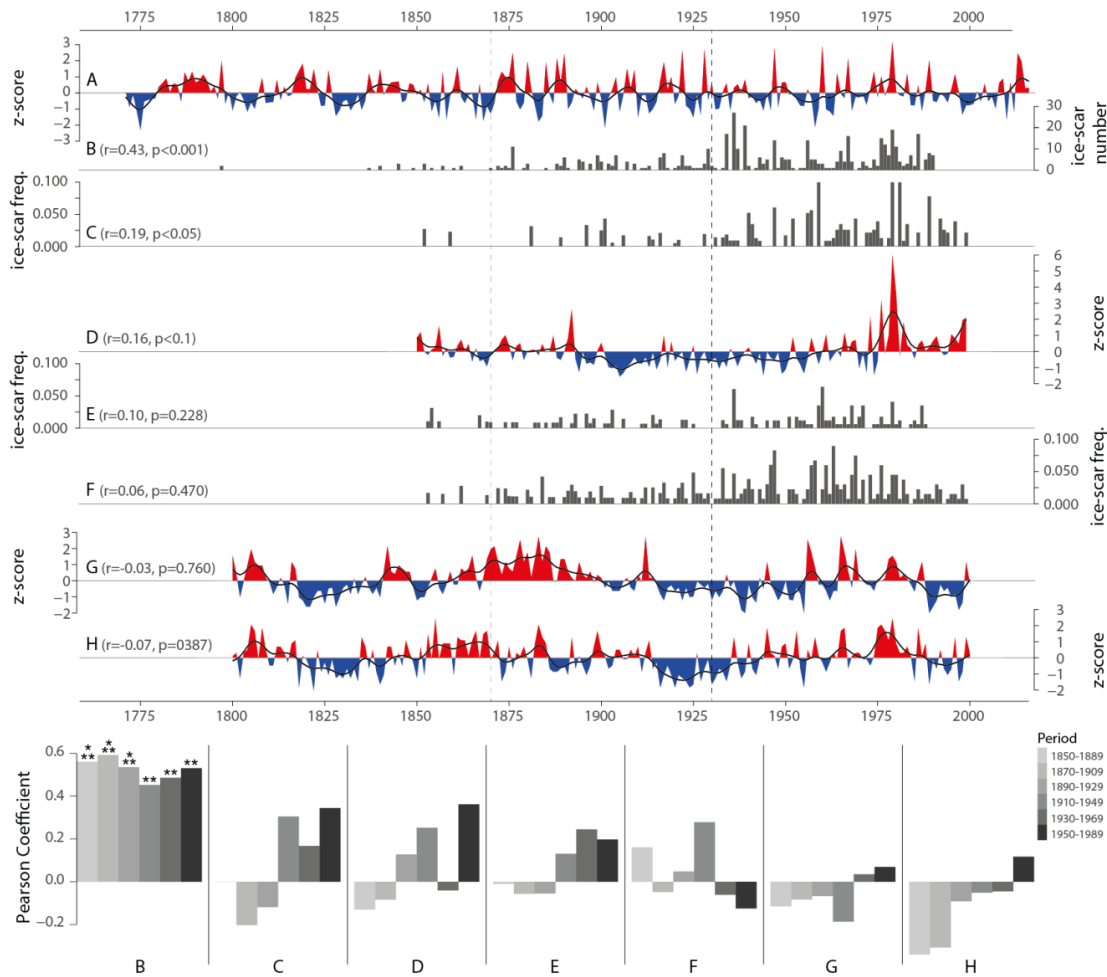


Figure 1.6 Comparison of ice-scar chronologies and reconstructed spring discharge from Northern Québec. Chronologies are presented in order of decreasing correlation with (A) Harricana River reconstructed spring discharge (REC1). Other chronologies are as follows: ice-scar frequencies of (B) Lake Duparquet (Tardif & Bergeron, 1997b), (C) Corvette Lake (Lemay & Bégin, 2008), (E) Bienville Lake (Bégin, 2001), (F) Montausier Lake (Boucher et al., 2011) and reconstructions of Caniapiscau reservoir (D) May discharge (Boucher et al., 2011), (G) annual discharge (Nasri et al., 2020), and (H) spring (March-April-May) discharge (Nicault et al., 2014). Ice-scar chronologies are presented in bar plot while discharge reconstructions are presented in positive (red) and negative (blue) area with a 10-years spline. Scales are the same between reconstructions, and between ice-scar chronologies. The bottom panel presents Pearson correlation coefficients calculated in 40-year moving windows lagged by 21 years between REC1 (A) and the above-described tree-ring proxies (B to H) with asterisks indicating p -value < 0.05 (*), < 0.01 (**) and < 0.001 (***).

1.6 Discussion

1.6.1 Strength of the Harricana spring discharge reconstruction

This work provides a unique annually resolved multi-century reconstruction of spring discharge and paleofloods for the Canadian northeastern boreal region. The performance statistics of the reconstruction are comparable to some of the most accurate tree-ring reconstructions of river discharge (Meko & Graybill, 1995; Woodhouse et al., 2006; Boucher et al., 2011). This study highlights the potential of using riparian trees as hydrological proxies and demonstrates the value of anatomical variability in tree rings to reconstruct low and high spring discharge with comparable accuracy. The greatest potential has been demonstrated with continuous measurements of the cross-sectional area of earlywood vessels (MVA) and number of earlywood vessels (N), and particularly with the MVA chronology, which is itself a proxy for spring discharge of the Harricana River. The juvenile tree growth in the total chronologies or the sample size in the first part of the chronologies were found to have a very limited influence on the common signal. Other anatomical and ring-width variables used as predictors of spring discharge (S25, L25, TVA, pE, dE, Dh, EW, LW, RW, EW%RW) showed less or no association to the spring discharge.

A recurring difficulty in dendrochronological reconstruction of river discharge is to capture adequately both high and low discharge. Most hydrological reconstructions have been derived from precipitation-sensitive trees growing in semi-arid environments (Meko et al., 2001; Woodhouse et al., 2006; Biondi & Meko, 2019; Martínez-Sifuentes et al., 2020) while few have used trees growing directly on floodplains (Agafonov et al., 2016, Meko et al., 2020). In arid environments, the difficulty lies in capturing high discharge given that sites and trees are sampled to maximize drought (low discharge) signal. Also, because flooding is linked to heavy rainfall, which can result in moisture no longer being the limiting factor to growth, tree-

ring width of drought-sensitive trees is not a good indicator of variations in high levels of flooding (Meko et al., 1995). In boreal environments, where high discharge is mostly associated with spring thaw (Aygün et al., 2019), reconstructions of spring discharge using trees from uplands have shown that tree-ring width may not record years of high spring discharge when thaw occurs before the beginning of the growing season (Nicault et al., 2014). Indeed, the variability of the latewood width in a given year is generally higher than that of the earlywood and may negatively influence the earlywood width in the following year (Tardif, 1996; Tardif & Conciatori, 2006b), which explains why early, late, and total tree-ring widths may not capture the full range of hydrological variability (Kames et al. 2016).

The use of ring-porous trees growing in flood-prone environments and their anatomical response to annual floods has demonstrated the usefulness of flood rings in dendrohydrology (St. George & Nielsen, 2000; St. George & Nielsen, 2003; Therrell & Bialecki, 2015; Kames et al., 2016; Meko & Therrell, 2020). More broadly, in environments where the period of flooding is sufficiently long and overlaps the period of formation of earlywood vessels in submerged stem portions, flood rings can be used to identify historical flood years. In addition, year-to-year measurements of earlywood vessel characteristics can extend hydrological records by reconstructing a wider hydrological spectrum i.e., from low to high discharge years.

1.6.2 Spatial coherency of spring discharge and flooding

Positive and highly significant correlations between REC1 and that of the nine surrounding hydrological stations compared well with the results of Kames et al. (2016). In addition, the similarities shared with other published paleorecords of spring flooding from sub-arctic Québec support a strong common hydrological signal across the study area and for the early 20th to early 21st centuries. In their analysis of spring flood duration and frequency, Javelle et al. (2003) identified our study area as part of a large

homogeneous region from central Ontario to southwestern Québec, mainly explained by the distribution of maximum snow depth between 1980 and 1995. When developing the regional flood equations for Ontario and Québec, Gingras et al. (1994) had already suggested a similar region around our study area where most of the flooding was generated by snowmelt from April to June.

While no latitudinal or longitudinal gradient in the strength of the associations between REC1 and hydrological stations was observed, regional differences can be distinguished between Lake Duparquet and subarctic Québec (to the north), the Great Lakes (to the south), Ontario and Manitoba (to the west of the study area). For example, the exceptional spring flood years recorded regionally were not always identical among regions, but some floods years were common across eastern Canada : the 1979 flood occurred in Manitoba, Ontario, Québec and New Brunswick after intense rainfall combined with heavy snowmelt late in the spring (Payette, 1980; Tardif and Bergeron, 1997b; Burton, 2015); the 2017 spring flood affected the province of Québec (Davies, 2017); and the more intense spring flood of 2019 affected Ontario and the Great Lakes, Québec, and New Brunswick (Bilefsky & Austen, 2019; McNeil, 2019; Turcotte et al., 2019). However, the return frequency of spring floods over the last 250 years appears to be higher in the study area than in Manitoba, for instance, where 10 floods were recorded on the Red River for the period 1750–1999 (St. George et al., 2003) compared to 26 floods reconstructed from 1770 to 2016 on the Harricana River.

At low frequencies, the long-term changes observed in REC1 are also consistent with changes identified in an ice-scar chronology from Lake Duparquet (Tardif & Bergeron, 1997b) and to changes observed in subarctic Québec, where periods of low discharge (1820–1850; 1920–1950) and high discharge (1870–1920) are associated with an increase in lake levels and glacial activity (frequency and maximum height of ice scars) since the 1850s and even more so since the 1950s (Tardif & Bergeron, 1997b; Bégin,

2000; Bégin, 2001; Lemay & Bégin, 2008, Boucher et al., 2011; Nicault et al., 2014; Nasri et al., 2020). Multi-century ice-scar chronologies from northern Québec share similar upward trends in spring flooding over the 20th century with REC1, although there are some regional contrasts. Multi-proxy reconstructions of spring discharge for the Caniapiscau reservoir (Boucher et al., 2011; Nicault et al., 2014; Brigode et al., 2016) also showed higher and more variable levels since 1965. In boreal Lake Duparquet, an increase in the frequency and magnitude of ice scarring was observed since the end of the Little Ice Age (LIA; 1850–1870 CE; Matthews & Briffa, 2005) with a peak increase in the 1930s followed by continued high ice scarring activity (Tardif & Bergeron, 1997b). Major spring flood years were also visible in these ice-scar chronologies, particularly in 1947, 1960 and 1979 (Tardif & Bergeron 1997b; Lemay & Bégin, 2008). Recruitment of *F. nigra* (Tardif & Bergeron, 1999) and *Thuja occidentalis* (Denneler et al., 2008a) trees on the shores of Lake Duparquet has also been shown to be reduced along the shorelines relative to higher elevations, in response to the increased frequency of flooding and ice scarring since the 19th century that has increased the exposure of riparian stands.

Despite the similarities (positive correlations) between REC1 and ice-scar chronologies from Lake Duparquet and subarctic Québec, these records do not always match and may represent regional differences and/or fundamental differences in the nature of the proxies used. For example, ice scars reflect mainly lake-ice phenology and ice-push abrasion while flood rings mainly reflect the persistence of flooding and anoxia. Tardif and Bergeron (1997b) suggested that records of ice scars on lakes may not adequately reflect flood levels on rivers. Lakes in the Abitibi region freeze earlier and thaw later than rivers, and lake ice is also thicker and less mobile than on rivers where the current is stronger. In addition, the accumulation of shore ice, the timing between the thaw and the maximum water level, or complex differences of ice regime and decay between sites are also known to affect the relationship between flood water levels and the height

and frequency of ice-scars (Tardif & Bergeron, 1997b; Lemay & Bégin, 2008; Boucher et al., 2011; Lindenschmidt et al., 2018). Ice-scar formation are also reflective of specific conditions (e.g., daily winds, lake morphology) occurring over a short temporal window associated with ice break-up (Tardif & Bergeron, 1997b; Lemay & Bégin, 2008) whereas flood rings integrate hydroclimate conditions occurring over a larger temporal window and including post ice break-up events like spring precipitation leading to prolonged flooding. Ice scars are also recorded at a time trees are dormant whereas flood rings and year-to-year changes in earlywood vessels reflects conditions leading to long lasting submersion of the stem during active radial growth.

Results strongly suggest that since 1770 the spring discharge dynamics in northeastern Ontario and northwestern Québec has undergone changes. While mean discharge in REC1 remained the same over the 1771 to 2016 period, changes were observed in the frequency of low to high discharge events through time. Even though reconstructed Harricana River spring discharge shows little year-to-year association with discharge records from the subarctic Québec, the comparison of datasets allows us to identify 1870 and the 1930s as breakpoints in the magnitude of spring-discharge increase. Evidence supporting a major climate shift at the end of the LIA also comes from independent data on fire cycles in the Lake Duparquet region. In eastern boreal Canada and since the end of the LIA, a pronounced decrease in the frequency and magnitude of forest fires has been linked to a decrease in the frequency of droughts and to an increase in precipitation (Bergeron & Archambault, 1993; Drobyshev et al., 2017). Bergeron et al., (2001) also support the idea that differences in forest fire frequencies and area burned between northeastern Ontario and central Québec may be driven by climatic changes since the end of the LIA.

1.6.3 Spring discharge, flooding and climatic changes

While there have been no consistent trends in flooding events for Canada as a whole (Aygün et al., 2019; Bush & Lemmen, 2019), century-long discharge data records from nival regime catchments in northern Ontario support our findings by showing an increasing trend in the average magnitude of spring snowmelt floods since 1916 (Burn & Whitfield, 2018). Trend toward earlier timing of spring break-up and flooding during the 19th and early-20th centuries has however been reported in discharge records across Canada (Bonsal et al., 2006; Vincent et al., 2018), northern Ontario (Fu & Yao, 2015; Burn & Whitfield, 2018) and the Great Lakes (Jensen et al., 2007). The 20th century flood regime is shown to be affected by faster snowmelt and more intense and frequent rain and rain-on-snow events (Bush & Lemmen, 2019). However, our results suggest the contrary or at least no trend as indicated by the positive correlation found between REC1 and snow-cover extent and a negative correlation with spring maximum temperature. No seasonality change has been found either in Harricana River instrumental records since 1915 or in tree-ring based chronologies of subarctic Québec (Boucher et al., 2011). Regarding the low spring discharge levels, our reconstruction has not perfectly captured the low discharge years recorded on the Harricana River between 1996 and 2016. This period may constitute a unique period of relatively low discharge and ending in 2012, as indicated by the recurrence of major flood in 2013, 2014, 2017, and 2019. The addition of precipitation-sensitive tree-ring proxies could be beneficial for capturing additional variance associated with the increase of spring water deficit and late summer droughts (Griffin et al., 2011) documented since the end of the LIA (Girardin et al., 2006).

In this study, recent fluctuations in REC1 were associated with long winters with significant snow cover and intense spring precipitation that promotes rapid melting, especially in late spring, over much of central-east Canada. The increase in Harricana

River spring mean discharge since the end of the LIA is also consistent with recorded increases in snow water equivalent, maximum snow depth in Canada (Zhao et al., 2013), and the duration of snow cover in northern Québec (Brown, 2010) since 1950. Although the influence of ENSO (and PDO) on snow cover variability in Québec has been limited in the mid to late-19th century (Bonsal et al., 2001; Bonsal et al., 2006), its influence during the 20th century has increased unprecedentedly compared to the last seven centuries (Li et al., 2013). The particularly significant associations of ENSO with monthly discharge in southern Ontario and Québec beginning in the 1960s (Nalley et al., 2012) also support the hypothesis that the increase in Harricana River maximum spring discharge could be driven by the increasing influence of ENSO.

Our reconstruction showed that the phase of NINO3.4 may influence the type and the timing of high discharge in the Harricana River. Warm, moist air masses in the equatorial Pacific Ocean (warm phase, El-Niño) may be associated with early springs and minor flooding, whereas cold, dry air masses (cold phase, La-Niña) may correlate with late thaw and maximum spring discharge. This is consistent with ENSO influence on inter-annual flood variability across North America. Flooding is influenced differently during El-Niño, which is associated with extreme-precipitation floods than during La-Niña, which is associated with snowmelt floods (Gurrapu et al., 2016; Kundzewicz et al., 2019). There is also evidence that ENSO has strongly influenced river ice phenology (freeze-up and break-up timing, duration of river ice-period) since 1850 in Québec (Bonsal et al., 2001; Bonsal et al., 2006) and that the phase and magnitude of the PDO index modulate the impact of ENSO on winter air temperature in the Great Lakes region (Rodionov & Assel, 2003). This influences the storage of ice and snow in winter, which can then feed the spring thaw floods.

In contrast to the reconstruction of spring discharge in the Harricana River, where the AO and NAO indices may be associated with discharge conditions in summer only,

spring snowmelt floods have been mainly associated with these indices in northeastern Québec (Boucher et al., 2011; Nicault et al., 2014; Brigode et al., 2016). Although NAO and AO had a limited influence on river ice phenology in Canada in the mid-19th century (Bonsal et al., 2001; Bonsal et al., 2006), their negative phases influenced the climatic conditions of previous winters and springs in northeastern Québec (Boucher et al., 2011; Nicault et al., 2014; Brigode et al., 2016). The AMO phase has also been associated with the multi-decadal magnitude of flooding across Canada (Burn & Whitfield, 2017) and been reported to modulate the relationship between the NAO and ENSO indices, particularly in late winter (Zhang et al., 2019). Across the North Atlantic Basin, Ballesteros-Cánovas et al. (2019) also hypothesized that flooding could be of higher magnitude during coupled negative AMO and PDO and positive AO and NAO phases, as in the case of the extraordinary 1936 winter flood in western Europe and eastern North America. The more positive phases of PDO since the 1970s are also consistent with more frequent El-Niño events (Bonsal et al., 2001). Simulating the future of extreme La-Niña and El-Niño events under greenhouse gas warming by 2100, Cai et al. (2015) suggested that a greater number of extreme El-Niño events would be compensated by La-Niña events about twice as frequent as today. Such La-Niña events may be associated with maximum spring discharge in our study. These simulations suggest that the frequency and magnitude of maximum spring discharge would continue to increase in our study area with future climatic changes.

The recent variability (especially in terms of frequency) of reconstructed spring discharge is therefore supported by climate variability. However, land use changes, or even beaver dams, may also have contributed to a lesser extent to the altering of regional runoff in the river basins (Kundzewicz et al., 2019). Indeed, the increase in maximum discharge in the spring could be linked to an increase in runoff due to snowmelt through factors other than climate alone, such as through forest clear-cutting or urbanization. However, in the boreal forest of eastern Canada the settlement periods

for large agricultural clearings and mine openings date from 1890 and 1910–1920 (Boileau, 1999), which does not correspond to the periods of change indicated by the reconstruction of spring discharge in the Harricana River (~1850 and 1950). In addition, Nolin et al. (2021b), using flood rings as a flood proxy in four river basins distributed across northeastern Ontario and northwestern Québec, demonstrated the high spatial coherence among natural rivers and for the last 250 years (1770–2016). Their results suggest that the long-term variability observed in the spring flood signal is of climatic origin given the coherency observed over an area covering more than 70,000 km². The influence of non-climatic factors (land use changes, beaver dams, etc.) may be limited.

1.7 Conclusion

This study demonstrates the usefulness of developing continuous chronologies of earlywood vessels (and of visual flood-rings identification) for high-resolution reconstruction of annual spring discharge. The reconstructed Harricana River spring discharge is robust, with both low and high discharge years being equally well reconstructed. Ring-porous species growing in flood-prone environments and the plasticity of their anatomical features in response to stem submersion during annual spring flood demonstrated to be useful hydrological proxies. In a context where the period of flooding is sufficiently long and overlaps the period of earlywood vessels formation in submerged stems, year-to-year measurements of earlywood vessel areas should allow us to improve the understanding of long-term changes in regional spring discharge. Our high-resolution multi-century reconstruction of spring discharge provides evidence of increased high discharge since the end of the Little Ice-Age. The likely cause is an increase in snow cover over much of central-east Canada rather than warmer air temperature. More work needs to be done to assess the stability of the association between REC1 and long-term circulation indices like ENSO, NAO and AMO. The strong spatial synchrony of the reconstructed spring discharge

reconstruction with instrumental gauge data over a large territory in boreal Québec and Ontario for the later 20th and early 21st centuries suggests that the observed increase in the frequency and magnitude of flooding (high discharge), especially since the 1950s, is likely a consequence of climate change. Given the level of management and dam construction on rivers and the lack of hydrological data in northern Canada, paleohydrological studies using high-resolution tree-ring proxies are particularly relevant and need to be further developed.

1.8 Acknowledgments

We thank the FERLD research station team and especially Danielle Charron and Raynald Julien for their continuous support over the two summers of field work. Great thanks go to the field assistants Cyrielle Ducrot, Chloé Lavelle, Isabelle Gareau and Stephane Hébert as well as to The University of Winnipeg laboratory assistants Dominique Levin, Johanna R.M. Robson and Hollie Swart. We thank Yves Bégin, Étienne Boucher, Pierre Brigode, Mickaël Lemay, and Antoine Nicault for sharing their tree-ring hydrological reconstructions and for precious discussions on this project. This research is a contribution of the Canada Research Chairs (NSERC-CRC) held by YB and JT and was funded by a Natural Sciences and Engineering Research Council of Canada Collaborative research program including Ouranos, Hydro-Québec, Ontario Power Generation (OPG) and The University of Winnipeg. Earlier versions of the manuscript benefited from constructive comments by Jacinthe Clavet-Gaumont and David Huard (Ouranos) as well as from Kurt C. Kornelsen (OPG). We also acknowledge the contributions of the Editor-in-Chief (Pr. Jed O. Kaplan) and both reviewers (Pr. Juan A. Ballesteros-Cánovas and Pr. Matthew Therrell) who provided constructive comments and suggestions on earlier drafts of the manuscript.

1.9 Data availability

Relevant data for this study are available from Nolin, A. F., Tardif, J. C., Conciatori, F., Kames, S., Meko, D. M. & Bergeron, Y. (2021). *Fraxinus nigra* tree-ring dataset for dendrohydrology study in the Lake Duparquet, and reconstruction of the Harricana River spring discharge, Québec, Canada. Mendeley Data, v2, <http://dx.doi.org/10.17632/d54gcxz9c5.2>. Data include earlywood vessels and tree-ring width chronologies derived from *Fraxinus nigra* trees growing in Lake Duparquet in eastern boreal Canada (Québec).

DUPARQUET_Chronologies.csv, as in Fig. 1.2, the 12 anatomical and ring-width chronologies developed for Lake Duparquet to reconstruct Harricana River spring discharge;

DUPARQUET_lat_lon.kml, the coordinate data for each station sampled on Lake Duparquet;

HARRICANA_rec&cal.csv, as in Fig. 1.5A, the instrumental and reconstructed Harricana River spring discharge for the two models REC1 and REC2;

metadatas.txt, a set of self-explanatory instructions and descriptions for data files.

All other data are available upon request to the corresponding author at alexandreflorent.nolin@uqat.ca (institutional email), alexandreflorent.nolin@gmail.com (permanent email).

1.10 Supplementary Materials

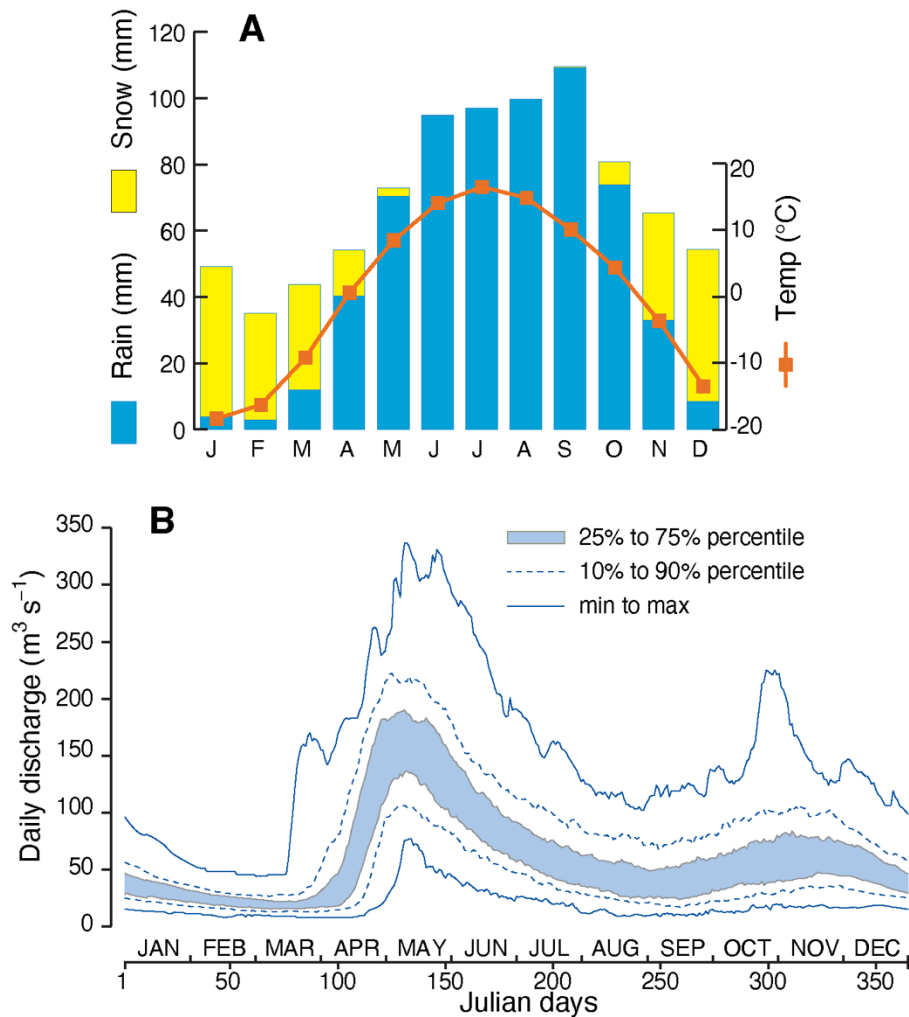


Figure 1.S1 Normals for climatic and discharge data. A) Mean monthly climate normals for La Sarre station 1971–2000, <http://climate.weather.gc.ca/>. B) Daily discharge for Water Survey Canada gages 04NA001 and 04NA002 Harricana River (1915–2020) indicating the range of recorded variability. Data obtained from the Canada water Survey, <https://wateroffice.ec.gc.ca/>.

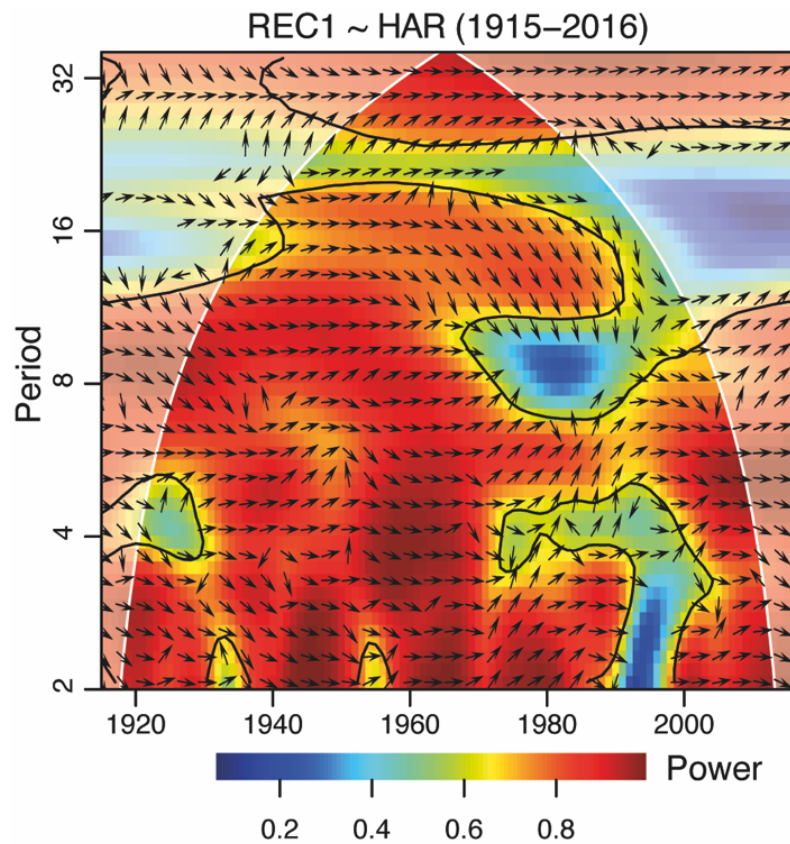


Figure 1.S2 Wavelet coherence between instrumental and reconstructed harricana river spring discharge. Cross power spectrum (XWT) between instrumental and reconstructed (REC1) Harricana River spring discharge (HAR) performed on the 1915–2016 period. Black lines encircle areas were p -value < 0.01 tested against white noise (as lag–1 autocorrelation in REC1 and in HAR were not significant) and on 1,000 Monte-Carlo iterations. Arrows pointing to the right indicates that the variables are in phase.

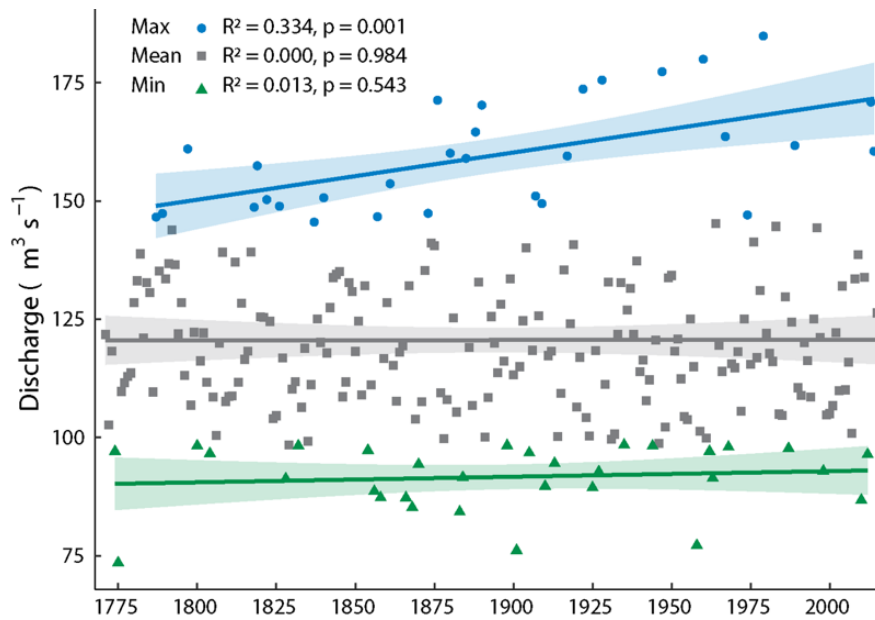


Figure 1.S3 Harricana River discharge characteristics. Scatter plot of the reconstructed Harricana River spring discharge (15 April to 30 June) from 1771 to 2016. Linear regressions are calculated for high discharge years (MAX, 30 highest values), the complete reconstruction (MEAN, all values), and low discharge years (MIN, 30 lowest values).

CHAPITRE II

SPATIAL COHERENCY OF THE SPRING FLOOD SIGNAL AMONG MAJOR RIVER BASINS OF EASTERN BOREAL CANADA INFERED FROM FLOOD RINGS

Alexandre F. Nolin, Jacques C. Tardif, France Conciatori, Yves Bergeron

Publié dans *Journal of Hydrology*

Février 2021

2.1 Abstract

In eastern boreal Canada, long-term perspective in water resources and hydroelectric dams management is currently limited by the lack of long-term hydrological records. The research for new paleohydrological proxies would help fill this hydrological data gap and provide regional hydroclimatic predictive trajectories in the context of climate change. The development of long annually resolved series of earlywood vessel cross-sectional area has recently demonstrated a high potential for reconstructing high and low discharges. This study analyzes a network of 10 sites scattered around Lake Duparquet. The region covers an area of about 20 000 km² including four river basins characterized by natural and regulated rivers, and unflooded control sites. The objectives were to assess 1) the spatial coherency in flood-rings chronologies among sites and Lake Duparquet, and among hydrological regimes (natural, regulated and unflooded control) and 2) their degree of association with i) annually resolved chronologies of earlywood vessel cross-sectional area and number, ii) a reconstruction of the Harricana River spring discharge and iii) discharge data from eleven hydrometric stations distributed in the study area. It was hypothesized that flood rings would be consistent among natural rivers and absent from regulated rivers. Results showed high spatial coherency among natural rivers with flood rings recording the major floods of the last 250 years. Flood ring and earlywood vessel chronologies were strongly correlated to both reconstructed and instrumental discharge data. On regulated rivers, trees were younger than at the other sites and mainly spring floods that occurred prior to dam creation and the few extreme floods after dam creation were recorded by flood rings. One hypothesis is that older trees (before dam) most likely recorded the natural dynamic of the river, while younger trees (after dam) most likely recorded dam management maneuvers and spring flood exceeding dam capacity. Flood rings and earlywood vessel chronologies provided comparable and complementary hydrological evidences. Flood rings were easily identified visually allowing fast determination of major flood years whereas developing earlywood vessel chronologies, while being more tedious and time consuming, allowed capturing a larger spectrum of hydrological conditions.

Keywords: *Fraxinus nigra*, spring floods, earlywood vessels, Lake Duparquet, dendrohydrology, flood ring

2.2 Résumé [Ajout à l'article original]

Dans l'est du Canada boréal, la perspective à long terme de la gestion des ressources en eau et des barrages hydroélectriques est actuellement limitée par le manque d'enregistrements hydrologiques à long terme. La recherche de nouveaux indicateurs paléo-hydrologiques permettrait de combler cette lacune en matière de données hydrologiques et de fournir des trajectoires hydroclimatiques régionales potentielles dans le contexte du changement climatique. Le développement de longues séries, à résolution annuelle, de l'aire de la surface des vaisseaux de bois initial (section transversale) a récemment démontré un fort potentiel pour reconstruire les hauts et bas débits. Cette étude analyse un réseau de 10 sites dispersés autour du lac Duparquet. La région couvre une superficie d'environ 20 000 km² comprenant quatre bassins fluviaux caractérisés par des rivières naturelles et régulées, et des sites témoins non inondés. Les objectifs étaient d'évaluer 1) la cohérence spatiale des chronologies de cernes de crues entre les sites et le lac Duparquet, et entre les régimes hydrologiques (naturel, régulé et témoin non inondé) et 2) leur degré d'association avec i) des chronologies à résolution annuelle de l'aire calculé en section transversale et du nombre de vaisseaux du bois initial, ii) une reconstitution du débit printanier de la rivière Harricana et iii) des données de débit provenant de onze stations hydrométriques réparties dans la zone d'étude. L'hypothèse était que les cernes de crues seraient cohérents entre les rivières naturelles et absents des rivières régulées. Les résultats ont montré une grande cohérence spatiale entre les rivières naturelles, les cernes de crues enregistrant les principales inondations des 250 dernières années. Les fréquences de cernes de crues et les chronologies de vaisseaux du bois initial étaient fortement corrélées aux données de débit reconstituées et instrumentales. Sur les rivières régulées, les arbres étaient plus jeunes que sur les autres sites et les cernes de crues ont enregistré principalement les crues de printemps qui se sont produites avant la création du barrage et les quelques crues extrêmes après la création du barrage. Une hypothèse est que les arbres plus âgés (avant le barrage) ont probablement enregistré la dynamique naturelle de la rivière, tandis que les arbres plus jeunes (après le barrage) ont probablement enregistré les manœuvres de gestion du barrage et les crues de printemps dépassant la capacité du barrage. Les cernes de crues et les chronologies des vaisseaux de bois initial ont fourni des preuves hydrologiques comparables et complémentaires. Les cernes de crues sont facilement identifiables visuellement, ce qui permet de déterminer les crues, tandis que le développement des chronologies des vaisseaux du bois initial, bien que plus fastidieux et plus long, a permis de capturer un plus large spectre de conditions hydrologiques.

Mots-clés : *Fraxinus nigra*, crues printanières, vaisseaux du bois initial, Lac Duparquet, dendrohydrologie, cerne de crue

2.3 Introduction

The hydrological variability observed in recent decades worldwide is unusual and raises questions about the potential impacts of climate change on water resources (IPCC, 2018). Worldwide, exceptional floods and droughts are becoming more frequent and intense and are expected to become even more severe under a warmer climate (Berghuijs et al., 2017; Kundzewicz et al., 2019). In Canada, the severity of floods in the last decade is unprecedented on the scale of 20th century hydrological records (Burn & Whitfield, 2016; Gaur et al., 2018). The Insurance Bureau of Canada for Natural Disaster reports nearly \$1 billion Canadian dollars spent annually on insurance payouts since 2010 (IBC, 2020). For example, the 2019 flood in the Ottawa River basin exceeded that of 2017 which was considered the 100-year flood (ECCC, 2020).

Since the 1950s northern Canada has warmed by an annual average of 2.3°C and total annual precipitation has increased by +35% (Zhang et al., 2000; Bush & Lemmen, 2019). Global warming directly affects seasonal flows in the boreal region because of snow and discharge interactions. The most significant changes observed from 1950 were in winter where the combination of changes in temperature and precipitation over snow cover resulted in higher winter discharges (Vincent et al., 2015; Mudryk et al., 2018; Aygün et al., 2019; Bush & Lemmen, 2019). Episodes of rain-on-snow or rain-in-place of snow, and mid-winter thaws feed winter discharge in the boreal rivers instead of storing water in the snow cover. Instrumental records of the past century in Canada also have shown a reduction in spring discharge and in summer discharge associated with a shorter ice season (Aygün et al., 2019; Bush & Lemmen, 2019).

Hydrological trends across Canada, however, show high spatial variability which mainly relates to complex climate and discharge interactions, regional landscape

complexities and the lack of long-term hydrological data (Mortsch et al., 2015; Aygün et al., 2019; Bush & Lemmen, 2019). In fact, most of the historical hydrometric stations in both northern Québec and Ontario were installed at the time of the creation of the hydroelectric generating stations which complicate the comparison of hydrological records between the pre- and post- dam periods (Table 2.S1). It also remains uncertain how the projected climate change will affect the frequency and magnitude of extreme floods and droughts (Gaur et al., 2018). Hydrological simulations for northern Manitoba, Ontario and Québec estimated the magnitude of the change in the probable maximum flood to be between -1.5 and $+21\%$ by 2070 (Clavet-Gaumont et al., 2017). The estimated 100-year snowpack variations ranged from -9% to $+8\%$ with large variations between the southern and northern parts of the provinces. Similarly, the simulations for Québec predict earlier spring floods and an increase in winter and mean annual discharge with a strong intensity gradient from south to north (Guay et al., 2015).

Projected changes in hydrological regimes will also affect the management of hydroelectric facilities, particularly in northern Canada (Boucher & Leconte, 2013; Cherry et al., 2017). One of the major issues concerns the stability of dams throughout their lifespan given that Canada's major facilities were built to last more than 100 years (Clavet-Gaumont et al., 2017). For Québec, where more than 95% of the energy demand is supplied by hydropower with sales representing more than \$2.9 billion Canadian dollars per year, considering mitigation and adaptation scenarios is essential (Hydro Québec, 2020).

Paleoclimatic proxy data have played an important role in extending hydroclimate records to help in planning for future water resource variability. Applications of tree-ring science to hydrology have allowed, among others, to extend instrumental discharge records in time (Meko & Woodhouse, 2011; Boucher et al. 2011; Nolin et al., 2021a). Proxy derived from annually resolved tree rings have been used to extend

times series of precipitation (Griffin et al., 2013), discharge (Agafonov et al., 2016; Nolin et al., 2021a), drought (Biondi & Meko, 2019), or lake levels (Tardif & Bergeron, 1997b; Bégin, 2001; Tardif et al., 2010), while few have assessed their potential for flood reconstruction (St. George & Nielsen, 2003; Tardif et al., 2010; Kames et al., 2016; Nolin et al., 2021a).

In recent years, flood rings that form in tree rings from riparian ring-porous species has allowed to identify major spring floods in various river basins and prior to instrumental records (St. George & Nielsen, 2000; St. George & Nielsen, 2003; Tardif et al., 2010; Wertz et al., 2013; Therrell & Bialecki, 2015; Kames et al., 2016; Meko & Therrell, 2020). In ring-porous tree species (e.g., *Quercus* and *Fraxinus*), flood rings are characterized by increased earlywood vessel density and/or reduced earlywood vessel cross-sectional areas (St. George & Nielsen, 2003; Tardif et al., 2010; Copini et al., 2016; Kames et al., 2016; Nolin et al., 2021a). Anatomical changes in earlywood vessels occur in the submerged portion of the tree stem if flooding happens to coincide with the period of active earlywood formation (St. George et al., 2002; Copini et al., 2016). At Lake Duparquet in northwestern Québec, chronologies of earlywood vessels from black ash trees (*Fraxinus nigra* Marsh.) better reflected spring discharge variability than tree-ring widths (Kames et al., 2016) and were successfully used to reconstruct Harricana River spring discharge from 1771 to 2016 (Nolin et al., 2021a).

In contrast to flood studies conducted at Lake Duparquet (Tardif et al., 2010; Kames et al., 2016; Nolin et al., 2021a) or the Red River (St. George & Nielsen, 2000; 2003), the use of flood rings in North America could be spatially hindered in areas where electricity generation has resulted in river regulation. Dam management alters the natural availability of water in terms of mean seasonal levels and frequency of flooding which in turn affect riparian forests (Stella & Bendix, 2019) and possibly their use as discharge proxy. In regulated rivers, correlations between tree-ring width chronologies

and discharge tend to decrease whereas those with precipitation tend to increase resulting in a decreased effectiveness in reconstructing discharge (Reily & Johnson, 1982; Schook et al., 2016a; Netsvetov et al., 2019). Up to now, no studies have assessed the impact of discharge regulation on flood-rings formation in riparian trees.

The objectives of this study were twofold. First, the spatial coherency in flood-ring chronologies was assessed among a network of ten sites located along four river basins in northeastern Canada (Mattagami, Abitibi, Harricana and upper Ottawa Rivers) and at Lake Duparquet, and under three different hydrological regimes (natural, regulated and at unflooded control). It was hypothesized that the flood-ring chronologies among natural river basins will be similar and that they will differ from those originating from regulated rivers, especially after the creation of dams. Second, we determined the degree of association between flood-ring chronologies and i) continuous annually resolved series of earlywood vessel cross-sectional area and number, ii) a reconstruction of the Harricana River spring discharge and iii) discharge data from eleven hydrometric stations distributed in the study area. It was hypothesized that these various datasets will be highly correlated thus illustrating the large-scale spatial coherency in the spring flood signal in eastern boreal Canada.

2.4 Material and methods

2.4.1 Study area

The study area encompasses Lake Duparquet and four major river basins (Mattagami, Abitibi, Harricana and upper Ottawa Rivers) located in northeastern Canada (Fig. 2.1). It roughly covers an area of about 20 000 km². The Mattagami, Abitibi and Harricana Rivers are flowing north and are major southern tributaries of the James Bay in the Hudson sea (Déry et al., 2011) while the upper Ottawa River is flowing south to the Saint-Lawrence estuary (Fig. 2.1). Lake Duparquet (48°28'N; 79°16'W) is situated in

the upstream section of the Abitibi River, near the continental divide (Fig. 2.1). The Mattagami and Abitibi Rivers are partially regulated with dams implanted since the 1910s (CEHQ, 2019; OMNRF, 2019; Table 2.S1) while the Harricana and upper Ottawa Rivers are naturally flowing (CEHQ, 2019; OMNRF, 2019). The regional hydrological regime is dominated primarily by snowmelt and summer precipitation, with most of the annual discharge flowing during the spring breakup flood. For example, the mean discharge of the Harricana River in May represents 11 to 30% of the total annual discharge over the period 1915–2020 (Nolin et al., 2021a).

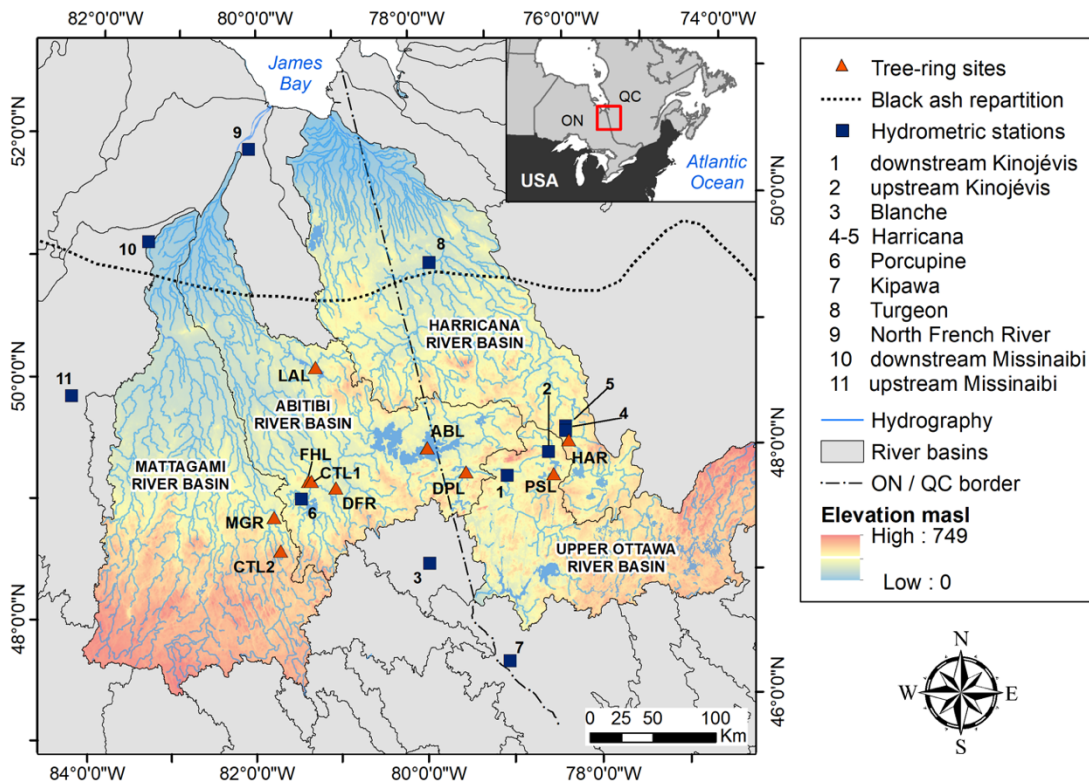


Figure 2.1 Map of the study area. Location of the study area within North America (upper inset). The tree-ring sampling sites (red triangles) and hydrometric stations (blue squares) are indicated as well as the four major river basins under study. The abbreviations refer to those listed in Table 2.1, Lake Duparquet is coded ‘DPL’.

The study area is part of the northern Clay Belt of Québec and Ontario where the soils are dominated by glacio-lacustrine deposits that transform into peatlands northward (Daubois et al., 2015). It is also the southern limit of the boreal forest where mixedwood associations are composed of balsam fir (*Abies balsamea* (L.) Mill.), black spruce (*Picea mariana* (Mill.) BSP), paper birch (*Betula papyrifera* Marsh.), white spruce (*Picea glauca* (Moench) Voss) and trembling aspen (*Populus tremuloides* Michx.) (Denneler et al., 1999). Riparian areas are dominated by eastern white-cedar (*Thuja occidentalis* L.), and occasionally balsam poplar (*Populus balsamifera* L.) (Tardif et al., 1992; Denneler et al., 1999). *Fraxinus nigra* can be found in this last associations or it can form pure stands (Tardif & Bergeron, 1997a). For this study, *F. nigra* trees were found in a variety of habitats such as oxbow lakes, sediment bars, meanders, or lake bays where the soil consists of a fine clay deposit and where the topography allows the water table to be accessible most of the year.

2.4.2 Sampling

Between 2017 and 2018, ten sites distributed along four river basins were sampled including four sites with natural hydrological regime (Lake Duparquet: DPL, Preissac Lake: PSL, Harricana River: HAR and Little Abitibi Lake: LAL); four sites with regulated hydrological regime (Abitibi Lake: ABL, regulated downstream by the Iroquois Falls dam built in 1914; Driftwood River: DFR, regulated downstream by the Monteith dam built in 1953, Frederick House Lake: FHL, regulated downstream by the Frederick House Lake dam built in 1938; and Mattagami River: MGR, regulated upstream by the Wawaitin Falls dam built in 1912, and downstream by the Sandy Falls dam, built in 1911; Table 2.S1) and two unflooded control sites in topographically flat upland forests (CTL1, CTL2; Fig. 2.1, Table 2.1). Among the regulated river sites, the ABL, DFR and FHL sites are located upstream of the dams while the MGR site is located between two dams. In total, 929 samples were collected from 470 *F. nigra* trees (Table 2.1). To aid in site selections, aerial photographs and Canada's National Forest

Inventory maps (<https://nfi.nfis.org>) coupled with SRTM elevation data (<https://earthexplorer.usgs.gov/>) were used. The Québec (CEHQ, 2019) and Ontario dam inventories (OMNRF, 2019) were used to characterize each sampling site according to hydrological regimes (presence of a dam and its distance to the sampling site). Increment cores were taken from living trees and stem discs were collected from dead trees with all samples collected as close to the ground level as possible. Wood samples were prepared and sanded following standard dendrochronological procedures (Phipps, 1985; Cook & Kairiukstis, 1990). Prior to visual identification of flood rings, the prepared sample wood surfaces were rubbed with white chalk to increase the contrast between earlywood vessels and other cell types (St. George et al., 2002; Tardif & Conciatori, 2006b).

Table 2.1 Number of *Fraxinus nigra* trees sampled, and cores collected per site. Sites are classified by hydrological regime. The field “Period” indicates the maximum period covered by the flood-ring and continuous series of earlywood vessel chronologies. The distance provided are in reference to Lake Duparquet’s location. Among the regulated river sites, the ABL, DFR and FHL sites are located upstream of the dams while the MGR site is located between two dams.

Discharge	Code	Distance (km)	Site	River Basin	Trees	Samples	Period
Natural	DPL	/	Duparquet Lake	Abitibi	65	123	1750–2016
	PSL	70	Preissac Lake	Upper Ottawa	37	74	1812–2016
	HAR	85	Harricana River	Harricana	120	239	1780–2016
	LAL	145	Little Abitibi Lake	Abitibi	48	96	1793–2016
Regulated	ABL	30	Abitibi Lake	Abitibi	12	24	1901–2016
	DFR	105	Driftwood River	Abitibi	43	86	1852–2016
	FHL	125	Frederick House Lake	Abitibi	67	132	1774–2016
	MGR	150	Mattagami River	Mattagami	32	64	1904–2016
Control	CTL1	120	Frederick House Lake	Abitibi	24	47	1904–2016
	CTL2	160	Bruce Lake	Mattagami	22	44	1755–2016

2.4.3 Tree-ring data

Each sample was systematically inspected with a dissecting microscope to visually determine the presence of flood ring and their presence was labelled on the core mount prior to visual crossdating. Flood rings were categorized into two classes in relation to their vessel size, vessel density and organization within the earlywood (Fig. 2.2). This visual identification step was carried out by two observers, who each had half of the samples amount. A dual numerical code was used, with a F1 indicating a weakly defined flood ring (noticeable increase in number of earlywood vessels supported with a decrease in earlywood vessel area) and a F2 indicating a well-defined flood ring as previously described in *F. nigra* (Tardif et al., 2010; Kames et al., 2016; Nolin et al., 2021a; Fig. 2.2). This characterisation of flood rings (F1 or F2) was chosen to account for the intensity of flood rings rather than a simple presence-absence index. Given that tree elevation and coring height varied within a site and that anatomical changes in earlywood vessels (flood ring) were reported to occur solely in the submerged portion of the tree stem during active earlywood formation (St. George et al., 2002; Copini et al., 2016), adopting a dual numerical code aimed to better capture the flood signal. After flood-ring identification on each sample was completed, visual crossdating was performed using *F. nigra* pointed years developed for Lake Duparquet (Tardif & Bergeron 1997a; Kames et al., 2016; Nolin et al., 2021a) and the list method (Phipps, 1985).

In addition to flood-ring identifications, annual measurements of tree-ring earlywood vessels were performed on a subset of trees. The mean cross-sectional lumen area (MVA) and the number of earlywood vessels (N) were measured in six *F. nigra* samples. These samples were selected to be the oldest and best-preserved wood samples (e.g., clear tree rings, no rot, etc.) from the four river basins and corresponded to natural and regulated hydrological regimes: Abitibi River basin (natural, site LAL, $n = 2$); Harricana River basin (natural, site HAR, $n = 2$); upper Ottawa River basin

(natural, site PSL, $n = 1$); Mattagami River basin (regulated, site MGR, $n = 1$; Fig. 2.1; Table 2.1). The MVA and N chronologies previously developed for Lake Duparquet (1771–2016, $n = 43$) by Nolin et al. (2021a) were used as references.

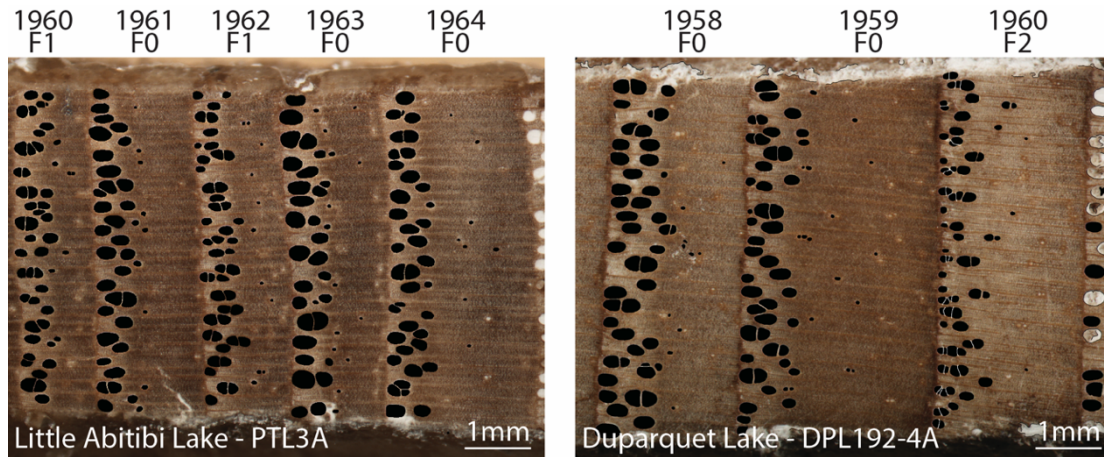


Figure 2.2 Segmented earlywood vessels in *Fraxinus nigra* tree rings. Vessels appear black as the result of the digitalization process. The years are given with the classification of flood rings: F0 = null, F1 = weakly defined flood ring and F2 = well-defined flood ring. Notice the difference in the strength of the flood rings between Little Abitibi Lake (left) and Lake Duparquet (right) for the year 1960.

Measurement of mean cross-sectional area (MVA) and number (N) of earlywood vessel in annually resolved tree rings was performed as described in Nolin et al. (2021a) using high-resolution scanned images of the tree rings. The images were acquired from a Nikon DS-Fi1 camera mounted on a NIKON SMZ1000 stereomicroscope to produce standardized tree-ring images format (1600 x 1200 dpi at x20 magnification). Earlywood vessels were automatically detected and digitalized using the Canny edge algorithm (Canny, 1986) implemented in ImageJ2X software (Rueden et al., 2017). Each earlywood vessel shape was checked and false automatic delimitations (*e.g.*, incomplete earlywood vessel lumen areas at the edge of the cores, grouped earlywood

vessels, tyloses) were manually corrected with a graphic tablet. After ensuring that each earlywood vessel contour delineation was correct, the measurements of annual MVA and N were performed using WinCell software Pro v2018c (Régent Instrument, 2018). Both MVA and N were measured on earlywood vessel areas greater than 3,000 μm^2 in cross-section (Tardif, unpublished data). The delimitation between earlywood and latewood has been qualitatively identified as the abrupt decrease in vessel cross-sectional area (Tardif & Conciatori, 2006b; Kames et al., 2016).

Series crossdating and measurements were validated with CDendro (Larsson, 2003a) and COFECHA (Holmes, 1983) prior to series' detrending. Each tree-ring series was divided by a cubic smoothing spline function with 50% frequency of response of 60 years (Cook & Kairiukstis, 1990). Six missing values have been interpolated by the Spline filling function of the 'dplR' package to detrend the series (Bunn, 2008). Detrended series were then combined into standardized chronologies per river basins and hydrological regimes using a bi-weight robust mean (when $n > 1$ series) to lower the influence of outliers. This was the case for the Abitibi and the Harricana rivers ($n = 2$ series). All statistical procedures of dendrochronology were conducted with the 'dplR' package (Bunn, 2008) in R environment (R Core Team, 2020).

2.4.4 Hydrological data

Daily discharges were downloaded from the Water Survey of Canada, the Reference Hydrometric Basin Network and the Centre d'Expertise Hydrique du Québec (Table 2.S2). Eleven hydrometric stations were selected on natural rivers not regulated by dams (Table 2.S2) and with a minimum of 24 years of data, but not necessarily in a continuous sequence. Daily discharges were averaged from April 15 to June 30. This period best represented the range of discharge variability during the spring flood season and can be equated with the period of earlywood formation in *F. nigra* (Nolin et al., 2021a). Only years with less than 10 % missing daily values for the period 15 April to

30 June (77 days) were considered. This arbitrary threshold was chosen to avoid statistical shortcomings in the interpolation of missing values. It should be noted that the data for Harricana River came from two hydrometric stations in close proximity (4 km) and for the same drainage area. They have therefore been grouped into a single time series because they overlap with no difference in daily discharge values (Kames et al., 2016; Nolin et al., 2021a). In addition to these hydrometric records, the Harricana River spring discharge reconstruction from Nolin et al. (2021a) was used for comparison.

2.4.5 Statistical analyses

The spatial coherency of flood rings among the four river basins and Lake Duparquet was assessed using four approaches. First, annual flood-ring series were compiled by tree, keeping for each year the code that had the maximum intensity between the two radii ($0 < F1 < F2$). Spearman's rank correlation coefficients were calculated between each flood-ring series per tree (categorical variable: value = 0, 1 or 2) and the reconstructed Harricana River spring discharge (continuous variable) over the maximum series length (n ranging from 113 to 246 years). The dispersion of correlation coefficients between sites, and between hydrological regimes were compared using box plots (Legendre & Legendre, 2012). When flood-ring series were compared to the reconstruction of the Harricana River spring discharge, which is derived from *F. nigra* trees growing on the floodplain of Lake Duparquet, the dispersion of correlation coefficients between sites was compared by geographic distance to Lake Duparquet.

Second, flood-ring series per tree were used to calculate, for each of the ten sampled sites, three flood-ring relative frequencies $F1$, $F2$ and $F12$ (hereafter flood-ring chronologies). $F1$ and $F2$ can be defined as the annual sum of flood rings for a given year, divided by the annual sum of samples for the same year and expressed as the percentage of $F1$ and $F2$ rings over the total number of samples in a given year. $F12$ is

the sum of F1 + F2 chronologies and was used to determine whether or not the F1 and F2 flood-ring classes carry different hydrological signal. Each flood-ring chronology (F1, F2, F12) was correlated using Spearman's rank correlation coefficient i) with the reconstructed spring discharge of the Harricana River, ii) with spring discharge records from 11 hydrometric stations, iii) among river basins, iv) and among hydrological regimes.

Third, and in the same way, earlywood vessel chronologies (MVA and N) were correlated using Pearson's correlation coefficient i) with the reconstructed spring discharge of the Harricana River (Nolin et al., 2021a), ii) with spring discharge records from 11 hydrometric stations, iii) among river basins, and iv) and among hydrological regimes. At last, the periodicities that dominate the variance through time were compared using continuous wavelet transform (CWT) on the mean standardized earlywood vessel chronologies (MVA and N) from the four river basins. CWT were computed on a $\omega_0 = 6$ Morlet power spectrum base so the Morlet wavelet scale be comparable to the Fourier period (Torrence & Compo, 1998). Significant peaks in spectra were tested against a white-noise background on 1,000 Monte Carlo iterations (Torrence & Compo, 1998). All analyses were conducted using R software (R Core Team, 2020) and the packages 'Hmisc' (Harrell, 2020) for correlations analyses, and 'biwavelet' (Gouhier et al., 2019) for continuous wavelet transformations.

2.5 Results

2.5.1 Flood ring coherency across river basins

The flood-ring chronologies covered the period 1770–2016 with one tree per river basin going back to 1770 (Fig. 2.3). The sample replication indicated that trees sampled from the four regulated rivers (ABL, DFR, FHL, MGR) were generally younger than in other hydrological regimes with few trees available before the 1850s ($n = 4$). The F1 and F2 chronologies (Fig. 2.3) were highly intercorrelated over the common period 1780–2016 on Lake Duparquet ($\rho = 0.68$, $p < 0.001$), natural rivers ($\rho = 0.59$, $p < 0.001$) and regulated rivers ($\rho = 0.55$, $p < 0.001$), but not on unflooded control sites ($\rho = 0.03$, $p = 0.606$). The F12 chronologies were more strongly correlated to instrumental and reconstructed spring discharge than either the F1 or F2 chronologies (Table 2.2, Table 2.3). The F12 chronologies for both Lake Duparquet (maximum value of 100%) and natural rivers (maximum value of 93.3%) demonstrated a higher proportion of flood rings than for regulated rivers (maximum value of 39.2%) and unflooded control sites (maximum value of 10.0% ; Fig. 2.3). Indeed, each correlation between flood-ring chronologies and the different datasets used in this study were highest for Lake Duparquet, higher in natural rivers than in regulated rivers, and centered around zero for the unflooded control sites (Fig. 2.3, Fig. 2.4, Table 2.2, Table 2.3). In the spatial structure of correlations, associations between each flood-ring chronologies and instrumental spring discharge records tended to weaken with increasing distance to Lake Duparquet and in regulated rivers (Fig. 2.4, Table 2.3); the lowest number of significant associations being found with the southernmost hydrometric station of Kipawa River (Table 2.3).

Table 2.2 Spearman's rank correlation coefficients (ρ) and p -values (p) between the flood-ring chronologies at each site and the reconstructed Harricana River spring discharge. F1 and F2 represent weakly and well-defined flood rings and F12 is the sum of their relative frequencies. Bold characters denote p -values < 0.05 .

Discharge	Sites	Period	N years	F1		F2		F12	
				ρ	p	ρ	p	ρ	p
Natural	DPL	1771–2016	246	0.57	0.000	0.63	0.000	0.66	0.000
	PSL	1812–2016	205	0.44	0.000	0.40	0.000	0.43	0.000
	HAR	1780–2016	237	0.36	0.000	0.48	0.000	0.44	0.000
	LAL	1793–2016	224	0.35	0.000	0.46	0.000	0.44	0.000
Regulated	ABL	1901–2016	116	0.13	0.181	0.10	0.263	0.15	0.106
	DFR	1852–2016	165	0.36	0.000	0.46	0.000	0.43	0.000
	FHL	1774–2016	243	0.05	0.432	0.21	0.001	0.07	0.267
	MGR	1904–2016	113	0.29	0.002	0.22	0.017	0.30	0.002
Control	CTL1	1904–2016	113	0.09	0.350	0.05	0.631	0.12	0.196
	CTL2	1771–2016	246	-0.04	0.574	0.02	0.763	-0.02	0.697

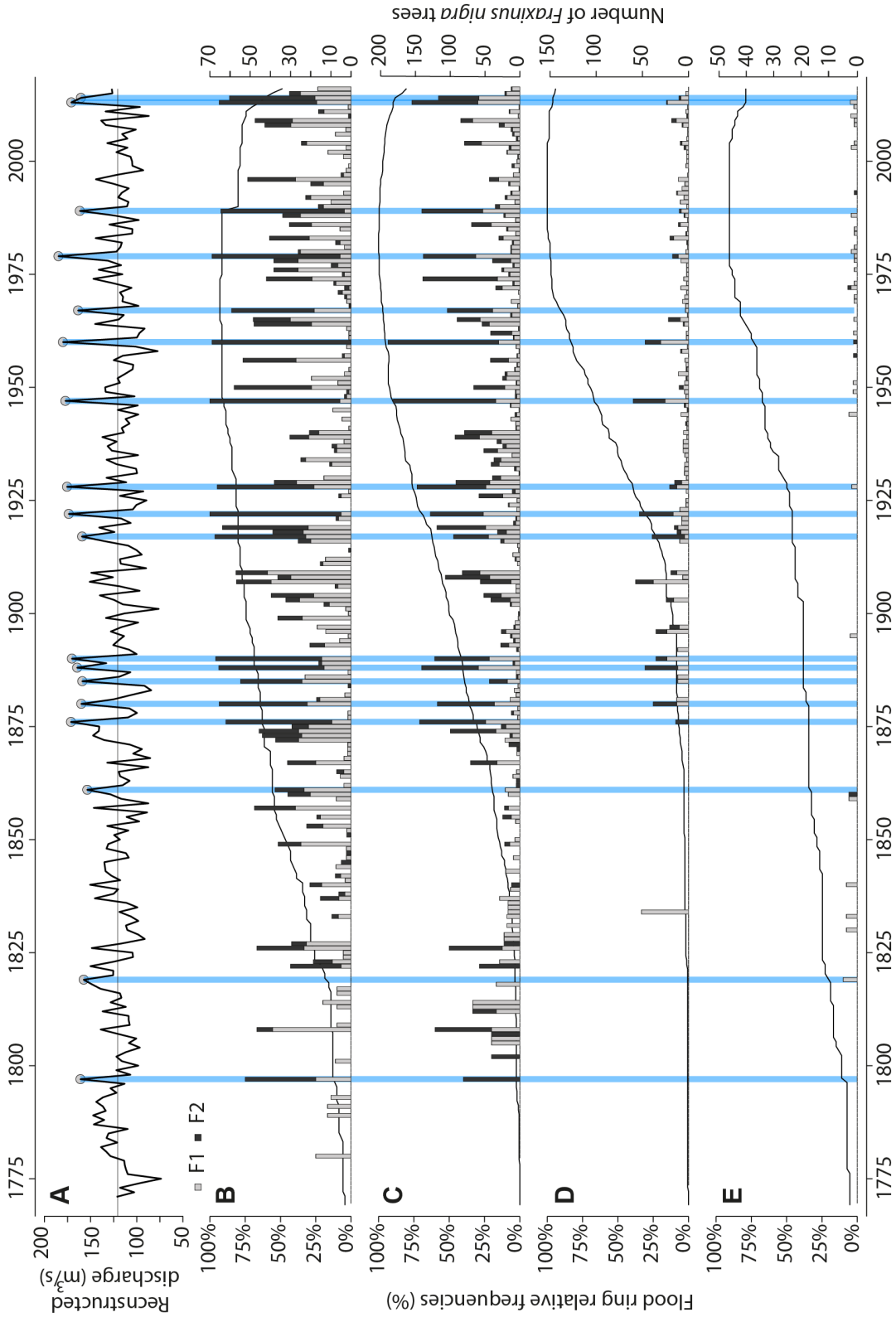


Figure 2.3 Flood-ring chronologies among hydrological regimes. Comparison between (A) the reconstructed Harricana River discharge flood-ring relative chronologies from *Fraxinus nigra* trees from (B) Lake Duparquet (DPL), (C) pooled natural rivers (PSL, HAR, LAL), (D) regulated rivers (ABL, DFR, FHL, MGR), and (E) unflooded control sites (CTL1, CTL2). Grey and black histograms are respectively F1 and F2 flood-ring relative frequencies. The background solid black lines indicate the number of trees per year. The dashed horizontal lines indicate the three thresholds used to extract the highest F12 values from the three hydrological regimes, and respectively $F12 \geq 75\%$ for Lake Duparquet, $F12 \geq 50\%$ for natural rivers and $F12 \geq 10\%$ for regulated rivers. The 18 years with the highest reconstructed spring discharge for the Harricana River and over the last 250 years are represented by grey dots on the upper A curve and extending as blue bars. Those 18 years were defined using a threshold corresponding to the mean + 1.5 SD (threshold value = 151.3 m³/s; Nolin et al., 2021a).

Table 2.3 Spearman's rank correlation coefficients (ρ) and p-values (p) between flood-ring chronologies from Lake Duparquet (DPL), natural (NAT), regulated rivers (REG) and unflooded control sites (CTL) and 10 instrumental records of April 15 to June 30 mean discharge across the study area. The field "Id" is the Canadian federal hydrometric station identification number. F1 and F2 are weakly and well-defined flood rings and F12 is the sum of the relative frequencies F1 and F2. The table is ordered by increasing distance between hydrometric station and DPL (left to right) to visualize spatial coherency in the correlation structure. Bold characters denote p-values < 0.05 .

Station	Kinojévis River	Kinojévis River	Blanche River	Harricana River	Porcupine River	Kipawa River	Turgeon River	Missinaibi River	North French River	Missinaibi River
Id	02JB013	02JB003	02JC008	04NA001-2	04MD004	02JE015	04NB001	04LM001	04MF001	04LJ001
Period	1971–2016	1938–1965	1970–2016	1915–2016	1977–2015	1963–2011	1969–1999	1973–2016	1967–2016	1921–2016
N years	46	28	47	102	26	38	24	43	50	96
Distance (km)	30	70	80	85	130	155	170	310	310	320
DPLF1	ρ 0.61	ρ 0.51	ρ 0.54	ρ 0.57	ρ 0.52	ρ 0.40	ρ 0.60	ρ 0.52	ρ 0.57	ρ 0.29
<i>p</i>	0.000	0.006	0.000	0.000	0.006	0.012	0.002	0.000	0.000	0.005
DPLF2	ρ 0.77	ρ 0.61	ρ 0.58	ρ 0.66	ρ 0.70	ρ 0.35	ρ 0.64	ρ 0.59	ρ 0.37	ρ 0.36
<i>p</i>	0.000	0.000	0.000	0.000	0.000	0.031	0.001	0.000	0.009	0.000
DPLF12	ρ 0.80	ρ 0.74	ρ 0.68	ρ 0.73	ρ 0.78	ρ 0.48	ρ 0.75	ρ 0.64	ρ 0.55	ρ 0.42
<i>p</i>	0.000	0.000	0.000	0.000	0.000	0.002	0.000	0.000	0.000	0.000
NATF1	ρ 0.76	ρ 0.66	ρ 0.67	ρ 0.75	ρ 0.77	ρ 0.34	ρ 0.77	ρ 0.71	ρ 0.57	ρ 0.54
<i>p</i>	0.000	0.000	0.000	0.000	0.000	0.035	0.000	0.000	0.000	0.000
NATF2	ρ 0.60	ρ 0.49	ρ 0.60	ρ 0.61	ρ 0.76	ρ 0.26	ρ 0.63	ρ 0.61	ρ 0.53	ρ 0.47
<i>p</i>	0.000	0.008	0.000	0.000	0.000	0.111	0.001	0.000	0.000	0.000
NATF12	ρ 0.75	ρ 0.62	ρ 0.63	ρ 0.73	ρ 0.78	ρ 0.34	ρ 0.79	ρ 0.73	ρ 0.58	ρ 0.54
<i>p</i>	0.000	0.000	0.000	0.000	0.000	0.035	0.000	0.000	0.000	0.000
REGF1	ρ 0.54	ρ 0.19	ρ 0.41	ρ 0.39	ρ 0.65	ρ 0.28	ρ 0.54	ρ 0.56	ρ 0.30	ρ 0.36
<i>p</i>	0.000	0.330	0.005	0.000	0.000	0.087	0.007	0.000	0.033	0.000
REGF2	ρ 0.42	ρ 0.45	ρ 0.38	ρ 0.36	ρ 0.54	ρ -0.14	ρ 0.34	ρ 0.37	ρ 0.25	ρ 0.19
<i>p</i>	0.004	0.016	0.008	0.000	0.004	0.400	0.105	0.015	0.082	0.068
REGF12	ρ 0.56	ρ 0.27	ρ 0.41	ρ 0.42	ρ 0.67	ρ 0.23	ρ 0.56	ρ 0.56	ρ 0.29	ρ 0.36
<i>p</i>	0.000	0.159	0.004	0.000	0.000	0.172	0.005	0.000	0.039	0.000
CTLF1	ρ -0.04	ρ 0.02	ρ 0.05	ρ 0.04	ρ 0.09	ρ 0.07	ρ 0.10	ρ 0.07	ρ 0.03	ρ -0.03
<i>p</i>	0.773	0.914	0.751	0.721	0.663	0.689	0.658	0.662	0.823	0.797
CTLF2	ρ -0.17	ρ 0.14	ρ -0.12	ρ -0.06	ρ 0.12	ρ -0.06	ρ -0.22	ρ 0.06	ρ -0.04	ρ 0.11
<i>p</i>	0.265	0.467	0.437	0.536	0.559	0.732	0.297	0.692	0.801	0.300
CTLF12	ρ -0.08	ρ 0.10	ρ 0.03	ρ 0.03	ρ 0.12	ρ 0.02	ρ 0.07	ρ 0.08	ρ 0.03	ρ 0.02
<i>p</i>	0.608	0.620	0.865	0.802	0.553	0.918	0.732	0.609	0.825	0.832

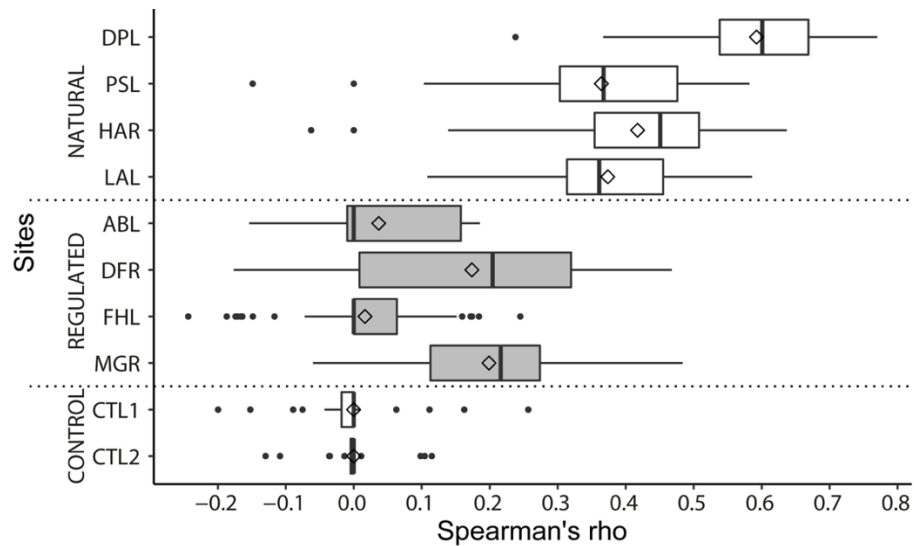


Figure 2.4 Box plot of the dispersion of Spearman's rank correlation coefficients between flood-ring series per tree and the reconstruction of the Harricana River spring discharge. Correlations are pooled by river hydrological regime (natural, regulated and unflooded control; separated by dotted lines and respectively from top to bottom) and by increasing distance from sites to Lake Duparquet. Site abbreviations are defined in Table 2.1. The left and right-most edges of the rectangles indicate the interquartile range between the 25th and 75th percentiles and the dots indicate outliers outside the 10th and 90th percentiles. The center line of the graph indicates the median, and the diamond indicates the mean.

Flood-ring chronology values (F12) were compared to the reconstructed spring discharge of the Harricana River for the period 1771–2016 (Fig. 2.3). Nolin et al. (2021a) estimated using the reconstruction mean value + 1.5 standard deviation ($151.3 \text{ m}^3/\text{s}$) that the most severe spring flood years had occurred in 1797, 1819, 1861, 1876, 1880, 1885, 1888, 1890, 1917, 1922, 1928, 1947, 1960, 1967, 1979, 1989, 2013 and 2014 (Fig. 2.3A). Given the variation in hydrological regimes and the number of sampled trees within each, an arbitrary threshold was determined to extract the highest F12 values from each regime. These threshold were respectively $F12 \geq 75\%$ for Lake Duparquet, $F12 \geq 50\%$ for natural rivers and $F12 \geq 10\%$ for regulated rivers (Fig. 2.3). According to these three thresholds, the highest values in the F12 flood-ring chronologies corresponded well with the 18 years of highest reconstructed discharge years since 1771 with respectively 16/18, 14/18 and 10/18 years captured for Lake Duparquet, natural rivers and regulated rivers.

In each of the hydrological regimes, some years with high F12 values (above the pre-determined thresholds) did not match with the 18 most severe spring floods identified using the reconstructed spring discharge of the Harricana River (Fig. 2.3; Table 2.S3). For the most part these years were, however, very close to the $151.3 \text{ m}^3/\text{s}$ threshold used to estimate the most severe spring floods (Table 2.S3). For Lake Duparquet, the five mismatched F12 years with values $\geq 75\%$ (1907, 1909, 1919, 1950 and 1956) corresponded to reconstructed discharges between 125.0 and $151.1 \text{ m}^3/\text{s}$. Similarly, the five F12 year with values $\geq 50\%$ for the natural rivers (1808, 1826, 1908, 1919 and 1974) corresponded to reconstructed discharges between 125.7 and $148.8 \text{ m}^3/\text{s}$. For the regulated rivers, ten F12 values $\geq 10\%$ also corresponded to reconstructed discharge ranging from 116.2 to $151.1 \text{ m}^3/\text{s}$.

Ten high F12 values in regulated rivers chronology were also not indicated by equivalent high F12 values in natural rivers, Lake Duparquet, or in the reconstructed spring discharge of the Harricana River (Fig. 2.3). The F12 chronologies from regulated rivers never reached more than 40% with a marked decrease in F2 flood-ring frequency observed after ca. 1920 (Fig. 2.3D). Looking at the individual regulated sites averaged to produce the regulated flood-ring chronologies revealed that both lake sites (ABL and FHL) recorded very little flood rings compared to the two river sites (DFR and MGR; results not shown). These differences in flood-ring chronologies (F1, F2, F12) were further emphasized by the regulated Driftwood River (DFR; 1852–2016) and Mattagami River (MGR; 1904–2016) being significantly correlated with the reconstructed Harricana River spring discharge and not the Abitibi Lake and Frederick House Lake (ABL, FHL; Table 2.2). Before the 1920s the chronologies presented few flood rings, and after the 1920s flood rings matched the highest spring discharge years reconstructed for the Harricana River.

In the unflooded control sites, the flood rings observed were mostly F1 and were never present in more than 10% of the trees (Fig. 2.3E). Flood-rings series per tree and flood-ring chronologies in the unflooded control sites showed no significant association with the reconstructed Harricana River spring discharge (Table 2.2; Fig. 2.4) or with the 11 hydrometric records (Table 2.3). Two values corresponded to the highest 18 spring discharge years reconstructed in the Harricana River (1819: 10%, 1 tree out of 10 ; 2013: 4.87%, 2 trees out of 41).

2.5.2 Continuous earlywood vessel chronologies

Continuous chronologies of earlywood vessels spanned different time periods for Lake Duparquet (1771–2016) and for the four river basins (Harricana: 1783–2016; upper Ottawa: 1814–2016; Abitibi: 1840–2016; and Mattagami: 1922–2016; Fig. 2.5 left panels). Inter-series correlations were high in chronologies produced from two tree series. For example, in MVA chronologies from Harricana and Abitibi River, $r = 0.73$ ($n = 129$, $p < 0.001$) and $r = 0.68$ ($n = 119$, $p < 0.001$; Fig. 2.5). Correlations between earlywood vessel and F12 chronologies were high in Lake Duparquet (respectively for MVA and N, $\rho = -0.73$ and 0.54 , $p < 0.001$, 1771–2016) and natural rivers ($\rho = -0.53$ and 0.43 , $p < 0.001$, 1783–2016). In regulated rivers, correlations were weaker (MVA : $r = 0.29$, $p = 0.004$, 1922–2016 ; N : $r = -0.14$, $p = 0.186$, 1922–2016). Generally, the amplitude of interannual variability was higher in MVA than in N chronologies (Fig. 2.5) and these two variables were negatively intercorrelated (Lake Duparquet: $r = -0.65$, $p < 0.001$, $n = 244$; Harricana: $r = -0.47$, $p < 0.001$, $n = 232$; upper Ottawa: $r = -0.41$, $p < 0.001$, $n = 199$; Abitibi: $r = -0.58$, $p < 0.001$, $n = 175$; and Mattagami River: $r = -0.28$, $p < 0.05$, $n = 92$). The highest spring discharge years reconstructed for the Harricana River were well captured by MVA and N chronologies from Lake Duparquet, and natural rivers. Each of those chronologies showed 1947 and 1960 as the highest spring discharge magnitude in the last 250 years and the years 1880, 1890, 1922, 1989, 2013, and 2014 also shared particularly high values (Fig. 2.5).

Correlations of earlywood vessel chronologies among river basins and hydrological regimes (Table 2.4) and with hydrometric records (Table 2.5; Fig. 2.1) were highly significant. As with flood-ring chronologies, associations with earlywood vessel chronologies were found to be highest with Lake Duparquet, higher among natural rivers than for regulated rivers and to weaken with increasing distance from Lake Duparquet (Table 2.4, Table 2.5). The lowest correlations were found between the

MVA and N chronologies from the upper Ottawa River and the southernmost hydrometric record of Kipawa River, both flowing South to the Saint-Lawrence River (Table 2.4, Table 2.5). Compared to the N chronologies, the MVA chronologies were less associated among river basins and showed a greater number of significant correlations (10/10 vs 4/10 for MVA; Table 2.4). In the structure of correlations between earlywood vessel chronologies and hydrometric records, the opposite was observed. The associations between MVA and hydrometric records were about twice as high as with N and showed a greater number of significant associations (Table 2.5).

Table 2.3 Pearson's correlations (r) and p -values (p) between continuous earlywood vessels chronologies from the naturally flowing Lake Duparquet ($n = 43$), Harricana River (site HAR, $n = 2$), Abitibi River (site LAR, $n = 2$), upper Ottawa River (site PSL, $n = 1$) and the regulated Mattagami River (site MGR, $n = 1$). Chronologies abbreviation are as follows: (MVA) mean cross-sectional lumen area of earlywood vessels, (N) number of earlywood vessels. Pearson's correlation coefficients are given for the common period 1922–2016 and bold characters denote p -values < 0.05 .

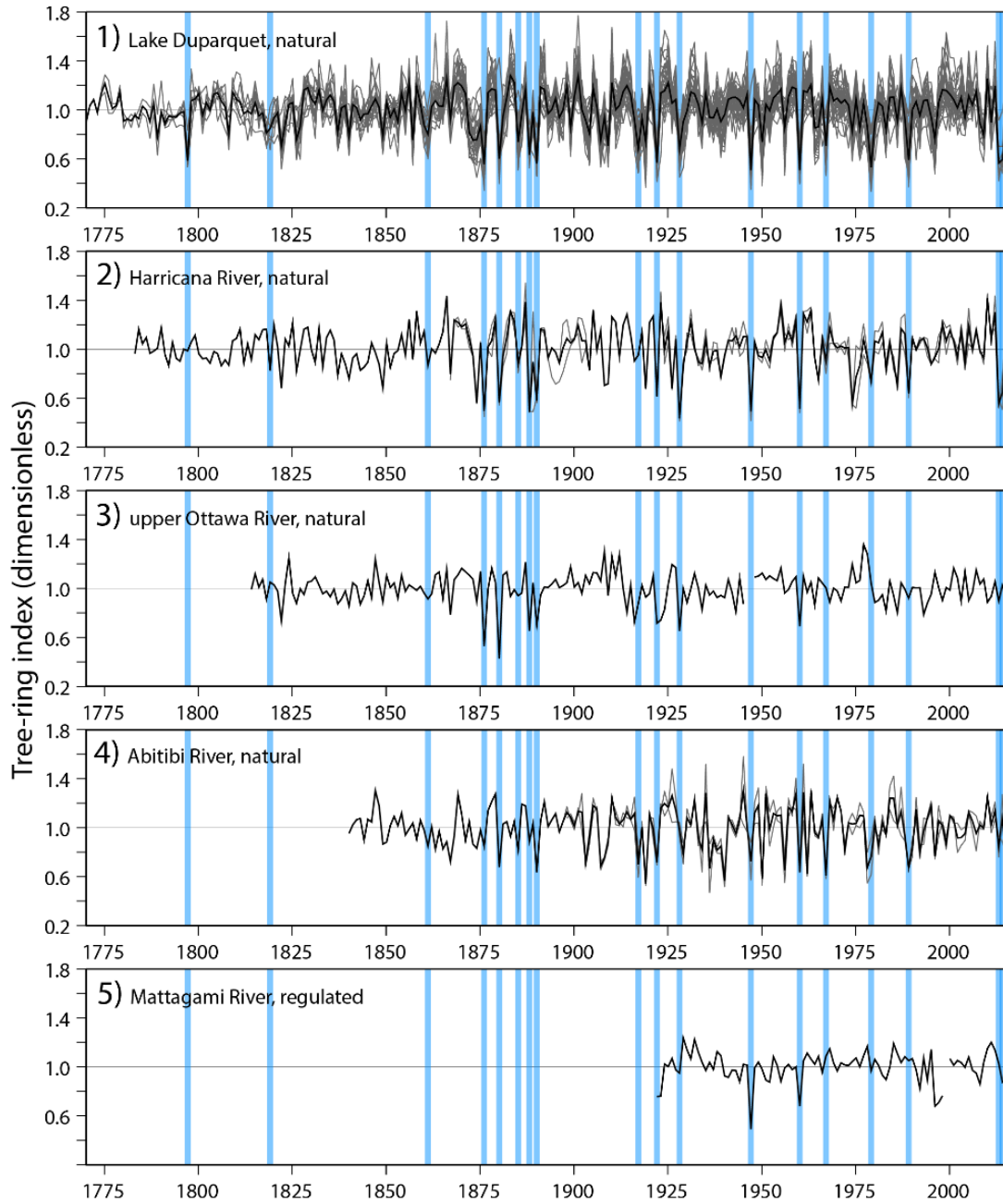
Sites / Chronologies		MVA	N
Duparquet / Harricana	r	0.81	0.71
	p	0.000	0.000
Duparquet / Abitibi	r	0.61	0.59
	p	0.000	0.000
Duparquet / upper Ottawa	r	0.20	0.51
	p	0.055	0.000
Duparquet / Mattagami	r	0.31	0.50
	p	0.003	0.000
Harricana / Abitibi	r	0.41	0.41
	p	0.000	0.000
Harricana / upper Ottawa	r	0.15	0.40
	p	0.141	0.000
Harricana / Mattagami	r	0.19	0.43
	p	0.060	0.000
Abitibi / upper Ottawa	r	0.17	0.37
	p	0.100	0.000
Abitibi / Mattagami	r	0.19	0.35
	p	0.066	0.000
Mattagami / upper Ottawa	r	0.15	0.28
	p	0.160	0.007

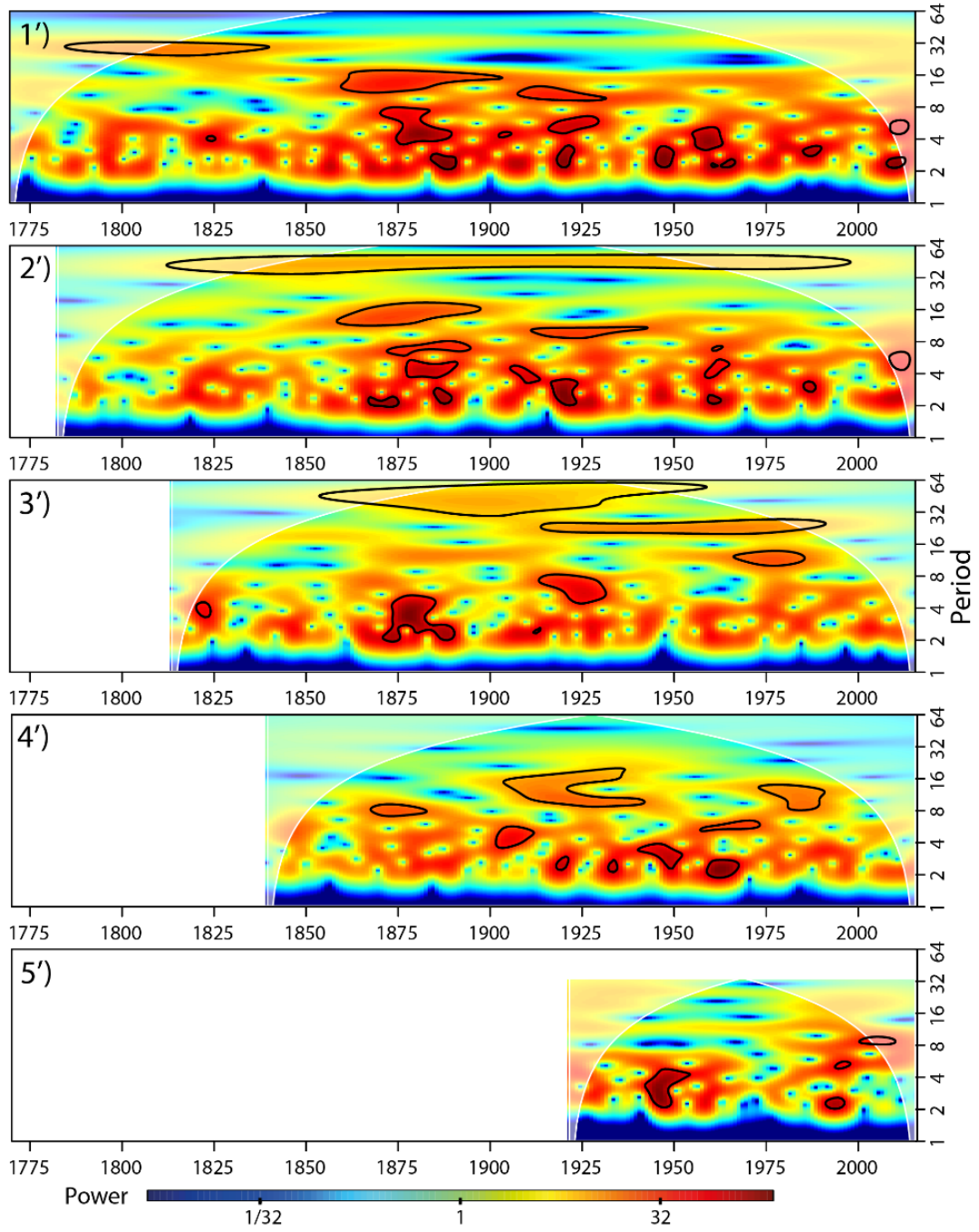
Table 2.4 Pearson's correlation coefficients (r) and p -values (p) between chronologies of mean lumen cross-sectional area (MVA) and number (N) of earlywood vessels, from four river basins and 10 instrumental records of April 15 to June 30 mean discharge across the study area. The field "Id" is the Canadian federal hydrometric station identification number. The table is ordered by increasing distance between hydrometric stations and Lake Duparquet (left to right) to visualize spatial coherency in the correlation structure. Bold characters denote p -values < 0.05 .

Station	Kinojévis River	Kinojévis River	Blanche River	Harricana River	Porcupine River	Kipawa River	Turgeon River	Missinaibi River	North French River	Missinaibi River
Id	02JB013	02JB003	02JC008	04NA001- 2	04MD004	02JE015	04NB001	04LM001	04MF001	04LJ001
Period	1971– 2016	1938– 1965	1970– 2016	1915–2016	1977– 2015	1963– 2011	1969– 1999	1973– 2016	1967– 2016	1921– 2016
N years	46	28	47	102	26	38	24	43	50	96
Distance (km)	30	70	80	85	130	155	170	310	310	320
RECI (1771–2016)	r 0.86 p 0.000	r 0.93 p 0.000	r 0.76 p 0.000	r 0.82 p 0.000	r 0.80 p 0.000	r 0.55 p 0.000	r 0.73 p 0.000	r 0.69 p 0.000	r 0.52 p 0.000	r 0.57 p 0.000
MV	r -0.83 p 0.000	r -0.84 p 0.000	r -0.74 p 0.000	r -0.78 p 0.000	r -0.80 p 0.000	r -0.49 p 0.002	r -0.76 p 0.000	r -0.66 p 0.000	r -0.54 p 0.000	r -0.56 p 0.000
Lake Duparquet (1770–2016)	r 0.67 p 0.000	r 0.72 p 0.000	r 0.61 p 0.000	r 0.62 p 0.000	r 0.75 p 0.000	r 0.22 p 0.179	r 0.64 p 0.001	r 0.57 p 0.000	r 0.55 p 0.000	r 0.46 p 0.000
MV	r -0.84 p 0.000	r -0.8 p 0.000	r -0.6 p 0.000	r -0.81 p 0.000	r -0.69 p 0.000	r -0.57 p 0.000	r -0.57 p 0.004	r -0.56 p 0.000	r -0.34 p 0.017	r -0.49 p 0.000
Harricana River (1783–2016)	r 0.47 p 0.001	r 0.60 p 0.001	r 0.40 p 0.006	r 0.53 p 0.000	r 0.40 p 0.043	r 0.18 p 0.268	r 0.17 p 0.438	r 0.23 p 0.132	r 0.32 p 0.026	r 0.24 p 0.017
MV	r -0.41 p 0.005	r -0.49 p 0.009	r -0.25 p 0.097	r -0.48 p 0.000	r -0.65 p 0.000	r -0.27 p 0.105	r -0.66 p 0.001	r -0.61 p 0.000	r -0.51 p 0.000	r -0.52 p 0.000
Abitibi River (1840–2016)	r 0.44 p 0.002	r 0.42 p 0.027	r 0.48 p 0.001	r 0.42 p 0.000	r 0.75 p 0.000	r 0.21 p 0.199	r 0.49 p 0.015	r 0.61 p 0.000	r 0.44 p 0.001	r 0.51 p 0.000
MV	r 0.21 p 0.156	r -0.44 p 0.018	r 0.14 p 0.338	r -0.18 p 0.065	r -0.14 p 0.510	r 0.42 p 0.009	r 0.33 p 0.120	r 0.09 p 0.570	r 0.17 p 0.235	r -0.10 p 0.317
Upper Ottawa River (1814–2016)	r 0.29 p 0.052	r 0.53 p 0.004	r 0.37 p 0.011	r 0.38 p 0.000	r 0.33 p 0.102	r 0.20 p 0.224	r 0.09 p 0.671	r 0.13 p 0.403	r 0.06 p 0.661	r 0.24 p 0.019
MV	r -0.07 p 0.651	r -0.46 p 0.015	r -0.05 p 0.741	r -0.22 p 0.031	r -0.33 p 0.095	r -0.28 p 0.093	r 0.33 p 0.110	r -0.26 p 0.093	r -0.12 p 0.391	r -0.27 p 0.008
Mattagami River (1922–2016)	r 0.34 p 0.022	r 0.45 p 0.016	r 0.42 p 0.004	r 0.43 p 0.000	r 0.45 p 0.022	r 0.30 p 0.069	r 0.15 p 0.491	r 0.42 p 0.005	r 0.26 p 0.069	r 0.30 p 0.004

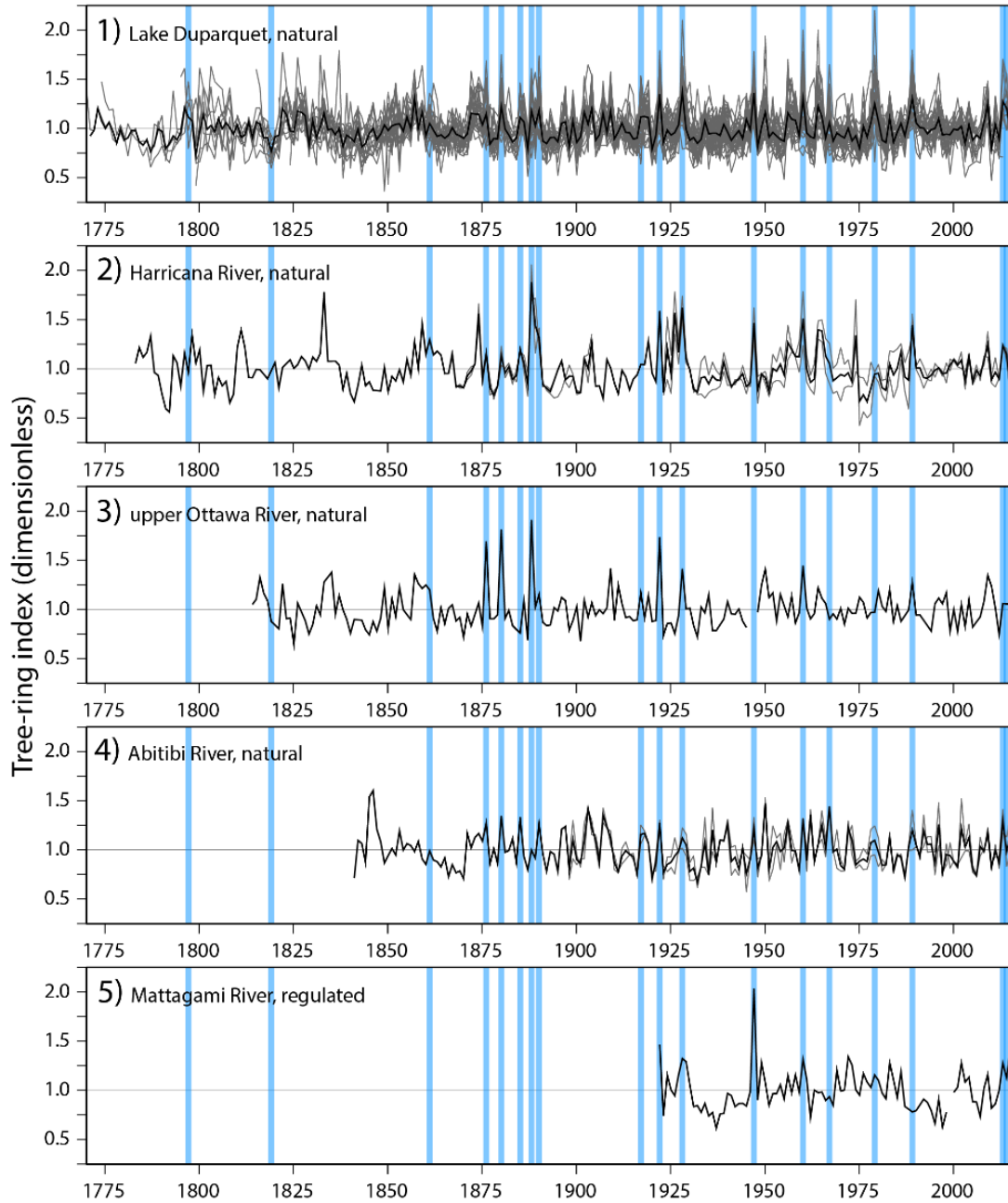
► Figure 2.5 Comparison between continuous earlywood vessel chronologies and their continuous wavelet transform among river basins. A) Chronologies of mean earlywood vessel cross-sectional (MVA). B) Chronologies of number of earlywood vessels (N). Left panel is the comparison between chronologies from Lake Duparquet and from the four river basins. The vertical blue bars indicate the 18 years with the highest reconstructed spring discharge for the Harricana River and over the last 250 years. Those 18 years were defined using a threshold corresponding to the mean + 1.5 SD (threshold value = 151.3 m³/s; Nolin et al., 2021a). Right panel is the decomposition of mean standardized chronologies into Morlet 6th power in continuous wavelet transform. The color bar gives the range of variance intensity from low (blue) to high (red) and black lines encircle significant high variance tested against a white noise background at a *p*-value < 0.05. The cone of influence is figured in white and delimit areas where wavelets are altered by edge-effect. For both A) and B) right and left panels, chronologies are as follow: 1) Lake Duparquet, 1771–2016, *n* = 43; 2) Harricana River basin, site HAR, 1783–2016, *n* = 2; 3) upper Ottawa River basin, site PSL, 1814–2016, *n* = 1; 4) Abitibi River, site LAL, 1840–2016, *n* = 2 and 5) Mattagami River, site MGR, 1922–2016, *n* = 1. The Lake Duparquet, Harricana, Abitibi and upper Ottawa River chronologies were developed from trees growing with natural discharge, while the Mattagami River basin index is from a site where the river is regulated by a dam.

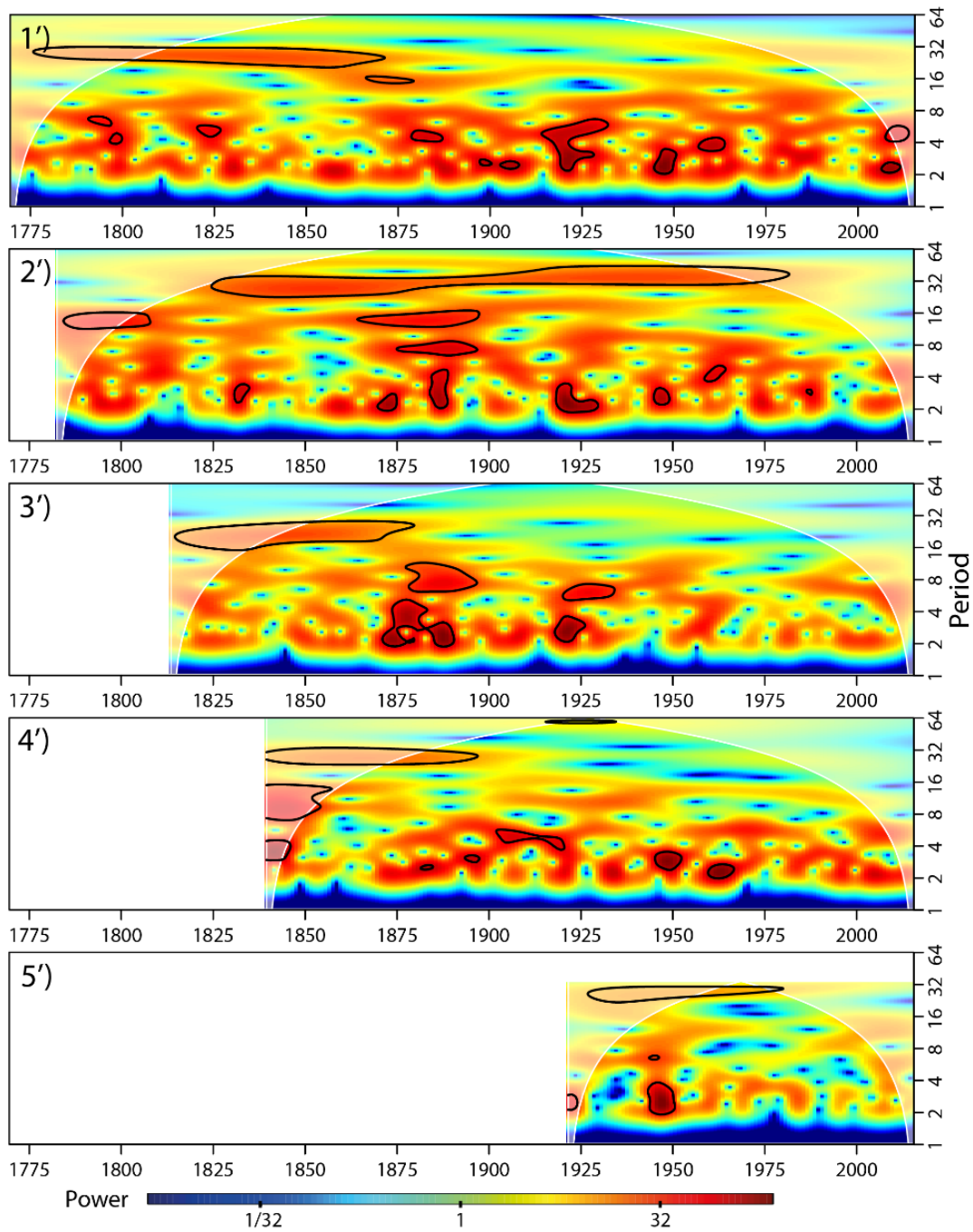
A) Mean earlywood vessel area (MVA)





B) Number of earlywood vessels (N)





Continuous wavelet transformation allowed to investigate the temporal coherency of the earlywood vessel chronologies from the different hydrological regimes ($n = 1$ or $n = 2$ trees) to the more robust Lake Duparquet MVA and N chronologies ($n = 43$ trees). Since the MVA and N chronologies were significantly correlated with the regional spring discharge records, it can be hypothesized that the decomposition of their periodicities may reflect the decomposition of periodicities affecting regional spring discharge. Three major patterns of significant high variance were observed in the power spectrum of chronologies from natural regimes (Fig. 2.5 right panels). A first pattern of 32-year significant periodicity was persistent in MVA and N chronologies from Lake Duparquet up to ~1850 and persisted from ~1800 to 1975 in the Harricana River chronologies. In the upper Ottawa River chronologies, only the MVA showed a significant 32-year periodicity affecting the variance from ~1850 to 1950. A second pattern near a 16-year periodicity was more variable over time and between river basins than the 32-year pattern. It started around 1850 in Lake Duparquet and around 1900 in other chronologies from natural rivers. A third pattern was the apparition of decadal periodicities of 8-years and less from ~1875 and 1900 in chronologies from natural rivers except the upper Ottawa River. The chronologies from the regulated Mattagami River began in 1922 and were not long enough to support the accurate calculation of high periodicities (low frequencies). However, the N chronology showed significant high variance similar to that found in natural rivers chronologies. Notably, around a decadal periodicity in 1940 and around a 32-year periodicity from 1925 to 1980, although outside the cone of influence (Fig. 2.5).

2.6 Discussion

2.6.1 Spatial coherency among spring flood proxy from natural rivers

In this study, results showed that both flood-ring chronologies (F1, F2, F12) and earlywood tree-ring anatomical chronologies (MVA and N), hereafter referred to as spring flood proxies, were highly intercorrelated. Spring flood proxies were strongly correlated to Harricana River spring discharge and to instrumental data from eleven hydrometric records distributed across a wide boreal territory (above 70 000 km²). Spring flood proxies provided synchronous evidence of flooding across the four river basins with most of the major spring floods reconstructed for the Harricana River for the last 250 years being recorded by *F. nigra* trees growing along Lake Duparquet and natural rivers. Major spring floods were also recorded by *F. nigra* trees from regulated rivers but i) in comparison by very few trees and ii) more often in the form of weakly defined flood rings. The signal strength although appears to decrease with geographical distance to Lake Duparquet and in regulated rivers. The high proportion of individual tree showing significant correlation to the reconstructed Harricana River spring discharge among natural and, to a lesser extent, regulated rivers also support strong spatial coherency. These results confirm the hypothesis of a common hydroclimatic variability among the four river basins sampled. These results are also in line with studies reporting highly significant associations between mean cross-sectional earlywood vessel lumen area (MVA) chronologies from Lake Duparquet and the instrumental regional spring discharge data (Tardif et al., 2010; Kames et al., 2016; Nolin et al., 2021a). These results also support the fact that the increase in spring flood frequency and magnitude reported by Nolin et al. (2021a) since the end of the Little Ice Age is regionally coherent.

The similarities found at low frequencies in earlywood vessel chronologies also support spatial coherency between Lake Duparquet and natural rivers and point towards a

decrease in the periodicities of high spring discharge since at least 1850. The frequency of high spring discharge may have changed from a persistent multi-decadal periodicity in the late 19th to early 20th century to a decadal and then interannual periodicity in the late 20th century. This result compares well with those of previous studies conducted in Lake Duparquet (Tardif & Bergeron, 1997b; Nolin et al., 2021a) and hypothesizing a long-term increase in the frequency and magnitude of spring flooding since the end of the Little Ice Age (1850–1870; Matthews & Briffa, 2005). Ideally, the CWT analysis would have been conducted on a large number of samples per river basins to extract the strongest possible common signal, as it was done with the MVA and N chronologies from Lake Duparquet. Indeed, it is possible that factors related to age or stand dynamics may interfere with the hydroclimatic signal in earlywood vessel chronologies (Tardif & Conciatori, 2006b). For example, the sample from upper Ottawa River presented a lot of suppressed years (very small annual ring width) and its MVA chronology was not significantly correlated with that of Lake Duparquet. However, the consistency expressed by the MVA and N chronologies consisting of 1 to 2 trees per river basin compared to the robust Lake Duparquet chronologies ($n = 43$) still demonstrates a strong common signal at both high and low frequencies. It was also demonstrated that five *F. nigra* samples may be sufficient to reconstruct most of the interannual variability of the Harricana River spring discharge during the 20th century ($EPS > 0.85$, $Rbar > 0.20$; Nolin et al., 2021a). Given the similarities observed in the power spectrum of the sampled rivers, it would nevertheless be interesting to conduct this CWT analysis on a larger number of samples and to study their associations with large-scale atmospheric circulations in North America and at different periodicities.

2.6.2 Comparison of spring flood proxies among natural rivers, regulated rivers, and unflooded control sites.

Compared to *F. nigra* trees growing along the floodplain of naturally flowing rivers, those from regulated rivers (and from unflooded sites) recorded flood rings less

frequently and mainly of the weaker type (F1). Flood-ring chronologies from regulated rivers showed little interannual variability and were also less correlated with hydrometric records. Spring floods identified by flood rings were most coherent with those of natural rivers prior to dam creation in the 1920s and for a few extreme floods thereafter (*e.g.*, 1947, 1960). Some weak flood rings (F1) were also recorded on regulated rivers although they have not been recorded on natural rivers and Lake Duparquet and could be the result of dam management maneuvers. Furthermore, trees were generally younger in floodplain sites located along regulated rivers compared to that along natural rivers and Lake Duparquet, suggesting that the construction of the dams may have had a detrimental effect on the existing ash forests. In hydrological system that were regulated, DeWine & Cooper (2007) demonstrated for instance, that dam construction threatened the recruitment and the persistence of old-growth riparian forests in the upper Colorado River. Historically in Ontario, most dams were built to raise the water level to the high-water mark identified by surveyors using signs on the landscape (Ontario Geological Survey, 1920). Since the dams were built to hold water until the maximum natural flood elevation, it is likely that the old riparian forests have been permanently flooded and removed from the landscape. The potential to accurately reconstruct the historical variability of today's regulated rivers can therefore be lower due to a lack of ancient trees. However, the few trees sampled on the regulated rivers did record flood rings and this demonstrates that flood ring can be suitable proxy to retrieve partial historical discharge records from the trees growing in the shoreline of regulated rivers.

In addition, further work is needed to assess sites differences in regulated hydrological systems. Our results indicated variations in the recording of flood rings by *F. nigra* trees located along lakes regulated by downstream dams (single-dam system) and rivers regulated by both upstream and downstream dams (multi-dam system). It would be interesting to systematically compare flood rings in trees located upstream and

downstream of dams, and according to their position on the bank relative to the shoreline, to determine if the hydrological signal provided by flood ring can be improved by a more targeted sampling strategy. Differences in height between dams may also have impacted downstream water levels and flood rings differently.

In the unflooded control sites, the trees were as old as at Lake Duparquet but had little or no flood rings with solely few F1 being observed. The maximum value of F12 never reached more than 10% and flood rings were not consistent among samples. They also did not match the years for which flooding was observed in other river basins, either from the spring flood proxies, the reconstruction of the Harricana River spring discharge or from the regional hydrometric records. This confirms that *F. nigra* trees from flooded and unflooded sites carry different climatic signals, mainly because their exposures to water stress and drought are different (Tardif & Bergeron, 1997a; Kames, 2009). Previous studies in the Lake Duparquet region showed, for example, that earlywood vessel chronologies from unflooded non-riparian *F. nigra* stands were i) not significantly correlated to those developed from flooded riparian stands and ii) presented no significant correlations with instrumental spring discharge (Kames, 2009). This is also sustained by ring-width chronologies developed by Tardif & Bergeron, (1997a) and Kames (2009) showing a lack of crossdating between riparian and non-riparian *F. nigra* trees. The physiological mechanisms of flood-ring formation are still poorly understood, but it was hypothesized that stem submersion induces the production of ethylene which, in turn, interacts with other growth regulators thus affecting the formation of earlywood vessels (Yamamoto et al., 1995; St. George et al., 2002; Copini et al., 2016). It is therefore unlikely that periods of high humidity (runoff, rainfall, etc.) in topographically flat upland forests will cause a physiological response similar to that of flooding in riparian forests.

2.6.3 Adequacy between spring flood proxies, advantages and limitations

Spring flood proxies developed in this study (F1, F2, F12, MVA, N) were shown to provide similar and complementary information on high spring discharge variability at an annual resolution. The continuous quantitative measurement of earlywood vessels allowed the extraction of a broader spectrum of hydrological variability compared to the semi-quantitative visual identification of flood rings which provided event-year chronologies.

Among the flood-rings chronologies, F1 and F2 in Lake Duparquet and natural rivers captured very comparable signal but their summation (F12) captured a slightly broader spectrum of hydrological conditions associated with high spring discharge. This result suggest that it is worth identifying both weak (F1) and strong (F2) flood-ring types. It is hypothesized that differences between F1 and F2 in *F. nigra* trees for a given year may be reflecting differences in coring height or tree exposure (elevation and topography) to flooding. In flood years, it has been shown that the decrease in earlywood vessel size is maximum at the base of the trees with a gradual decrease along the trunk height (St. George & Nielsen, 2002; St. George et al., 2002). Furthermore, the timing, intensity and duration of spring floods will also impact the ability of riparian *F. nigra* trees to record a flood ring. St. George et al. (2002) had showed, for instance, that the duration of flooding had a greater influence than the peak flood stage on the size of earlywood vessels in flooded *Quercus macrocarpa*.

Among the anatomical chronologies, MVA and N showed comparable associations to instrumental and reconstructed spring discharge. Although we cannot robustly assert this result given the limited number of samples that have been used, associations between N chronologies and spring discharge were generally higher between river basins and in regulated rivers than with MVA chronologies. It could thus be hypothesized that earlywood vessels area and number carry slightly different

hydrological signal associated with spring flooding in natural and regulated rivers. Kames et al. (2016) showed that the MVA and N chronologies extracted from flooded *F. nigra* trees from Lake Duparquet were associated with climate at slightly different periods. The MVA and N chronologies were associated with mean monthly temperatures and total precipitation from April to May and April to June, respectively.

In terms of advantages and limitations, the use of the various spring flood proxies, (F12, MVA or N) depends on the objectives pursued and the resources available (*e.g.*, number of trees, equipment). While quick to develop, visually derived flood-ring chronologies like that of numerous pointer years involve processing a larger number of samples and require conventional dendrochronology equipment (Tardif & Conciatori, 2006a; Therrell & Bialecki, 2015; Meko & Therrell, 2020). Continuous earlywood vessels chronologies require fewer samples but is demanding in image analysis equipment and software, as well as extensive analysis time (Kames et al. 2016, Nolin et al., 2021a). Relative frequencies provide information on the number of samples affected per year, while continuous chronologies provide annual quantitative information (Tardif & Conciatori, 2006a). However, it could be hypothesized that, as the number of samples increases, the relative frequency of flood rings could approximate the hydrological signal extracted by earlywood vessel chronologies composed of far fewer samples. It would thus be possible to use relative frequencies of flood rings as spring discharge predictors in reconstruction models, even if conventionally flood-ring frequencies has been used to identify past flooding and not for the purpose of quantitative reconstruction (St. George & Nielsen, 2002; Therrell & Bialecki, 2015; Meko & Therrell, 2020). Examples of approaches combining both discrete and continuous flood proxies to reconstruct spring discharge can be found in Boucher et al. (2011) and in Nicault et al. (2014).

2.7 Conclusion

In a context of climate change, river regulation, and disappearance of old riparian forests, the study of spring flood proxies is becoming a necessity in water management and flood risk assessment in northern territories. This study demonstrated the strong spatial coherency associated with the use of two spring flood proxies in naturally flowing rivers from eastern boreal Canada. It also stressed the potential limitation associated with the use of flood rings from trees growing along regulated water bodies. Flood rings and direct measurement of the earlywood vessels captured high-resolution, comparable, and complementary spring flooding evidence. Even in regulated rivers, partial spring flooding history can be inferred from flood rings prior to dam creation. Results underline the potential and utility of extending the use of these spring flood proxies in dendrohydrology. Future work could study flood rings over a larger area by sampling, for example, one natural river per watershed to monitor historical trends in large-scale spring floods and study the potential effects of climate change. Flood-ring methods could be applied to more southern river basins such as Saint-Lawrence River or Ottawa River. It would then be necessary to study the presence of flood rings in species such as green ash (*Fraxinus pennsylvanica* Marsh.) or potentially in diffuse-porous species.

2.8 Acknowledgments

We acknowledge the special support of Mélanie Desrochers (UQÀM), Martin P. Girardin (CFL), Lars Hildebrandt and Gordon Kayahara (Ontario Forest Service) for their help in the production of the detailed forest maps. We thank field assistants Cyrielle Ducrot, Stéphane Hébert, Chloé Lavelle, Isabelle Gareau, and Ralitsa Mincheva, as well as Johanna M. Robson and Hollie Swart from the University of Winnipeg DendroEcology Lab. We also thank the FERLD research station team and especially Danielle Charron and Raynald Julien for their continuous support over the two summers of field work. This study was a contribution of Canada Research Chairs (NSERC-CRC) hold by YB and JT and was funded by the Natural Sciences and Engineering Research Council of Canada Collaborative research program including our partners Ouranos, Hydro-Québec, Ontario Power Generation (OPG) and The University of Winnipeg. This work was also supported by a scholarship from RIISQ – Intersectorial Flood Network of Québec (2nd Program 2020–2021) awarded to AN. Earlier versions of the manuscript benefited from constructive comments by Susanne Kames (U of Winnipeg), Jacinthe Clavet-Gaumont and David Huard (Ouranos), as well as Kurt C. Kornelsen (OPG). We also acknowledge the contributions of the Editor-in-Chief (Pr. Marco Borga) and both reviewers (Pr. Matthew Therrell, and anonymous) who provided constructive comments/suggestions on earlier drafts of the manuscript.

2.9 Data availability

Relevant data for this study are available from Nolin, A. F., Tardif, J. C., Conciatori, F., & Bergeron, Y. (2021). *Fraxinus nigra* tree-ring dataset for flood history study among major river basins near the Lake Duparquet, eastern boreal Canada. Mendeley Data, v1. <http://dx.doi.org/10.17632/94vjr69fb2.1>. Data include flood ring (F1, F2) and earlywood vessel chronologies (MVA, N) derived from *Fraxinus nigra* trees growing in eastern boreal Canada near Lake Duparquet (Québec, Canada).

F1_F2_chrono.csv, as in Fig. 2.3, the F1 and F2 flood-ring chronologies per sites (sites are coded as in Table 2.1) with sample replication (n) to reproduce flood-ring frequencies;

LAT_LON.kml, the coordinate data for each site and sampled tree;

MVA_N_chrono.csv, as in Fig.2.5, the MVA and N chronologies per river basins (river basins are coded as in Table 2.1);

RECI.csv, the reconstruction of the Harricana River spring discharge from 1771 to 2016 reported in "Multi-century tree-ring anatomical evidence reveals increasing frequency and magnitude of spring discharge and floods in eastern boreal Canada" published in "Global and Planetary Change" by Nolin et al. 2021a.

metadatas.txt, a set of self-explanatory instructions and descriptions for data files.

All other data are available upon request to the corresponding author at alexandreflorent.nolin@uqat.ca (institutional email), alexandreflorent.nolin@gmail.com (permanent email).

2.10 Supplementary Materials

Table 2.S1 Comparison of years of hydropower dam commissioning and years of operation of water survey of Canada (WSC) hydrologic stations. References are given besides in-service years and listed at the bottom of the table.

River	Dam	In-service year	WSC Station	WSC record length
Abitibi River	Abitibi Canyon	1933 ^{1,3}	04ME002	1929–1994
Abitibi River	Frederick House Lake	1938 ³	04MD001	1938–1994
Abitibi River	Iroquois Falls	1914 ²	04MC001	1920–1995
Abitibi River	Island Falls	1925 ^{2,3}	04ME001	1924–1967
Abitibi River	Monteith Dam	1953 ⁶	04MB002	2006–2019
Abitibi River	Otter Rapids	1961 ^{1,3}	04ME004	1961–1994
Abitibi River	Twin Falls	1921 ³ ; 1922 ²	04MC002	1949–1995
Mattagami River	Little Long Rapids	1963 ^{1,3}	04LG003	1963–1994
Mattagami River	Peter Long Lake*	1916 ¹	/	/
Mattagami River	Sandy Falls*	1911 ¹	/	/
Mattagami River	Smoky Falls	1926 ⁵ ; 1928 ³	04LG001	1926–1963
Mattagami River	Smooth Rock Falls	1916 ³	04LB001	1920–1997
Mattagami River	Wawaitin Falls*	1912 ¹	/	/

* dam is not equipped with a hydrologic station.

(1) Ontario Power Generation (2020) Hydroelectric power & River System data. <https://www.opg.com/powering-ontario/our-generation/hydro/river-system-data/> [2020, June 23];

(2) H2O Power (2020) H2O Power Locations. <https://www.h2opower.com/our-locations/> [2020, June 23];

(3) Natural Resources Canada (2009) Atlas of Canada 1,000,000 National Frameworks Data. Hydrology – Dams. FTP Archived Open Government Catalogue. http://ftp.geogratis.gc.ca/pub/nrcan_rncan/archive/vector/framework_cadre/hydrology/analytical/drainage_supplemental/dams/ [2020, June 23];

(4) Centre d'Expertise Hydrique du Québec (CEHQ). (2019). Répertoire des barrages. Ministère de l'Environnement et de la Lutte contre les Changements climatiques. Gouvernement du Québec, Ottawa. Available at <https://www.cehq.gouv.qc.ca/barrages/default.asp> [June 23, 2020];

(5) Ontario River Alliance (2014) Smoky Falls Generating Station, Mattagami River. <http://www.ontarioriversalliance.ca/smoky-falls-generating-station-mattagami-river/> [June 23, 2020]

(6) Ontario Shared Services (2020) Notice of Proposed Procurement for the Monteith Dam Replacement n° 00002081816.

<https://www.merx.com/public/solicitations/nce/852737790/abstract#:~:text=Monteith%20Dam%20is%20located%20on%20the%20Driftwood%20River%2C,is%20in%20poor%20condition%20and%20must%20be%20replaced.> [January 25, 2021]

Table 2.S2 List of hydrometric stations. The abbreviations of the data sources are as follows: Water Survey of Canada (WSC), Reference Hydrometric Basin Network (RHBN) and Centre d'Expertise Hydrique du Québec (CEHQ). The field No. correspond to the legend in Fig. 2.1. The field "Distance (Km)" is the relative distance to Lake Duparquet.

No.	Station Name	Federal Id	Source	Distance (km)	Lat/Lon	Drainage Area (km ²)	Period	N years	N missing daily values
1	Kinojévis River	02JB013	CEHQ	30	48°22' N; 78°51' W	2,590	1971–2016	46	0
2	Kinojévis River	02JB003	CEHQ	70	48°27' N; 78°21' W	1,680	1938–1965	28	0
3	Blanche River	02JC008	RHBN	80	47°53' N; 79°52' W	1,780	1970–2016	47	0
4	Harricana River	04NA002	RHBN	85	48°34' N; 78°07' W	3,680	1915–1933	19	0
5	Harricana River	04NA001	RHBN	85	48°36' N; 78°06' W	3,680	1934–2016	83	0
6	Porcupine River	04MD004	WSC	130	48°33' N; 81°03' W	408	1977–2015	26	0
7	Kipawa River	02JE015	WSC	155	47°04' N; 79°18' W	5,980	1963–2011	38	0
8	Turgeon River	04NB001	CEHQ	170	49°59' N; 79°05' W	11,200	1969–1999	24	6
9	Missinaibi River	04LM001	WSC	310	50°35' N; 82°05' W	22,900	1973–2016	43	0
10	North French River	04MF001	RHBN	310	51°04' N; 80°46' W	6,680	1967–2016	50	0
11	Missinaibi River	04LJ001	RHBN	320	49°36' N; 83°16' W	8,570	1921–2016	96	0

Table 2.S3 Comparison between the 18 highest reconstructed spring discharge years and the F12 flood-ring relative frequencies. Values highlighted in grey denote F12 flood-ring frequencies greater than 75% at Lake Duparquet (DPL), 50% at natural rivers (NAT) and 10% for regulated rivers (REG). On the left side are represented the 18 highest spring discharge years for which the average discharge from April 15 to June 30 reconstructed from 1771–2016 (REC1) value was greater than 151.3 m³/s. This threshold was calculated over the 1771–2016 period as the mean + 1.5 standard deviation. On the right side, are the other years for which the F12 flood-ring relative frequencies were above the thresholds (75%, 50% and 10% in DPL, NAT and REG sites) and compared to REC1.

Year	REC1	DPL	NAT	REG	Year	REC1	DPL	NAT	REG
1797	161.00	75.0	40.0	0.0	1808	139.16	66.7	60.0	0.0
1819	157.43	0.0	0.0	0.0	1826	148.88	66.7	50.0	0.0
1861	153.64	53.8	10.3	0.0	1834	118.86	0.0	8.3	33.3
1876	171.29	88.6	71.0	9.1	1896	128.15	18.0	13.0	23.1
1880	160.10	93.3	58.3	25.0	1897	116.17	24.0	4.3	13.3
1885	159.00	78.3	21.5	7.7	1903	124.67	46.2	20.4	15.8
1888	164.57	93.6	69.5	30.8	1907	151.05	81.1	27.9	37.5
1890	170.25	95.8	60.2	23.1	1908	125.70	51.9	52.7	4.2
1917	159.52	96.4	46.8	25.7	1909	149.43	81.5	40.7	12.5
1922	173.66	100.0	63.3	34.8	1919	140.75	91.1	58.6	10.0
1928	175.57	94.7	72.7	13.3	1950	134.24	82.8	32.6	6.6
1947	177.34	100.0	89.6	39.2	1956	125.02	76.6	20.7	2.5
1960	179.95	98.4	93.3	30.7	1965	119.56	69.2	44.4	14.3
1967	163.59	84.6	51.3	2.2	1974	147.05	60.0	68.7	3.4
1979	184.86	98.4	68.3	11.3	1983	144.61	57.8	14.8	13.2
1989	161.72	92.2	69.3	6.5	2009	138.62	67.9	41.8	11.9
2013	170.90	93.3	76.4	15.6					
2014	160.52	86.0	57.5	6.8					

CHAPITRE III

FLOOD-RING PRODUCTION MODULATED BY RIVER REGULATION IN
EASTERN BOREAL CANADA

Alexandre F. Nolin, Jacques C. Tardif, France Conciatori, Yves Bergeron

Publié dans *Frontiers in Plant Science*
*Functional Plant Ecology - Quantitative wood anatomy to explore tree responses to
global change* (special issue)

Octobre 2021

3.1 Abstract

In northeastern boreal Canada long-term perspective on spring flooding is hampered by the absence of long gauge records. Changes in tree-ring anatomy of periodically flooded trees have allowed reconstruction of historical floods in unregulated hydrological systems. In regulated rivers, the study of flood rings could recover past flood history, assuming that the effects of hydrological regulation on their production can be understood. This study analyzes the effect of regulation on the flood ring occurrence (visual intensity and relative frequency) and on ring widths in *Fraxinus nigra* trees growing at five sites distributed along the Driftwood River floodplain. Driftwood River was regulated by a dam in 1917 that was replaced at the same location in 1953. Ring width revealed little to no evidence of the impact of river regulation, in contrast to the flood-rings. Prior to 1917, high relative frequencies of well-defined flood rings were recorded during known flood years, as indicated by significant correlations with reconstructed spring discharge of the nearby Harricana River. After the construction and the replacement of the dam, relative frequencies of flood rings and their intensities gradually decreased. Flood-ring relative frequencies after 1917 and particularly after 1953 were mostly composed of weakly defined (less distinct) flood rings with some corresponding to known flood years and others likely reflecting dam management. Strength of the correlations with the instrumental Harricana River discharge also gradually decrease starting after 1917. Compared to upper floodplain trees, shoreline trees at each site recorded flood rings less frequently following the construction of the first but especially of the second dam, indicating that water level regulation limited flooding in the floodplains. Compared to the downstream site to the dam, the upstream ones recorded significantly more flood rings in the post dam period, reemphasizing the importance of considering the position of the site along the river continuum and site conditions in relation to flood exposure. The results demonstrated that sampling trees in multiple riparian stands and along various hydrological contexts at a far distance of the dams could help disentangle the flooding signal from the dam management signal.

Keywords : dendrohydrology, black ash, *Fraxinus nigra*, earlywood vessels, Ontario

3.2 Résumé [Ajout à l'article original]

Dans le nord-est du Canada boréal, l'étude de la variabilité à long terme des inondations printanières est restreinte par l'absence de longs enregistrements hydrométriques. Les changements dans l'anatomie des cernes des arbres périodiquement inondés ont permis de reconstruire les inondations historiques dans les systèmes hydrologiques non régulés. Dans les rivières régulées, l'étude des cernes de crues pourrait permettre de retrouver l'histoire des inondations passées, en supposant que les effets de la régulation hydrologique sur leur production puissent être compris. Cette étude analyse l'effet de la régulation sur l'occurrence des cernes de crues (intensité visuelle et fréquence relative) et sur la largeur des cernes chez les arbres *Fraxinus nigra* poussant sur cinq sites répartis le long de la plaine inondable de la Driftwood River en Ontario. La Driftwood River a été régulée par un barrage en 1917 qui a été remplacé au même endroit en 1953. La largeur des cernes annuels a révélé peu ou pas de preuves de l'effet de la régulation de la rivière, contrairement aux cernes de crues. Avant 1917, des fréquences relatives élevées de cernes de crues bien définis ont été enregistrées pendant les années de crue connues, comme l'indiquent les corrélations significatives avec le débit printanier reconstitué de la rivière Harricana voisine. Après la construction et le remplacement du barrage, les fréquences relatives des cernes de crues et leurs intensités ont progressivement diminuées. Les fréquences relatives des cernes de crues après 1917 et surtout après 1953 étaient principalement composées de cernes de crues faiblement définis (moins distincts), certains correspondant à des années de crue connues et d'autres reflétant probablement la gestion du barrage. La valeur des corrélations avec le débit instrumental de la rivière Harricana a également diminué progressivement à partir de 1917. Sur chaque site, et par rapport aux arbres des plaines inondables, les arbres des berges ont enregistré des cernes de crues moins fréquemment après la construction du premier mais surtout du second barrage, ce qui indique que la régulation du niveau d'eau a limité les inondations dans les plaines inondables éloignées. Par rapport au site en aval du barrage, ceux en amont ont enregistré plus de cernes de crues dans la période post-barrage, ce qui souligne à nouveau l'importance de la position du site dans le continuum fluvial et des conditions du site par rapport à l'exposition aux inondations. Les résultats ont démontré que l'échantillonnage des arbres dans de multiples peuplements riverains et dans divers contextes hydrologiques (grande distance des barrages) pourrait aider à démêler le signal d'inondation du signal de gestion du barrage.

Mots-clés : dendrohydrologie, frêne noir, *Fraxinus nigra*, vaisseaux du bois initial, Ontario

3.3 Introduction

Over the last decades, extreme floods and droughts have become more recurrent and severe in eastern boreal Canada (Buttle et al., 2016; Bush and Lemmen, 2019; Aygün et al., 2019). Understanding if these recent trends are part of the natural hydrological variability is critical and studies remain complicated due to a lack of long instrumental hydrological series (Mortsch et al., 2015; Bush and Lemmen, 2019; Pellerin, 2019). Most gauge stations in remote northern rivers were installed in the 1920s following the construction of water regulation systems or hydroelectric facilities which reduced the availability of natural records (Pellerin, 2019; Nolin et al., 2021b). Therefore, biological proxies such as tree rings have provided hydrological time series in areas that lack instrumental records and have allowed dendrohydrologists to extend existing instrumental records when available.

Tree-ring proxies, among others, have been used to successfully reconstruct monthly, seasonal, and annual discharge (Boucher et al., 2011; Nolin et al. 2021a), lake level fluctuations (Lemay and Bégin, 2008), droughts (Girardin et al., 2006) and floods (Boucher et al., 2011; Tardif and Bergeron, 1997b). Recent studies of anatomical changes in tree rings of periodically flooded trees (*i.e.*, flood rings) have demonstrated their effectiveness in detecting major historical floods and comparing their magnitude (St. George et al., 2002; St. George et al., 2003; Tardif et al., 2010; Therrell and Bialecki, 2015; Kames et al., 2016; Meko and Therrell, 2020; Nolin et al., 2021a; Tardif et al., 2021a). In riparian ring-porous genus (*e.g.*, *Quercus*, *Fraxinus*) flooding of tree stems at the time of earlywood formation resulted in decreased earlywood vessel cross-sectional areas (*i.e.*, flood ring; St. George et al., 2002; Copini et al., 2016). Flood ring induced under experimental flooding conditions for amplitudes ranging from 3, 6 or 8 weeks in 4-years-old pedunculate oak (*Quercus robur* L.) trees indicated that their occurrence was independent of flooding duration (Copini et al., 2016).

Developing quantitative earlywood vessel chronologies led to significant reconstruction of high spring river discharge compared to the sole use of ring-width chronologies (Nolin et al., 2021a). Indeed, ring width of riparian trees showed little, and often contrasting, association with flooding (Kames et al., 2016; Tardif et al., 2021b). For example, in Lake Duparquet, the radial growth of black ash (*Fraxinus nigra* Marsh.) in lowland floodplains (Tardif and Bergeron 1993, Tardif and Bergeron, 1997a; Kames et al. 2016; Nolin et al., 2021a, Tardif et al., 2021b) and tamarack (*Larix laricina* K. Koch) in alluvial bogs (Girardin et al. 2001) showed a negative impact of spring flooding, while radial growth of eastern white-cedar (*Thuja occidentalis* L.) in upper floodplains showed a positive impact of spring flooding (Denneler et al., 2010). Few consistent responses have been found between tree-ring width and discharge in riparian bur oak (*Quercus macrocarpa* Michx.) along the Red River (Manitoba, Canada; St. George and Nielsen, 2003), but tree-ring widths of riparian European ash (*Fraxinus excelsior* L.), sampled along the Warta River in Poland, demonstrated a positive and significant correlation with previous fall (Sep. to Jan.) and current July and September maximum river discharge (Koprowski et al., 2018). The presence and/or absence of flood rings in tree rings of ring-porous trees depends however on their exposure to spring flooding. Depending on the hydrological context, flood rings varied in relative frequency and intensity (Nolin et al., 2021b; Tardif et al., 2021b). For instance, Tardif et al. (2021a) and Tardif et al. (2021b) demonstrated that flood rings were formed mainly in *F. nigra* trees located in lower floodplain but not in trees exposed to the same hydrological regime but growing at higher elevation.

Fewer trees recorded flood rings in floodplains of regulated rivers compared to those of natural rivers, and flood rings in regulated rivers were also less distinct (intense) than those in natural rivers (Nolin et al., 2021b). Compared to the hydrological records from natural rivers, the natural discharge variability is masked by dam regulation and management manoeuvres in regulated river hydrological records (Déry et al., 2016)

with a particular reduction in maximum daily and annual peak discharge downstream of dams (Williams and Wolman, 1984; Magilligan and Nislow, 2005; Graf, 2006). After water-level regulation, floodplain trees would be inundated less frequently due to flood attenuation by the dam. The tree rings would therefore be less likely to record all the same years of flooding as in nearby natural rivers. The impact of dam regulation on riparian forests could thus alter their ability to provide proxy (natural) hydrological data when trees have coped to altered hydrological regimes.

River regulation and dam management alter water availability for both upstream and downstream riparian forests in space and time, and are further influenced by an interplay of factors such as species' plasticity, soil moisture, microtopography, etc. (Nilsson and Berggren, 2000; Magilligan and Nislow, 2005; Stella and Bendix, 2019). Downstream of a dam the water table may be lowered, and the flood peaks attenuated with the frequency and magnitude of flooding reduced, suppressed, or shifted in time depending on reservoir management (Nilsson and Berggren, 2000; Ashmore and Church, 2001; Magilligan and Nislow, 2005; Graf, 2006). The composition of floodplain forests downstream of a dam often shifts to more drought tolerant species than in the pre-dam period with a loss of old growth trees (DeWine and Cooper, 2007; Stallins et al., 2010; Schook et al., 2016b). The response time of riparian forests varies widely across hydrological contexts. For example, Smith et al. (2013) found that the regulation of the Apalachicola River, initiated 40 years ago in the 1970s, reduced flood disturbance which positively affected tree age, and negatively affected radial growth and recruitment.

Hydrological effects upstream of dams have been less commonly studied (Petts, 1980; Evans et al., 2007; Baena-Escudero et al., 2021). In the short term, water regulation raises the water level for riparian forests upstream of a dam in the portion of the river under the influence of the dam (reservoir) resulting in forest mortality or composition

change (Nilsson and Berggren, 2000), or in the loss of trees/species presenting flood rings. In the longer term, a dam can also cause progressive siltation reducing the river cross-section upstream of the dam. For example, Baena-Escudero et al. (2021) demonstrated that the siltation induced by dams on the Guadalquivir River in Spain, laden with silty sand sediments, resulted in a reduction in the river's discharge capacity during floods less than one-hundred years after the dams were built. As a result, higher water levels were reached after siltation, for an equivalent discharge before siltation, increasing the frequency and duration of flooding of the floodplains along the reservoir (Baena-Escudero et al., 2021). Slater and Villarini (2016) also noted that trends in flood frequencies among American rivers were different for some river basins that had undergone regulation or reduction in the capacity of the main river channel (urbanization). However, the length of the dam reservoir varies depending on the characteristics of the river and of the dam (Nilsson and Berggren, 2000). Further upstream of the reservoir, riparian forests and flood dynamics are not affected and retain their natural attributes.

The impact of river regulation on radial tree growth has been little studied, but dendrochronological studies suggest that river damming generally has an adverse effect on the radial growth of riparian trees. Downstream of dams, regulation increases the sensitivity of riparian tree growth to drought and to low water levels (Reily and Johnson, 1982; Salzer et al., 1996; Coble and Kolb, 2012). As a result, tree growth is more highly correlated to discharge during the pre-dam period and to drought (low discharge) and precipitation during the post-dam period (Reily and Johnson, 1982; Stromberg and Patten, 1990; Salzer et al., 1996; Coble and Kolb, 2012; Netsvetov et al., 2019). The damming also tends to reduce the ring-width variability in the post-dam period (Salzer et al., 1996). Reily and Johnson (1982) compared regulation effects on radial tree growth of several riparian species along elevation gradients in the Missouri River and

demonstrated that tree growth downstream of an altered hydrological regime responds in variable ways depending on, among others, tree species and elevation to water levels.

The aim of this study was to determine how discharge regulation by dams affects both ring width and the production of flood rings along various regulated hydrological contexts. More precisely, we asked how is radial growth and flood-ring production of riparian *F. nigra* trees impacted by the construction of hydrological dams, and if the trees' ability to record high magnitude flood rings differ according to distance to the shoreline and among different sites located upstream and downstream of the dam. It was hypothesized i) that flood rings would present no differences between sites prior to dam construction whereas ii) after dam construction, flood rings would be recorded more abundantly and be of higher intensity upstream. It was also hypothesized that dam construction would reduce ring width and its variability, as well as alter the correlation structure with discharge and precipitation. In addition to enhancing our understanding of the impact of dam regulation on the ability of riparian *F. nigra* trees to record hydrological events, this study addresses sampling strategies that maximize the success of generating flood records of riparian trees in a context of hydrological regulation.

3.4 Material and methods

3.4.1 Study area

The study area is located on the Driftwood River, meandering in the clayey and peatland plains of northeastern Ontario at the southern fringe of the boreal forest (Fig. 3.1). The source of Driftwood River is located near Lipsett Lake (48°19'49" N; 80°42'46" W). After flowing north to reach Moose Lake, the river ends in the Abitibi River (Fig. 3.1). Because the head of the Driftwood River basin is not easily accessible,

the sampling started on the shores of Moose Lake (11 km²) to the confluence with the Abitibi River (Fig. 3.1). The Driftwood River was flowing naturally until the construction of a log dam in 1917–1918 at Monteith (OMNRF, 2019; Fig. 3.1, Fig. 3.2). The height of the log dam is not known but the structure was built with two spillways to store the water in a reservoir and to supply electricity (60-cycle power) to a Demonstration Farm for the Ontario Government. In 1941, the generator was downsized to a 25-cycle electric power to light a prisoners-of-war camp. The reservoir and spillways were maintained but apparently abandoned. In 1952 to April 1953, the old log-dam was replaced at the same location by a 5.9-meter-high and 52-meter-long concrete gravity structure to supply water for an industrial farm (The old and the new on Driftwood River, 1953). It is possible that the dam was built on an existing rapid or on a natural constriction of the riverbed as is the case for other rivers in the region. Monteith dam is owned and operated by the Ontario Ministry of Natural Resources to control the Driftwood River as far upstream as Moose Lake. Most of the year the dam is maintained at a fixed operating level of 260.36m (Fig. 3.3; OMNR, 2004). The dam is operated solely at spring for flood mitigation with manually operated stop-logs to maintain Moose Lake level at, or below, 260.66m (Fig. 3.3; OMNR, 2004).

Upstream of the Monteith dam a gauge station (04MB002; WSC, 2021; Fig. 3.1 and Fig. 3.3) has been in service since 2006 to record water levels about 10 meters upstream of the dam. While of short duration, the daily hydrographs indicate that the Driftwood River follows a boreal regime with a peak response to ice and snowmelt in spring lasting for several weeks. Relatively high-water levels are maintained through the summer, probably because of the dam, and with a late recession in winter a few months before the freshet (Fig. 3.3). There is no record of the Driftwood River hydrological regime prior to the dam, making it impossible to assess the exact impact of the dam on flood magnitude or mean water levels upstream and/or downstream. The nearest unregulated hydrological record is for the Porcupine River (04MD004), located about

50 km to the west with data from 2007–2019. The drainage areas of the gauge stations on the Driftwood and Porcupine Rivers are similar (537 km² compared to 408 km²) allowing a direct comparison. The nearest, longest unregulated records are for the Harricana River (04NA001 & 04NA002), located about 200 km to the East, with data from 1915–2021, over a larger drainage area (3 680 km²).

Table 3.1 Location of sampling sites. Data are ordered by increasing distance to the dam from top to bottom. Period is the length of flood-ring records.

Site	No. Trees	Position to dam	Latitude / Longitude	Period
RPR 1	8	1 km downstream	48°38'53"N ; 80°40'42"W	1930–2017
DFR 1	6	10 km upstream	48°34'31"N ; 80°40'05"W	1917–2017
DFR 2	10	25 km upstream	48°31'03"N ; 80°42'15"W	1879–2017
MOL 1	8	27 km upstream	48°31'15"N ; 80°43'13"W	1898–2017
MOL 2	11	31 km upstream	48°30'44"N ; 80°44'39"W	1852–2017

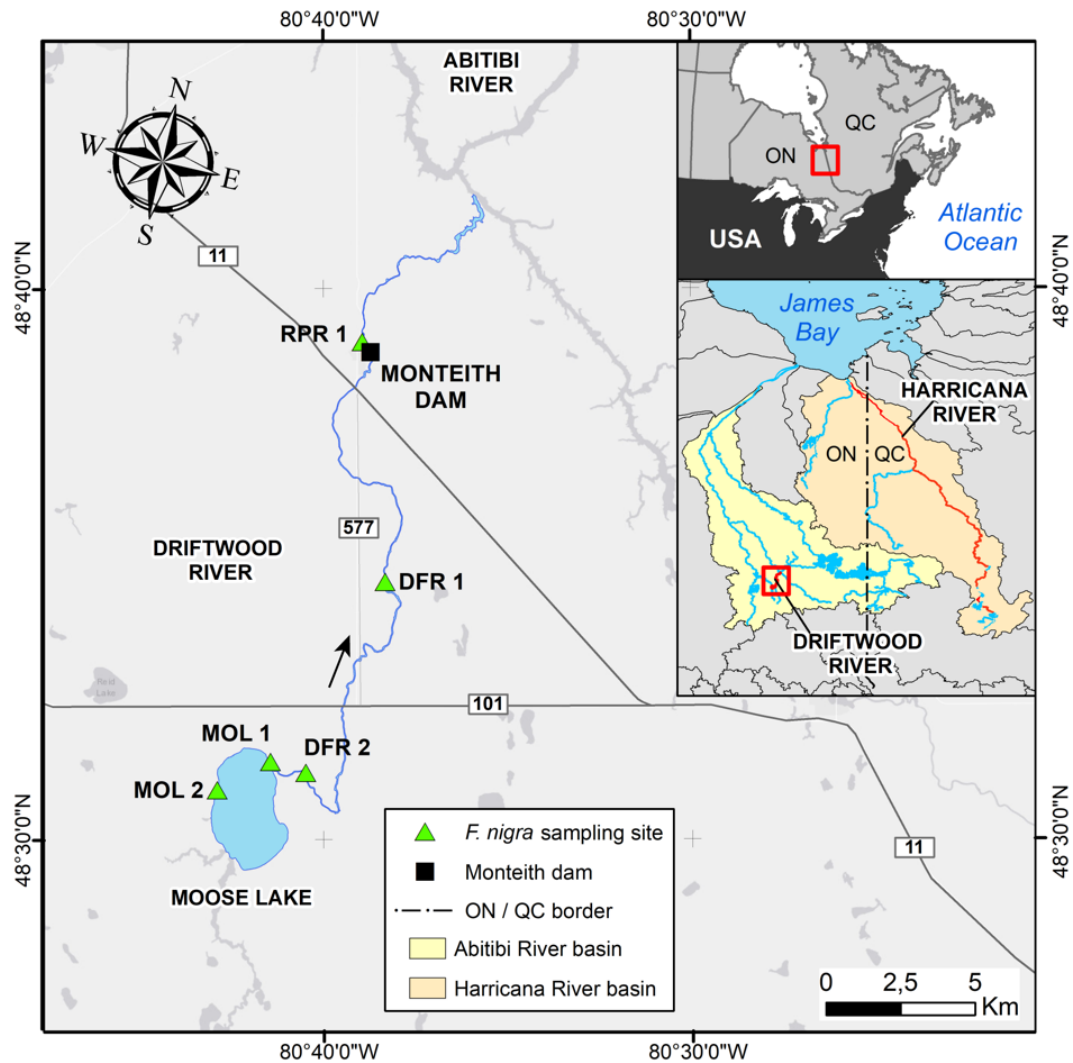


Figure 3.1 Map of the study area. Geographic location of the Driftwood River at the border between Ontario and Québec in Canada (upper right inset) and within the Abitibi River basin (lower right inset). Locations of the *Fraxinus nigra* sampling sites along the Driftwood River are coded as follows: MOL - Moose Lake; DFR - Driftwood River; RPR - Rapid River.

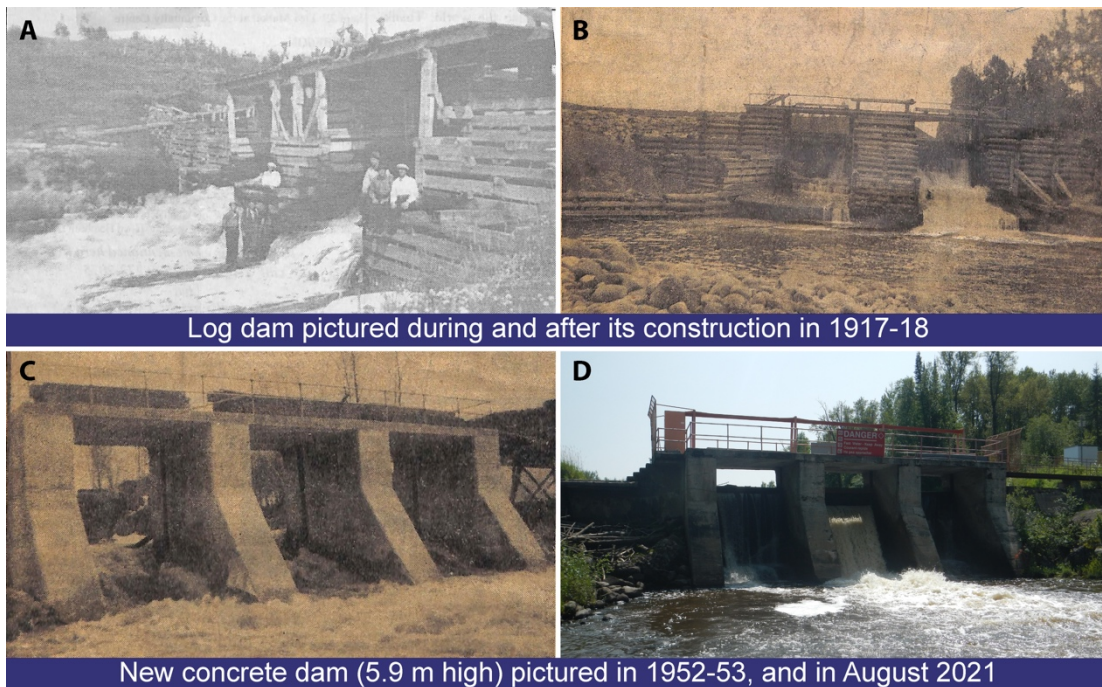


Figure 3.2 The old and the new on Driftwood River at Monteith. First log dam (a, b) and second concrete dam (c) in the years of their construction as compared to today structure (d). Historical photos b) and c) by Mrs. C. Clifford were published in an unknown local newspaper on May 6, 1953. All historical photos retrieved from the digitalized archives of the Monteith Women Institute Tweedsmuir Community History, a courtesy of the Federated Women's Institutes of Ontario (FWIO; <https://collections.fwio.on.ca>). Photo in August 2021 by AFN.

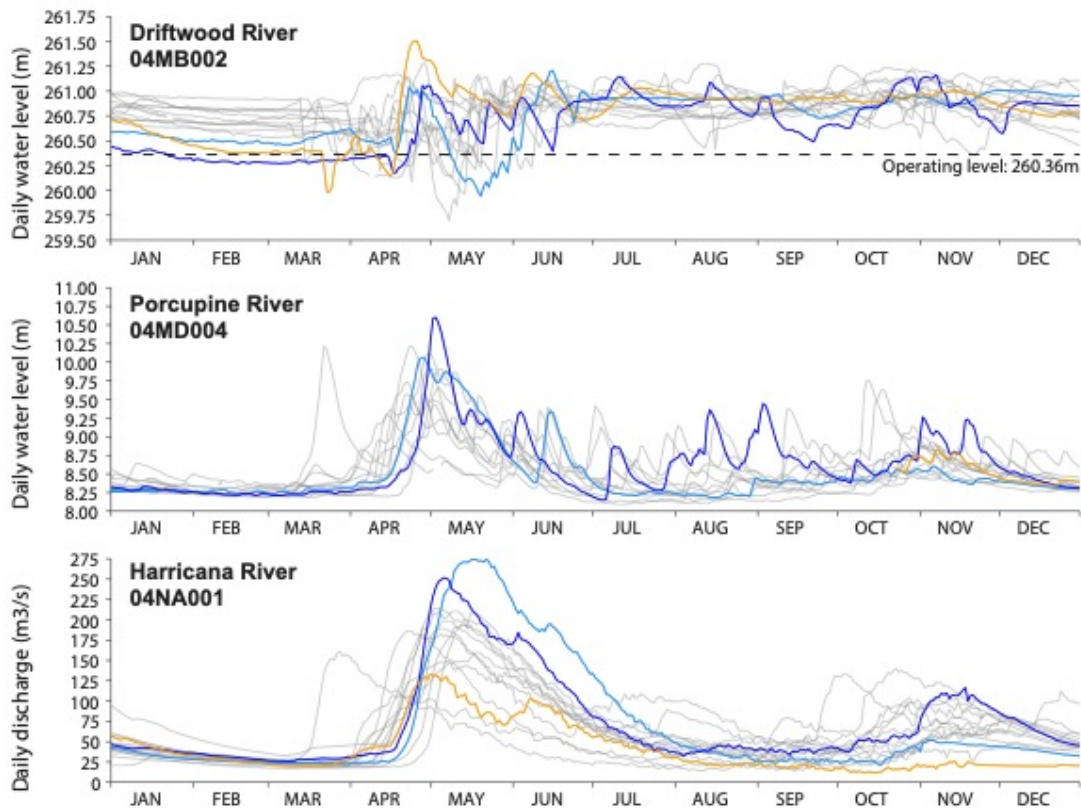


Figure 3.3 Comparison of the daily water level of the Driftwood River downstream of the Monteith dam (2006–2020) with the daily water levels of the unregulated Porcupine River at Hoyle (~50km west; 2007–2019) and the daily discharge of the unregulated Harricana River at Amos (~200km east; 2006–2020). Daily data for the year 2007 are incomplete at the Porcupine River gauge station. Data were extracted from the historical hydrological station data of the Water Survey Canada. The years of maximum discharge or water level found during the 2006–2020 period and in the three rivers are highlighted in color. The light blue line represents the year 2019 (maximum discharge in the Harricana River), the dark blue line represents the year 2013 (maximum water level found in the Porcupine River), and the orange line represents the year 2007 (maximum level found in the Driftwood River). Dashed line in the upper panel depict the operating level (260.36m) of the Monteith dam.

3.4.2 Tree-ring data

Tree-ring were collected in the summer 2017 to investigate the spatial coherency of spring floods in eastern boreal Canada (Nolin et al. 2021b). A total of 43 living *F. nigra* trees were sampled in 5 sites representing different hydrological contexts with site RPR 1 located 1 km downstream of Monteith dam; site DFR 1, located 10 km upstream of the dam; site DFR 2 located 25 km upstream on the tip of a meander and 1km downstream of the estuary of Moose Lake; site MOL 1 located 27 km upstream at the estuary of Moose Lake; and site MOL 2 located 31 km upstream on the opposite shore of Moose Lake estuary (Fig. 3.1; Table 3.1). *Fraxinus nigra* trees growing on the shoreline of the Driftwood River are situated close to their northern distribution limit. The species grows on fine waterlogged clay soils and occurs in pure or mixed stands in association with eastern white-cedar and balsam poplar (*Populus balsamifera* L.; Tardif et al., 1992; Tardif and Bergeron, 1999; Denneler et al., 2008b). The species is tolerant to water level fluctuations (Sims et al. 1990) and was sampled in the lower floodplains where sensitive fern (*Onoclea sensibilis* L.) is indicative of long-lasting floods (Tardif and Bergeron, 1992). Dominant trees were selected, and two cores were collected on trees with the largest diameter with the aim to produce long chronologies. Coring was done with a 5mm increment borer on two opposite directions to reach the tree center and as close to the tree base as possible. Diameter at breast height was recorded as well as the distance of each tree to the shoreline. Each core sample was prepared according to standard dendrochronological procedures (Phipps, 1985) and sanded with a progressively finer grit. Prior to crossdating, each sample was inspected for the presence of flood rings by two observers, each processing half of the samples. In *F. nigra*, flood rings are characterized by a noticeable increase in earlywood vessels number which is accompanied by a noticeable decrease of earlywood vessels area (Tardif et al., 2010; Kames et al., 2016; Nolin et al., 2020ab; Tardif et al., 2021a). A dual numerical code was used to record the level of distinctiveness of flood rings with

a F1 code indicating a weakly-defined flood ring and a F2 code indicating a well-defined flood ring (Nolin et al., 2021b, Tardif et al., 2021a). Crossdating was then performed using the previously defined regional *F. nigra* pointers years (Tardif and Bergeron, 1997a; Kames et al. 2016; Nolin et al., 2021b). The age of each tree was determined from the oldest core sample and was either the age of the pith or the age of the last visible tree ring when the pith was not present on the core. Ring widths were measured with CooRecorder (v9.0.1; Larsson, 2003a) on 2400dpi scanned images and were validated with CDendro (v9.0.1; Larsson, 2003b) and COFECHA (Holmes, 1983).

3.4.3 Statistical analysis and independent data

Both, flood-ring relative frequencies and ring-width chronologies, were generated. Flood-ring series were produced from visual identification of flood rings and of their intensity (F1 and F2) by two expert observers. Tardif et al., (2021a) demonstrated that both flood rings and their intensity could be identified with high consistency by novice and expert observers and that visual identification of flood rings could provide accurate and reproducible semi-quantitative data. Flood-ring series were pooled by tree, keeping the code with the maximum intensity for each year ($0 < F1 < F2$; Nolin et al., 2021b). Flood-ring categories have been shown to respond to the same hydroclimatic variables and to be complementary with F1 observed in most years, F2 observed in known high flood years, and both F1 and F2 being almost absent from unflooded control sites (Nolin et al., 2021b; Tardif et al., 2021a). The relative frequencies of F1 and F2 by sites were then calculated by dividing their respective sum by the number of trees per year. Both F1 and F2 relative frequencies were also summed (F12). Ring-width measurement series were averaged by tree ($n = 2$ cores) and the old non-overlapping portion was kept ($n = 1$ core) to maximize temporal coverage. Ring-width series were standardized by dividing each tree series by its mean to conserve the integrity of the low-frequency variations (Cook and Kairiukstis, 1990). Standardized ring-width series and F1, F2, F12 relative frequencies were then averaged by sites. To assess a possible

effect of distance from the shoreline, each of those series were grouped into two distance classes representing shoreline trees [0–10m] and floodplain trees]10–100m].

Nonparametric change-point analysis was performed on mean site ring-width chronologies using the "ecp" package (v3.1.3; James and Matteson, 2014). A univariate change point analysis was performed for each site, and a multivariate analysis was performed using all mean site chronologies at once. Multivariate analysis of change points was performed by successive common periods, removing the youngest chronology each time until there were only two chronologies left. Change points were estimated by iterative hierarchical segmentation of chronologies and tested for significance using 1,000 Monte Carlo permutation tests (Matteson, and James, 2014).

Flood-ring relative frequencies and ring-width chronologies were finally compared to four independent instrumental and proxy series. First, daily discharge data from the unregulated Harricana River (1915–2021; WSC, 2021) were used (Fig. 3.1). Second, both a reconstruction of the spring (April 15-June 30) discharge and a chronology of flood-ring relative frequency for the Harricana River were available for the period 1771–2016 (Nolin et al., 2021ab). The reconstructed Harricana River discharge data are highly correlated with the instrumental data ($r = 0.819$, $p < 0.001$, 1915–2016) and can be used as a proxy for the period before 1915 (Nolin et al., 2021a). At last, precipitation data were also retrieved from gridded CRU TS4.04 (Harris et al., 2020) using the KNMI Climate Explorer (<https://climexp.knmi.nl>; Trouet and Van Oldenborgh, 2013). Spring (March-April-May) precipitation data were averaged over the $0.5^\circ \times 0.5^\circ$ grid cells corresponding to the spatial extent of the sampling sites (48°N ; -80°E to 48.5°N ; -80.5°E ; Fig. 3.1) and covering 1901 to 2019.

The flood-ring relative frequencies (F1, F2, F12) were compared among sites using bootstrapped Spearman correlation coefficients (Legendre and Legendre, 2012). Each

correlation was calculated on 10,000 random samplings of the chronologies to approximate the sampling distribution of the Spearman correlation coefficient and to return its mean (Efron, 1979), using the ‘boot’ package (Canty and Ripley, 2021). Ring-width chronologies were compared among sites and with the aforementioned hydroclimatic data using 40-year moving windows of bootstrapped Pearson correlation coefficients lagged backward by 5 years (Legendre and Legendre, 2012) using the ‘treeclim’ package (Zang and Biondi, 2015). All statistical analyses were conducted in the R statistical Environment (R Core Team, 2021).

3.5 Results and discussion

3.5.1 Impact of regulation on stand structure

The comparison of daily hydrographs of regulated and unregulated rivers illustrates the reduction of spring flood peaks and the maintenance of high-water levels throughout the year in the Driftwood River compared to a natural regime (Fig. 3.3). Comparing the years of the highest water levels and discharge in the Driftwood, Porcupine, and Harricana Rivers also shows that years of high-water levels in the regulated Driftwood River do not necessarily correspond to years of high-water levels or high discharge in the two other natural rivers (2007 orange line in Fig. 3.3). In the natural Porcupine, and Harricana Rivers, the years 2013 and 2019 are known major flood years and show comparable high-water level and discharge (blue lines in Fig. 3.3).

The ages of the trees sampled on the Driftwood River ranged from 32 to 166 years with differences observed from upstream to downstream (Table 3.2). The oldest and largest *F. nigra* trees were located at the greatest distance upstream of Monteith dam (MOL 2) while the youngest and smallest trees were found at the site right downstream of the dam (RPR 1) and at the closest site upstream of the dam (DFR 1; Table 3.2; Fig. 3.4). Site DFR 2 presented the most dispersed age class compared to others with tree age

ranging from 38 to 138 years (Table 3.2; Fig. 3.4). The difference in age between upstream and downstream sites was consistent although the maximum age of a few trees was underestimated because of rotten parts (14 of 43 trees) and could therefore be assumed to be older. The maximum ages of the trees suggest that sites DFR1, DFR2, MOL1, and MOL2 were present prior to the construction of the log-dam in 1917–1918 and that RPR1 was established prior to the construction of the second dam in 1952–1953 (Table 3.2; Fig. 3.4). On the shores of Moose Lake (MOL 1, MOL 2) *F. nigra* trees formed dense and thick fringe forests from the shoreline to a maximum of 100m in the floodplain.

Further downstream on the Driftwood River (DFR 2, DFR 1, RPR 1) *F. nigra* trees were organized in narrow linear stands along the river and extended to a maximum of 30m in the floodplain. The old age and extent of the stands suggests that *F. nigra* trees at Moose Lake have survived the dam constructions. In the nearby Lake Abitibi, the first damming of the lake in 1915 raised the water level of ca. 1.2 m and caused the mortality of the riparian fringe forest (Denneker et al., 2008b). Investigating the spatial coherency of flood rings, Nolin et al. (2021b) found significantly shorter flood-ring records in regulated rivers compared to natural rivers which suggested that regulation may have permanently eliminated old-growth floodplain forests. Several studies also reported a negative effect of peak flow regulation recruitment and establishment of riparian trees downstream of a dam (DeWine and Cooper, 2007; Smith et al., 2013; Schook et al., 2016b). In this study, no additional stands of *F. nigra* were found downstream of RPR 1.

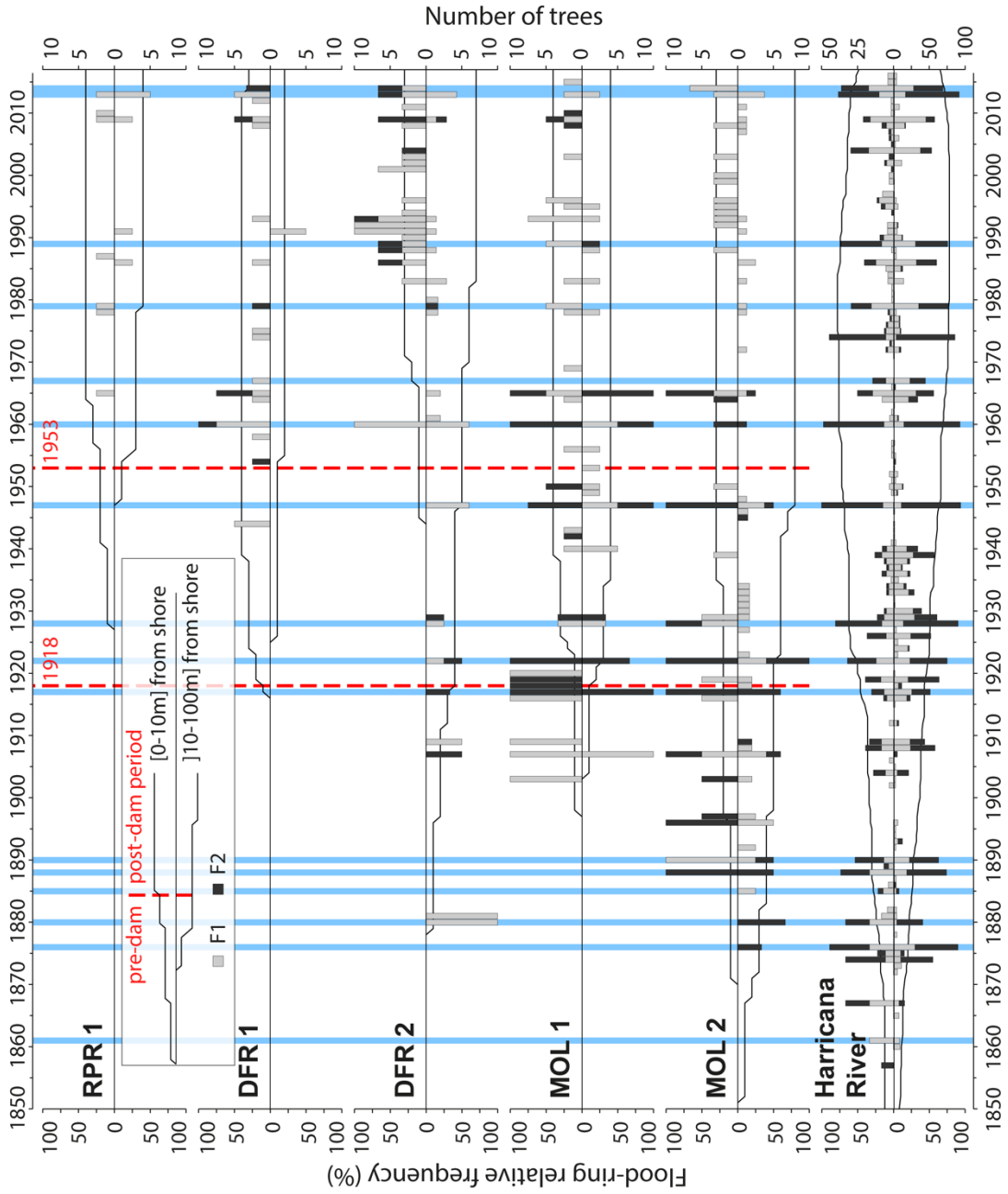
Beside an effect of regulation, other factors could also explain the age difference between sites (oldest upstream, youngest downstream) such as land use changes, timber harvest, or natural dynamic of seeds propagation. However, no evidence of land use changes and lowland forest harvesting were found in the archives consulted

(Geography of Monteith, n.d.; The old and the new on Driftwood River, 1953). Seeds of *Fraxinus* trees (samaras) are morphologically adapted to be dispersed by wind, and dispersal by water current in periodically flooded riverine lowlands has also been reported (Merritt and Wohl, 2002; Schmiedel and Tackenberg, 2013).

Fraxinus nigra sexual regeneration at Lake Duparquet was also positively influenced by high water levels during spring and early summer, while the species also regenerates by vegetative reproduction (Tardif et al., 1994). In the Saône River in France, flooding favored *Populus* regeneration by eliminating seedlings of other flood-intolerant species (Astrade and Bégin, 1997). It can thus be hypothesized that river regulation may result in a regeneration deficit of riparian *F. nigra* downstream of the dam and upstream at the reservoir. Since only old trees were sampled in this study, the data do not provide evidence of an effect of Monteith dams on *F. nigra* recruitment in the Driftwood River floodplains. A future research avenue should thus investigate age classes and seedling perennity among floodplain forests and between hydrological contexts.

Table 3.2 Characteristics of *Fraxinus nigra* stands. Mean values and standard deviation by site indicating (1) stem diameters at breast height, (2) maximum tree age, and (3) their position in the floodplain relative to the shoreline. Data are ordered by increasing distance to the dam from top to bottom.

Site	Diameter	Age	Distance to shore
RPR 1	27.5 ±6.3	68.9 ±15.3	13.4 ±11.8
DFR 1	26.7 ±5.8	89.3 ±10.2	6.8 ±6.4
DFR 2	35.4 ±10.9	85.0 ±31.2	35.9 ±18.0
MOL 1	33.9 ±7.1	98.4 ±14.9	8.8 ±5.5
MOL 2	48.5 ±9.9	122.1 ±31.3	29.5 ±25.6



◀ Figure 3.4 Flood-ring chronologies for each of the five sites and organized by distance classes to the shoreline (0–10m and 10–100m) and for the naturally flowing Harricana River. Trees close to the shoreline (0–10m) are shown with positive bars and trees from the floodplain (10–100m) with negative bars. Grey and black histograms are respectively F1 and F2 flood-ring relative frequencies, and the black solid line in the background indicates temporal replication among the trees sampled per year. Vertical red dashed lines indicate dates of construction of the first and second Monteith dam. Blue vertical bars indicate the years with the highest reconstructed spring discharge for the Harricana River (threshold value = 151.3 m³/s; Nolin et al., 2021ab).

3.5.2 Flood-ring relative frequencies (pre-dam period)

The flood-ring chronologies covered 1852–2017 with a common overlap period between 1930 to 2017 (Table 3.1). Little flood-ring data were available prior to the construction of the first log-dam (1917–1918; Fig. 3.4). The most consistent flood-ring record for the pre-dam period were found at the most ancient and upstream site MOL 2 (Fig. 3.4). The high spring discharge years evidenced in the F12 relative frequencies from the Harricana River were identified by the years 1880, 1888, 1890, and 1917 recorded by 33 to 100% of the trees growing on the shoreline and in the floodplain of Moose Lake with mainly F2 flood rings (Fig. 3.4). F12 relative frequencies from MOL 2, MOL 1 and DFR 2 also correlated positively ($r = 0.25$ to 0.50) and significantly ($p < 0.05$) with the reconstructed Harricana River spring discharge (Table 3.3). Few years exhibited high F1 and F2 relative frequencies while not being equaled in the Harricana River records and supported the regional contrasts evidenced in years 1896 and 1907 by Nolin et al. (2021ab). Those two years were similarly characterized by high spring discharge and mid to high frequency of flood rings at Lake Duparquet (20% and 81%, respectively) and in the Little Abitibi River (38% and 76%, respectively; Nolin et al., 2021ab). Other years with high F12 relative frequencies for this period in the Driftwood River (DFR1, DFR2) demonstrated a good agreement with MOL 2 and with the reconstructed Harricana River spring discharge (Fig. 3.4, Table 3.3). Of importance is that the relative frequencies of F1 and F2 were higher in trees growing on the shoreline

than in the floodplain, where more abundant F1 with lower relative frequencies were found (Fig. 3.4). Not all years with F2 values in shoreline trees were matched by comparable F2 values in floodplain trees, as is the case for the Harricana River flood ring record (Fig. 3.4). Tardif et al. (2021ab) showed that flood rings gradually disappeared from low to high elevation floodplains to non-flooded upland stands and that microtopography led to differences in trees' exposure to flood. This result suggest that natural historical floods may have flooded for short distances to the shoreline which would further increase the sensitivity of the *F. nigra* forests to a change in flood regime or water levels by dams. Overall, the results from the pre-dam period compared well with the findings from other regulated rivers in the area which showed a high spatial coherency with most flood rings recorded in natural rivers prior to the period of dam implementations in the region (1920–1930s; Nolin et al., 2021b).

3.5.3 Flood-ring relative frequencies (post-dam period)

In contrast to the flood-rings chronology from the unregulated Harricana River, those from the Driftwood River tracked the hydrological changes that occurred after the implementation (1917) and the replacement (1953) of Monteith dam. The most striking features were the decrease flood-ring relative frequencies and the decrease in the number of F2 in the post-dam period (Fig. 3.4). This response was also seen in the decrease in the number of sites with a significant correlation of F12 relative frequencies with the mean Harricana River instrumental spring discharge (Table 3.3).

Table 3.3 Comparison of F12 flood-ring relative frequencies with instrumental and reconstructed mean spring (April 15 to June 30) discharge of the naturally flowing Harricana River and by distance to shoreline (0–10m and 10–100m). Spearman correlation coefficients (ρ) are given after calculating 10,000 bootstrap iterations. Bold characters denote significant ρ coefficients at $p < 0.05$. Spearman coefficients were calculated for four periods (1) the pre-dam period before the first log dam (1850–1917), (2) after the first log dam (1918–2016); (3) in between the first log dam and the second concrete dam (1918–1952); and (4) after the second concrete dam (1953–2016). (*) Note that for the pre-dam period, the number of years varies among sites and distance classes with DFR 2 (1879–1917), MOL 1 (1898–1917), MOL 2 (1852–1917; Fig. 3.4; Table 3.1). The pre-dam period has been calculated with the reconstructed Harricana River discharge, the other periods with the instrumental Harricana River discharge. nd: no data.

	pre-dam period (*)		after the first dam: 1918–2016		in-between the two dams: 1918–1952		after the second dam: 1953–2016									
	[0–10m]	110–100m]	[0–10m]	110–100m]	[0–10m]	110–100m]	[0–10m]	110–100m]								
	ρ	p	ρ	p	ρ	p	ρ	p								
RPR 1	nd	nd	nd	nd	nd	nd	0.04	0.742	0.23	0.075						
DFR 1	nd	nd	0.23	0.024	nd	nd	nd	nd	0.41	0.001	0.674					
DFR 2	nd	nd	0.35	0.005	nd	nd	0.49	0.006	0.28	0.034	0.160					
MOL 1	0.31	0.013	0.25	0.051	0.27	0.007	0.32	0.002	0.48	0.008	0.27	0.041	0.20	0.120		
MOL 2	0.38	0.003	0.50	0.000	0.28	0.007	0.15	0.152	0.60	0.000	0.05	0.721	0.11	0.427	0.20	0.131

During the period between the first and the second dam (1918–1952), high F12 relative frequencies with high values of F2 were still recorded during the known high spring discharge years of 1922, 1928, and 1947 at upstream sites MOL 2, MOL 1 and DFR 2 (Fig. 3.4). The F12 relative frequencies from those sites still correlated positively and significantly with the instrumental Harricana River mean spring discharge. However, the correlations from shoreline trees at MOL 1 presented a non-significant ($p < 0.05$) correlation while in a range of the correlation strength found in the other periods (Table 3.3). Few high values of F12 relative frequencies were observed in floodplain trees growing on the MOL 2 site compared to the pre-dam period. Abundant F1 flood rings of low relative frequency ($< 20\%$) were also observed in floodplain trees at the MOL 2 site during 1917–1952 period, but not in shoreline trees, which contrasts with the other flood-ring records from the other four sites (Fig. 3.4). Like the pre-dam period, higher F12 relative frequencies, and mostly F2 flood rings were found for trees close to the shoreline compared to floodplain trees (Fig. 3.4).

After the replacement of the dam in 1953, values of F12 relative frequencies decreased at all sites compared to the previous two periods, with mainly F1 being recorded. The lowest F12 relative frequencies were found near the dam (RPR 1 and DFR 1) and the highest values found upstream and at a far distance from the dam (MOL 2, MOL 1, DFR 2). Site RPR 1 showed almost no flood rings (37.5% at maximum in 3 out of 8 trees) although the age of the stand does not allow comparison with a pre-dam period. Experimentally induced flood rings however have shown to form in 4-year-old pedunculate oak (*Quercus robur* L.) trees suggesting that young riparian forests should be able to record flood history (Copini et al., 2016). The absence of flood rings at RPR 1 might thus reflect the river regulation.

At the other sites, flood rings were primarily F1, with high F2 relative frequencies found in both known regional flood years and in random years. High spring discharge

years 1960, 1967, 1979, 1989, 2013 and 2014 were evidenced in the Harricana River record (Fig. 3.4). The 1960 flood was reconstructed as the highest discharge of the last 250 years in the Harricana River (Nolin et al., 2021a) and showed very high F12 relative frequencies (approaching 100%) in multiple natural regional rivers (Nolin et al., 2021b). In the Driftwood River, high flood-ring relative frequencies of F1 and F2 types were still found in 1960 after the dam was replaced (Fig. 3.4). Other years with high F12 relative frequencies such as 1965 or 2007 may result from the dam management in the Driftwood River, or from regional contrasts in spring flooding (Fig. 3.4). For instance, year 1965 was characterized by high ice-scar frequency in Lake Duparquet (Tardif and Bergeron, 1997b) and by mid to high F12 flood-ring relative frequencies in Lake Duparquet (69%) and regional natural rivers (44%; Nolin et al., 2021b). Year 2007 was the highest spring water level recorded in the Driftwood River upstream of the Monteith dam and over the period 2006–2020, which was not the case in the natural Harricana River (Fig. 3.3). The mean spring discharge of the Harricana River for year 2007 ($91.5 \text{ m}^3/\text{s}$) was well below the discharge threshold used to define high spring discharge years in this river ($151.3 \text{ m}^3/\text{s}$, Nolin et al., 2021ab).

Floodplain trees recorded very low F12 relative frequencies compared to the shoreline trees at all sites (Fig. 3.4). No significant correlation with instrumental mean Harricana River spring discharge was either found for F12 from floodplains trees at all sites (Table 3.3). Trees of site MOL 2 almost stopped recording flood rings after 1960 and it can be assumed that the decrease in the flood peak regime induced by the dam has ended the flooding of this site, while maintaining the old-growth forest. The F12 records from shoreline trees at other sites upstream of the dam (MOL 1, DFR 2, DFR 1) still correlated positively and significantly with the instrumental Harricana River mean spring discharge (Table 3.3). Higher F12 relative frequencies were found after ~1980 in the shoreline trees at site DFR 2, which may indicate an intensification of

spring water storage by the dam over this period compared to the other sites over the same period, and to the period before 1980 at site DFR 2 (Fig. 3.4).

Throughout the flood-ring records in the post dam period, no extremely high relative frequencies were found during known date of town settlement, or road and bridge construction. The small village of Driftwood city established on the east side of the Driftwood River was destroyed in the 1916 fire. The first buildings of the actual Monteith were built in 1916, after the fire, and on the opposite side of the river (Geography of Monteith, n.d.). No particularly high flood-ring relative frequencies were neither found for the years of the construction or modification of roads and bridges. The Ontario Highway 11 and Secondary Highway 577 (Fig. 3.1) were built in 1920 and 1956 respectively, and were modified in 1953, 1958 and 1959 (Highway 11) and in 1978 (Highway 577) sometimes associated with muskeg excavations (<http://www.thekingshighway.ca/list.htm>). While the number of samples used in this study is a limiting factor, the overall findings agree with those from regional regulated rivers where trees recorded few flood rings and of low intensity (F1) after the period of dam constructions in the region (1920–1930s; Nolin et al., 2021b).

The exclusion of low F12 frequencies or partitioning of F12 frequencies between F1 and F2 flood rings may allow to separate years of major flood from years of high-water stage induced by dam management or other anthropogenic alterations (e.g., bridge construction, muskeg excavations). This may become important in a context where it is not possible to compare flood-ring relative frequencies to regional hydrologic records (instrumental or reconstructed). The high F12 relative frequencies that are present in both, shoreline trees (F12 > 75%) and floodplain trees (F12 > 50%), indicate that the spring discharge from 1960 and 1965 flooded the shoreline and the floodplain trees after the Monteith dam construction. The years for which F2 were recorded in both, shoreline, and floodplain trees, also indicated that the years 1960, 1965 and the

year 2009 inundated the distant floodplain. Different flood-ring responses to those flood years at sites MOL 1 (high relative frequencies) and MOL 2 (low relative frequencies; Fig. 3.4) emphasized that sampling sites with different elevation and flood exposure gradient might help in disentangling major flood years from water-level management events. Moreover, in this study, cores were taken at varying heights due to varying wood quality (*i.e.*, rot, frost scars...). It would be interesting to include sampling height in future analyses since flood rings has been shown to solely occur below water level (Copini et al., 2016) and/or to weaken along with stem height and with increasing distance to the ground (St. George et al., 2002). Studying the flood-ring distribution in relation to stem height could provide a proxy for flood height and it would add to information that can be provided by flood-ring intensity. For instance, Tardif et al. (2021a), noted that flooded *F. nigra* trees in close proximity could record flood ring of different intensity (F1, F2) supporting the idea that sampling height and tree elevation might affect the distinctiveness of flood ring signature. The authors also noted that the identification error between two observers was greater for weakly-defined flood rings (F1) than for well-defined flood rings (F2).

3.5.4 Ring-width chronologies

Over the 1930–2017 common period, the mean correlation between the five site chronologies was generally high ($r = 0.49 \pm 0.24$ sd) except for the site RPR1 which was weakly correlated with the other sites ($r = 0.19 \pm 0.28$ sd). The highest significant correlation among ring-width chronologies was found between the most upstream sites MOL 1 and MOL 2 ($r = 0.69$, $p < 0.001$). The univariate change point analysis identified no change in mean and/or variance in each mean site ring-width chronologies that could be related to the first or second dam construction (Fig. 3.5; Table 3.S1). Significant change points were detected with low consistency in multivariate analysis in years 1909, 1914, 1917, 1941, 1945 and 1974 and 1975 ($p < 0.05$) over most of the common periods used for the multivariate change point analysis (Table 3.S1). The most

significant change point was the year 1974, identified in three different combinations of mean site chronologies (Table 3.S1). This year does not correspond to any of the years of village (1916), road, bridge (1920, 1953, 1956, 1958, 1959, 1978), or dam (1917, 1953) constructions that may have possibly affected the hydrology of the Driftwood River. Grouping the mean site chronologies into distance classes (shoreline and floodplain trees) resulted in no improvement of the results (results not shown). At each site, ring-width chronologies showed little association with instrumental Harricana River mean spring discharge or average spring precipitation for all period considered (before and after 1953, common period 1930–2016). For example, considering the common period 1930–2016, correlations between ring-width chronologies and respectively, river mean spring discharge or average spring precipitation were close to zero (mean $r = -0.02 \pm 0.07$; mean $r = -0.07 \pm 0.07$; $n = 5$).

Investigation of the temporal stability of these associations also suggested that radial growth at none of the sites was significantly and consistently correlated with mean spring discharge or precipitation (Fig. 3.6). After the 1970s each mean site chronology however demonstrated a change from negative to positive correlations ($p > 0.05$) between the radial growth and mean spring discharge (Fig. 3.6). The correlation between radial growth and average spring precipitation was mostly negative, with a trend toward positive correlations since about the 1990s at three of five sites (Fig. 3.6). Overall, these weak evidences of a dam effect on riparian tree growth demonstrated the advantages of flood-rings over ring-width records in flood history studies when ring-porous species are available. It is also possible that the change created by the Monteith dam was not strong enough to affect radial tree growth but still affected the earlywood vessels. In this case, further study on a larger number of rivers and hydrological contexts is needed to determine if ring widths can be used to supplement flood rings.

However, little to no consistent responses between total and sub-annual tree-ring width and spring flood discharge has neither been found in riparian *Q. macrocarpa* (St. George and Nielsen, 2002, 2003) nor in *F. nigra* (Tardif and Bergeron, 1993; Tardif and Bergeron., 1997b; Kames et al. 2016; Nolin et al., 2021a, Tardif et al., 2021b). The inversion of correlation sign found between ring width and discharge after damming is consistent with previous studies of North American rivers (Reily and Johnson, 1982; Stromberg and Patten, 1990; Salzer et al., 1996; Coble and Kolb, 2012; Netsvetov et al., 2019). Although in our study, the change in sign was the opposite, from a negative correlation before 1970 to a positive correlation after 1970. The weak and poorly significant correlations in the case of the Driftwood River also contrast with the strong and significant changes found in these studies. Most of these studies has however been conducted in arid to semi-arid environments where water (precipitation and/or discharge) constitutes a limiting factor to growth, which is rarely the case near boreal rivers. Since the first dam was built about 100 years ago, it is also possible that the riparian forests of the Driftwood River are surviving forests within which the trees whose ring widths were severely affected may have died already and thus not appear in the data.

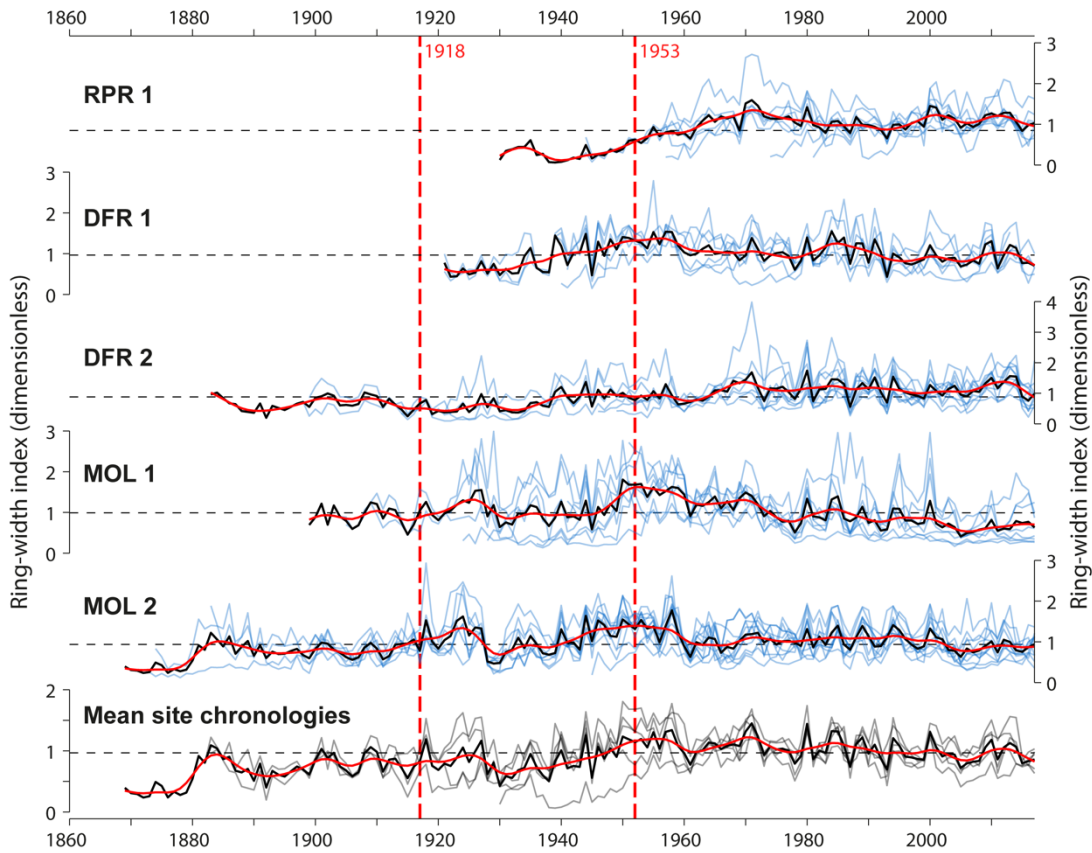


Figure 3.5 Standardized tree-ring width series (pale blue line) and mean site chronologies (dark black lines), and comparison of mean site chronologies among the five sites. Vertical red dashed lines indicate dates of construction of the first and second Monteith dam. The red curves are 10-year spline functions and depict decadal variations in the mean radial tree growth at each site.

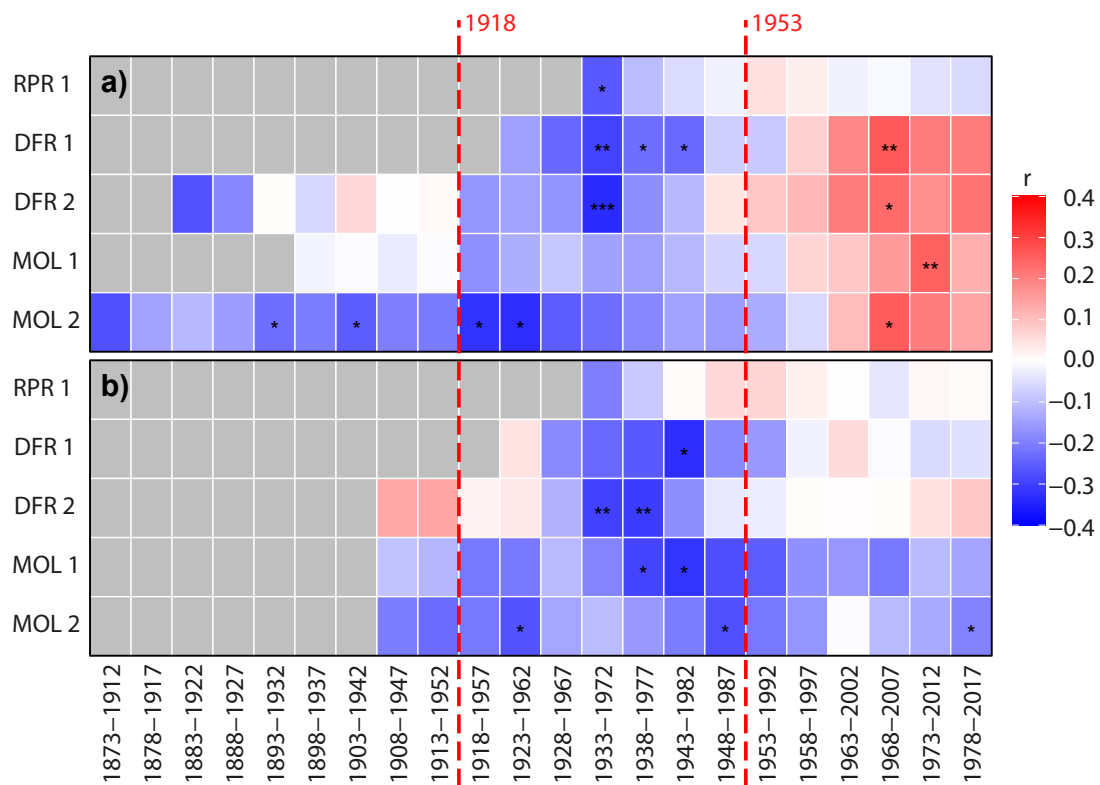


Figure 3.6 Bootstrapped moving Pearson correlations between individual site ring-width chronologies a) Harricana River spring (April 15 to June 30; 1869–2017) discharge, and b) the CRU TS 4.04 mean spring precipitation (MAR-APR-MAY-JUN; 1901–2017). The mean spring discharge of the Harricana River used in this analysis is constructed from the reconstructed (1869–1914) and instrumental (1915–2017) series. Pearson correlation coefficients were calculated by 40-year moving windows lagged backward by 5 years and range from red (positive correlation) to blue (negative correlation). Grey color indicates no data. Asterisks in a) and b) panels indicate p -value < 0.1 (*), < 0.05 (**), and < 0.01 (***). Vertical red dashed lines indicate dates of construction of the first and second Monteith dam.

3.6 Conclusion

This study demonstrated the feasibility of extracting hydrological information from regulated rivers and in particular in the pre-dam period. The flood rings successfully recorded the spring floods in the pre-dam period as indicated by comparison with instrumental and reconstructed records from nearby unregulated rivers. The number of trees recording flood rings as well as their intensity within tree rings (F1, F2 types) decreased after the construction of the first dam in 1917–18 and particularly after its replacement in 1952–53. Compared to flood-ring chronologies, ring width chronologies in the sampled trees were weakly correlated to the instrumental and reconstructed discharge of the Harricana River and did not record river regulation and at any distance to the shore. On the contrary, trees within 10m from the shoreline recorded more well-defined flood rings and of higher intensity (F2) than those further away, thus presenting a better association with known regional flood years. Comparing to the downstream site to the dam, the upstream ones recorded significantly more flood rings in the post-dam period, reemphasizing the importance of considering the position of the site along the river continuum and site conditions in relation to flood exposure. Our results suggests that a sampling strategy taking advantage of tree sampling at a far distance upstream from the dam and along various hydrologic contexts may maximize the flood signal recorded by riparian ring-porous trees in regulated rivers. A good strategy might be to sample upstream of any natural or rapid restrictions in a river, as these restrictions back up some of the water to the riparian zone during flood events. Given the importance of hydropower in northern Canada and the need for hydrological proxies in a context of climate change, it remains critical to continue developing dendrohydrological research using riparian trees and to better understand the interaction between hydrological proxies and water level regulation.

3.7 Data availability statement

Relevant data for this study are available from Nolin, A.F., Tardif, J.C., Conciatori, F., & Bergeron, Y. (2021) *Fraxinus nigra* flood ring dataset for the study of flood history (1850–2017) of the Driftwood River, northwestern Ontario. Mendeley Data, v1., <http://dx.doi.org/10.17632/6pgc25nk27.1>. Data include sample replication (N) and flood-ring frequencies (F1, F2) derived from *Fraxinus nigra* trees growing in the floodplain of the Driftwood River in northwestern Ontario.

DriftwoodFR.csv, as in Fig. 3.4, F1 and F2 flood-rings chronologies per sites and distance class with sample replication (N) to reproduce the flood-ring frequencies. Harricana River F1 and F2 flood ring chronologies from Nolin et al., 2021b are also provided.

DriftwoodRW.csv, as in Fig. 3.5, the mean site chronologies of total ring width with sample replication (N).

LAT_LON_Driftwood.kml, the coordinate data for each *F. nigra* stand sampled on the Driftwood River, including Monteith dam location, in Google Earth format (.kml).

meatadatas.txt, a set of self-explanatory instructions and descriptions for data files.

All other data are available upon request to the corresponding author at alexandreflorent.nolin@uqat.ca (institutional email), alexandreflorent.nolin@gmail.com (permanent email).

3.8 Acknowledgments

We acknowledge Martin Girardin (CFL), Lars Hildebrandt and Gordon Kayahara (Ontario Forest Service) for their precious help in locating *Fraxinus nigra* tree's habitats. We also thank the Forêt d'enseignement et de recherche du Lac Duparquet team, and especially Danielle Charron and Raynald Julien for their continuous support during the field campaigns, as well as field assistants Stéphane Hébert, Cyrielle Ducrot and Chloé Lavelle. Earlier version of the manuscript benefited from constructive discussions and comments by David Huard (Ouranos), Susanne Kames (University of Winnipeg), and Kurt C. Kornelsen (OPG). We also acknowledge the contribution of the Editor, Pr. Ignacio García González, and two reviewers (Michael J. Clifford and Radoslaw Puchalka) who provided constructive comments and suggestions to improve earlier draft of the manuscript.

3.9 Supplementary Materials

Table 3.S1 Change point analysis of mean site chronologies of tree-ring width. Results are given for each site (univariate analysis, $n = 1$ chronology) and each combination of mean site chronologies tested (multivariate analysis, $n = 2, 3, 4$ or 5 chronologies). Multivariate analyses were performed on the period common to the chronology or to the chronology combination used. Years were identified as significant change points when $p < 0.05$.

Site(s)	Common		No. of change points	Years identified as significant ($p < 0.05$) change points	
	period	change points			
RPR1	1930–2017	0			
DFR1	1917–2017	0			
DFR2	1879–2017	0			
MOL1	1898–2017	0			
MOL2	1852–2017	1	1914		
RPR1, DFR1, DFR1, MOL1, MOL2	1930–2017			1945	1975
DFR1, DFR2, MOL1, MOL2	1917–2017	2		1941	1974
DFR2, MOL1, MOL2	1879–2017	3	1909	1941	1974
MOL1, MOL2	1898–2017	2		1917	1974

CHAPITRE IV

A 247-YEARS TREE-RING RECONSTRUCTION OF SPRING
TEMPERATURE AND RELATION TO SPRING FLOODING IN EASTERN
BOREAL CANADA

Alexandre F. Nolin, Martin P. Girardin, Jacques C. Tardif, Xiao Jing Guo, France
Conciatori, Yves Bergeron

Publié dans *International Journal of Climatology*,

Mars 2022

4.1 Graphical abstract



Charred jack pine snags provide unique paleoclimatic data in the Canadian boreal forest. Spring temperature reconstructions from these trees indicate cooler than average springs at the end of the Little Ice Age, with multi-decadal cold and warm phases, before transitioning to warmer springs since ~1940. Most of the highest regional spring discharge are also consistent with the reconstructed variability in cool spring temperatures and show high spatial coherence with the historical extent of snow cover in central and northeastern Canada.

4.2 Abstract

Few records of spring paleoclimate are available for boreal Canada, as biological proxies recording the beginning of the warm season are uncommon. Given the spring warming observed during the last decades, and its impact on snowmelt and hydrological processes, searching for spring climate proxies is receiving increasing attention. Tree-ring anatomical features and intra-annual widths were used to reconstruct the regional March to May mean air temperature from 1770 to 2016 in eastern boreal Canada. Nested principal component regressions calibrated on 116 years of gridded temperature data were developed from one *Fraxinus nigra* and ten *Pinus banksiana* sites. The reconstruction indicated three distinct phases in spring temperature variability since 1770. Ample phases of multi-decadal warm and cold springs persisted until the end of the Little Ice Age (1850–1870 CE) and were gradually replaced since the 1940s by decadal to interannual variability associated with an increase in the frequency and magnitude of warm springs. Significant correlations with other paleotemperature records, gridded snow cover extent and runoff support that historical high flooding were associated with late, cold springs with heavy snow cover. Most of the high magnitude spring floods reconstructed for the nearby Harricana River also coincided with the lowest reconstructed spring temperature per decade. However, the last 40 years of observed and reconstructed mean spring temperature showed a reduction in the number of extreme cold springs contrasting with the last few decades of extreme flooding in the eastern Canadian boreal region. This result indicates that warmer late spring mean temperatures on average may contribute, among other factors, to advance the spring break-up and to likely shift the contribution of snow to rain in spring flooding processes.

Keywords: Climate change, dendroclimatic reconstruction, spring temperature, generalized additive mixed models (GAMM), *Fraxinus nigra*, *Pinus banksiana*.

4.3 Résumé [Ajout à l'article original]

Peu de données paléoclimatiques printanières sont disponibles dans l'est du Canada boréal car les indicateurs biologiques enregistrant le début de la saison de végétation sont rares. Étant donné le réchauffement printanier observé au cours des dernières décennies, et son effet sur la fonte des neiges et les processus hydrologiques, la recherche d'indicateurs paléoclimatiques printaniers est d'importance. Les caractéristiques anatomiques des cernes et les largeurs intra-annuelles ont été utilisées pour reconstruire la température moyenne régionale de l'air de mars à mai et de 1770 à 2016. Des régressions en composantes principales imbriquées, calibrées sur 116 ans de données de température, ont été élaborées à partir d'un site de *Fraxinus nigra* et de dix sites de *Pinus banksiana*. La reconstitution a indiqué trois phases distinctes dans la variabilité des températures printanières depuis 1770. Des phases multi-décennales de printemps chauds et froids ont persisté jusqu'à la fin du Petit Âge Glaciaire (1850–1870 CE) et ont été progressivement remplacées depuis les années 1940 par une variabilité décennale à interannuelle associée à une augmentation de la fréquence et de la magnitude des printemps chauds. Les corrélations significatives trouvées avec d'autres données de paléotempératures, l'étendue des couverts neigeux et le ruissellement, soutiennent que les crues historiques majeures étaient associées à des printemps tardifs et froids avec un couvert neigeux important. La plupart des crues printanières reconstituées pour la rivière Harricana voisine ont également coïncidé avec les plus basses températures printanières reconstituées par décennies. Cependant, dans les 40 dernières années des températures printanières moyennes plus chaudes contrastent avec les dernières décennies d'inondations extrêmes dans l'est du Canada boréal. Ce résultat indique que des températures moyennes plus chaudes à la fin du printemps peuvent contribuer, entre autres facteurs, à avancer la crue printanière et probablement à favoriser la contribution de la pluie au lieu de la neige dans les processus d'inondation printanière.

Mots-clés : Changement climatique, reconstitution dendroclimatique, température printanière, model additif mixte généralisé (GAMM), *Fraxinus nigra*, *Pinus banksiana*

4.4 Introduction

Boreal territories are prone to the impacts of climate warming given the importance of snow accumulation and snowmelt in their hydrological cycle (Buttle et al., 2016; Aygün et al., 2019). In northern Canada, and particularly since 1948, annual average temperature has increased three times faster (+2.3°C) than the Earth's global rate (Bush and Lemmen, 2019). The greatest observed warming occurred in winter and spring months resulting in a significant decrease in the length of the ice season (Bush and Lemmen, 2019). Spring snowmelt and ice break-up have occurred earlier since the beginning of the 20th century and this trend has been consistent across Canada (Zhang et al., 2001a; Burn and Hag Elnur, 2002; Prowse and Bonsal, 2004; Duguay et al., 2006; Cunderlik and Ouarda, 2009; Déry et al., 2009; Fu and Yao, 2015; Jones et al., 2015; Vincent et al., 2015; Aygün et al., 2019; Chen and She, 2020). Similarly, and since the 1950s, monthly mean discharge across Canada has shown significant increases in March and April, and significant decreases in May (Zhang et al., 2001a). The timing of river and lake ice break-up has also been found to be significantly and negatively correlated with spring air temperature across Canada (Duguay et al., 2006; Fu and Yao, 2015; Chen and She, 2020). As a result, snow cover extent and duration declined and particularly in the eastern part of the country (Brown, 2010; Mudryk et al., 2018; Aygün et al., 2019). Snow water equivalent (SWE) has generally declined in Canada since the 1950s except in northern and central Québec where it has increased (Brown, 2010; Aygün et al., 2019). In this region, increased mid-winter thaw, winter rainfall instead of snow, and rain-on-snow events (Brown, 2010; Jeong et al., 2018; Vincent et al., 2018) may also contribute to increase the SWE by ice layering, and thus the water available for spring runoff from snowmelt. Increasing air temperatures increase the rate of evaporation and atmospheric humidity, which is particularly noticeable in winter at high latitudes because total precipitation (snow and rain) is normally limited by below-freezing temperatures and low atmospheric humidity (Davis et al., 1999; Zhang et al.,

2000). The warming of northern and eastern Canada since 1900 was then associated with an increase in the number of heavy rainfall events in spring and in the number of heavy snowfall events in autumn and winter (Zhang et al., 2001b). Warm extremes are also becoming warmer and more frequent, while cold extremes are becoming less cold and less frequent, particularly in northern Canada and since the 1950s (Vincent et al., 2018; Wan et al., 2019).

Trend analyses in flood frequency and magnitude in northeastern Canada consequently demonstrated increases during the 20th and 21st centuries (Burn and Whitfield, 2016; Buttle et al., 2016; Burn and Whitfield, 2017; Bush and Lemmen, 2019; Nolin et al., 2021a). In the Lake Duparquet area (northwestern Québec) the frequency and magnitude of spring flooding increased since 1850–1870 (Tardif and Bergeron, 1997; Nolin et al., 2021a) which correspond to the end of the Little Ice Age in northeastern Canada (Viau and Gajewski, 2009). Particularly since the last century (1900–2016), high spring discharges therein have been positively associated to cold and early winter and to cold and late spring with a persistent snowpack (Nolin et al. 2021a). However, an increase in the rainfall-to-total-precipitation ratio during the spring-summer season in the Arctic (1979–2015; Han et al., 2018) suggests that the increase in snowfall currently observed in northeastern Canada might be transitory. Climate change scenarios for northern Canada project a 2 to 17% increase in total precipitation by 2100, with a shift from snow to rain in the spring and fall (Bush and Lemmen, 2019).

Future climate projections for Canada consider multiple possible regional changes in mean air temperature, with low emissions scenarios projecting a +2.0°C increase and high emissions scenarios projecting a +6.0°C increase by 2100 (Bush and Lemmen, 2019). Climate change scenarios indicate an increase in flood risk over northern Canada and a decrease in flood risk over northeastern Québec (Gaur et al., 2018). Snow cover projections point toward a general decrease in snow accumulation in winter

(Mudryk et al., 2018) and toward a quicker spring snowmelt over the next hundred years (Minville et al., 2008). Regional climate model projections for northern Québec and Ontario consequently indicate that rain may contribute more to seasonal discharge in winter by 2050 compared to the 20th century (Guay et al., 2015; Wang et al., 2015; Clavet-Gaumont et al., 2017).

The 20th century warming trend associated with anthropogenic activities (Bush and Lemmen, 2019) is now superimposed to the natural internal climate variability (Vincent et al., 2015; Wan et al., 2019). Knowledge of this natural variability remains dependent on instrumental and observational data, but the availability of climate and hydrological data is poor in northeastern Canada, with very few records predating the 1950s (Mortsch et al., 2015; Bush and Lemmen, 2019; Nolin et al., 2021b). Analyses of past variability in spring flood risk and projected hydroclimatic changes remain limited (Mortsch et al., 2015; Buttle et al., 2016; Gaur et al., 2018; Nolin et al., 2021a). In addition, given that most of Canada's electricity generation relies on hydropower plants located in the north (Cherry et al., 2017), understanding natural hydroclimatic variability and placing ongoing hydroclimatic changes in a historical context is crucial for flood risk management (Ashmore and Church, 2001; Boucher et al., 2011; Bush and Lemmen, 2019).

Tree rings have proven to be one of the most versatile proxy for studying climate variations on the scale of the last centuries to millennia and various tree-ring records have been developed to reconstruct precipitation (Griffin et al., 2013), temperature (Jacoby et al., 1988; Girardin et al., 2009; Tardif et al., 2011), snowpack (Shamir et al., 2020; Mood et al., 2020; Touchan et al., 2021), or extreme events such as droughts (Girardin et al., 2006; Hoffer and Tardif, 2009) and floods (Boucher et al., 2011; Ballesteros-Cánovas et al., 2020; Nolin et al., 2021a). Across northern North America, temperature reconstructions have been successfully derived from annual tree-ring

widths (Jacoby and D'Arrigo, 1989) and/or maximum latewood density data (Briffa et al., 1994; Briffa et al., 2001; Davi et al., 2003; Youngblut and Luckman, 2008; Anchukaitis et al., 2013; Gennaretti et al., 2014) as well as its surrogate blue intensity (Wilson et al., 2014) or in use with combination of stable isotopes (Barber et al., 2004; Gennaretti et al., 2017). Light rings were also successfully used to reconstruct summer temperatures in Interior North America (Girardin et al., 2009; Tardif et al., 2011). In the boreal region, tree-ring records are obviously biased toward the active growing season and most of the reconstructions (*Alaska and Yukon*: Davi et al., 2003; Barber et al., 2004; Youngblut and Luckman, 2008; Anchukaitis et al., 2013; Northern North America: Briffa et al., 1994; *Interior North America*: Girardin et al., 2009; Tardif et al., 2011; *Northern Québec*: Jacoby et al., 1988; Gennaretti et al., 2014; Gennaretti et al., 2017; *Fennoscandia*: Briffa et al., 1988) have focused on the maximum temperature of the warm season or summer temperature with very few attempts to reconstruct spring or winter temperature variability from tree rings (Guiot, 1987).

As the largest temperature changes reported by instrumental records since the early 20th century in northern Canada occur during the ice season (Bush and Lemmen, 2019; Aygün et al., 2019), it is important to develop temperature reconstructions for winter and spring. Chronologies developed from intra-annual tree-ring widths may contain such climate signals compared to those of annual tree-rings. Total tree-ring widths integrate climate signals over several months during the preceding and current growing seasons, while earlywood (EW) and latewood (LW) width may integrate climate during the season of their formation (Tardif, 1996; Meko and Baisan, 2001; Therrell et al., 2002; Stahle et al., 2009). In coniferous tree species and across the Northern Hemisphere, the EW tends to correlate with climate during the months prior to or during the beginning of the growing season (late winter to early spring) while the LW tends to correlate with climate during the late growing season (late spring to summer; Fritts, 1976; Meko and Baisan, 2001; Therrell et al., 2002; Stahle et al., 2009; Hoffer

and Tardif, 2009; Griffin et al., 2013). Functional dependencies between the formation of EW and LW tissues are also involved. The formation of EW depends on carbohydrates synthesized during the previous growing season and accounts for most of the ring width and hydraulic conductivity, while the formation of LW depends on photoassimilates synthesized during the current growing season (Kozlowski and Pallardy, 1997; Rossi et al., 2013). The inter-correlation between EW and LW can be assessed by removing the linear dependency of the LW width on the preceding EW width using simple linear regression (Meko and Baisan, 2001; Therrell et al., 2002; Griffin et al., 2011) or allometric equation based on the number of tracheids formed during the growing season (Camarero et al., 2021). Seasonal climate forcing on EW and LW production may, nonetheless, be site and species specific. For example, in boreal Sweden EW and LW growth of Scots pine (*Pinus sylvestris* L.) responded positively to spring temperature, although there was a higher correlation between EW width and May temperature (Miina et al. 2000). Therrell et al. (2002) showed that LW chronologies of Douglas fir (*Pseudotsuga menziesii* Franco.) from northern New Mexico responded positively to summer precipitation while LW chronologies from southern New Mexico responded positively to spring precipitation. In central Canada, only the LW chronology responded positively to mean temperature from April to May in jack pine (*Pinus banksiana* Lamb.) while the EW and LW chronologies of black spruce (*Picea mariana* Mill.) responded negatively to early summer temperature (July and July-August respectively; Hoffer and Tardif, 2009).

Dendroclimatic analyses of black ash (*Fraxinus nigra* Marsh.) and jack pine (*Pinus banksiana* Lamb.) trees conducted over eastern and central boreal Canada demonstrated consistent growth responses to spring climate (Hofgaard et al., 1999; Tardif and Bergeron, 1999; Tardif et al., 2001; Girardin and Tardif, 2005; Girardin et al., 2006; Huang et al., 2010; Genries et al., 2012; Kames et al., 2016). At Lake Duparquet, a warm beginning of the growing season (March - April) negatively

affected the number of earlywood vessels of floodplain *F. nigra* and positively influenced their mean cross-sectional area (Kames et al., 2016), while a warm early summer (May - June) negatively affected radial growth (Tardif et al., 2001). Warm and early spring (March - April) temperatures also favored the radial growth of *P. banksiana* (Hofgaard et al. 1999; Tardif et al., 2001; Girardin and Tardif, 2005; Girardin et al., 2006; Hoffer et al., 2009; Huang et al., 2010; Genries et al., 2012). The formation of light-colored latewood (so called “light ring”) in *P. banksiana* was moreover correlated to the effect of late winter snowfall and cool early springs delaying the onset of cambial activity at the beginning of the growing season (Girardin et al. 2009; Tardif et al., 2011). It can thus be hypothesized that chronologies of intra-annual tree-ring widths of *P. banksiana* and of earlywood vessels of *F. nigra* trees may contain specific climatic signals related to spring temperature variability, making them suitable candidate tree species for spring temperature reconstruction.

The objectives of this study were threefold: (1) to develop a network of spring-temperature sensitive tree-ring chronologies in eastern boreal Canada from *P. banksiana* and *F. nigra* trees, (2) to reconstruct and assess the variability of spring temperatures for the last 250 years, and (3) to investigate the associations between variations in spring temperature and the recent trends in regional spring flooding since the end of the Little Ice Age.

4.5 Material and methods

4.5.1 Study Area

The study area encompasses a longitudinal gradient within the northern Clay Belt of Québec and Ontario near Lake Duparquet, and at the southern fringe of the boreal forest (Fig. 4.1). The region is defined by the glaciolacustrine flat sediment deposits composing its soils and resulting from the drainage of the proglacial lakes Barlow and Ojibway during the last deglaciation (Daubois et al., 2015). The sub-boreal climate of the area is characterized by a near freezing mean annual air temperature (0.7°C), a high summer humidity (mean annual precipitation of 890mm) and a considerable amount of snowfall in fall to spring (mean annual snowfall of 250mm) as indicated for the period 1971–2000 by climate normals from ‘La Sarre’ weather station (48°48’ N, 79°11’ W; Canadian Climate Normals, http://climate.weather.gc.ca/climate_normals; Fig. 4.1).

Fire is the main natural disturbance in the study area. Post-fire forests are dominated by *P. banksiana* on nutrient-poor and sandy soils, or in associations with paper birch (*Betula papyrifera* Marsh.) and trembling aspen (*Populus tremuloides* Michx.) in more mesic conditions (Bergeron and Dansereau, 1993). After 80 to 100 years after a fire, forest stands transit toward an association of balsam fir (*Abies balsamea* (L.) Mill.), black spruce and white spruce (*Picea glauca* (Moench) Voss) (Cayford and McRae, 1983; Bergeron, 2000). Old-growth *F. nigra* forests grow on the lowland floodplains and in association with trembling aspen and eastern white-cedar (*Thuja occidentalis* L.) (Tardif and Bergeron, 1992; Denneler et al., 1999). The oldest living *F. nigra* specimens at Lake Duparquet have been dated to 1750–1770 (Tardif and Bergeron, 1999). *Pinus banksiana* is less long-lived (< 100 year on average; Cayford and McRae, 1983; Rudolph and Laidly 1990; Hofgaard et al. 1999), and in the absence of prolonged fire disturbance, the species is replaced by late successional ones (Cayford and McRae, 1983; Despons and Payette 1992). *Pinus banksiana* chronologies can, however, be

extended by using charred snags which are highly resistant to falling and decomposition compared to *Picea* and *Abies* spp. (Dansereau and Bergeron, 1993; Angers et al., 2010). Standing dead trees charred during one or several fires can remain under the canopy for several hundred years and thus reflect the growing conditions of one or more generations of trees prior to fire (Dansereau and Bergeron, 1993; Angers et al., 2010).

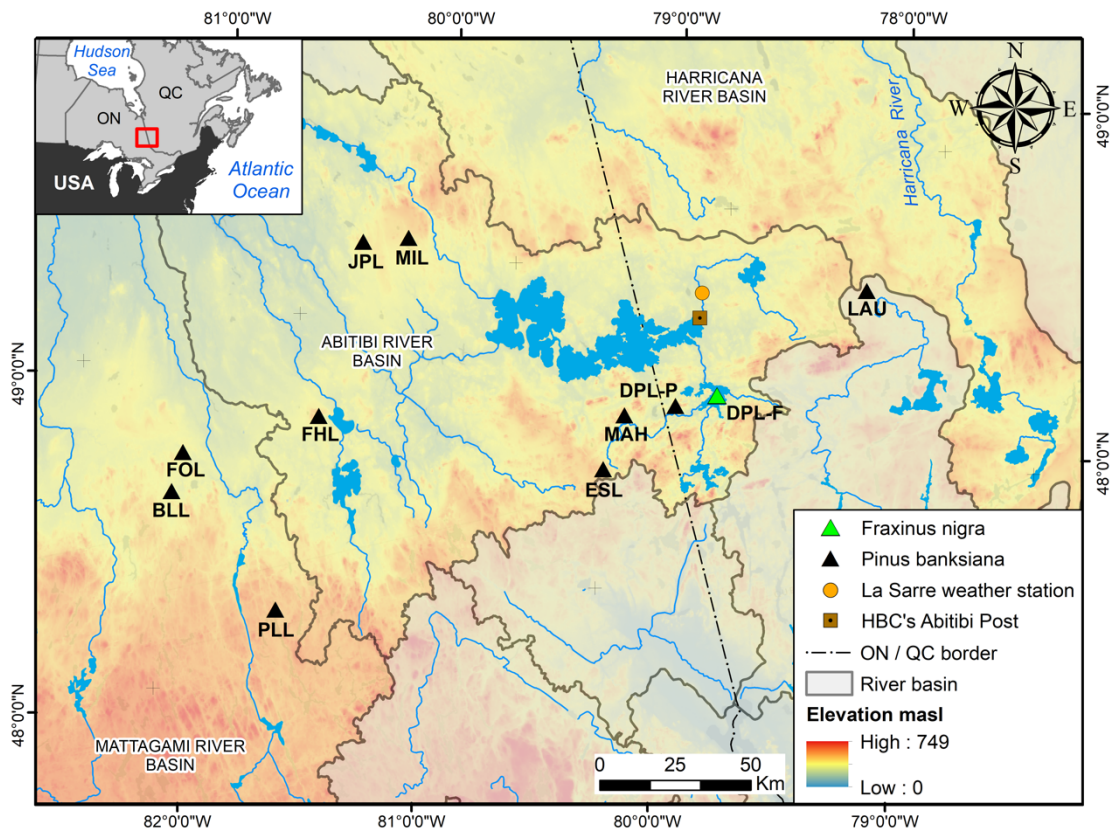


Figure 4.1 Map of the study area. *Pinus banksiana* (black triangles) and *Fraxinus nigra* (green triangle) sampling sites at the border between Ontario and Québec. River basin extents are provided for base map, and site codes are listed in Table 4.1.

4.5.2 Tree-ring data

During summer 2018, 722 samples were collected from 345 *P. banksiana* trees at ten sites (Fig. 4.1; Table 4.1) and including 45 samples (22 trees) from Dansereau and Bergeron (1993). Samples were prepared according to standard dendrochronological procedures (Cook and Kairiukstis, 1990) and crossdated using previous multi-century chronologies developed for *P. banksiana* (Bergeron and Dansereau, 1993; Hofgaard et al. 1999; Girardin et al., 2006). Earlywood (EW), latewood (LW), and total ring-width (RW) were measured using Coorecorder (v 9.6; Larsson, 2003a) and validated using both CDendro (v 9.6; Larsson, 2003b) and COFECHA (Holmes, 1983). Further dendrochronological details about the preparation of samples, pre-processing of chronologies to avoid biases from the influence of past fires on tree growth, as well as a climate-growth sensitivity analysis can be found in the Supplementary Materials.

Additionally, *F. nigra* anatomical and ring-width series developed in the floodplain of Lake Duparquet by Nolin et al. (2021a) were included in the tree-ring dataset and comprised an additional 62 series from 43 trees. *Fraxinus nigra* series were constituted of 12 variables including four ring-width variables (RW, EW, LW, and EW / RW proportion) and eight anatomical variables derived from the analysis of earlywood vessels (mean lumen cross-sectional area of the total, 25% largest, and 25% smallest vessels; total lumen cross-sectional area; number of vessels; porosity within the earlywood; density of vessels; and hydraulic conductivity diameter). Further details about these series are given in Nolin et al. (2021a).

4.5.3 Climate data

Because few weather stations in our study area predate the 1950s (Girardin et al., 2011) climate data were extracted from the KNMI Climate Explorer (<https://climexp.knmi.nl>; Trouet and Van Oldenborgh, 2013).

Table 4.1 Tree-ring chronologies provenance. Species are *Pinus banksiana* (PIBA) and *Fraxinus nigra* (FRNI). Code refers to Figure 4.1. (Period is the period after truncation to $n > 3$ samples to account for post-fire regeneration gaps in each site chronologies).

Species	Site	Code	Lat/Lon	N trees	N series	Period	Avg series length (years)
PIBA	Blue Lake	BLL	48°34'N; 81°44'W	19	39	1855–2017	105
PIBA	Lake Duparquet	DPL	48°28'N; 79°27'W	45	91	1776–2017	108
FRNI	Lake Duparquet	DPL	48°28'N; 79°16'W	43	62	1770–2016	64
PIBA	Esker Lake	ESL	48°20'N; 79°50'W	35	76	1833–2017	75
PIBA	Frederick House Lake	FHL	48°41'N; 81°01'W	40	80	1874–2017	103
PIBA	Footprint Lake	FOL	48°40'N; 81°39'W	45	93	1746–2017	86
PIBA	Jack Pine Lake	JPL	49°10'N; 80°39'W	29	65	1809–2017	90
PIBA	Launay	LAU	48°39'N; 78°30'W	18	40	1867–2017	125
PIBA	Magusi hills	MAH	48°29'N; 79°41'W	26	58	1777–2017	89
PIBA	Mistango Lakes	MIL	49°08'N; 80°26'W	25	53	1766–2017	113
PIBA	Peter Long Lake	PLL	48°09'N; 81°24'W	63	127	1723–2017	79

Monthly mean gridded CRU TS4.04 (Harris et al., 2020) temperature data were extracted from 1901 to 2019 and from a coordinate polygon corresponding to the spatial extent of the 11 sampling sites (48°N; –78°E to 49°N; –81.5°E; Fig. 4.1). From the same coordinate polygon, average land spring (March to May) temperatures from the Gridded Berkeley Earth Surface Temperature Anomaly Field (1750–2019; Rohde et al., 2013) and the 20th Century Reanalysis V3 (1836–2015; Slivinski et al., 2019) were downloaded as independent verification datasets for the reconstruction diagnostic. The Berkeley spring temperature is based on interpolation of an enhanced set of weather stations data and given as anomalies relative to Jan 1951 to Dec 1980 (Rohde et al., 2013). For the study area, the earliest climate observation of the Berkeley data corresponded to the spring of 1897 (Abitibi Post), and within a 500 km radius, the spring of 1866 (location(s) unknown). The Hudson's Bay Company fur trading post on Lake Abitibi (Abitibi Post, 48°43' N; 79°22' W; Fig. 4.1) is the oldest local source of

monthly temperatures with data recovered from 1897 to 1935 (years 1900, 1901, 1917 and 1922 missing; <https://climatedata.ca/>) and significantly correlating with Berkeley spring temperatures ($r = 0.96$, $p < 0.001$). Berkeley temperature for the earlier period (1750–1866) are the result of interpolation of data from climate stations further away than 500km (locations unknown) (<http://berkeleyearth.lbl.gov/locations/49.03N-78.37W>). The 20th Century Reanalysis, on the other hand, assimilates surface pressure observations and an ensemble of ocean-atmosphere circulation models to generate estimates of historical weather data (Slivinski et al., 2019). This dataset provides a reliable historical context of surface temperature fields from synoptic to climatic time scale (Slivinski et al., 2021).

To investigate the relationship between spring (March to May) temperature and regional to large-scale spring discharge, both instrumental (1915–2020; Water Survey of Canada, <https://wateroffice.ec.gc.ca>) and reconstructed Harricana River spring discharge (April 15 to June 30; 1771–2016; Nolin et al., 2021a), NOAA/NCDC Rutgers Snow Cover (March, April, May; 1967–2016; Estilow et al., 2015) and monthly GRUN global gridded runoff (March, April, May; 1902–2014; Ghiggi et al., 2019) were used. The reconstruction of the Harricana River spring discharge is derived from earlywood vessel cross-sectional area and ring width of *F. nigra* trees growing along the shores of Lake Duparquet, and periodically flooded in spring. The reconstruction captured 69% of the variance over a 102-year calibration period (1915–2016) and showed high coherency with regional flood-ring frequencies (Nolin et al., 2021b) and various hydrological paleorecord from subarctic Québec (Nolin et al., 2021a). Rutgers snow cover is a mapping of Northern Hemisphere snow extent, based on digitizing hand-drawn maps from shortwave satellite imagery (1967–1972; resolution ~4km) and very high-resolution radiometer satellite imagery (after October 1972, resolution ~1km; Estilow et al., 2015). GRUN runoff is a multi-model ensemble of hydrological simulations trained with observational discharge data and climate data

from a downscaled and corrected version of the 20th Century Atmospheric Reanalysis and provided at a 5° x 5° spatial scale (Ghiggi et al., 2019). The association with Lake Duparquet spring ice break-up water level reconstructed from maximum ice-scar heights (Tardif and Bergeron, 1997b) was also determined, as well as with observational ice break-up dates (site DPL; Mongrain et al., 2014; Mongrain, comm. pers. 2018). To detect and characterize linear trends in observed hydrological and climatic time series, non-parametric Mann-Kendall trend statistic was used (Burn and Hag Elnur, 2002; Monk et al., 2011; Mortsch et al., 2015).

4.5.4 Reconstruction of temperatures

A composite temperature reconstruction was developed from nested principal component regression models (Cook et al., 2003; Frank and Esper, 2005; Girardin et al., 2006) to maximize both spatial and temporal coverage of the predictor chronologies constituted of 30 *P. banksiana* (10 sites x 3 variables) and 12 *F. nigra* (1 site x 12 variables) chronologies. This method involves splicing the total time span of the tree-ring data into sub-periods of common intervals to maximize the number of tree-ring predictors in sub-periods. Principal components analysis (PCA) was performed on each sub-period from a correlation matrix to transform the standard chronologies into a reduced number of linear combinations of the original chronologies with reduced multicollinearity (Meko and Graybill, 1995; Hidalgo et al., 2000). Eigenvectors with an eigenvalue > 1 were retained as potential predictors following the Kaiser-Guttman rule in each model (Hidalgo et al., 2000; Frank and Esper, 2005). Since tree growth can be influenced by temperature from the previous year, principal components lagged forward by one year ($t + 1$) were also included in the predictors set to reconstruct temperature for the current year (t) (Fritts, 1976; Briffa, 1988).

Generalized additive mixed models (GAMMs; Wood, 2017) were used for the calibration of transfer function models needed for the spring temperature reconstruction. A GAMM is like a generalized linear mixed model (GLMM), except that smooth terms are incorporated, which allows for a rich collection of the nonlinear relationships, including multiple forms of spline functions. First, a screening of PCA-reduced standard chronologies (t and $t + 1$) was done using stepwise multiple linear regression analysis (p -value to enter = 0.05; p -value to remove = 0.01). The model took the form:

$$T_{i,t} = \beta(i^{th}_{t,t+1}) + \varepsilon_{i,t} \quad (4.1)$$

where T is the spring temperature, i^{th} represents n^{th} principal components, t represents the year, and ε the residual error of each model. The preselected candidate predictors were then entered in a GAMM corresponding to each sub-period. Each GAMM model included non-linear predictors (tree-ring data) to predictand (temperature data) relationships. The GAMM equations took the form:

$$T_{i,t} = f(i^{th}_{t,t+1}) + \nu_i + \varepsilon_{i,t} \quad (4.2)$$

where ν_i is an error term with an AR1 ($p = 1, q = 0$) correlation structure. Smoothing function (f) of the GAMM were cubic regression splines with a degree of smoothness determined using a built-in cross-validation fitting process (Wood, 2003). The significance of predictors was re-evaluated within the GAMM models ($p < 0.10$) to avoid variance inflation in the final regression equations. The variables for which the smoothing terms were not significant in this first iteration were passed in a second GAMM iteration, this time in a linear form:

$$T_{i,j,t} = f(i^{th}_{t,t+1}) + \beta(j^{th}_{t,t+1}) + \nu_{i,j} + \varepsilon_{i,j,t} \quad (4.3)$$

where j^{th} represents n^{th} principal components represented using a linear function (β). Predictors that did not satisfy the $p < 0.10$ requirement were removed. GAMM iterations were repeated until only significant predictors were included in the models. Fitted coefficients per periods (transfer functions) were then extracted from each GAMM model and applied to their respective PCs to get estimates of spring temperature over the period not covered by the instrumental data. Models' assumptions were validated using a standard analysis of the residuals, and each model was individually cross-calibrated and validated using the maximum period of overlap with instrumental data (116 years) split in half (1901–1958 / 1959–2016; 58 years). Final models were calibrated over the entire period of available temperature data (1901–2016). GAMM modeling was performed using the 'mgcv' package v.1.8-36 (Wood, 2021). Reconstruction efficiency and stability was assessed from the adjusted explained variance ($AdjR^2$) and Fisher's F statistic as well as from standard dendrochronological statistics reduction of error (RE, Briffa et al. 1988) and coefficient of efficiency (CE, Cook and Kairiukstis, 1990), product-mean test (PMT), sign test and mean absolute error (MAE, Cook et al., 1999). All statistical procedures were conducted in R v.4.0.3 (R Core Team, 2021).

4.6 Results

4.6.1 Reconstruction of spring temperatures

Twelve transfer functions were developed from the principal components of the tree-ring intra-annual width and anatomical chronologies and constituted 12 regression models covering 12 sub-periods and spanning at most 1723–2016 and at least 1947–2016 (Fig. 4.2ab; Fig. 4.S1; Table 4.S1). Stepwise regressions selected the current year PC1 as the main predictor in each model. The first model (1954–2016) explained 54% of the variance in the observed data with five predictors selected. It also performed

similarly in the split calibration-verification procedure (Table 4.S1). Calibration R^2 and verification statistics of the following models decreased with the decline of the number of potential predictors (Fig. 4.2c, Table 4.S1). Positive RE and CE, and $RE > CE$ indicated that nine of the 12 models covering the period 1770–2016 had predictive skill and that they could be merged in a composite reconstruction of mean spring temperature (Table 4.S1). The three remaining models extending to the year 1723 were thus excluded from the following analyses ($Adj.R^2 = 0.12, 0.12, 0.09$ respectively; Table 4.S1). The mean inter-correlation between the nine selected models also demonstrated a high consistency in the reconstructed regional temperature signal, with a mean Pearson $r = 0.83 \pm 0.08$ std (Fig. 4.S1). Overall, the reconstruction demonstrated good skill to track interannual variability and to reproduce the low-frequency patterns found in the instrumental spring temperature data with a slightly higher accuracy to capture mean negative (mean departure from instrumental data for negative values, $\bar{x} = -0.48 \pm 0.89$ std) than mean positive spring temperatures (mean departure from instrumental data for positive values, $\bar{x} = 0.95 \pm 0.77$ std) over the calibration period (1901–2016; Fig. 4.2; Table 4.S1). The accuracy of the reconstruction to capture extreme spring mean high and low temperatures, however, indicated a lower accuracy in capturing extreme low temperatures at the beginning of the century (1912, 1917, 1923, 1926, 1943 and 1950) and then a lower accuracy to capture extreme high temperatures at the end of the century (1977, 1986, 1987 and 2010; Fig. 4.2; Fig. 4.S1). The average residuals for the 10 years of highest and lowest spring temperatures remained comparable between the two half-calibration periods but also evidenced the better reconstruction of lowest spring temperatures at the end of the century (1901–1958, average residuals for the 10 warmest springs 1.21 ± 0.85 std, and the coldest -1.38 ± 0.80 std; 1959–2016, average residuals for the 10 warmest springs 1.38 ± 0.83 std and the coldest -0.51 ± 0.83 std). The reconstructed mean spring temperature was significantly correlated with the Berkeley mean spring temperature record during the entire reconstructed period ($r = 0.49, p < 0.001, 1770–2015$, Fig. 4.3c) and consistently

across much of central-to-northeastern Canada (Fig. 4.4a; Fig. 4.5a). Comparison with the mean spring temperature from the 20th Century Reanalysis also indicated a consistent correlation with our spring temperature reconstruction ($r = 0.42$, $p < 0.001$, 1836–2015) and across a comparable spatial extent (Fig. 4.5). To test the temporal and spatial stability of the associations between the reconstructed mean spring temperature over Canada, the Berkeley averaged spring temperature anomalies, and the spring mean temperature of the 20th Century Reanalysis, 50-years Pearson correlation' windows lagged backward by 25 years were used (Fig. 4.5). The results showed temporally consistent correlations centered on the study area, with the exception of the 1892–1941 interval where the spatial association decreased in the Great Lakes region in both data sets. The highest and most significant spatial correlations ($r > 0.60$; $p < 0.001$) with both datasets were found for the recent period and extending back to the beginning of the 19th century. The lower spatial correlation for the late 18th and early 19th centuries reflects the interpolation that has been done from climate stations located more than 500km from the study area in the Berkeley record and revealing associations being significantly higher with northcentral USA than central Canada (Fig. 4.5).

Three different periods can be distinguished in the reconstruction (Fig. 4.2a, Fig. 4.3a). A first period lasting from 1770 to ~1875 was marked by persistent multidecadal cold and warm phases of comparable amplitudes. This period lasted until the end of the Little Ice Age. From ~1875 to 1940, the amplitude in the decadal variability was reduced as highlighted by the 10-year smoothing spline (Fig. 4.2a, Fig. 4.3a). After ~1940, both the mean spring air temperature reconstruction and observational data were marked with a warm period contrasting with the last 250 years and a higher frequency of extreme warm spring temperatures. This third period (1940–2016) was also marked by the absence of multidecadal cold phase, and by the persistence of a warm phase lasting ~25 years (Fig. 4.2a, Fig. 4.3a). The cold phase that lasted from the end of the Little Ice Age until the 1900s and the warming enhancement post the 1950s

were more marked and persistent in the Berkeley record, albeit the two records (reconstruction and Berkeley) remained coherent at low frequency across those two periods (Fig. 4.3).

Given that the mean monthly and seasonal CRU, and Berkeley temperature timeseries showed no AR (1) autocorrelation, Mann-Kendall linear trend investigation was conducted. Significant ($p < 0.05$) linear warming trend were indicated in the month of May and overall spring from 1901 to 2019 in observed CRU temperature ($\tau_{\text{MAR}} = 0.10$, $p = 0.110$; $\tau_{\text{APR}} = 0.10$, $p = 0.116$; $\tau_{\text{MAY}} = 0.17$, $p = 0.007$; and $\tau_{\text{SPRING}} = 0.17$, $p = 0.007$) and Berkeley records ($\tau_{\text{MAR}} = 0.13$, $p = 0.044$; $\tau_{\text{APR}} = 0.08$, $p = 0.175$; $\tau_{\text{MAY}} = 0.18$, $p = 0.005$; and $\tau_{\text{SPRING}} = 0.18$, $p = 0.004$). The Berkeley records also showed a significant warming trend in March, which was not detected in the CRU dataset. As for the mean spring temperature reconstruction, it showed a modest linear warming trend over a comparable period ($\tau = 0.14$, $p = 0.022$, 1901–2016). Over the three periods (1770–1875, 1875–1940, 1940–2016) standard deviation in reconstructed mean spring temperature increased particularly since ~1940 in both positive (respectively, $\text{sd} = 0.57$, 0.47 , 0.74) and negative values (respectively, $\text{sd} = 0.43$, 0.57 , 0.64 ; Fig. 4.2a, Fig. 4.3a). Compared to the Berkeley record, which only showed a steady increase in mean spring temperature, the calibration data and the reconstruction showed particularly low peaks of mean spring temperatures and especially after the 1930s (Fig. 4.2a and Fig. 4.3). The last 40 years also showed less occurrence of extreme low spring temperature in each record (reconstruction, calibration data, Berkeley; Fig. 4.2a and Fig. 4.3). For instance, over the period 1901–2019, observed spring mean temperature values below the mean minus 1.5SD threshold (-1.85°C) occurred in years 1917, 1923, 1926, 1939, 1943, 1947, 1950 and 1956, with the coldest temperature recorded being the spring of 1926 (-2.87°C). In comparison, during the last 40 years (1980–2019) the coldest recorded temperature was -1.66°C in 1996.

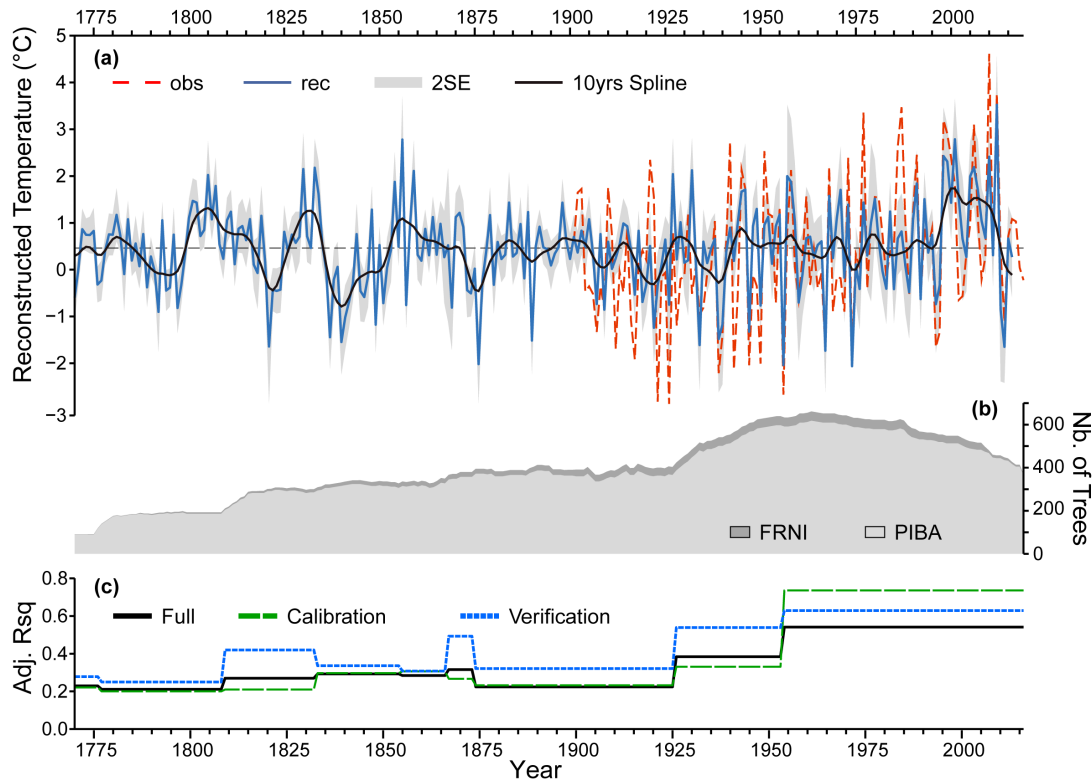


Figure 4.2 Characteristics of the composite temperature reconstruction. (a) Reconstruction of spring (March to May) temperature from 1770 to 2016 with two-standard-error confidence interval (grey) and decadal variation highlighted by a 10-year smoothing spline (black). Observed temperature data is illustrated by the dashed red line. A horizontal line delineates the reconstructed temperature mean at 0.41°C. (b) Sample depth of *Fraxinus nigra* (FRNI, dark grey) and *Pinus banksiana* (PIBA, light grey). (c) Adjusted multiple correlation coefficient (AdjR²) for each model periods and for the calibration (green), verification (blue) and full model (black) equations.

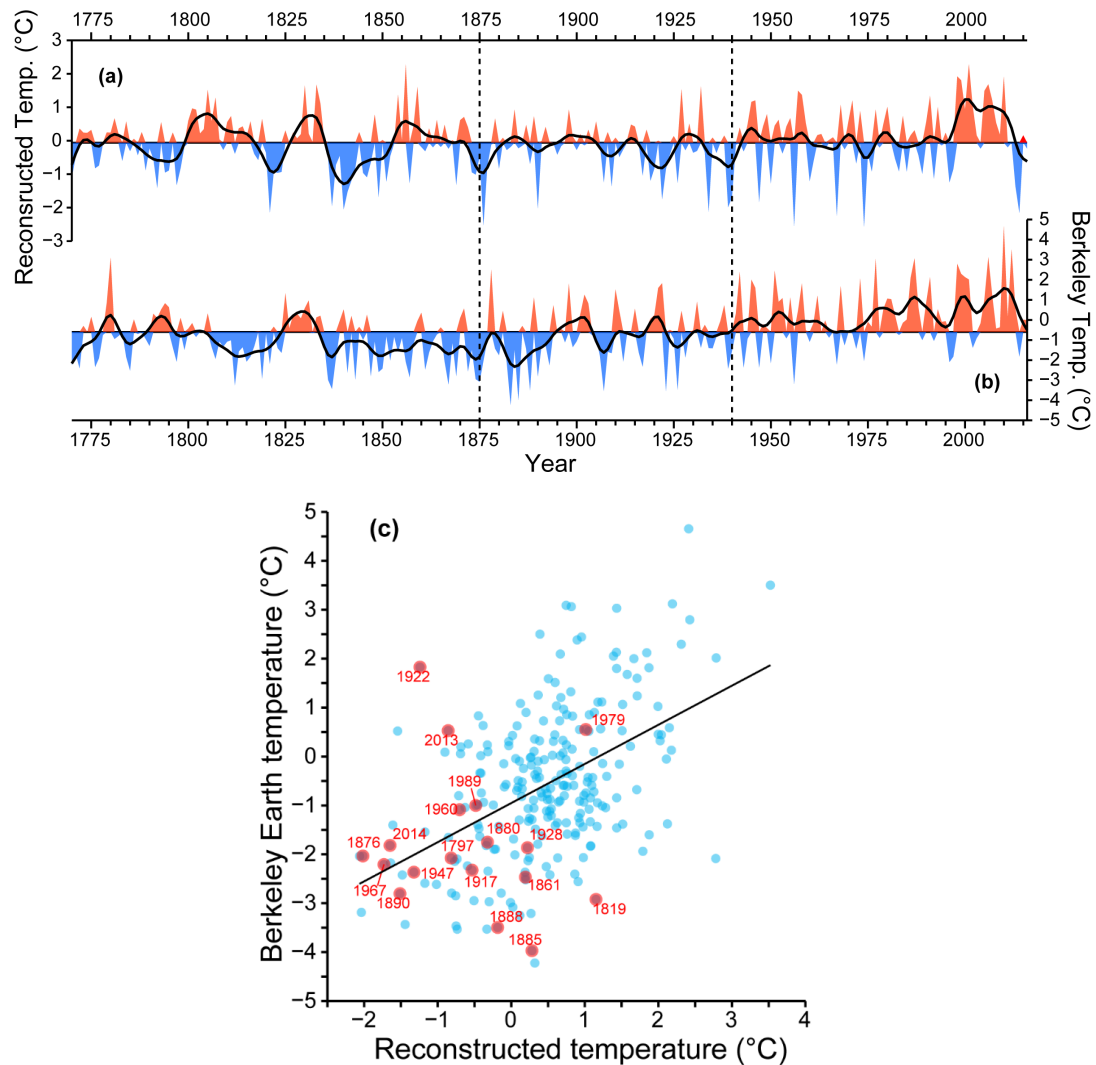


Figure 4.3 Comparison from 1770 to 2016 between (a) reconstructed mean spring air temperature and (b) Berkeley mean spring air temperature. Warm and cold phases are illustrated respectively by red and blue areas and supported by a 10-yr spline highlighting the decadal variability. Note that the two series are presented with a different y-axis range. Vertical dashed lines indicate the three periods (1770–1875, 1875–1940, 1940–2016) distinguished in the reconstruction. (c) Scatterplot of the two time-series showing the dispersion of their respective values (blue circles). Years highlighted by red circles indicate the ones with the highest discharge values in the reconstructed spring mean discharge of the Harricana River since 1770 (discharge higher than $151.3 \text{ m}^3/\text{s}$; Nolin et al., 2021a).

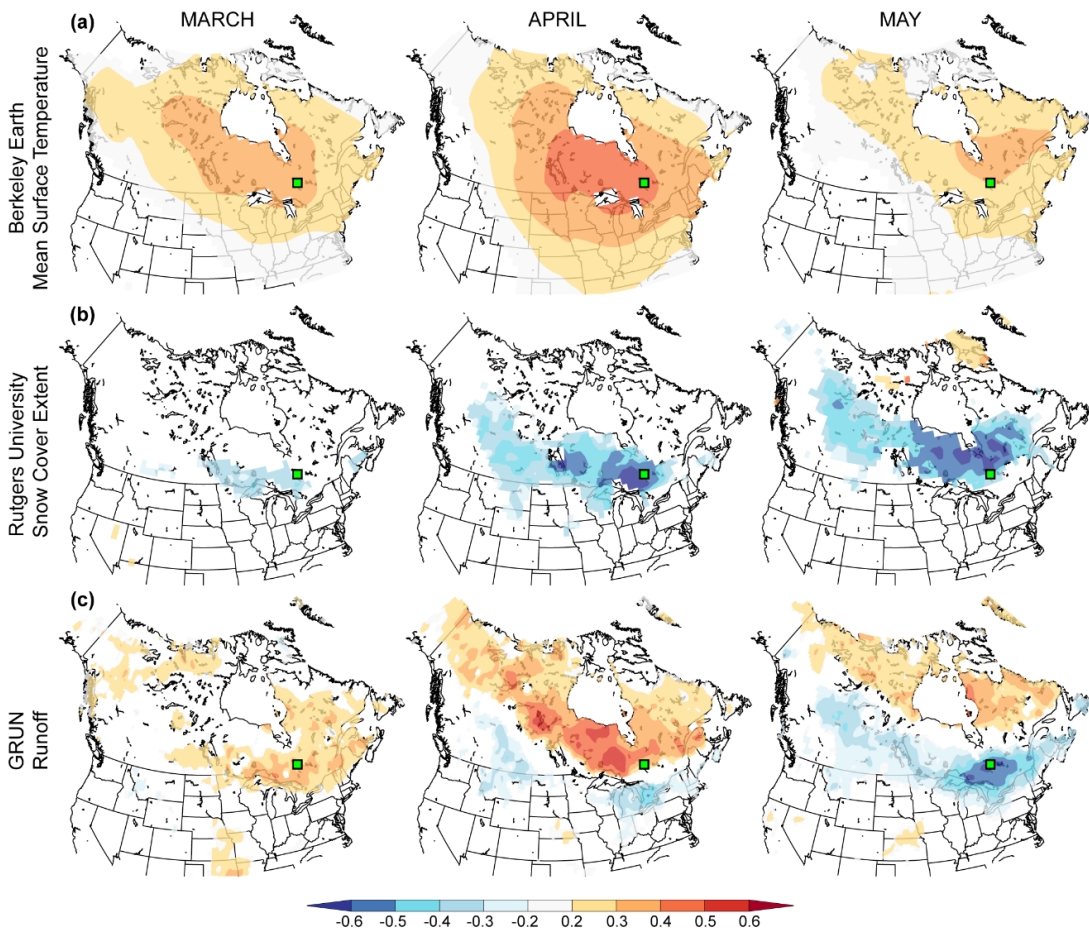


Figure 4.4 Spatial correlation maps ($p < 0.1$) between reconstructed spring mean air temperature and March to May (a) Berkeley average temperature anomalies (1770–2016), (b) NOAA Rutgers snow cover (1967–2016) and (c) GRUN runoff (1902–2014). Correlation coefficients range from positive (red) to negative (blue). Spatial correlations were done using the KNMI Climate Explorer engine (<https://climexp.knmi.nl>; Trouet and Van Oldenborgh, 2013). Green square symbol indicates the study area.

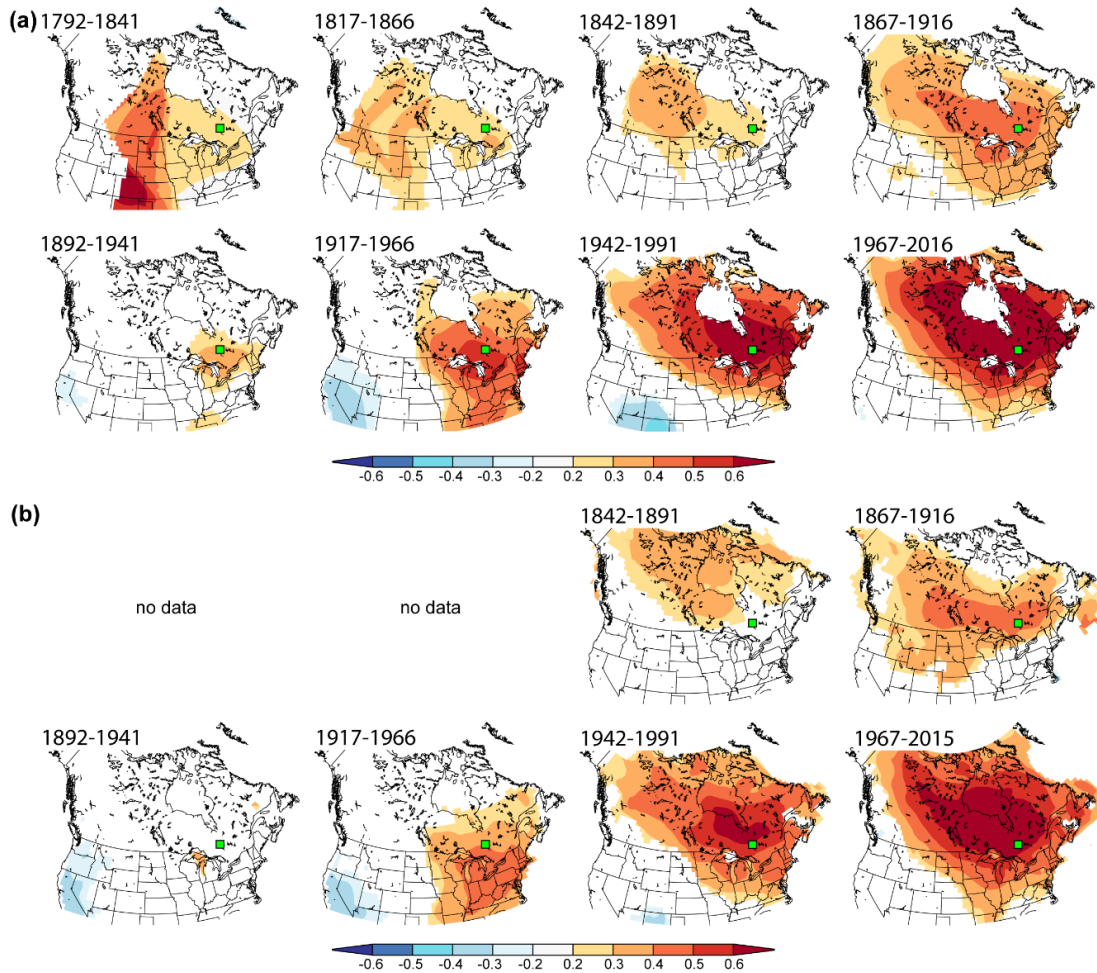


Figure 4.5 Spatial correlation maps ($p < 0.1$) between reconstructed mean spring air temperature and (a) Berkeley spring average temperature anomalies, and (b) 20th Century Reanalysis average spring temperature. Correlations are given for 50-years moving windows lagged backward by 25 years and were done using the KNMI Climate Explorer engine (<https://climexp.knmi.nl>; Trouet and Van Oldenborgh, 2013). Green square symbol indicates the study area.

4.6.2 Relationship to spring flooding

The reconstructed spring mean temperature showed high coherency with spring paleoflood evidence from Lake Duparquet. The reconstruction was negatively and significantly correlated with the Harricana River spring (April 15 to June 30) mean discharge in both reconstructed ($r = -0.52$; $p < 0.001$; 1771–2016) and instrumental ($r = -0.55$; $p < 0.001$; 1915–2016) dataset. Correlations with instrumental monthly mean and maximum discharge of the Harricana River (1915–2016) also showed that the reconstructed mean spring temperature was more strongly associated to late spring stage ($r_{\text{mean MAY}} = -0.61$; $r_{\text{max MAY}} = -0.54$; $r_{\text{mean JUN}} = -0.58$; $r_{\text{max JUN}} = -0.62$; all $p < 0.001$) than to early spring stage of the river ($r_{\text{mean MAR}} = 0.23$; $p = 0.019$; $r_{\text{max MAR}} = 0.29$; $p = 0.003$; $r_{\text{mean APR}} = 0.33$; $p = 0.001$; $r_{\text{max APR}} = 0.11$; $p = 0.271$). Correlations with averaged spring discharge (March to May) further demonstrated that the reconstructed mean spring temperature was more strongly associated to the spring maximum ($r = -0.50$, $p < 0.001$) than to spring mean discharge ($r = -0.22$; $p = 0.030$). In the Harricana River, maximum discharge occurred on average on May 8 and ranged between April 14 and May 29 (1915–2020). The mean spring temperature reconstruction was also negatively and significantly correlated with observed ice break-up date ($r = -0.54$; $p < 0.001$; 1968–2016) and spring lake water levels reconstructed from a maximum ice-scar height chronology ($r = -0.25$; $p < 0.001$; 1770–1990) for Lake Duparquet. The ice break-up at Lake Duparquet over the period 1968–2016 occurred on average on May 9 and ranged between April 20 and May 24. No significant linear trend toward earlier ice break-up was found in annual ice break-up dates for Lake Duparquet (Mann Kendall $\tau = -0.14$, $p = 0.162$; 1968–2018).

In the spring temperature reconstruction, most years with the lowest mean spring temperature calculated per decade (1771–1779, 1780–1789, ..., 2000–2009, 2010–2016; Table 4.2) corresponded to the most severe spring flood years reconstructed for

the last 250 years (1771–2016). A total of 14 years of minimum spring temperature (1797, 1861, 1876, 1880, 1888, 1890, 1917, 1922, 1947, 1960, 1967, 1989, 2013, 2014, and 2019 also but outside of the calibration period) matched 14 of the 18 years of highest spring discharge reconstructed since 1771 (the 1819, 1885, 1928 and 1979 floods did not match; Table 4.2). Similar results were obtained using the instrumental Harricana River spring discharge over the 1920–2016 period (1922, 1947, 1960, 1967, 1989, 2013, 2019 also but outside the calibration period), at the exception of year 2014 (127.21 m³/s; Table 4.2). While most of the minimum mean temperatures per decade were below zero, no apparent threshold at which the temperature corresponds to a high spring flood discharge was discernible (Table 4.2). The coldest reconstructed spring years also did not always correspond to the highest spring discharge (Table 4.2).

Significant and negative association was found between the reconstructed mean spring temperature and the last day with snow on the ground over the study area, calculated from daily Rutgers Snow Cover values as the first day with a value < 0.1 in spring ($r = -0.42$, $p < 0.001$; 1967–2016). Investigating spatial field correlations indicated strong and negative associations between reconstructed spring mean temperature and spring snow cover extent across much of central to northeastern boreal Canada (Fig. 4.4b). Associations were strongest in late spring (April, May) and particularly in May with the highest correlations found over the study area and extending to the James Bay and the Great Lakes (Fig. 4.4b). Used for validation purposes, spatial correlations of the reconstructed mean spring temperature with GRUN runoff indicated positive associations in March-April across much of northern Canada switching to negative associations in May over our study area (Fig. 4.4c), which is in line with the change in the sign of correlation found in the correlation with instrumental Harricana River mean and maximum discharge.

Table 4.2 Comparison of reconstructed mean spring (March to May) temperature minimums and of reconstructed and instrumental mean spring (April 15 to June 30) discharge maximums. Values are compared by decade and for the last 247 years. ‘REC discharge’ is the reconstructed mean spring discharge of the Harricana River (1771–2016) and is taken from Nolin et al. (2021a). ‘HAR discharge’ is the instrumental mean Harricana River spring discharge (1915–2020). Both mean spring discharges are average from April 15 to June 30 daily discharge data, while temperature reconstruction is average March to May. Years in bold highlight the years that are part of the highest mean spring discharge years since 1771. Grey cells highlight the years for which, per decade, the minimum spring temperature corresponds to the maximum spring discharge. The first (1771–1779) and last (2010–2016) periods used for comparisons are not complete decades.

Decade	REC Temperature		REC Discharge		HAR Discharge	
	1 st min	2 nd min	1 st max	2 nd max	1 st max	2 nd max
1771–1779	1770 (-0.60)	1776 (-0.32)	1771 (121.75)	1773 (118.24)	/	/
1780–1789	1789 (-0.38)	1783 (-0.09)	1789 (147.36)	1787 (146.60)	/	/
1790–1799	1792 (-0.90)	1797 (-0.82)	1797 (161.00)	1792 (143.92)	/	/
1800–1809	1809 (0.23)	1808 (0.54)	1808 (139.16)	1802 (122.11)	/	/
1810–1819	1818 (-0.07)	1816 (0.11)	1819 (157.43)	1818 (148.66)	/	/
1820–1829	1821 (-1.64)	1823 (-0.45)	1822 (150.29)	1826 (148.88)	/	/
1830–1839	1837 (-1.44)	1838 (-0.21)	1837 (145.53)	1838 (125.09)	/	/
1840–1849	1840 (-1.55)	1849 (-1.18)	1840 (150.69)	1845 (135.12)	/	/
1850–1859	1857 (-0.76)	1851 (-0.72)	1857 (146.67)	1853 (132.10)	/	/
1860–1869	1869 (-0.81)	1861 (0.19)	1861 (153.64)	1867 (132.11)	/	/
1870–1879	1876 (-2.02)	1874 (-0.51)	1876 (171.29)	1873 (147.39)	/	/
1880–1889	1880 (-0.32)	1888 (-0.19)	1888 (164.57)	1880 (160.10)	/	/
1890–1899	1890 (-1.51)	1895 (0.09)	1890 (170.25)	1899 (133.51)	/	/
1900–1909	1909 (-0.85)	1907 (-0.74)	1907 (151.05)	1909 (149.43)	/	/
1910–1919	1919 (-0.69)	1917 (-0.53)	1917 (159.52)	1919 (140.75)	/	/
1920–1929	1922 (-1.24)	1926 (-0.75)	1928 (175.57)	1922 (173.66)	1928 (191.15)	1922 (165.27)
1930–1939	1934 (-1.61)	1939 (-1.48)	1939 (137.34)	1930 (132.86)	1933 (160.68)	1939 (151.64)
1940–1949	1947 (-1.32)	1940 (-1.17)	1947 (177.34)	1949 (133.73)	1947 (189.79)	1949 (143.99)
1950–1959	1956 (-2.04)	1950 (-0.77)	1950 (134.24)	1956 (125.02)	1952 (128.15)	1956 (128.02)
1960–1969	1967 (-1.73)	1960 (-0.7)	1960 (179.95)	1967 (163.59)	1960 (196.10)	1967 (171.12)
1970–1979	1974 (-2.06)	1976 (-0.41)	1979 (184.86)	1974 (147.05)	1974 (179.85)	1979 (167.19)
1980–1989	1989 (-0.48)	1985 (-0.42)	1989 (161.72)	1983 (144.61)	1986 (152.84)	1989 (149.16)
1990–1999	1996 (-0.74)	1992 (-0.63)	1996 (144.31)	1995 (125.07)	1997 (131.21)	1990 (125.91)
2000–2009	2004 (0.27)	2003 (0.66)	2009 (138.62)	2008 (133.51)	2004 (141.97)	2009 (141.58)
2010–2016	2014 (-1.65)	2013 (-0.86)	2013 (170.90)	2014 (160.52)	2013 (156.90)	2017 (152.35)

4.7 Discussion

The reconstructed spring mean air temperature demonstrated evidence of a warming phase over the last century compared to the successive warm and cold persistent decadal phases observed up to the end of the Little Ice Age (1850–1870 CE). The coldest interval reconstructed *i.e.*, for the period ~1815–1855, is in line with tree-ring reconstruction of summer temperature published in sub-arctic Québec (Jacoby et al., 1988; Briffa et al., 1994; Gennaretti et al., 2014; Gennaretti et al., 2017) depicting this period as the coldest in the last millennium. The ~1815–1865 cold phases in northern Québec coincide with low solar activity (Guiot, 1987) and active volcanic decades (notably the April 1815 eruption of Mount Tambora, Indonesia; Jacoby et al., 1988; Briffa et al., 1994; Gennaretti et al., 2014; Gennaretti et al., 2017). Both the observed CRU temperature and Berkeley records demonstrated significant warming of May and overall, of spring over the 1901–2019 period and the greatest reconstructed warming in spring mean air temperature has been detected starting since about 1940.

Observed maximum discharge of the Harricana River (1915–2020) and ice break-up dates for Lake Duparquet (1968–2018) also indicated that the onset of spring flooding over the 20th century occurred on average in late April and early May. This suggest that air temperature in March and April may have had a greater influence on flood initiation than air temperature in May. While across Canada, minimum, mean, and maximum spring temperatures have generally warmed since 1950 (Zhang et al., 2001a), the projected mid-century (2030–2059) monthly temperature changes of the Great Lakes Basin also suggest that future increases in maximum temperatures are likely to be higher from May to October than in any other months, and with the smallest increase found in April (Zhang et al., 2018). The influence of the warming phase of spring temperatures reconstructed since ~1940 must therefore be put into perspective when

analyzing the relationship between spring temperature and flooding since significant linear warming trend in observed data was mostly found in May.

Independent regional studies already identified the 1850–1870s and 1930–1950s as breakpoints in the regional hydroclimate history. For instance, ice-scar frequencies and lake level changes for Lake Duparquet (Tardif and Bergeron, 1997b) and other lakes from high-boreal Québec (Lemay and Bégin, 2008; Boucher et al., 2011) pointed toward an increase in the magnitude and frequency of flooding since the end of the Little Ice Age and increasing since the 1930 to 1950s. Reconstruction of spring discharge in the Harricana River associated recent increases in flood frequency and magnitude with cold, snowy winters and late springs. Late spring snowmelt under the combined effect of spring precipitation and cold spring temperature marked the highest discharges of the century (Nolin et al., 2021a). High spatial coherency was found in this study between spring mean air temperature, the snow cover extent and the GRUN runoff. This result demonstrates the consistent control of spring temperature over snowmelt and runoff over central to northeastern Canada and particularly in late spring. The change in the sign of correlation between temperature, instrumental Harricana River discharge, and GRUN runoff suggests that discharge in March and April was associated to warm and early springs (positive correlation), and that discharge in May (and June) was associated to cold and late springs (negative correlation) with a persistent and thick snowpack. However, no significant linear trend was found in annual ice break-up dates for Lake Duparquet to support a trend toward earlier spring flooding. Indeed, per decade, much of the late and cold spring years were associated with the highest spring discharge years reconstructed for the Harricana River over the last 250 years (except for the years 1819, 1885), which was also supported by instrumental discharge data (except for year 2014). The years 1819 and 1885 represent regional contrasts in spring flooding with moderate flood-ring relative frequencies

recorded in regional rivers contrasting with high flood-ring frequencies and earlywood vessel records in Harricana River and Lake Duparquet (Nolin et al., 2021ab).

It should be noted that the *F. nigra* series from Lake Duparquet (43 trees) were used to reconstruct the mean spring discharge of the Harricana River. The present reconstruction of mean spring temperature contains these same 43 series (11% of the trees used), reduced in PC components with 345 other *P. banksiana* tree series (Table 4.1). The detrending of *F. nigra* series was also not the same in both studies (smoothing spline with a 50% frequency of response at 60 years in Nolin et al. 2021a; generalized negative exponential model detrending in the present study; cf. Suppl. Mat.). The use of the same proxies (43 trees) in both the Harricana River mean spring discharge and regional mean spring temperature reconstructions may influence the correlation between the two reconstructions. The decadal comparison between mean spring temperature and Harricana River mean spring discharge (1920–2016; Table 4.2), however, showed that results between instrumental and reconstructed Harricana River mean spring discharge were similar.

The variance explained by the present reconstruction (23 to 54%) is somewhat in the range of summer temperature reconstructions conducted over northeastern Canada using total ring-width of coniferous trees (Jacoby et al., 1988; Gennaretti et al, 2014) or multiproxy tree-ring approaches (Jacoby et al., 1988; Briffa et al., 1994). The present reconstruction underestimates extreme cold spring temperatures at the beginning of the century, and extreme high temperatures at the end of the century. Possible reasons include (1) the difficulty to capture a spring climate signal at the beginning of the growing season using dendrochronological proxies (Schweingruber, 1996; Rossi et al., 2013), (2) the spatial and temporal heterogeneity of historical data in the early calibration period (Girardin et al., 2011), (3) the diminution of tree-ring predictors going back in time, and (4) spring temperature variability and extremes that are not

captured by tree ring proxies as tree-growth is never 100% explained by climate factors (McCarroll et al., 2015). Indeed, the initiation of the tree-ring growth remain difficult to defined climatically (Schweingruber, 1996; Rossi et al., 2013) and some of the variance in early spring temperatures might not be fully captured by *P. banksiana* trees if warm temperatures arise when trees have not yet begun their cambial activity. For example, in this reconstruction, the springs 1987 and 2010 showed the largest underestimation of extreme high spring temperature observed during the calibration period. The years 1987 and 2010 are among the three earliest breakups recorded at Lake Duparquet since 1968, along with the year 1998 (1987: April 23, 1998: April 23, and 2010: April 22, 1968–2018 average being May 9). Observed CRU mean April temperature since 1901 were also highest in years 1955, 1984, 1987 and 2010 with values ranging from 4.84 to 5.25°C, as compared to a mean April temperature of 0.77°C over the 1901–2019 period.

Increases in the magnitude of both extreme warm and extreme cold reconstructed spring mean temperatures during the 1930s–1970s contrast with those reconstructed over the 1770–2016 period. These extremes also contrast with the Berkeley record but are consistent with our calibration data set. During the early stages of global warming (1930s), it is likely that the increase in near-freezing temperatures instead of below-freezing temperatures in winter and spring favored precipitation (snow and/or rain) and quicker melting (Davis et al., 1999; Zhang et al., 2000; Zhang et al., 2001b). One hypothesis could be that the occurrence of both cold (late spring, long-lasting snow cover) and warm extremes (early spring, quicker snowmelt) increased the frequency and magnitude of flooding observed in the region since 1930–1950 (Tardif and Bergeron, 1997b; Nolin et al., 2021ab) although this hypothesis still requires to be confirmed. Tardif et al. (1997b) had hypothesized that earlier spring melt with heavy rainfall could increase the risk of ice-breakup at a time the ice cover is thick, thus increasing the magnitude of flooding. The reduction in the number of cold springs in

the last 40 years of the reconstructed and observed spring mean temperature would also contrast with the assumption that spring floods are for the most part due to snowmelt during cold and late springs. This result indicates that warmer late spring mean temperatures on average may contribute, among other factors, to advance the spring break-up and to likely shift the contribution of snow to rain in spring flooding processes. Such change in flooding processes have already been reported in Canada since about the 1950s (Burn and Whitfield, 2016; Aygün et al., 2019; Bush and Lemmen, 2019) and similar trends are projected by most hydrological simulations across Canada and for Québec (Guay et al., 2015; Gaur et al., 2018; Bush and Lemmen, 2019). Warmer winter temperatures in northern Canada are expected to reduce snow accumulation and promote mid-winter melt, which should contribute to a decrease in SWE, while warmer spring temperatures are expected to accelerate snowmelt (Bush and Lemmen, 2019; Aygün et al., 2019). Warmer spring temperature in northern Canada should also increase the likelihood of rain-on-snow events as well as the spring rainfall to snowfall ratio in future years (Zhang et al., 2000; Ashmore and Church, 2001; Bush and Lemmen, 2019). Snow water equivalent had however increased in northern and central Québec since 1950 (Brown, 2010; Aygün et al. 2019). In terms of timing, earlier freeze-up and break-up trends have been observed in south-central Ontario since the 1900s (Fu & Yao, 2015), but not at Lake Duparquet. Using a cluster analysis of the Harricana River daily hydrographs, Nolin et al. (2021a) also noted that early spring break-ups with minimal to intermediate discharge dominated between 1998 and 2012 when compared to the period 1915–2020. Our present results further showed an inverse relationship between the reconstructed mean spring temperature and the last day with snow on the ground over our study area and for the 1967–2016 period.

Climate model simulations for the whole Québec project a +10% to +15% increase in precipitation (from south to north) by 2050 with a net change in winter and spring precipitation forms, contributing to a 0 to 5% increase (again from south to north) in

the contribution of winter months to annual streamflow, and an increase in average spring flood volume of about 5% (Guay et al., 2015). The frequency of extremes and their maximum magnitudes are also expected to increase by up to +20% for Québec by 2070 led by rain instead of snow (Clavet-Gaumont et al., 2017). At this point, it remains hazardous to clearly dissociate a snowmelt-driven flood from a rainfall-driven flood in our study area, and it remains to be determined how the increase in spring temperatures, the reduction in snow cover, and the increase in rainfall will interact with the flood regime in snowmelt driven river basins. For instance, the years 1989 and 1999 in the Harricana River were characterized by two peaks triggered by the snowmelt in late spring, and by heavy precipitation event in early summer (not shown).

Future research could aim at a reconstruction of precipitation or of snow parameters (e.g., snow cover extent, snow depth or snow water equivalent) to further investigate the relationship between precipitation, snowmelt and flooding and allow to predict consistent hydroclimatic trajectories under various climate change scenarios. For instance, Mood et al. (2020) developed a reconstruction of the snowpack variability from annual ring-widths of high-elevation Pacific Silver Fir (*Abies amabilis* Douglas ex. J. Forbes) in British Columbia. Similar reconstructions also come from areas where tree growth is more water limited. For instance, Touchan et al. (2021) reconstructed multi-millennial variability on April 1st SWE from EW and LW width chronologies of Giant Sequoia (*Sequoiadendron giganteum* J. Buchh. ex Lindl.) in California and Colorado, US. The studies of Mood et al., (2020) and Touchan et al., (2021) benefited from manual snow records since the 1950s to calibrate the tree-ring predictors. In the same way, Shamir et al. (2020) used principal components analysis of snowpack-related climatic variables, derived from a high-resolution hydrological model, to explain respectively 48 and 35% of the variance in earlywood and latewood width chronologies of four coniferous tree species growing in mountains of central Sierra Nevada, US. Overall, these results suggest that tree species responding to climate

parameters of the early growing season, such as *P. banksiana* and *F. nigra* might be suitable candidates to reconstruct snow variability and further investigate the relationships between spring snow cover, temperature and flooding.

4.8 Conclusion

This work presents a new *Pinus banksiana* tree-ring network and a well-verified reconstruction of regional spring mean air temperature consistent across much of central-to-northeastern Canada and since year 1770. The 12 transfer functions calculated explained 23 to 54% of the observed spring mean temperature variability over the last 247 years with a decreasing efficiency back in time which correspond mainly to the decrease in the number of available tree-ring data in the early years of the reconstruction. The end of the Little Ice Age was characterized by cooler than average springs and multidecadal cold and warm phases before transitioning toward a warming of late spring (May) temperature, and particularly after the 1940s and in the last 40 years. Most of the highest spring flooding reconstructed in the nearby Harricana River matched with the decadal variability reconstructed in low spring temperature. The coherency found with the snow cover extent and the gridded runoff across much of central-to-northeastern Canada also support that high historical spring flooding were mainly triggered by long lasting snow cover in late spring. However, over the last 40 years of the reconstruction, the reduction in the number of cold springs may suggest that spring flooding may now be related less to the persistence of late spring snow cover, but rather to earlier snowmelt and increased precipitation contribution to discharge. These changes in boreal hydrology and flooding appear to be a likely consequence of the recent warming trend observed in mean spring temperatures. Further research is needed to understand whether changes have occurred in the distinct contributions of current snow and precipitation to spring flooding to allow for reliable regional hydroclimatic trajectory projections. Among other things, it will be necessary

to determine whether or not future changes in spring temperature will lead to changes in the relative supply of rain and snow to the spring flood dynamics in eastern boreal Canada.

4.9 Data Availability statement.

Relevant data for this study are available from Nolin, A. F., Girardin, M. P., Tardif, J. C., Guo, X. J., Conciatori, F., & Bergeron, Y. (2021) *Pinus banksiana* and *Fraxinus nigra* dataset for the study of spring temperature in eastern boreal Canada. Mendeley Data, v1. <http://dx.doi.org/10.17632/kk2rsk7rj6.1>. Data include tree-ring width and wood anatomical chronologies (*PIBA_FRNI_Chronos.csv*) with their respective sample depth (*PIBA_FRNI_SampDepth.csv*) and the reconstructed spring mean temperature (*PIBA_FRNI_RecSpringTemp.csv*), as well as the gps position of the sampling sites (*LAT_LON_RecSpringTemp.kml*), and a set of self-explanatory instructions and descriptions for data files (*metadatas.txt*). All other data are available upon request to the corresponding author at alexandreflorent.nolin@uqat.ca (institutional email), alexandreflorent.nolin@gmail.com (permanent email).

4.10 Acknowledgments

We thank the field and laboratory assistants Marion Cartier, Cyrielle Ducrot, Ralitsa Mincheva, and especially Isabelle Gareau for their thorough work. We also acknowledge the special support of the Forêt d'Enseignement et de Recherche du Lac Duparquet (FERLD) research station team for their support during the field campaigns and laboratory procedures and especially Danielle Charron and Raynald Julien. Locating old growth *P. banksiana* stands in northern Ontario was made possible with special support from Lars Hildebrandt and Bonny Fournier (Ontario Forest Service). This study was a contribution of Canada Research Chairs (NSERC-CRC) hold by YB

and JT and was funded by the Natural Sciences and Engineering Research Council of Canada Collaborative Research program including our partners Ouranos, Hydro-Québec, Ontario Power Generation (OPG) and The University of Winnipeg. This work was also supported by a scholarship from RIISQ – Intersectorial Flood Network of Québec (2nd program 2020–2021) awarded to AN. Earlier versions of the manuscript benefited from constructive comments by Susanne Kames (University of Winnipeg), David Huard (Ouranos), and Kurt Kornelsen (OPG). We also thank the contributions of the Associate Editor Dr. Jose Marengo and two anonymous reviewers who provided constructive comments and suggestions on earlier drafts of the manuscript.

4.11 Supplementary Materials

4.11.1 Construction of tree-ring chronologies

Prior to detrending of the individual tree-ring series (*P. banksiana* and *F. nigra*), the first 10th years of growth were removed when the tree center was present to remove noise associated with post-fire establishment and differing rates of canopy closure. The series exceeding 200 years long (restricted at MIL site) were limited to 125 years in the following analyses in order to minimize age-related biases of old trees whose LW width decreases significantly and tends towards a variance in LW width close to zero (Griffin et al., 2011; Girardin et al., 2012; Fig. 4.S2). As many burned trees and snags did not have a center due to rot, and to overcome shortcomings in missing center interpolation, the iterative detrending method proposed by Girardin et al. (2012) was applied to individual tree-ring series of *P. banksiana* and *F. nigra*. Series were first standardized using a power transformation based on Cook and Peters (1997) and detrended using a generalized negative exponential modelling (GNE). In this procedure the GNE function is first used as detrending and when it does not converge, the detrending curve is selected between a Hugershof function and a linear model based on the highest coefficient of determination (R^2). One advantage of this method is the equivalent

weight assigned to slow and fast-growing trees allowing to reduce noise related to site and biological effect without altering the low-frequency trends (Girardin et al. 2012). To further reduce the localized noise in tree-ring data and emphasize the common (climatic) signal, tree-mean series were averaged by sites using a Tukey's bi-weight robust mean to lower the influence of outliers (Cook and Kairiukstis, 1990). Due to post-fire related recruitment of *P. banksiana* trees in time, the chronologies had internal missing parts and did not always overlap. Parts of mean-site chronologies with low replication ($n \leq 3$) were excluded as most of those parts were the results of old snags transitioning between generations of pines and may have reflected conditions of sudden fire-opened forests. If less than three successive years were missing in each site chronology, the missing entries were filled by the corresponding years in the average chronology of all sites (representing 15 over 9750 annual values). Alternatively, when more than three successive years were missing, missing entries were filled by the corresponding site mean (straight line) to keep the site in the predictors pool (representing 363 over 9750 annual values and confined to the recent part of the MIL site series: no internal values were replaced by the mean). From this step, tree-ring chronologies were not pre-whitened to preserve as much low-frequency variability as possible in the temperature reconstruction model. Temporal autocorrelation was corrected on the model's residuals. However, for the sole purpose of climate-growth sensitivity analysis, chronologies of the two tree species with significant autocorrelation were prewhitened using a best-fit autoregressive model (Cook and Kairiukstis, 1990) before being compared to instrumental monthly minimum, maximum and mean temperature.

4.11.2 Strength of tree-ring chronologies

A total of 388 *P. banksiana* and *F. nigra* trees (784 series; Table 4.1; Fig. 4.S2) were included in the climate-growth sensitivity analysis. After truncation resulting from the corrections for young and old series and parts with low replication ($n < 3$ trees), *P. banksiana* width chronologies spanned a common period of 1770–2016 and a maximum period of 1723–2016 covered only by the PLL site (Table 4.1, Fig. 4.2b; Fig. 4.S2). Common growth signals in *P. banksiana* indices were analogous between chronologies and sites. The common signal was also stable over the two common periods calculated between sites to maximize the number of years and series per site (1874–1953 and 1930–2017) with mean inter-series correlation coefficients (R_{bar}) being respectively $RW = 0.29 \pm 0.05$; $EW = 0.27 \pm 0.04$; $LW = 0.27 \pm 0.04$ (Table 4.S2). The mean expressed population signal (EPS) indicated that the sample-size was sufficient to capture the regional population growth-signal with respectively $RW = 0.85 \pm 0.07$; $EW = 0.85 \pm 0.07$; $LW = 0.85 \pm 0.06$ over the two common periods, and that a minimum of about 30 trees per site was required to obtain $EPS > 0.85$ (Table 4.S3).

4.11.3 Sensitivity of tree-ring chronologies to temperature

The highest correlations were found between the chronologies of the two tree species and the mean temperature of March and April and, to a lesser extent with mean May temperature, with good consistency between sites and species (min and max not shown; Fig. 4.S3). Overall, *Pinus banksiana* LW chronologies demonstrated the most consistent and positive responses to mean temperature in March, April, and May, compared to *Pinus banksiana* RW and EW chronologies and to *Fraxinus nigra* chronologies (Fig. 4.S3). Strongest positive spring responses were found in the month of April and with *P. banksiana* LW chronologies showing the highest correlation coefficients at 9 out of 10 sites and ranging from $r = 0.28$ to 0.51 ($p < 0.001$; 1931–2017). *Pinus banksiana* RW, EW, and LW chronologies responded positively to mean temperature in March, April, and May at the FOL and JPL sites, in March and April at

the BLL site, in April and May at the DPL site, and in April at the BLL, DPL, FHL, FOL, JPL, LAU, MAH, and PLL sites (8 out of 10 sites; Fig. 4.S3). Chronologies generated from trees of site MIL showed low correlations to spring mean temperature, which could be related to the difference in the common period used for the sensitivity analysis (1901–1953; Fig. 4.S3). Warm autumns were favorable to EW, LW and RW growth of *P. banksiana* at 4 to 7 sites out of 10. Chronologies of EW of *F. nigra* and LW of *P. banksiana* also responded to summer mean temperatures at few sites (Fig. 4.S3). Among the *F. nigra* chronologies from Lake Duparquet (DPL), anatomical variables displayed a higher response to early-spring mean temperatures (March, April) compared to ring-width variables. Maximum correlations were found in April with variables related to vessel dimensions (mva, tva, l25, s25; $r = 0.40 \pm 0.03$, $p < 0.001$) and few responses with variables related to vessel number (pe and n respectively; $r_{pe} = 0.27$, $r_n = -0.27$; $p < 0.001$; Fig. 4.S3). No latitudinal or longitudinal gradient was found among the strength of site-associations to monthly spring mean temperature. As chronologies showed consistent and comparable responses to the regional temperature signal, nested regression of the mean spring air temperature (March to May) was conducted using all available chronologies reduced to n^{th} principal components.

Exploratory analyses conducted by reproducing the GAMM models with variable seasonal windows (March, April, May, March to April, April to May, March to May) and different temperature variables (min, mean, max) demonstrated that the calibration-verification procedure performed better with the mean spring temperature (March to May), and using non-prewhitened (standard) chronologies.

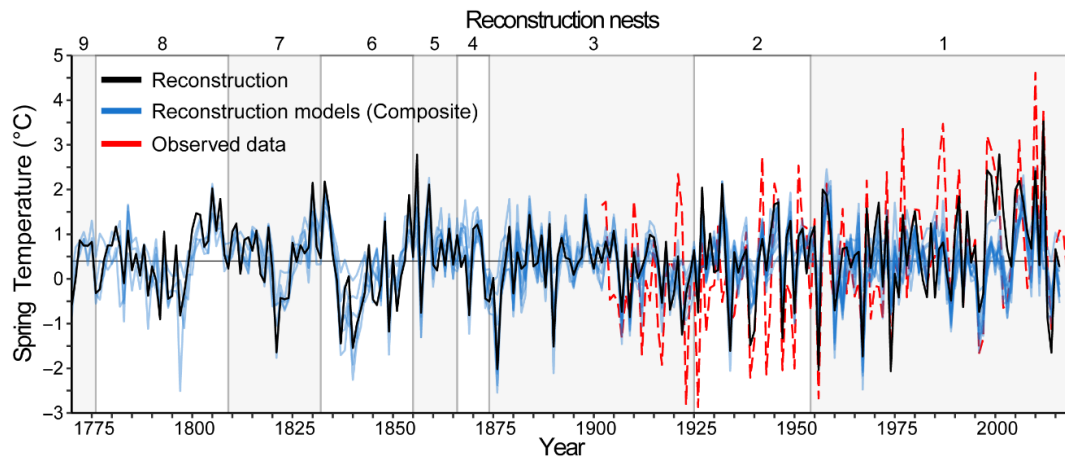


Figure 4.S1 Consistence between the nine composite reconstruction models. Reconstructed mean spring air temperature as result of the nine GAMM models that passed the verifications tests (in blue) compared to the observed mean spring air temperature CRU data used for calibration (1901–2016; in dashed red), and to the final reconstruction (in black). The nine sub-periods of common interval corresponding to nine models are represented by alternating grey and white background color.

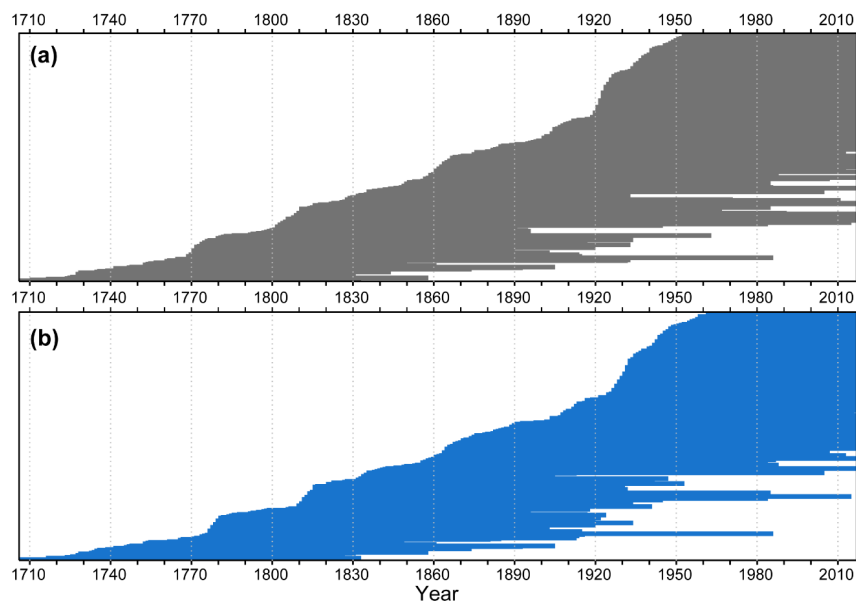


Figure 4.S2 Segment plot depicting the length of each of the 345 crossdated *Pinus banksiana* tree mean chronologies (a) before and (b) after age truncation to correct for young and old series and low replication ($n < 3$).

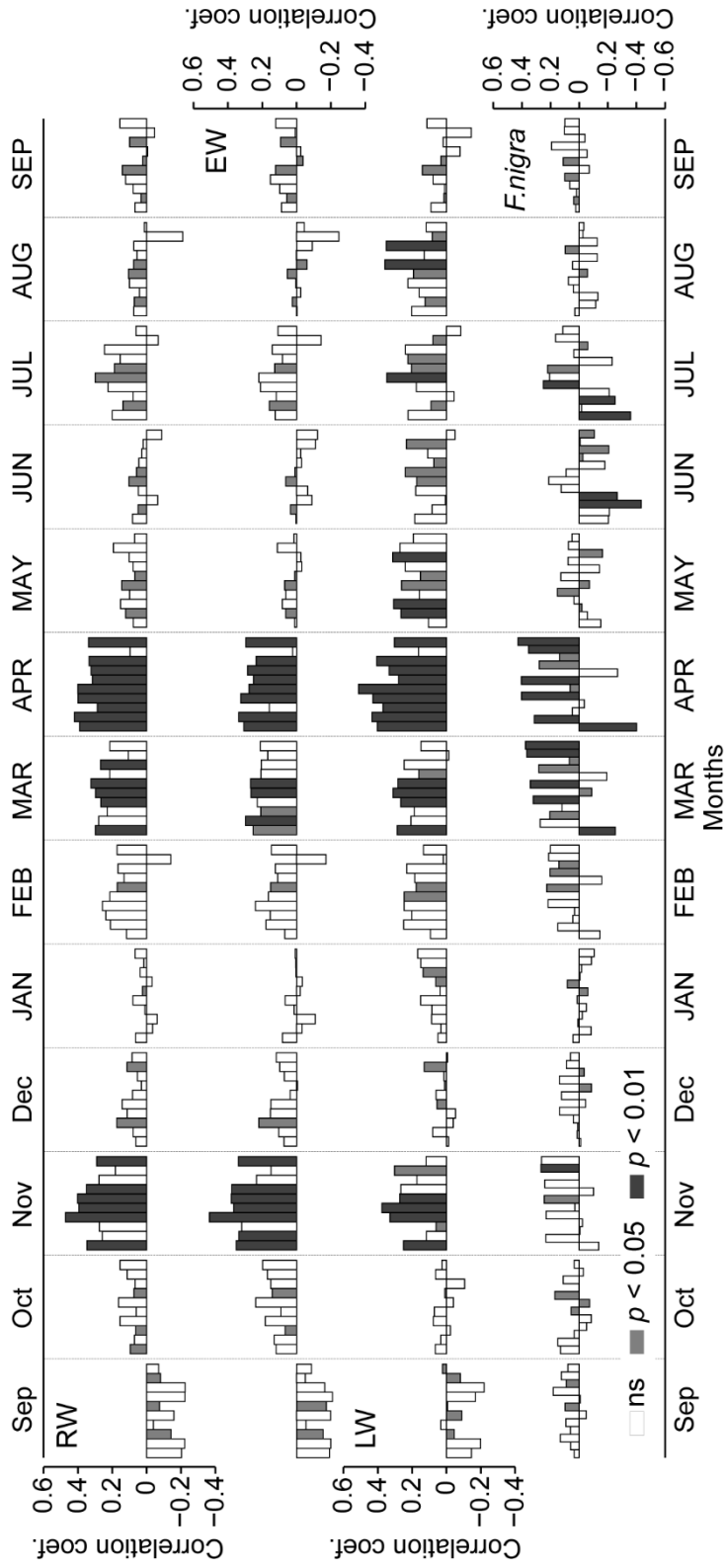


Figure 4.S3 Correlation coefficients between residual tree-ring chronologies and monthly CRU 4.04 temperature from previous to current September. Values are 1,000 times bootstrapped Pearson correlation coefficients for *Pinus banksiana* (RW) total ring width, (EW) earlywood width, (LW) latewood width chronologies from the 10 sites, and ordered as in Table 4.1 (BLL, DPL, ESL, FHL, FOL, JPL, LAU, MAH, MIL, PLL), and for the 12 *Fraxinus nigra* variables ordered as (de, Dh, ew, ewrw, l25, lw, mva, n, pe, rw, s25, tva, see Nolin et al., 2021a for details). Common period is 1931–2017 except for the *P. banksiana* MIL site (1901–1953) because chronologies were cut to remove the oldest portions > 125 years. Significant correlations are indicated with medium grey ($p < 0.05$) and dark grey ($p < 0.01$) histograms.

Table 4.S1 Calibration and verification statistics for each model. Abbreviations are as follows: adjusted and multiple R-squared (AdjR^2 and R^2), Pearson's correlation coefficient (r), reduction of error statistic and coefficient of efficiency (RE and CE), root mean square error (RMSE), mean absolute error (MAE), Fisher's F statistic (F), product mean test (PMT) and sign test. Model that didn't pass the verification tests, and therefore were not retained for the composite reconstruction, are highlighted with a grey background.

	No. potential predictors	No. selected predictors	Period	Calibration	Verification	AdjR^2	R^2	r	RE	CE	RMSE	MAE	Fstat	PMT	Sign test
1	16	5	1954–2016	1954–1985 1985–2016	1985–2016 1954–1985	0.54 0.74	0.58 0.78	0.76 0.91	0.57 0.90	0.57 0.88	0.97 0.55	0.76 1.32	15.59 18.25	5.02 4.16	47+16– 20+12–
2	18	4	1926–2017	1926–1971 1971–2016	1971–2016 1926–1971	0.38 0.33	0.41 0.39	0.66 0.65	0.43 0.66	0.43 0.52	1.14 1.04	0.92 1.22	15.05 6.57	5.53 3.06	63+28– 27+19–
3	20	3	1874–2017	1901–1958 1959–2016	1959–2016 1901–1958	0.23 0.32	0.27 0.36	0.52 0.64	0.48 0.49	0.34 0.34	1.19 1.13	1.14 1.33	6.73 9.97	3.39 –0.05	35+23– 36+22–
4	18	5	1867–2017	1901–1958 1959–2016	1959–2016 1901–1958	0.27 0.49	0.33 0.54	0.58 0.75	0.53 0.62	0.40 0.51	1.13 0.97	1.06 1.41	5.15 12.09	3.45 3.12	39+19– 35+23–
5	20	4	1855–2017	1901–1958 1959–2016	1959–2016 1901–1958	0.28 0.31	0.31 0.36	0.55 0.59	0.30 0.54	0.30 0.41	1.23 1.12	0.99 1.11	12.41 7.30	5.75 3.61	78+38– 39+19–
6	16	4	1833–2017	1901–1958 1959–2016	1959–2016 1901–1958	0.29 0.30	0.32 0.38	0.56 0.58	0.32 0.50	0.32 0.40	1.22 1.13	0.97 1.07	12.90 7.01	5.26 2.82	71+45– 37+21–
7	14	4	1809–2017	1901–1958 1959–2016	1959–2016 1901–1958	0.27 0.21	0.30 0.27	0.64 0.50	0.29 0.47	0.29 0.32	1.24 1.20	1.00 1.08	11.65 4.80	4.98 2.92	70+46– 38+20–
8	12	2	1777–2017	1901–1958 1959–2016	1959–2016 1901–1958	0.21 0.42	0.22 0.46	0.47 0.69	0.22 0.55	0.22 0.42	1.30 1.05	1.04 1.35	16.35 11.32	5.10 2.93	73+43– 36+22–
9	12	2	1770–2017	1901–1958 1959–2016	1959–2016 1901–1958	0.20 0.25	0.23 0.28	0.46 0.54	0.44 0.39	0.29 0.21	1.23 1.23	1.09 1.23	8.12 10.51	2.54 2.43	38+20– 37+21–
				1901–1958 1959–2016	1959–2016 1901–1958	0.22 0.28	0.25 0.30	0.50 0.55	0.46 0.40	0.32 0.22	1.21 1.22	1.15 1.29	9.09 11.97	2.75 3.23	36+22– 36+22–

Table 4.S1 (suite)

Model	No. potential predictors	No. selected predictors	Period	Calibration	Verification	adjR ²	R ²	r	RE	CE	RMSE	MAE	Fstat	PMT	Sign test
10	6	1	1766–2017	1901–1958 1959–2016	1959–2016 1901–1958	0.12 0.14	0.13 0.15	0.36 0.39	0.13 0.40	0.13 0.23	1.38 1.28	1.11 1.14	16.53 10.00	4.50 1.84	66+50– 33+25–
11	4	1	1746–2017	1901–1958 1959–2016	1959–2016 1901–1958	0.12 0.16	0.13 0.18	0.36 0.41	0.13 0.40	0.13 0.24	1.37 1.27	1.12 1.18	17.20 11.85	4.20 1.75	66+50– 33+25–
12	2	1	1723–2017	1954–1985 1985–2016	1985–2016 1954–1985	0.09 0.00	0.10 0.04	0.32 0.24	0.10 0.49	0.10 0.38	1.41 1.24	1.16 1.29	6.82 1.08	3.74 3.30	32+31– 18+14–
				1985–2016	1954–1985	0.16	0.19	0.45	0.11	–0.20	1.40	1.37	7.01	2.50	17+15–

Table 4.S2 Mean inter-series correlation coefficient (R_{bar}) on detrended tree mean time series after age correction (10 first years of growth removed, and MIL site cut at 125 years old). R_{bar} was calculated over two common periods maximizing the number of years and series per site. Slashes (“/”) indicate that series did not span entirely the common period. Number of trees per site in both common periods is indicated in the last right column.

Sites	Ring Width (RW)		Earlywood Width (EW)		Latewood Width (LW)		N trees	
	R_{bar} (1930–2017)	R_{bar} (1874–1953)	R_{bar} (1930–2017)	R_{bar} (1874–1953)	R_{bar} (1930–2017)	R_{bar} (1874–1953)	1930–2017	1874–1953
BLL	0.32	0.33	0.28	0.34	0.29	0.28	17	16
DPL	0.28	0.24	0.27	0.25	0.27	0.23	27	41
ESL	0.29	/	0.26	/	0.29	/	17	/
FHL	0.34	0.33	0.30	0.30	0.33	0.29	38	40
FOL	0.29	0.23	0.27	0.23	0.22	0.27	19	36
JPL	0.29	0.21	0.25	0.24	0.25	0.23	19	13
LAU	0.25	0.25	0.23	0.24	0.28	0.28	18	17
MAH	0.31	0.25	0.29	0.27	0.29	0.23	18	22
MIL	/	0.39	/	0.40	/	0.35	/	22
PLL	0.27	/	0.25	/	0.29	/	36	/

Table 4.S3 Expressed population signal (EPS) of the tree-mean chronologies after age correction (10 first years of growth removed, and MIL site cut at 125 years old). EPS was calculated over two common periods maximizing the number of years and series per site. Slashes (“/”) indicate that series did not span entirely the common period. Number of trees per site in both common periods is indicated in the last right column.

Sites	Ring Width (RW)		Earlywood Width (EW)		Latewood Width (LW)		N trees	
	EPS (1930–2017)	EPS (1874–1953)	EPS (1930–2017)	EPS (1874–1953)	EPS (1930–2017)	EPS (1874–1953)	1930–2017	1874–1953
BLL	0.83	0.88	0.80	0.88	0.81	0.85	17	16
DPL	0.88	0.86	0.88	0.87	0.88	0.86	27	41
ESL	0.91	/	0.89	/	0.91	/	17	/
FHL	0.95	0.92	0.94	0.92	0.94	0.91	38	40
FOL	0.87	0.80	0.86	0.79	0.83	0.83	19	36
JPL	0.82	0.72	0.79	0.76	0.79	0.75	19	13
LAU	0.83	0.84	0.82	0.83	0.85	0.86	18	17
MAH	0.86	0.71	0.85	0.73	0.85	0.69	18	22
MIL	/	0.90	/	0.91	/	0.89	/	22
PLL	0.92	/	0.91	/	0.93	/	36	/

CHAPITRE V

OBSERVED AND PROJECTED TRENDS IN SPRING FLOOD
DISCHARGES FOR THE UPPER HARRICANA RIVER, EASTERN
BOREAL CANADA

Alexandre F. Nolin, Martin P. Girardin, Jan F. Adamowski, Rahim Barzegar, Marie-
Amélie Boucher, Jacques C. Tardif, Yves Bergeron

Soumis pour révision dans

Journal of Hydrology – Regional Studies,

Septembre 2022

5.1 Abstract

Reliable hydrological projections are needed to manage and plan for the potential effects of climate change on water resources and associated flood risks. In eastern boreal Canada, however, current assessments of future hydroclimatic trajectories are confronted to discharge data scarcity and water regulation. In this study, we present a long-term perspective (past to future) on the Upper Harricana River discharge associated with spring flood episodes (April 15 to June 30, A15J30). Climate predictors for mean A15J30 discharge, which included observed rainfall, temperature and snow data, were screened using an iterative Boruta Random-Forest selections applied to 107 years of observations, capturing 72% of the variance. The retained machine learning model was then applied to climate projections from a CMIP5 ensemble of 10 Global Climate Models (GCMs) under RCP4.5 and RCP8.5 scenarios and compared to a tree-ring based reconstruction of past discharges to evaluate whether future variability was projected outside the historical range (1771–2021). Trend analyses for the 20th century show that warmer winter and spring average temperatures contributed to a decrease in the amount of snowpack and its water equivalent, while rainfall has increased. Spring ice break-up also appears to have become earlier. Compared to the reconstructed Little Ice Age discharge, observations indicated increased frequency and magnitude of high mean A15J30 discharge. Projected hydroclimatic trajectories suggested a higher contribution of rainfall to winter and spring discharge, offset by a sharp decrease in snowpack, thereby resulting in a modest decrease in discharge by the end of the 21st century. Of note, however, is that projections from two GCMs out of ten reproduced the historical conditions leading to high spring flooding and projected increasing magnitude and frequency of the mean A15J30 discharge. At the scale of the 10-GCMs ensemble, this scenario remains unlikely, but it should be taken into consideration by stakeholders as a precautionary principle, when planning for mitigating future effects of climate change on water resources and flood risks for eastern boreal Canada.

Keywords: boreal hydrology, climate change, spring flooding, Random Forest, CMIP5, Global Climate Models

5.2 Résumé

Des projections hydrologiques fiables sont nécessaires pour gérer et planifier les effets potentiels du changement climatique sur les ressources en eau et les risques d'inondation. Dans l'est du Canada boréal, les évaluations actuelles des trajectoires hydroclimatiques futures se heurtent à la rareté des données de débits et à la régulation des rivières. Dans cette étude, nous présentons une perspective à long terme (du passé au futur) sur le débit de la rivière Upper Harricana associée aux épisodes de crues printanières (15 avril au 30 juin, A15J30). Les prédicteurs climatiques du débit moyen A15J30, qui comprenaient des données observées sur les précipitations, la température et la neige, ont été sélectionnés à l'aide d'une sélection itérative de Boruta - Forêt d'arbres décisionnel ('*Random Forest*') appliquée à 107 années d'observations et capturant 72 % de la variance. Le modèle par apprentissage automatique retenu a ensuite été appliqué aux projections climatiques d'un ensemble CMIP5 de 10 modèles climatiques globaux (GCM) dans le cadre des scénarios RCP4.5 et RCP8.5. Les projections du modèle par apprentissage automatique ont ensuite été comparées à une reconstitution des débits passés basée sur les cernes d'arbres pour évaluer si la variabilité future était projetée en dehors de la gamme de variabilité historique (1771–2021). Les analyses de tendances pour le 20^e siècle démontrent que le réchauffement des températures moyennes hivernales et printanières contribue à diminuer la quantité de neige accumulée et son équivalent en eau, au contraire de la pluie qui a augmenté. Le dégel des rivières au printemps semble aussi être devenu plus hâtif. Par rapport au débit reconstitué du Petit Âge Glaciaire, les observations indiquent une augmentation de l'ampleur et de la fréquence du débit moyen de la période A15J30. Les trajectoires hydroclimatiques projetées suggèrent aussi une contribution plus importante des précipitations au débit hivernal et printanier, compensée par une forte diminution du manteau nival, entraînant ainsi une modeste diminution du débit d'ici la fin du 21^e siècle. Toutefois, deux GCM sur dix reproduisent les conditions historiques entraînant de fortes crues printanières et prévoient une augmentation de la magnitude et de la fréquence du débit moyen de la période A15J30. À l'échelle de l'ensemble de 10 GCM utilisé, ce scénario demeure toutefois peu probable, mais il devrait être pris en considération par les parties prenantes en tant que principe de précaution, lors de la planification de l'atténuation des effets futurs du changement climatique sur les ressources en eau et le risque inondation dans l'est du Canada boréal.

Mots-clés : hydrologie boréale, changement climatique, crue printanière, Random Forest, CMIP5, modèles climatiques globaux (GCM).

5.3 Introduction

A warmer future climate will have impacts on the frequency, magnitude, timing and location of extremes floods across the Northern Hemisphere (Cunderlik & Ouarda, 2009; Hirabayashi et al., 2013; IPCC, 2014; Burn & Whitfield, 2018; Gaur et al., 2018). While temperature has risen by +2.3°C in eastern boreal Canada since 1950 at a rate two times higher than the rest of North America (IPCC, 2014; Bush & Lemmen, 2019), there are trends towards both increasing and decreasing frequency and magnitude of river spring flooding over the past two centuries (Whitfield & Cannon, 2000; Burn & Whitfield, 2016; Buttle et al., 2016; Burn & Whitfield, 2017; Aýgun et al., 2019; Bush & Lemmen, 2019; Zadeh et al., 2020). As most rivers of eastern boreal Canada are snowmelt-driven, there are major concerns that future changes in both temperature and precipitation could lead to more extreme flooding than those currently observed (Whitfield & Cannon, 2000; Ashmore & Church, 2001; Adam et al., 2009; Aýgün et al., 2019; Bush & Lemmen, 2019). Indeed, the magnitudes attained by the floods of the past decade (2010–2020) across Canada were unprecedented on the scale of the 20th century hydrological records (Burn & Whitfield, 2016; Gaur et al., 2018). Nonetheless, a greater proportion of decreasing flood magnitude trends were observed when investigating longer records (60 years), indicating that flood magnitude did rise in the past (Zadeh et al., 2020).

Given that about 70% of Canada's hydropower capacity is located in northern Québec and Ontario (Cherry et al., 2017), changes in spring flood dynamics may have profound consequences on the economy, dam safety management and the design of future hydraulic structures (Bush & Lemmen, 2019). Reliable hydrological projections are thus needed to better manage and plan for the potential effects of climate change on water resources and associated flood risks (Boucher & Leconte, 2013; Cherry et al., 2017). The assessment of future hydroclimatic trajectories in eastern boreal Canadian

rivers is however hampered by the scarcity of discharge data and by the regulation of rivers and water bodies by hydraulic structures (Clavet-Gaumont et al., 2013a; Mortsch et al., 2015; Cherry et al., 2017; Kundzewicz et al., 2018; Pellerin, 2019). In our study area most of the gauges were installed during dam construction in the 1920 and 1930s (Nolin et al., 2021b). Dam management is now superimposed on natural discharge variability, which limits the study of long-term trends in discharge and floods, particularly at the watershed scale (Burn & Hag Elnur, 2002; Burn et al., 2010; Mortsch et al., 2015).

Future hydroclimatic trajectories in eastern boreal Canada have been investigated at the regional scale (Huziy et al., 2013; Clavet-Gaumont et al., 2013a; Guay et al., 2015; Clavet-Gaumont et al., 2017) or at smaller watershed scales (Cunderlik & Simonovic, 2005; Dibike & Coulibaly, 2005; Minville et al., 2008, 2009, Oubennaceur et al., 2021). Overall, geographical differences in observed hydroclimatic trends indicate that climate change may have various impacts on river processes at the watershed scale (Ashmore & Church, 2001; Burn & Hag Elnur, 2002; Cunderlik & Ouarda, 2009; Gaur et al., 2018; Wang et al., 2021), accompanied by complex spatial and temporal variability. Overall, it remains difficult to compare the varying hydrological projections due to the diversity of climate scenarios, climate projections and spatial resolution, hydrological models, and difficulties in quantifying uncertainties (Clavet-Gaumont et al., 2013a; Lucas-Picher et al., 2021). The different working scales also hinder comparisons. For instance, small river watersheds remain more sensitive to climate variability since the discharge of small drainage areas does not incorporate the same natural climate variability and climate factors than large drainage areas (Hirabayashi et al., 2013; Rokaya et al., 2018; Castaneda-Gonzalez et al., 2019; Lucas-Picher et al., 2021). Fine-scale climate parameters, such as the effects of lakes on regional temperature and precipitation, or the effects of a localized convective rainstorm on runoff, can be difficult to model with coarse spatial resolution climate models for small

watersheds (Lucas-Picher et al., 2021). Spring floods simulated with coarse climate data can thus result in smaller peak discharge than those simulated with finer-resolution climate data (Clavet-Gaumont et al., 2013ab; Castaneda-Gonzalez et al., 2019). Especially at the scale of small river watersheds, these uncertainties make long-term planning of territories development and water management difficult when projections are not available locally.

Potential changes in the seasonal discharge over eastern Canada have been projected for various river basins (*Québec*: Huziy et al., 2013; Guay et al., 2015; MELCC, 2018; *Western Québec*: Oubennaceur et al., 2021; *Eastern Québec*: Riboust & Brissette, 2015) and for various river sections (*southern Ontario*: Cunderlik & Simonovic, 2005; Grillakis et al., 2011; *Lac St. Jean tributaries*: Dibike & Coulibaly, 2005; Minville et al., 2008; Minville et al., 2009; Minville et al., 2010; *St. Lawrence River tributaries*: Quilbé et al., 2008; Boyer et al., 2010). Each projection suggested a reduction in summer minimum discharges, an increase in fall and winter maximum and mean flows, as well as earlier spring maximum discharges. However, how projected hydroclimatic changes will affect the frequency and magnitude of extremes events still remain unclear. Uncertainties arise because modeling the complexity of hydroclimatic factors involved in spring flooding remains difficult and because the projections themselves remain dependent on the quality of the climate and hydrological data used as model inputs (Dibike & Coulibaly, 2005; Quilbé et al., 2008; Huziy et al., 2013; Clavet-Gaumont et al., 2017). In general, in Québec, return frequencies of high magnitude discharges were projected to increase by 2050 and 2070, with the largest increases expected in northern rivers (Frigon et al., 2010; Huziy et al., 2013; Clavet-Gaumont et al., 2013a, 2017; MELCC, 2018). The projected increase in the magnitude of spring flooding in northern Québec is supported by increases in both maximum rainfall and snowpack (Guay et al., 2015; Clavet-Gaumont et al., 2017), although an increase in snowmelt contribution is likely to be transient (Guay et al., 2015; Bush & Lemmen, 2019). There is thus a need

to compare observed and projected hydroclimatic changes with historical data to better assess the potential changes in the contributions of climatic factors involved in spring flooding, particularly at the scale of small river watershed. This study took advantage of a multicentury-long record of reconstructed and observed spring discharge in the naturally flowing Harricana River, in eastern boreal Canada, to assess potential hydroclimatic changes as consequences of projected climate change. The objectives of this paper were threefold: (1) to estimate the potential trajectories of discharge associated with spring flooding of the natural Harricana River by 2100, (2) to evaluate the change in the relative contribution of climatic variables to spring discharge and flooding, and (3) to compare future trends (2021–2100) with the reconstructed trends in spring mean discharge (1771–2020). In addition to improving our understanding of the impact of climate change on the spring regime of the Harricana River, this study addressed a straightforward method to provide future hydrological data needed to frame climate change adaptation and decision making.

5.4 Material and Methods

5.4.1 Study area

The Upper Harricana River is located in northwestern Québec and encompasses the total area of the Harricana River watershed upstream of the Amos hydrometric station (48°35'52"N, 78°06'37"W; Fig. 5.1). The Upper Harricana River watershed was selected from the Canadian Reference Hydrometric Basin Network (Brimley et al. 1999) because it is naturally flowing, under limited human influence (<10% land use change over time). It has a 107-year discharge record (1915–2021) consisting of less than 5% estimated daily discharge values (Whitfield et al. 2012; Koshida et al. 2015). The watershed has an area of 3,724 km², a flat topography (295 to 505 masl; Fig. 5.1) and is largely forested (71%) with few urban areas (3%; Natural Resources Canada, 2015).

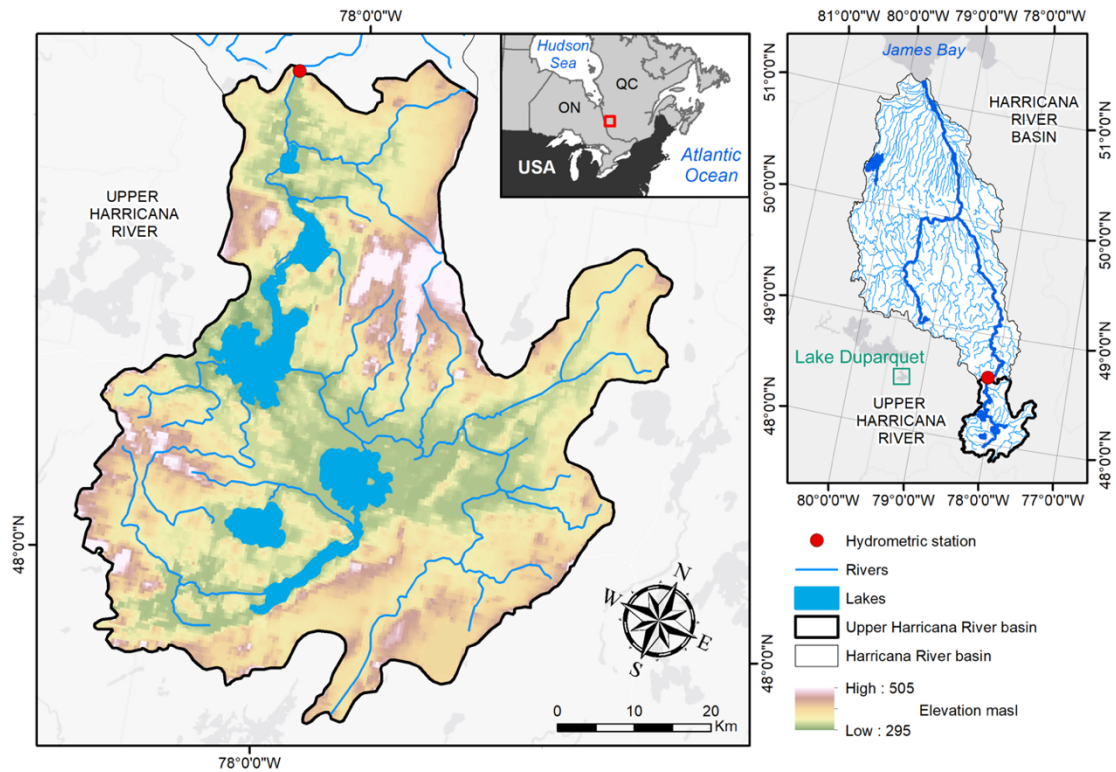


Figure 5.1 Map of the study area. Location of the study area within North America at the border between Ontario and Québec, Canada (right panel upper inset). HARRICANA River basin is flowing north to James Bay in the Hudson Sea (right panel). The study area encompasses the Upper HARRICANA watershed (left panel), located on the upper reach of the HARRICANA River and delimited by the Amos hydrometric station (red dot).

Climate normal temperatures from the Amos meteorological station (7090120; 48°34'N 78°08'W, 310masl; http://climate.weather.gc.ca/climate_normals; Fig. 5.S1) showed for the reference period (1971–2000), an average annual temperature of 1.2 °C with a wide range from winter minimum (−52.8°C) to summer maximum (37.2°C). The mean average annual snowfall was 248.4mm with seasonal accumulation of 21% in fall, 54% in winter and 25% in spring. The snow depth at month-end averaged 0.60m in winter and reached a maximum of 1.42m. The mean annual total precipitation averaged 918.4mm with heavy rainfall events occurring in the early summer up to a

daily maximum of 101.4mm. The Upper Harricana River flows north to James Bay (Fig. 5.1) and has an average annual discharge of 60 m³/s (1915–2020) and a high seasonal variability of a boreal regime driven by snowmelt. At the end of the winter, the snowpack melts and transforms the low winter discharge (average 1915–2020 = 35 m³/s) into a spring ice break-up flood that can reach up to 337 m³/s (maximum daily discharge observed during the flood of May 1960). The total amplitude of the spring flood extends on average from 15 April to June 30 (Nolin et al., 2021a; Fig. 5.S1).

5.4.2 Hydroclimatic data

Daily observed discharges for the Upper Harricana River were obtained for the period 1915 to 2021 from the ministère de l'Environnement et de la Lutte contre les changements climatiques du Québec and for gauge 04NA001-2. A dendrochronological reconstruction of the mean April 15 to June 30 discharge of the Upper Harricana River, from 1771 to 2016 (Nolin et al., 2021a) was used to extend the observations. This reconstruction was developed using tree-ring proxies from riparian black ash (*Fraxinus nigra* Marsh.) trees periodically flooded in spring. The reconstruction showed high spatial coherency with other palaeohydrological records from eastern boreal Canada and subarctic Québec (Nolin et al., 2021ab). Observed ice break-up date for Lake Duparquet, located 85km west of the Upper Harricana River (Fig. 5.1), were also available from 1968 to 2021 (Mongrain et al., 2014; pers. comm. 2021). Ice break-up refers to the date when Lake Duparquet was free of ice.

Given that few meteorological stations predate the 1950s in eastern boreal Canada (Girardin et al., 2011), climate data and particularly snow data were interpolated for the period 1900–2020 and averaged over the spatial extent of the Upper Harricana River watershed using BioSIM (v.10; Régnière et al., 2014; <https://cfs.nrcan.gc.ca/projects/133>). BioSIM uses spatial regressions to interpolate daily minimum and maximum air temperature and total precipitation data from nearby

Environment and Climate Change Canada meteorological stations, and adjusts for elevation, latitude, and longitude differentials with regional gradients (Régnière et al., 2014). Hereafter, BioSIM data will be referred to as observed meteorological data.

5.4.3 Climate projections and scenarios

Projected future changes in daily temperature and total precipitation for the Upper Harricana River watershed used the Ouranos standard ensemble of bias-adjusted climate scenarios (Charron, 2016), which is based on 10 downscaled global climate models (GCMs; Table 5.1) from the Coupled Model Intercomparison Project - Phase 5 (CMIP5 - Taylor et al., 2012). The Ouranos standard ensemble is postprocessed and refined at a 10 x 10 km spatial resolution and at a daily time step between 1950 and 2100 (Charron, 2016). Two future greenhouse gas emission (GHGs) scenarios, or representative concentration pathways (RCP) of 4.5 W/m² and 8.5 W/m² by 2100 were used (IPCC, 2014). Scenario RCP4.5 ('optimistic') simulates moderate GHGs emissions, +3.2°C worldwide warming by 2100, and a stabilization of the GHGs emissions by the end of the century. Scenario RCP8.5 ('pessimistic') corresponds to high GHGs emissions, +6.3°C worldwide warming by 2100, and few GHGs reduction measures taken at the global scale by 2100. Climate ensemble data were averaged for the Upper Harricana River spatial extent and for each of the 10 GCMs and two RCPs using Ouranos' Power Analytics and Visualization for Climate Science platform (PAVICS; Ouranos, 2022).

5.4.4 Snowfall and rainfall amounts

Snowfall and rainfall amounts had to be estimated from the total precipitation amounts available in the 10-GCM ensemble. First, for the observed period of weather observations (1900–2020), snowfall and snow water equivalent (SWE) were derived using the physics equated in Brown et al. (2003) and implemented in BioSIM software.

Table 5.1 Climate simulations (r1i1p1) from CMIP5 ensemble used in this study. This set of 10 standard scenarios (cb-oura-1.0) was produced by Ouranos to cover the range of expected changes in daily temperature and precipitation in the province of Québec.

No	Code	Model	Institution
1	BNU	BNU-ESM	College of Global Change and Earth System Science, Beijing Normal University, China
2	CE2	CanESM2	Canadian Centre for Climate Modelling and Analysis, Canada
3	CMS	CMCC-CMS	Centro Euro-Mediterraneo per I Cambiamenti Climatici, Italy
4	A13	ACCESS1.3	Commonwealth Scientific and Industrial Research Organisation, and Bureau of Meteorology, Australia
5	INM	INM-CM4	Institute for Numerical Mathematics, Russia
6	IAL	IPSL-CM5A-LR	Institut Pierre-Simon Laplace, France
7	IBL	IPSL-CM5B-LR	Institut Pierre-Simon Laplace, France
8	MPL	MPI-ESM-LR	Max Planck Institute for Meteorology, Germany
9	NOE	NorESM-1M	Norwegian Climate Centre, Norway
10	GFM	GFDL-ESM2M	Geophysical Fluid Dynamics Laboratory, USA

These functions determine the temperature at which precipitation falls as snow and at which snow melts, using air temperature, longitude, and latitude. To simplify this physics-based model, an empirical binary logistic regression model was used to estimate the proportion of snow and rain from the projected daily total precipitations occurring as a function of the projected mean daily temperatures (Kienzle, 2008; Jennings et al., 2018; Fig. 5.S2). The snow-to-rain regressions were derived using generalized linear models of a 4-parameter logistic curve:

$$Y = c + \frac{d-c}{1+\exp(b(X-e))} + \varepsilon \quad (5.1)$$

where b is the slope of the inflection point and e is X value producing a response half-way between the higher (d) and lower asymptote (c), and where ε is the error term. To return a percentage of daily total precipitation, the s-shape curve was constrained between $c = 0$ and $d = 100$. Drizzle and precipitation events below 0.5 mm were

removed before calibrating the model and days without precipitation were not considered. The final equation took the form:

$$\%Snow = 0 + \frac{100-0}{1+\exp(0.3401(T_{Mean}-0.0878))} + \varepsilon \quad (5.2)$$

$$\%Rain = 100 - \%Snow \quad (5.3)$$

The model successfully reproduced BioSIM daily rainfall and snowfall estimates with a highly significant ($p < 0.001$) linear relationship ($R^2 = 0.999$, $n = 21,481$ and $R^2 = 0.995$, $n = 16,079$ respectively; Fig. 5.S2), low residual standard error (RSE = 0.04 ± 0.28 mm and -0.01 ± 0.26 mm respectively), and approximately normally distributed residuals.

5.4.5 Potential evaporation

Daily potential evaporation (E_d) was estimated from the daily maximum temperature (T_{max}) data of each GCM. The following empirical model of Thornthwaite and Mather (1955) equated in Girardin and Wotton, (2009) was used:

$$E_d = 0.36 \times (T_{max}) + L_f \quad (5.4)$$

where L_f is a standard day length adjustment factor varying by month: January to March = -1.6 , April = 0.9 , May = 3.8 , June = 5.8 , July = 6.4 , August = 5.0 , September = 2.4 , October = 0.4 , and November to December = -1.6 . In this model, only values of $T_{max} > 0$ were considered, and negative E_d values resulting from negative L_f values were set to 0.

5.4.6 Machine Learning model

A regression model linking the observed Upper Harricana River A15J30 mean discharge to the set of climate data covering the period 1915–2020 was developed as follows. First, monthly and seasonal indices including the A15J30 period were calculated along with other climatic indices related to flood generating mechanisms (Table 5.S1; Suppl. Mat.). These additional indices included, among others, the total accumulated precipitation (TAP; sum of daily snowfall accumulated from November to December plus the daily total precipitation accumulated from January to April, modified from Romolo et al., (2006); Table 5.S1; Suppl. Mat.), and the estimated timing of ice break-up (IBU; 100 melting degree days accumulated from a mean daily temperature above 0°C, adapted from Williams (1971) and Lamontagne et al., (2021); Table 5.S1; Suppl. Mat.).

To reduce the dimensionality of the dataset which included 259 climate predictors, a random forest (RF) classifier trained with the Boruta variable selection algorithm (BRF; Kursa et al., 2010) was used to screen optimum predictor variables (Gädeke et al., 2020; Masrur Ahmed et al., 2021). Compared to a RF regression (*e.g.*, Fouad et al., 2018), BRF incorporates the interactions between variables and iteratively removes the irrelevant predictors, using a comparison between predictors and randomized version of predictors (shadow variables; Kursa et al., 2010). In other words, BRF tests for each variable whether its *z*-score (*i.e.*, the mean of accuracy loss divided by standard deviation of accuracy loss) is higher than the maximum *z*-score recorded among the shadow variables. It then compares the number of times that a variable contributes significantly ($p < 0.05$) more to the model than the best contribution of the shadow variables using a binomial distribution. The BRF was computed using the 'Boruta' R-package (v.7.0.0, Kursa, 2020) and for 1,000 iterations of 500 RF tree bootstrap samples. Parametrization of the RF models were set to default as (1) the number of variables randomly sampled as candidates at each split (*mtry*) equal to the number of

variables divided by three; and (2) the number of terminal nodes trees in the forest set to maximum.

A stepwise multiple linear regression model was then developed to estimate the mean A15J30 discharge of the Upper Harricana River, and took the form:

$$\hat{Y} = \beta_0 + \beta_1 X_1 + \dots + \beta_i X_i + \varepsilon \quad (5.5)$$

where \hat{Y} is the predicted annual mean A15J30 discharge value of the 1 to i observed climate variables X ; β_0 is the regression constant indicating the value of Y when all $X_{1 \rightarrow i}$ are zero; $\beta_{1 \rightarrow i}$ are the estimated regression coefficients from the linear functions; and ε is the error term.

The linearity and normality of the machine learning (ML) model, as well as the independence and constant variance of the errors were checked using standard analysis of the residuals (Legendre & Legendre, 2012). The final ML model was validated using split sampling (Snee, 1977) where half the period of available observed discharge and climate data (1915–1967, 53 years) was used to calibrate the model, and the second half (1968–2020, 53 years) was used to verify the model. This procedure was then inverted (1968–2020 for calibration; 1915–1967 for validation) to ensure the stability of the model over the two split-periods. Variance inflation factor (VIF; eq. 5.6) was used to screen the final set of predictors for multicollinearity. The p -value of each predictor and the Fisher's F statistic of the regression, as well as the coefficients of determination (R^2) and the R^2 adjusted for the number of predictors ($\text{Adj}R^2$) were used to further assessed the model performance in projecting the Upper Harricana River mean A15J30 discharge. Average model errors were quantified using the root mean square error (RMSE; eq. 5.7) and the RMSE to observations standard deviation ratio (RSR; eq. 5.8; Moriasi et al., 2007), as well as the mean absolute error (MAE; eq. 5.9)

expressing errors in the unit of the data. Finally, to assess the predictive skill of the hydrological model, the Nash-Sutcliffe model efficiency coefficient (NSE; eq. 5.10; Nash & Sutcliffe, 1970) and the percent bias (PBIAS; eq. 5.11; Moriasi et al., 2007) were used during the calibration / verification exercise. The verified ML model was used to project the Upper Harricana River A15J30 mean discharge (2021–2100) using the 10-GCMs as inputs.

$$VIF_{(\hat{\beta}_i)} = \frac{1}{1-R_i^2} \quad 1 \leq VIF \leq +\infty \quad (5.6)$$

$$RMSE = \frac{1}{N} \sum_{i=1}^n (E_i - O_i)^2 \quad 0 \leq RMSE \leq 1 \quad (5.7)$$

$$RSR = \frac{RMSE}{\sigma_O} \left[\frac{\sum_{i=1}^n (O_i - E_i)^2}{\sqrt{\sum_{i=1}^n (O_i - \bar{O})^2}} \right] \quad 0 \leq RSR \leq +\infty \quad (5.8)$$

$$MAE = \frac{1}{n} \sum_{i=1}^n |E_i - O_i| \quad 0 \leq MAE \leq +\infty \quad (5.9)$$

$$NSE = \frac{\sum_{i=1}^n (O_i - \bar{O})^2 - \sum_{i=1}^n (E_i - O_i)^2}{\sum_{i=1}^n (O_i - \bar{O})^2} \quad -\infty \leq NSE \leq 1 \quad (5.10)$$

$$PBIAS = \left[\frac{\sum_{i=1}^n (O_i - E_i) \times 100}{\sum_{i=1}^n (O_i)} \right] \quad 0\% \leq PBIAS \leq 100\% \quad (5.11)$$

where for 1 to n years i , O_i is the observed discharge of mean \bar{O} and standard deviation σ_O , and E_i is the ML-model estimated discharge of mean \bar{E} . During the split calibration-verification exercise, E_i is the estimated discharge from simulation over the verification period, not inferred from the pool of observed values used for calibration.

5.4.7 Independent hydrological simulations using a 10-GCM ensemble

The 10-GCM ensemble hydrological simulation done using the ML model were compared to those of the Hydroclimatic Atlas of Southern Québec 2022 (DEH22). The DEH22 simulations for the Upper Harricana River (river section ABIT01483, drainage area = 3,719.5 km²) used the Ouranos standard 10-GCM ensemble set (Table 5.1) with the same ensemble members (realization 1, initialization 1, physics 1: r1i1p1) and the same climate scenarios (RCP4.5, RPC8.5) as the ML model. The DEH22 simulations are currently built as part of a Québec-wide effort to assess future trajectories of river dynamics under climate change and used the HYDROTEL distributed physics-based model (Fortin et al., 2001) and were provided upon personal request to the ministère de l'Environnement et de la Lutte contre les changements climatiques du Québec (atlas.hydroclimatique@environnement.gouv.qc.ca). To correct for the difference in the variability of discharge between the ML and DEH22 simulations, empirical quantile mapping (EQM; Gudmundsson et al., 2012; Cannon et al., 2015; Crochemore et al., 2016) was used to scale each simulation to the distribution of observed discharge over a period of common overlap (1971–2000). The EQM method adjusts the empirical cumulative distribution function of the simulated discharge data to that of the observed discharge data. The correction was then applied to the projected data and allowed for a constant extrapolation of extreme values by considering the non-stationarity of the correction between the simulated and the projected series (*i.e.*, the correction applied on the projected period was not restricted to the discharge values taken during the observed period; Gudmundsson et al., 2012; Cannon et al., 2015; Crochemore et al., 2016). The EQM correction was performed using the ‘hyfo’ R package (v. 1.4.3; Xu, 2020), and using a built-in algorithm allowing extrapolation of extremes.

5.4.8 Hydroclimatic trend analysis

Long-term changes in A15J30 discharge and climate were compared among the reconstructed (1771–1920), observed (1921–2020, BioSIM data) and the projected

changes (2021–2100) timeseries, as well as among the hydrological models (ML, DEH22), the 10 GCMs, and the climate scenarios (RCP4.5, RCP8.5). The significance of linear monotonic trends in annual timeseries was assessed using the non-parametric Mann-Kendall test (Mann, 1945; Kendall, 1975) after ensuring that no significant serial autocorrelation could increase the probability of detecting a trend (Hamed & Rao, 1998; Yue et al., 2002). In the case of significant AR (1) autocorrelation, modified Mann-Kendall test by Hamed & Rao (1998) was preferred to the classical Mann-Kendall test. The magnitudes of the annual trend slopes were studied using Theil-Sen's test, which estimated the median of the slopes among all lines through pairs of points (Sen, 1968). Patterns of change between hydroclimatic variables and units were compared using percent change from the average of the first 10-years of the Theil-Sen's trend line. When estimating the percentage change in the trend line over the entire time series, the average value for the first 10 years was preferred to the first data point in the time series to avoid the potential effect of an extreme value. To assess trends in the magnitude of extremes, linear quantile regressions were used instead of Theil-Sen's slope, to account for the reduction in the degree of freedom in selecting only values above an arbitrary threshold within the timeseries (Passow & Donner, 2019). To characterize and investigate the projected changes in frequency of extreme high mean A15J30 discharge in the Upper Harricana River, a threshold value of 151.3 m³/s was used (Nolin et al., 2021ab). This value was defined as the average mean A15J30 discharge between 1771 and 2016 plus 1.5 times the standard deviation and was previously used to investigate historical changes in the high spring discharge of the Upper Harricana River. The frequency of high mean A15J30 discharge (above 151.3 m³/s) was then assessed per decade from 1771 to 2100. Finally, the inter-climate-simulations agreement, defined as the number of GCMs used as inputs for DEH22 and for the ML model presenting the same sign of change was used to assess the likelihood of the projected changes.

5.5 Results

5.5.1 Machine Learning model conception and evaluation

Correlation analyses over the 1915–2020 period indicated mostly highly significant associations ($p < 0.001$) between the mean A15J30 discharge of the Upper Harricana River and spring (March-April-May) climate variables (Fig. 5.2). The mean A15J30 discharge was positively associated with snowpack conditions (snowfall, snow depth, SWE, TAP), spring timing (SSL, IBU) and with variable involved in snowmelt flooding (ROS, MEL, HR10; and Table 5.S1 for definition of abbreviations). It also indicated negative associations with mean and maximum temperature. Overall the mean A15J30 discharge showed no significant ($p < 0.05$) AR(1) autocorrelation and only a few weak correlations with climate variables in the months preceding January (Fig. 5.2).

The BRF conducted on the complete climate dataset selected 36 climate predictors and that conducted on the climate variables excluding the SWE data, retained 31 climate predictors (Fig. 5.3). The two BRF selections ranked TAP, total precipitation in spring and annual snowfall as the most important climate variables to estimate the A15J30 mean discharge. Both BRF selections retained comparable predictors (22 identical variables) except for 13 variables using SWE (Fig. 5.3). Multiple linear stepwise selection performed over the two BRF-selected sets of climate predictors (with and without SWE) led to comparable model performances ($\text{Adj}R^2 = 72.3\%$ and 72.0% ; $F = 69.5$ and 68.6 ; $\text{RMSE} = 14.2$ and 14.2 , respectively). The model with SWE retained the timing of SWE minimum while the second model retained the estimated timing of ice break-up (IBU). Since daily SWE data were not available in the downscaled climate projections for Québec, the ML model excluding SWE was selected for the subsequent analyses. Climate variables used in the ML model included TAP ($R^2 = 39.7\%$), total A15J30 rainfall amount (Delta $R^2 = 14.4\%$), IBU (Delta $R^2 = 14.1\%$) and snowfall

maximum in May (Delta $R^2 = 4.9\%$; Table 5.2a; Fig. 5.4). Variance inflation factors remained close to 1 with for each predictor ensuring no multicollinearity in the final set of climate predictors (Table 5.2a).

Overall, the ML model demonstrated robust representation of the observed Upper Harricana River A15J30 mean discharge and successfully tracked interannual variability and reproduced low-frequency trends (Fig. 5.4) as indicated by a high F-statistic and NSE (Table 5.2b). Correlations calculated for each of the 10 GCM between the projections from the ML model and the independent projections by the DEH22 model showed very high consistency ($r_{RCP4.5} = 0.84 \pm 0.05$ std, $r_{RCP8.5} = 0.83 \pm 0.04$ std; 2021–2100). Cross calibration and verification statistics indicated approximately normally distributed residuals and a higher performance estimating the mean A15J30 discharge over the second (1968–2020) compared to the first half-period (1915–1967), although both RMSE and MAE remained low over the two calibration periods (Table 5.2b; Fig. 5.4). Slightly higher accuracies were found in capturing extreme low (mean departure from observed data for the 10 highest observed discharges, $\bar{x} = -18.5 \pm 15.8$ std) than extreme high mean discharge (mean departure from observed data for the 10 lowest observed discharges, $\bar{x} = 12.2 \pm 11$ std; Fig. 5.4), as also indicated by negative and positive PBIAS value over the first and second calibration periods respectively (Table 5.2b).

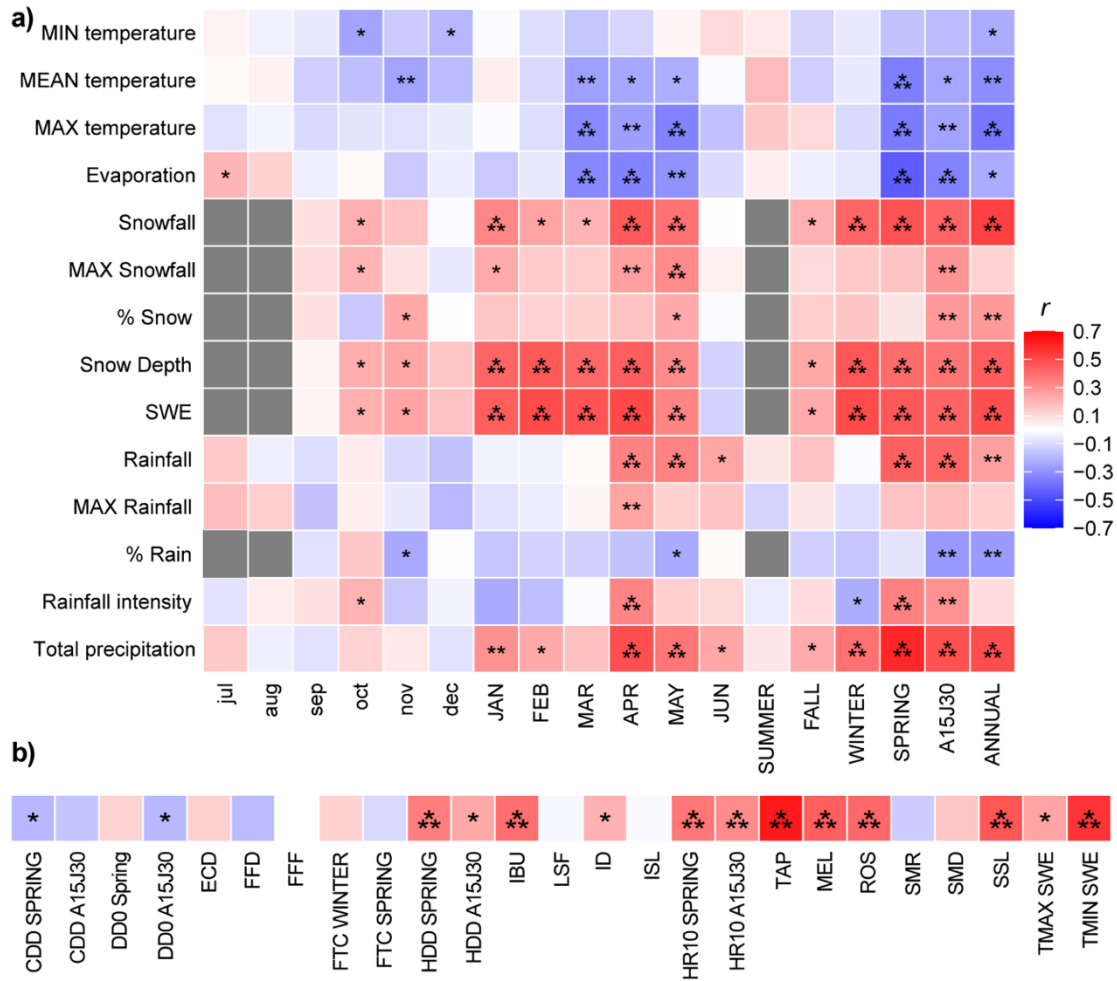


Figure 5.2 Associations between mean April 15 to June 30 discharge and selected climate variables over the 1915–2020 period. a) monthly and seasonal variables as detailed in Table 5.S1. b) climate variables aggregated according to different time periods as detailed in Table 5.S1. Note that the X axes are different between a) and b) panels. Pearson correlation coefficients range from red (positive correlation) to blue (negative correlation). Asterisks indicate p -value < 0.01 (*), < 0.05 (**), and < 0.001 (***)). See Table 5.S1 for definition of abbreviations.

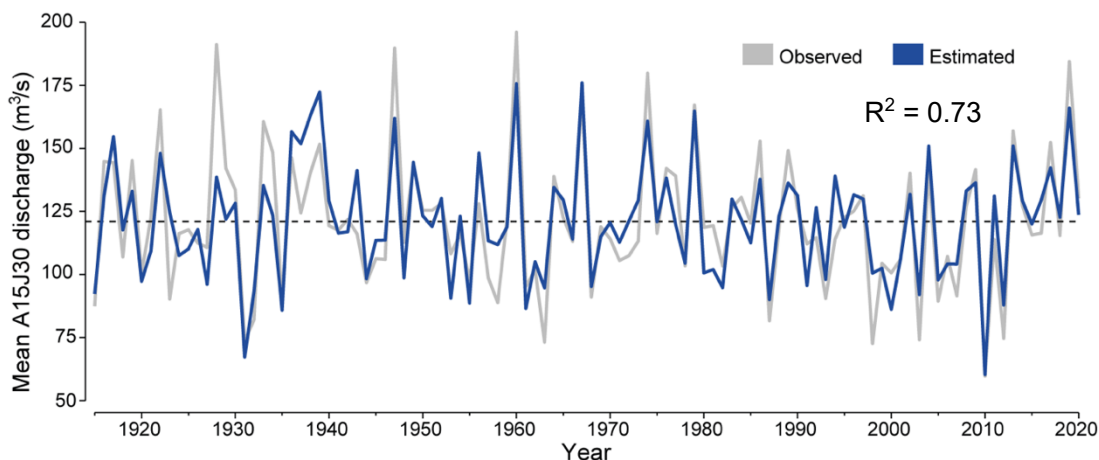


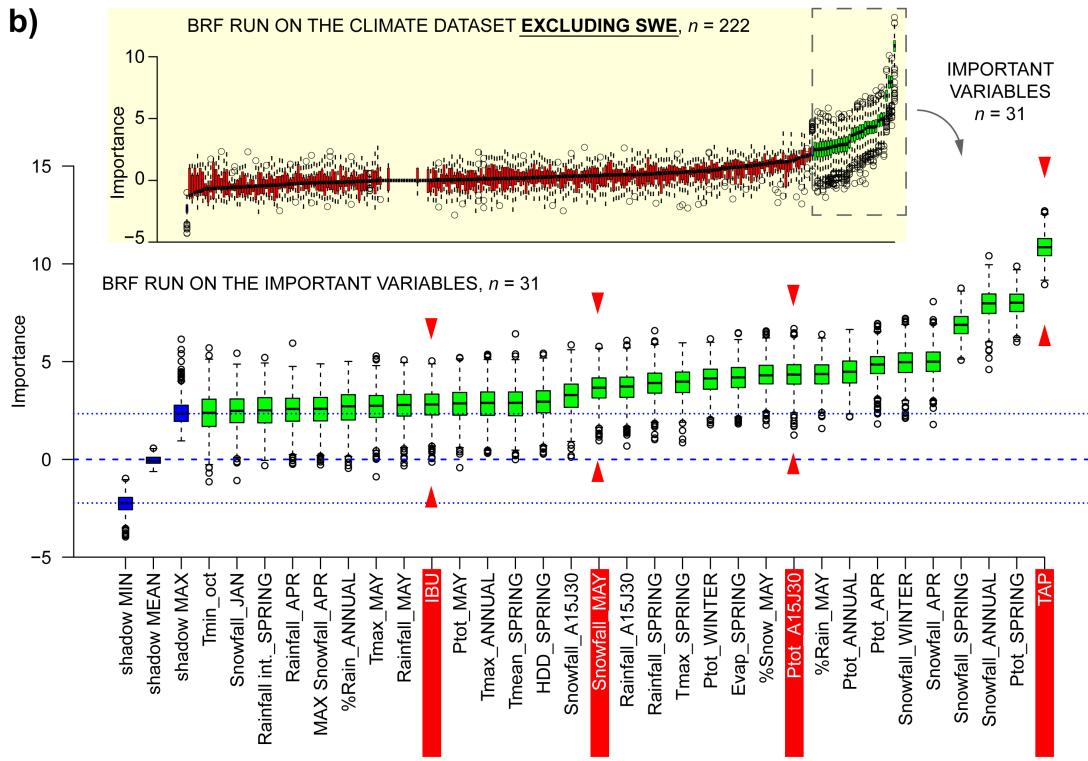
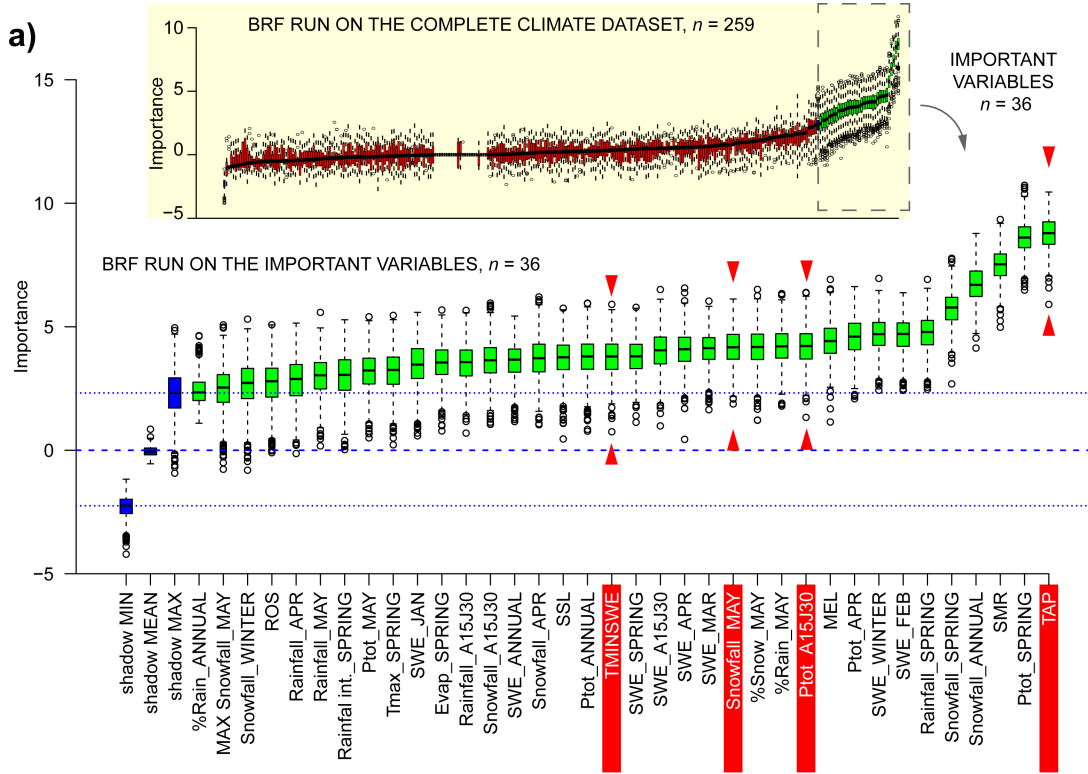
Figure 5.3 Comparison between observed (grey) and estimated (blue) Harricana River mean April 15 to June 30 discharge over the calibration period (1915–2020). Dashed line highlights the mean of the observed discharge at 121.01 m³/s.

Table 5.2a Annual Stepwise selection statistics for the full period calibration (1915–2020). See Table 5.S1 for definition of abbreviations.

Variable	R ²	AdjR ²	RMSE	Std. Error	p-value	VIF
TAP	0.40	0.39	21.02	0.03	2.00e ⁻¹⁶	1.01
Rainfall A15J30	0.54	0.53	18.42	0.03	1.48e ⁻⁰⁹	1.03
IBU	0.68	0.67	15.42	0.15	4.31e ⁻⁰⁹	1.03
Snowfall MAY	0.73	0.72	14.25	0.72	4.07e ⁻⁰⁵	1.06

Table 5.2b Annual Regression statistics for the split-sampling calibration and verification procedure, and the full period calibration. See Table 5.S1 for definition of abbreviations.

Calibration	Verification	AdjR ²	R ²	RSR (%)	RMSE	MAE (m ³ /s)	Fstat	NSE	PBIAS (%)
1915–2020	1915–2020	0.72	0.73	0.52	13.91	10.96	68.56	0.73	0
1915–1967	1968–2020	0.65	0.68	0.60	15.91	9.91	25.14	0.63	-1.30
1968–2020	1915–1967	0.79	0.81	0.46	11.06	13.28	51.23	0.78	0.89



◀ Figure 5.4 Boruta – Random Forest (BRF) selection of the climate predictors of the mean April 15 to June 30 Upper Harricana River discharge. The BRF selection results are presented for (a) the complete climate dataset, and (b) the climate variables excluding the SWE data, both over the period 1915–2020. Both a) and b) panels are box plots of the z-scores (Importance, Y-axes) ranking the variables (X-axes) according to their contribution to the model over 1,000 iterations and compared to the that of the shadow variables. Blue box plots are minimal, mean, and maximum importance of a shadow variable. Red and green box plots are importance of respectively rejected (non-significant contribution compared to that of the shadow variables) and confirmed ($p < 0.05$) variables. The top insert (beige background) in (a) and (b) presents the full selection of the BRF and then the details of the ranking for the selected variables (white background). The stepwise multiple linear regression performed among the variables indicated important by the BRF in panels a) and b) selected the variables highlighted with a red background on each X-axis. See Table 5.S1 for definition of abbreviations.

5.5.2 Historical trends in discharge and climate

Significant linear trends were found in the monthly and seasonal data used to characterize the hydrological regime since 1915 (Table 5.3). Trend analysis indicated that August and September mean and maximum discharges have decreased, and that mean discharges from February to April have increased. September and February demonstrated significant negative trends in minimum, mean and maximum discharges. Observed changes in discharge ranged within ~20-30% with the most significant trends being the decrease in maximum discharge in September and the increase in minimum discharge in March (Table 5.3). No change in discharge was determined over the A15J30 season nor in the maximum spring discharge since 1915 (Table 5.3). Over the reconstructed (1771–1920) and observed (1921–2020) periods, high mean A15J30 discharge above 151.3 m³/s occurred on average one time per decade, and up to a maximum of three times per decade in the 1880s (Fig. 5.5). The estimated timing of ice break-up calculated using BioSIM data (IBU, Table 5.S1) showed no changes since 1915 (Table 5.3). Over the longer term (1901–2020) however, it showed a significantly earlier trend by seven days. The observed timing of ice break-up at Lake Duparquet

demonstrated no change between 1968 and 2021, occurring on average on 9 May, and between 12 April and 24 May (not shown).

Significant monthly and seasonal linear trends were also identified in the observed climate data since 1915 (Table 5.3). Temperature warming has mainly been observed using mean temperature with minimum and maximum showing same trends when significant (Table 5.3). The most significant warming trends were observed in the maximum temperature of January and in the spring mean temperature. While fall to spring mean seasonal temperatures have warmed since 1915, there has been no change in the frequency of extreme cold days with minimum temperature below -25°C , which have implications in the river and lake ice development (ECD, Table 5.S1; Table 5.3). The warming of average winter and spring temperatures has coincided with decreases in the proportion of precipitation falling as snow and of the snowpack, characterized by both a decrease in snow depth and SWE. In contrast, winter and spring rainfall increased. For instance, in January, an increase of 2°C in maximum temperature (from 1.1°C to 2.1°C) coincided with a rainfall increase of 30% and to a snow cover and SWE decrease of 20% (Table 5.3). No change was found in the maximum snowfall, the frequency of rain-on-snow, nor in the duration of snowmelt. While precipitation maximum and intensity have increased in almost each month (most significant increase in March), no change were detected in the frequency of freeze-thaw cycles in winter and spring. The number of snowmelt events from January through May has even decreased (Table 5.3). The timing of the SWE minimum, which estimate the last day with snow on the ground in spring (Table 5.S1), decreased by seven days which is as early as the magnitude found in the trend for the estimated ice break-up timing (Table 5.3).

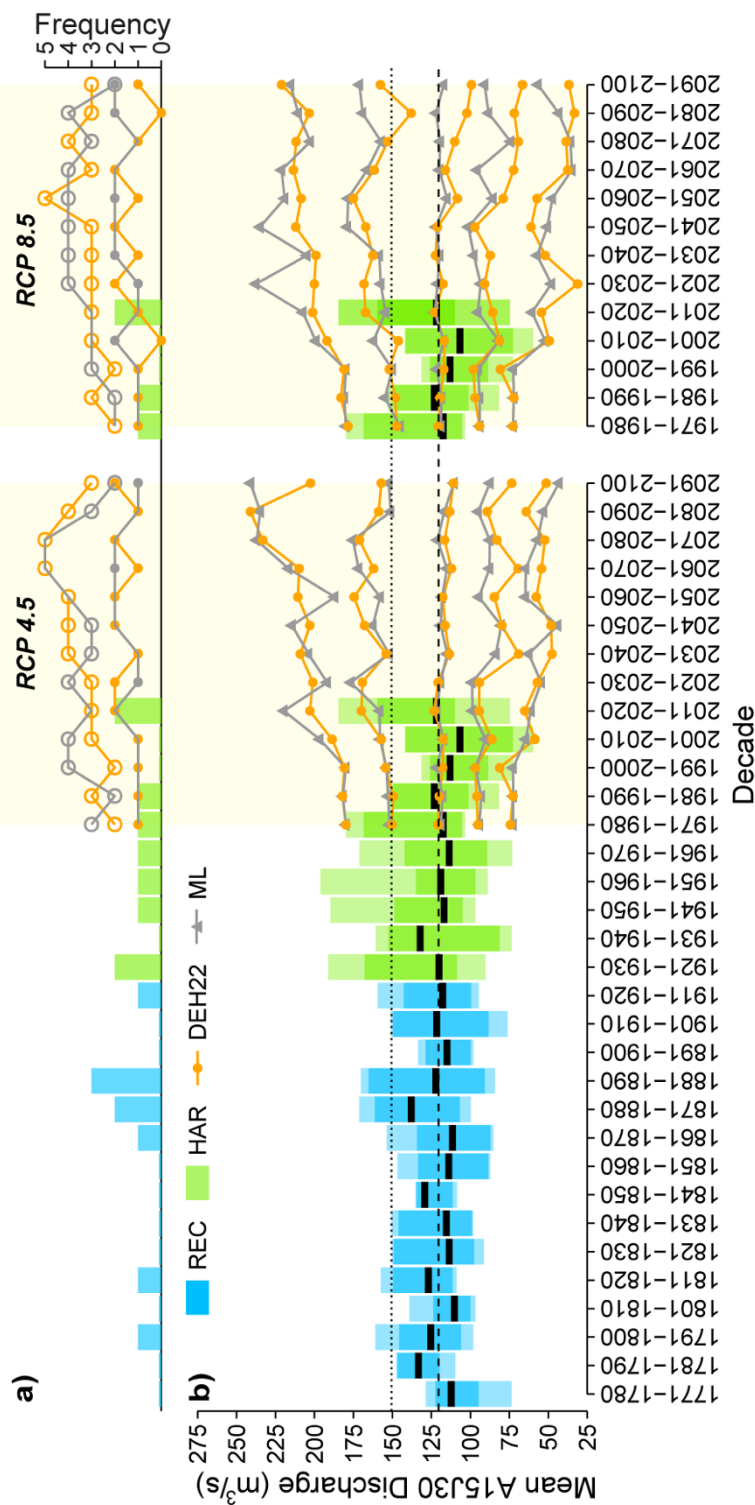


Figure 5.5 Comparison over 10-years windows between historical (blue), observed (green), and projected mean discharges from April 15 to June 30 (A15J30) of the Upper Harricana River. Projected discharges are those simulated by the machine learning model (ML, grey) and those from the Hydroclimatic Atlas of Southern Québec 2022 (DEH22). a) Frequency of mean A15J30 discharges higher than 151.3 m³/s and represented by the median (solid dots) and maximum (empty dots) values produced by 10-GCMs ensemble. b) Mean A15J30 discharge. Historical discharges are represented by crossbars where the median value is a thick black line, the interval containing 80% of the values is a solid color, and the minimum to maximum range of values is a shading color. Projected discharges under the RCP4.5 and RCP8.5 scenarios are represented by lines of minimum, 80% lower bound, median, 80% upper bound and maximum values produced among the 10-GCMs ensemble and for ML (grey triangles) and DEH22 (orange circles) projections respectively. Horizontal dashed line indicates the median of the observed discharge for 1971–2000 period at 121.03 m³/s.

Table 5.4a Scenario RCP4.5. Projected hydroclimatic trends in the Upper Harricana River watershed from 1971 to 2100 and calculated using the median of the 10-GCM ensemble. Non-significant ($p < 0.05$) trends are shown. Sen's slopes are expressed as 130-year change in the original data units. Percent change is relative to the 1971–1980 (10-year) average which is assumed to be representative of the beginning of the trend line. Value below the trend is the inter-GCMs agreement and expresses the number of positive trend / negative trend / non-significant change found among the ten GCMs when calculating the Sen's slope for each of GCM projection separately. Variables abbreviations are listed in Table 5.S1.

1971-2100 (RCP4.5)		jul	aug	sep	oct	nov	dec	JAN	FEB	MAR	APR	MAY	JUN	SUMMER	FALL	WINTER	SPRING	A15J30	ANNUAL	
MIN temperature		Slope	4	4.4	3.7	3.3	8.7	8.1	7.2	6.8	6.7	2.9	3.4	3.5	6.5	8.3	6.9	5	8.3	
		% Change	165%	517%	127%	38%	25%	21%	19%	21%	37%	55%	336%	298%	31%	20%	21%	44%	20%	
		Agrmt	10/0/0	10/0/0	9/0/1	7/0/3	10/0/0	10/0/0	10/0/0	10/0/0	10/0/0	9/1/0	10/0/0	10/0/0	9/0/1	10/0/0	10/0/0	10/0/0	10/0/0	
MEAN temperature		Slope	3.9	4.4	4.2	4.1	5.9	6.2	4.8	3.6	4	3.6	3.5	4.1	4.1	5.5	3.7	3.7	4.4	
		% Change	23%	29%	40%	113%	44%	34%	32%	43%	261%	40%	25%	27%	121%	36%	521%	37%	433%	
		Agrmt	10/0/0	10/0/0	10/0/0	10/0/0	10/0/0	10/0/0	10/0/0	10/0/0	9/0/1	10/0/0	9/0/1	10/0/0	10/0/0	10/0/0	10/0/0	10/0/0	10/0/0	
MAX temperature		Slope	3.5	3.8	4.8	4.3	2.7	1.1	3.4	3.4	4.8	3.5	3.5	3.6	4.9	3	3.4	3.6	3.6	
		% Change	12%	13%	20%	24%	93%	112%	40%	40%	26%	13%	12%	12%	20%	57%	13%	12%	11%	
		Agrmt	9/0/1	10/0/0	9/0/1	9/0/1	8/0/2	2/0/8	5/3/2	7/0/3	8/1/1	9/0/1	9/0/1	9/0/1	9/0/1	7/0/3	8/1/1	9/0/1	9/0/1	
Evaporation		Slope	4.1	4.6	4.6	4.2	2.4		0.9	3.9	4	3.8	3.8	3.8	4.6	0.2	2.7	4	1.6	
		% Change	18%	21%	30%	54%	168%		88%	50%	25%	18%	18%	18%	30%	195%	33%	24%	9%	
		Agrmt	9/0/1	10/0/0	9/0/1	10/0/0	10/0/0		6/1/3	8/0/2	9/0/1	9/0/1	9/0/1	9/0/1	9/0/1	0/0/10	9/0/1	9/0/1	5/0/5	
Snowfall		Slope	-	-	-	-8.4	-10.2	4.6	7.9	-6.8	-0.8	-	-	-	-19.2	10.9	-9.8	-5.9	-23.2	
		% Change	-	-	-	-75%	-32%	11%	27%	-56%	-51%	-	-	-	-41%	9%	-20%	-83%	-10%	
		Agrmt	-	-	-	0/8/2	0/6/4	1/0/9	5/0/5	0/7/3	0/0/10	-	-	-	0/10/0	1/0/9	0/3/7	0/10/0	0/4/6	
MAX Snowfall		Slope	-	-	-	-	-	1.3	1.3	-1.5	-0.6	-	-	-	-1.4	1.2	-	-1.8	1	
		% Change	-	-	-	-15%	-	20%	20%	-35%	-57%	-	-	-	-18%	12%	-	-56%	8%	
		Agrmt	-	-	-	0/2/8	-	2/0/8	2/0/8	0/6/4	0/0/10	-	-	-	0/3/7	1/0/9	-	0/10/0	1/0/9	
%Snow		Slope	-	-	-	-11.8	-21.4	-8.6	-7.4	-17.9	-1.2	-	-	-	-9.4	-12	-11	-3.1	-5.8	
		% Change	-	-	-	-80%	-43%	-20%	-8%	-20%	-67%	-53%	-	-	-51%	-14%	-39%	-77%	-21%	
		Agrmt	-	-	-	0/10/0	0/10/0	0/9/1	0/5/5	0/5/5	0/9/1	0/0/10	-	-	0/10/0	0/10/0	0/8/2	0/10/0	0/10/0	
Rainfall		Slope	8.5	19.3	17.9	11.1	4	3.9	3.9	9.5	19.4	13.6	18.9	18.9	52.5	21.8	41	34.5	125.7	
		% Change	10%	28%	70%	172%	224%	137%	137%	58%	57%	23%	7%	7%	28%	185%	35%	20%	21%	
		Agrmt	1/1/8	5/0/5	7/0/3	9/0/1	6/0/4	6/0/4	6/0/4	4/0/6	7/0/3	3/0/7	1/0/9	1/0/9	7/0/3	10/0/0	7/0/3	6/0/4	8/0/2	
MAX Rainfall		Slope	2.4	3.8	3.4	2.5	1.8	1.6	1.6	3.1	5	2.6	2.6	2.6	5.3	3.2	5.1	2.5	5.8	
		% Change	12%	23%	42%	78%	132%	97%	97%	46%	46%	16%	16%	16%	20%	74%	30%	11%	18%	
		Agrmt	1/0/9	2/0/8	6/0/4	7/0/3	6/0/4	5/0/5	5/0/5	3/0/7	7/0/3	4/0/6	4/0/6	4/0/6	4/0/6	9/0/1	6/0/4	3/0/7	4/0/6	
Rainfall intensity		Slope	0.4	0.9	1.1	0.8	0.8	0.9	0.8	0.6	1.3	0.8	0.5	0.5	0.9	0.6	0.9	1.1	0.6	
		% Change	7%	14%	21%	21%	41%	77%	58%	17%	28%	14%	7%	7%	16%	27%	18%	19%	10%	
		Agrmt	2/0/8	3/0/7	4/0/6	5/0/5	4/0/6	4/0/6	4/0/6	3/0/7	9/0/1	1/0/9	1/0/9	1/0/9	6/0/4	5/0/5	6/0/4	5/0/5	5/0/5	
1971-2100 (RCP4.5)		CDD	CDD	DD	DD	DD0	ECD	FDD	FFF	FTC	FTC	HDD	HDD	HDD	IBU	LSF	ISL	HR10	HR10	TAP
		SPRING	A15J30	SPRING	A15J30															
		12.8	74.2	3234	3234	3234	3234	723.8	15.9	3.7	-13.7	-587.6	-426.3	-15.2	-21	-17.1	2.1	1.2	29.8	
Additional variables		% Change	847%	279%	3%	3%	-70%	38%	34%	41%	-34%	-20%	-36%	-14%	-18%	-12%	73%	22%	11%	
		Agrmt	8/0/2	9/0/1	9/0/1	9/0/1	0/10/0	10/0/0	9/0/1	8/1/1	0/10/0	0/10/0	0/10/0	0/9/1	1/8/1	0/9/1	8/0/2	3/0/7	5/0/5	

Table 5.4b Scenario RCP8.5. Projected hydroclimatic trends in the Upper Harricana River watershed from 1971 to 2100 and calculated using the median of the 10-GCM ensemble. Non-significant ($p < 0.05$) trends are shown. Sen's slopes are expressed as 130-year change in the original data units. Percent change is relative to the 1971–1980 (10-year) average which is assumed to be representative of the beginning of the trend line. Value below the trend is the inter-GCMs agreement and expresses the number of positive trend / negative trend / non-significant change found among the ten GCMs when calculating the Sen's slope for each of GCM projection separately. Variables abbreviations are listed in Table 5.S1.

1971-2100 (RCP8.5)		jul	aug	sep	oct	nov	dec	JAN	FEB	MAR	APR	MAY	JUN	SUMMER	FALL	WINTER	SPRING	A15J30	ANNUAL		
MIN temperature	Slope	7.4	7.8	6.8	5.6	11.8	15.8	15.5	14	13.9	11.8	6.2	6.6	6.4	11.5	15.4	14	7.8	15.3		
	% Change	299%	923%	236%	66%	56%	45%	39%	37%	44%	66%	118%	60%	558%	54%	38%	44%	69%	37%		
	Agrmt	10/0/0	10/0/0	10/0/0	8/0/2	10/0/0	10/0/0	10/0/0	10/0/0	10/0/0	10/0/0	9/1/0	10/0/0	10/0/0	10/0/0	10/0/0	10/0/0	9/0/1	10/0/0		
MEAN temperature	Slope	7.1	8.2	7.6	6.9	7.1	9.9	10.9	9	7	6.5	6.2	6.3	7.3	7.3	9.9	6.4	6.3	7.8		
	% Change	42%	54%	73%	191%	207%	74%	60%	60%	83%	421%	69%	44%	47%	215%	64%	896%	63%	767%		
	Agrmt	10/0/0	10/0/0	10/0/0	10/0/0	10/0/0	10/0/0	10/0/0	10/0/0	10/0/0	10/0/0	10/0/0	10/0/0	10/0/0	10/0/0	10/0/0	10/0/0	10/0/0	10/0/0		
MAX temperature	Slope	7.4	7.8	8.2	7.3	7.6	6.2	3.1	1.6	7.1	7.2	6.1	6	7.5	8.2	6.1	6.1	5.8	7.4		
	% Change	25%	27%	33%	41%	74%	216%	340%	0.46	85%	38%	23%	20%	24%	33%	118%	23%	20%	24%		
	Agrmt	9/0/1	10/0/0	9/0/1	10/0/0	10/0/0	9/0/1	9/0/1	4/1/5	6/0/4	9/1/0	9/1/0	9/0/1	10/0/0	9/0/1	9/0/1	9/1/0	9/0/1	10/0/0		
Evaporation	Slope	7.3	8.5	8	7.2	4.8	0.6			2.1	6	6.3	6.4	6.4	8	0.5	4.5	6.6	1.9		
	% Change	32%	40%	52%	93%	345%	62.08			208%	78%	41%	31%	31%	52%	593%	54%	40%	11%		
	Agrmt	10/0/0	10/0/0	10/0/0	10/0/0	10/0/0	1/0/9			6/0/4	10/0/0	9/1/0	9/0/1	9/0/1	10/0/0	1/0/9	10/0/0	9/0/1	6/0/4		
Snowfall	Slope	-	-	-	-12.2	-19.3		7.4	4.6	-6	-8.8	-0.6	-	-	-32.7	11.4	-17	-7.4	-45.9		
	% Change	-	-	-	-109%	-61%		17%	15%	-0.18	-73%	-38%	-	-	-70%	9%	-35%	-106%	-20%		
	Agrmt	-	-	-	0/10/0	0/10/0		2/0/8	2/0/8	0/2/8	0/10/0	0/1/9	-	-	0/10/0	4/0/6	0/7/3	0/10/0	0/8/2		
MAX Snowfall	Slope	-	-	-	-3.1	-2.5		1.1	0.9	-2.2	-0.2	-	-	-	-2.7	1.1	-1.5	-2.9	-		
	% Change	-	-	-	-8	-35%		13%	13%	-50%	-21%	-	-	-	-36%	11%	-15%	-89%	-		
	Agrmt	-	-	-	0/10/0	0/8/2		4/0/6	1/0/9	0/7/3	0/1/9	-	-	-	0/9/1	2/0/8	1/2/7	0/10/0	-		
%Snow	Slope	-	-	-	-16.6	-36.3		-18.5	-15.7	-25.6	-24.2	-0.8	-	-	-14.7	-23.4	-16.5	-3.8	-9.3		
	% Change	-	-	-	-112%	-73%		-20%	-18%	-41%	-92%	-34%	-	-	-79%	-27%	-59%	-98%	-34%		
	Agrmt	-	-	-	0/10/0	0/10/0		0/10/0	0/9/1	0/7/3	0/10/0	0/1/9	-	-	0/10/0	0/10/0	0/10/0	0/10/0	0/10/0		
Rainfall	Slope	12.3	23.5	33.9	24.6	8.8	8	8.8	8	22.1	35.6	21.1	10.3		70.1	45.6	83.7	50.9	205.8		
	% Change	0.13	35%	132%	382%	501%	278%	135%	105%	105%	35%	35%	0.11		37%	390%	71%	29%	35%		
	Agrmt	1/0/9	7/0/3	10/0/0	10/0/0	10/0/0	8/0/2	8/0/2	8/0/2	8/0/2	10/0/0	6/0/4	1/0/9		10/0/0	10/0/0	9/0/1	10/0/0	10/0/0		
MAX Rainfall	Slope	6.2	7.6	6.1	3.7	3	6.2	8.2	8.2	8.2	4.8	2.8	4.1		5.7	6.6	8	4.9	10		
	% Change	38%	95%	189%	276%	184%	92%	76%	29%	76%	29%	0.13	0.14		21%	152%	47%	21%	30%		
	Agrmt	6/0/4	10/0/0	10/0/0	10/0/0	8/0/2	8/0/2	8/0/2	8/0/2	10/0/0	6/0/4	1/0/9	4/0/6		4/0/6	10/0/0	10/0/0	6/0/4	6/0/4		
Rainfall intensity	Slope	1.1	1.6	1.6	1.8	1.7	1.3	1.5	2.1	1.5	2.1	1.6	0.9		1.3	1.3	1.6	1.7	0.7		
	% Change	18%	31%	44%	88%	146%	94%	42%	45%	28%	28%	14%	7%		23%	55%	32%	31%	12%		
	Agrmt	5/0/5	8/0/2	8/0/2	10/0/0	10/0/0	7/0/3	7/0/3	10/0/0	10/0/0	6/0/4	6/1/3	4/1/5		8/0/2	10/0/0	10/0/0	9/0/1	5/0/5		
1971-2100 (RCP8.5)	CDD	SPRING	A15J30	SPRING	DD0	DD0	ECD	FDD	FFF	FTC	WINTER	FTC	HDD	HDD	IBU	LSF	ID	ISL	HR10	HR10	TAP
Additional variables	Slope	34.5	162.2		3726.7	-46	1234	24.7	8.7	-18.6	-1022	-690.2	-25.2	-6.1	-41.4	-30	3.6	1.7	70.2		
	% Change	2296%	604%		3%	-110%	65%	53%	96%	-46%	-35%	-58%	-23%	-3%	-35%	-20%	130%	29%	25%		
	Agrmt	9/0/1	10/0/0		9/0/1	0/10/0	10/0/0	10/0/0	8/1/1	0/10/0	0/10/0	0/10/0	0/10/0	0/7/3	0/9/1	0/10/0	9/0/1	7/0/3	10/0/0		

5.5.3 Projected impacts of climate change on the mean A15J30 discharge

The median of the 10-GCM ensemble projected a mean A15J30 discharge variability similar to that of the historical range of reconstructed (1771–1920) and observed (1915–2020) values with a slight (RCP4.5) to more pronounced decrease (RCP8.5) by the end of the century (Fig. 5.5). Under both climate scenarios, the ensemble median projected no significant change, and one out of ten GCM projected a decrease in mean A15J30 discharge. Similar discharge variability was projected using the 80% interval of the ensemble values, and under both climate scenarios. The 80% projected interval roughly corresponded to the range of values observed during the 20th century in high and low mean A15J30 discharge (Fig. 5.5). The projected mean A15J30 discharge compared well with the DEH22 projections, with high consistency between the ensemble minimum, median and maximum values (Fig. 5.5). While the ML model showed no change, the median of the DEH22 simulations projected a slight decrease in mean A15J30 discharge under both climate scenarios and supported by about half of the GCMs (RCP4.5: median = -7%, 5 GCMs showed a significant downward trend; RCP8.5: median = -14%, 6 GCMs showed a significant downward trend). Considering the extreme mean A15J30 discharge projected by the 10-GCMs ensemble, both hydrological model simulations demonstrated higher variability than the reconstructed and the observed values, in both low and high discharge.

5.5.4 Projected impacts of climate change on the low and high values and frequency of high mean A15J30 discharge

To assess the projected changes in both low and high mean A15J30 discharge, quantile regressions of the 10th and 90th quantiles were performed on both ML and DEH22 model simulations. It indicated that two to three GCMs (A13, GFM, and to a lesser extent CE2) projected an increase in the high mean A15J30 discharge above the reconstructed and observed levels (1771–2020; Fig. 5.6). One (RCP8.5) to two (RCP4.5) GCMs also projected a decrease in low mean A15J30 discharges below the

reconstructed and observed levels (Fig. 5.6). In contrast, the median frequency of high mean A15J30 discharge above 151.3 m³/s was projected to stay within the historical range of one to two floods per decade by 2100, and under both climate scenarios (Fig. 5.5). While the frequency of high mean A15J30 discharge over the hindcast period (1971–2020) demonstrated a good agreement between the median frequency projected by the 10 GCMs under both scenarios, it should be noted that the maximum frequency overestimated the observations by one to two events per decade. Without considering the values, the maximum frequency of high mean A15J30 discharge was projected to decrease by the end of the century under RCP4.5, and to a lesser extent under RCP8.5 (Fig. 5.5; Fig. 5.7). Comparing the projected maximum frequency among the 10 GCMs and hydrological models showed two trajectories between GCMs (Fig. 5.7). Five GCMs (BNU, CE2, CMS, IBL, NOE; Table 5.S1) projected similar and stable frequencies by 2100, with possible punctual increases up to five times per decade. The remaining five GCMs (A13, GFM, IAL, INM, MPL; Table 5.S1) projected increased frequency by mid to late century followed by a decrease to the historical frequency or below (Fig. 5.7).

5.5.5 Projected climate change trends by 2100

The projected mean annual temperature warming for the Upper Harricana River watershed ranged between 1°C (RCP4.5) and 2°C (RCP8.5) above the estimated global warming by 2100 (Table 5.4). The most significant warming trends were projected in the minimum temperature of late fall, winter, and spring. For instance, the mean temperature of November and the minimum temperature of May were projected to become positive by 2100 under both climate scenarios. These projected warming trends were accompanied by a decrease in days with a minimum temperature below –25°C and an increase in the frequency of freeze-thaw cycles in winter (Table 5.4). Snowfall amounts and contribution to precipitation decreased significantly in October, November, April, May (Table 5.4), and the A15J30 period (Table 5.4; Fig. 5.S3).

Under RCP8.5 scenario, snowfall amounts were projected to be near zero in May and both scenarios projected a near 100% decrease in snowfall amounts for the A15J30 period (Fig. 5.S3). It should be noted that, even over the hindcast period (1971–2020) and in contrast to the BioSIM data, all 10 GCMs did not simulate snowfall in June. The ensemble median projected increased snowfall in January and February, however associated to increased rainfall. In fact under both climate scenarios, rainfall amount and intensity were projected to increase in virtually each month, particularly in winter, and to a lesser extent, in early spring (Table 5.4).

Among the climate variables used as input to the ML model, the TAP was projected to increase driven by strong increases in November through April, and A15J30 rainfall (Table 5.4). In January and February both the snowfall and the rainfall amounts were projected to increase, and under both climate scenarios (Table 5.4). The contribution of snowfall to the total precipitation amount however, was projected to decrease in October-November, and in April-May, and particularly under RCP8.5 scenario (Table 5.4). The snowfall accumulation by 2100 was affected by a one-month reduction of the ice season length (ISL, Table 5.S1) under RCP8.5, and by a one-month reduction of ECD under both climate scenarios (Table 5.4). Consequently, the estimated timing of ice break-up in the Upper Harricana River was projected to occur between 15 (RCP4.5) to 25 days (RCP8.5) earlier by 2100.

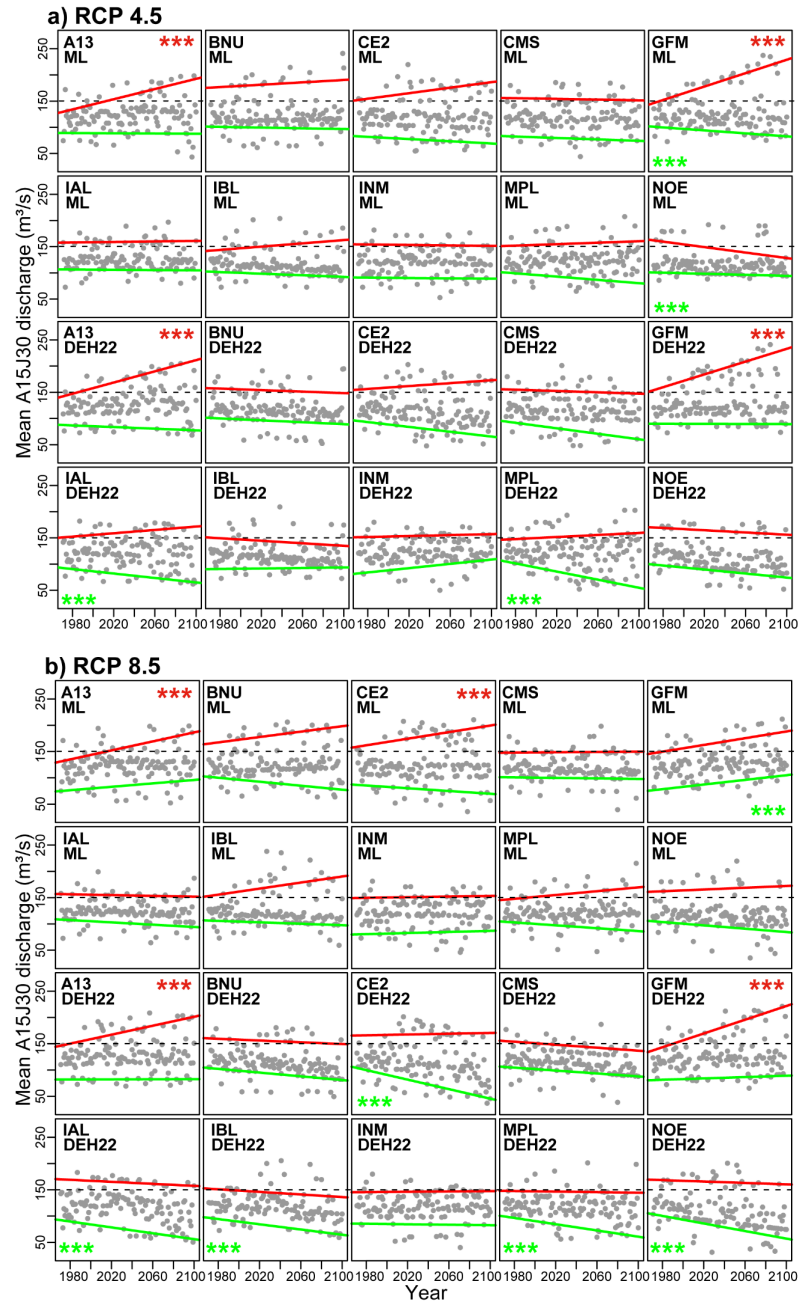


Figure 5.6 0.10 (green) and 0.90 (red) quantiles regressions calculated on the hydrological models' outputs (ML and DEH22) produced by each of the 10 GCMs and under the two climate scenarios (a) RCP4.5 and (b) RCP8.5. Significant ($p < 0.05$) quantiles regressions are indicated with “***”, respectively for the 0.10 (green) and 0.90 quantiles (red). Horizontal dashed lines indicate $151.3 \text{ m}^3/\text{s}$.

5.5.6 Assessment of the projected climate changes leading to increased high mean A15J30 discharge

To understand how projected climate changes might affect the upper Harricana River toward an increase in the A15J30 high mean discharge, particularly under the RCP4.5 scenario, the climate variables projected by the A13 and GFM climate models were compared to those projected by the 10-GCM ensemble (Fig. 5.6; Fig. 5.7). Each climate variable was screened to keep only the 95% extreme values (less than the 0.05 quantile or greater than the 0.95 quantile) and compared to the average discharge projected for the period A15J30 by the ML and DEH22 models (Fig. 5.8). It should be noted that because climate models are random and chaotic in nature, a particular high-water event cannot be compared between climate models to assess its climatic mechanisms.

For each GCM and under both climate scenarios, most of the predicted average high discharges for A15J30 were associated with high APR accumulations (accumulated snowfall from November to December, plus accumulated total precipitation from January to March; ML model: $r_{RCP4.5} = 0.68 \pm 0.05$ std, $r_{RCP8.5} = 0.67 \pm 0.08$ std; DEH22 model: $r_{RCP4.5} = 0.62 \pm 0.08$ std, $r_{RCP8.5} = 0.54 \pm 0.12$ std; 2021–2100). Under the RCP4.5 scenario, the GFM climate model differentiated from the other GCMs by predicting five snowfalls greater than 10 mm in May during the second half of the 21st century (2051–2100), while the other climate models predicted zero or two (Fig. 5.8a). This was also the only climate model that predicting no change in breakup timing by 2100 under RCP4.5 (Table 5.4a), with a mean timing predicted in April and some late breakups expected in mid- to late May. The high A15J30 mean discharges projected by the GFM model were therefore associated with the latest ice breakups and supported by the lowest May minimum temperatures and longest ice season length (ISL) in the 2021–2100 period (Fig. 5.8a). Most of the highest projected discharges also corresponded to the highest number of spring freeze-thaw cycles (FTC) and the highest amounts of snow in May (Fig. 5.8a). For each GCM, the highest A15J30 rainfalls and

highest daily rainfall events (HR10) were particularly consistent with projected high spring discharge and especially during the second half of the 21st century (Fig. 5.8a). Hydroclimatic associations to the high A15J30 mean discharge projected by the GFM climate model were found, to a lesser extent, with the A13 and CE2 climate model projections under the RCP4.5 scenario. Both climate models projected smaller increases in high A15J30 mean discharges than the GFM model (Fig. 5.6; Fig. 5.8a) and mostly associated with rainy spring than with a long ice season, high snowpack, and late breakup.

In the RCP8.5 projections, the climate variables associated with the A13, CE2, and GFM models were largely representative of those in the other GCM projections (Fig. 5.8b). The associations of climate variables with the highest A15J30 mean discharge among the climate ensemble showed two distinct trends in the first and second half of the century. For the first half of the 21st century, associations similar to those detailed in the RCP4.5 scenario were projected. Associations for the second half of the century were consistent only with most of the highest TAP index and most of the highest A15J30 rainfalls and the highest daily rainfall events (HR10; Fig. 5.8b).

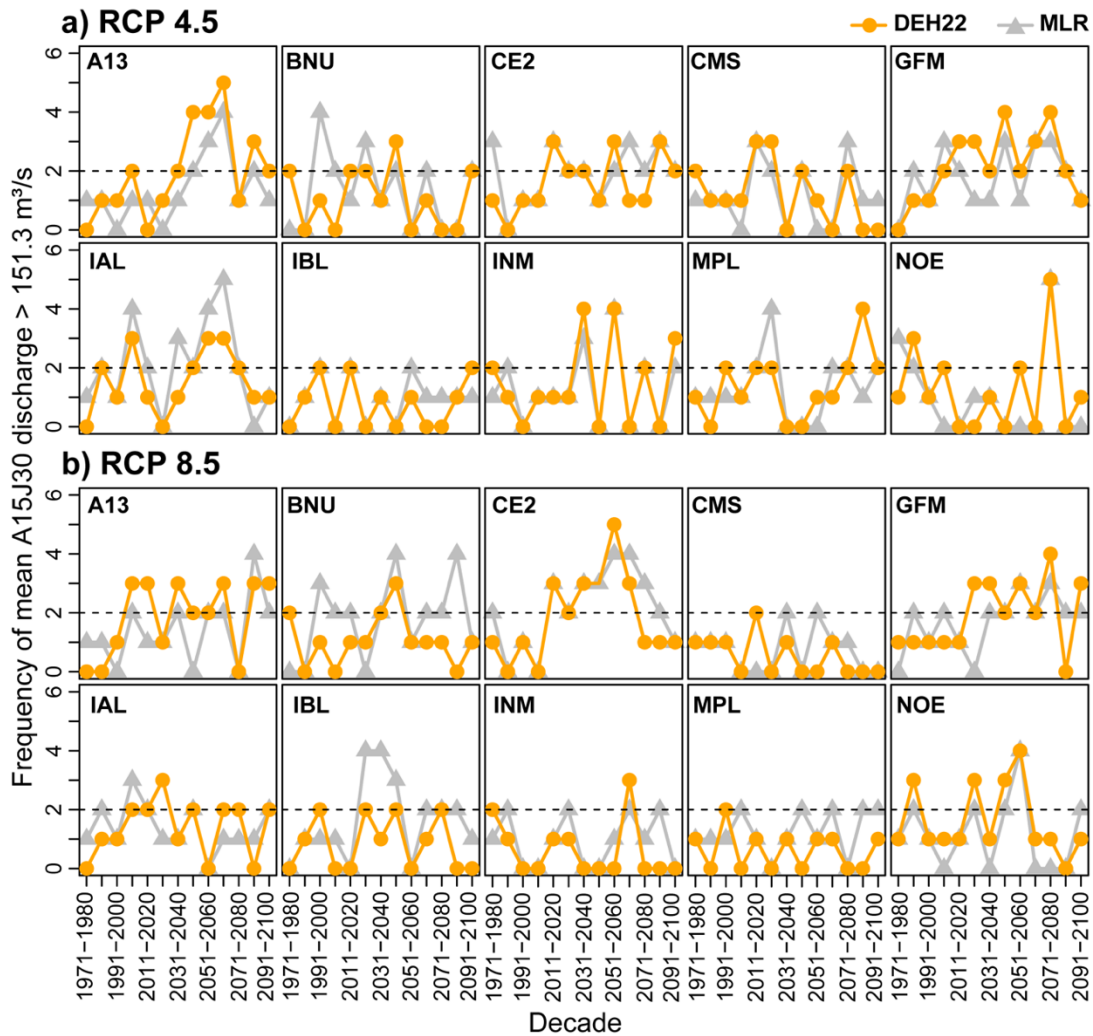
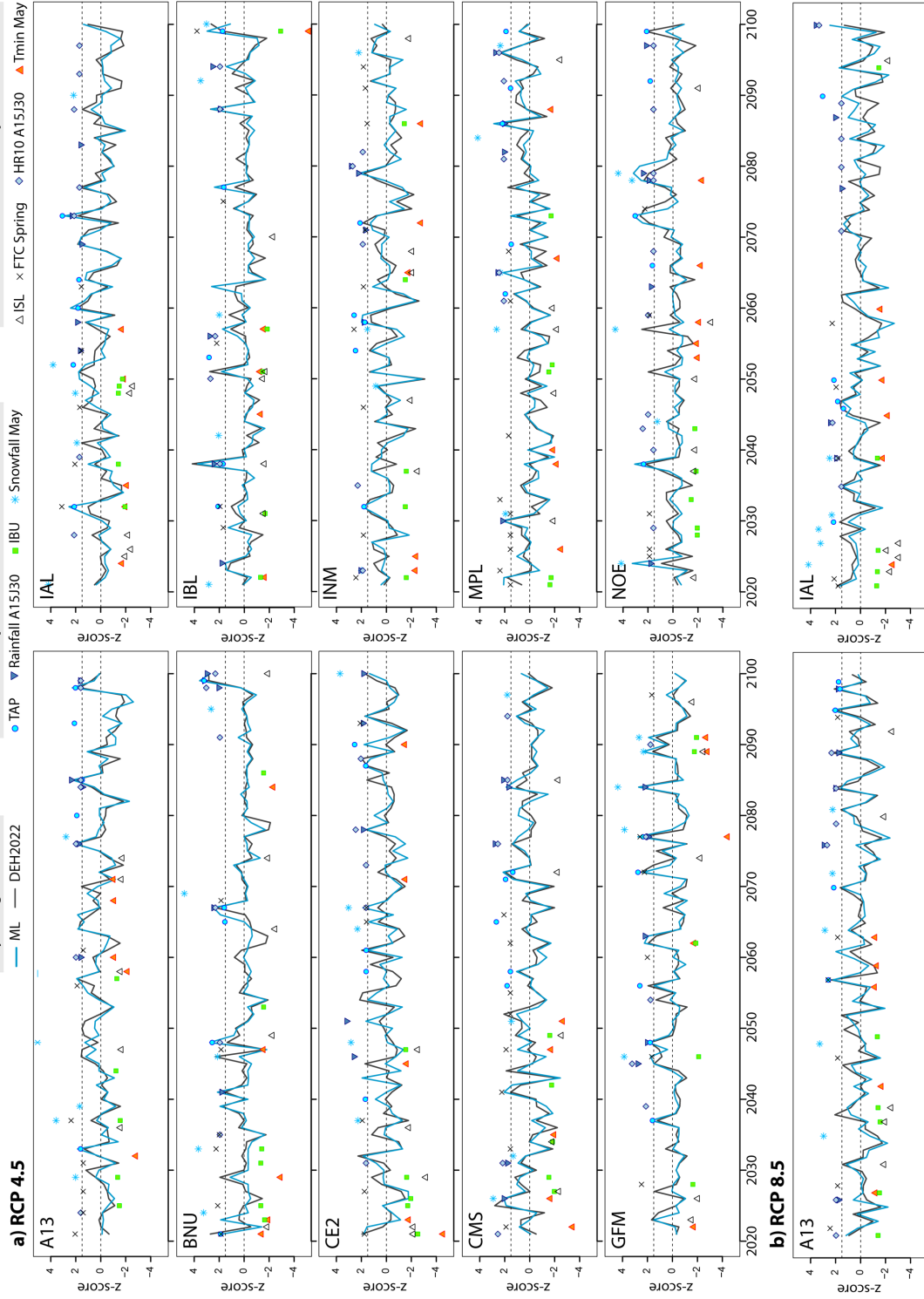


Figure 5.7 Comparison of the decadal frequencies of high floods (mean A15J30 discharge above 151.3 m³/s) among the 10-GCM ensemble and between (a) RCP4.5 and (b) RCP8.5 climate scenarios. Hydrological simulations are those by the machine learning model (grey triangle) and the Hydroclimatic Atlas of Southern Québec 2022 (DEH22, orange dots). Horizontal dashed line is two high floods per decade and can be used to compare graphs among others.



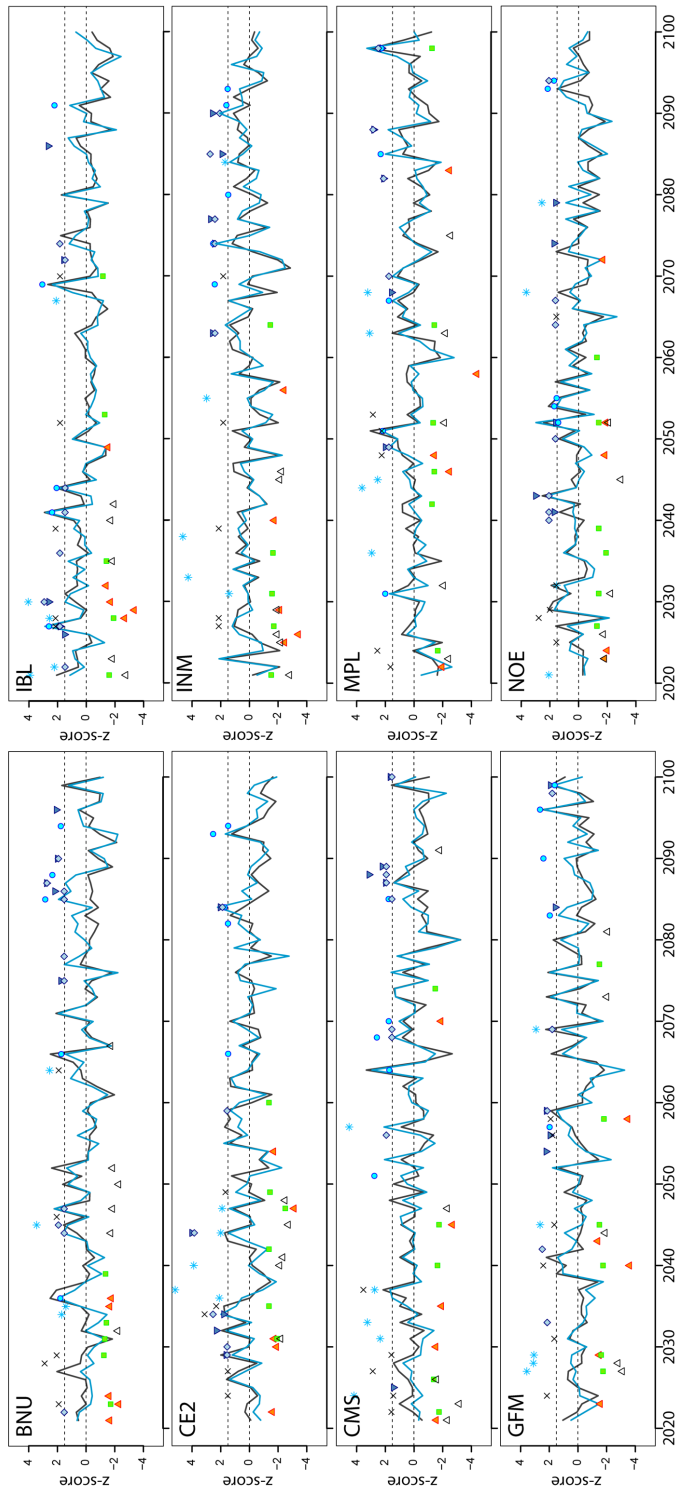


Figure 5.8 Comparison between the highest projected A15J30 mean discharge (2021–2100) and the extreme values projected in various climate predictors for (a) RCP4.5 and (b) RCP8.5 climate scenarios and each of the 10 GCM climate model. Each climate serie has been scale to z-score for comparison purposes. Extremes values in climate predictors were defined as below the 0.5 quantile of above the 0.95 quantile. High A15J30 mean discharge were defined as above the 151.3 m^3/s threshold (depicted as the upper dashed line). Discharge projections are depicted for the ML model (blue lines) and the DEH2022 model (grey lines). Climate predictors are figured with various shapes as explained in the upper graphic legend and coded as in Table 5.S1. For visualisation purposes, IBU and ISL values have been set negative.

5.6 Discussion

The Upper Harricana River has experienced significant hydroclimatic changes in the 20th century and quantifying, projecting, and understanding how climate change might further affect spring discharge trajectories is critical to the regional management of water resources and flood risks. This study provides a unique long-term perspective including past, present, and future mean A15J30 discharge variability in the Upper Harricana River from 1771 to 2100.

5.6.1 Observed hydroclimatic changes affecting the mean A15J30 discharge

The identified 20th century trends in the Upper Harricana River climate and discharge are consistent with other results from eastern boreal Canadian studies. Since the 1950s, shorter snow cover duration (Brown, 2010; Mudryk et al., 2018; Aýgun et al., 2019) and river and lakes ice cover duration (Fu and Yao, 2015; Rokaya et al., 2018; Aýgun et al., 2019; Bush & Lemmen, 2019; Chen and She, 2020) are consistently reported. Winter average temperature warming over eastern boreal Canada has also reduced the proportion of precipitation that falls as snow (Yagouti et al., 2008; Brown, 2010; Mudryk et al., 2018; Aýgun et al., 2019; Mudryk et al., 2020) while increasing the total precipitations (Zhang et al., 2000; Zhang et al., 2001b; Yagouti et al., 2008; Vincent et al., 2018). In the Upper Harricana River watershed SWE has significantly decreased, supporting available results for northeastern Canada which generally show decreases (Mudryk et al., 2018; Aýgun et al., 2019; Mudryk et al., 2020), but contrasting with increases found in northern Québec (Yagouti et al., 2008; Brown, 2010; Aýgun, et al., 2019).

While changes in maximum spring rainfall intensities observed in the Upper Harricana River during the 20th century remains moderate, others eastern boreal Canadian rivers demonstrated transition from snowmelt-driven spring floods towards mixed snowmelt

and heavy rainfall-driven spring floods, and particularly in the southernmost areas (Burn et al., 2010; Ouellet et al., 2012, Burn & Whitfield, 2018; Aýgun et al., 2019; Teufel & Sushama, 2021). No changes were found in the variables accounting for the melting mechanisms of the Upper Harricana snowpack such as in the freeze-thaw cycles, rain-on-snow events, or the duration of snowmelt in spring, which would suggest that the snowmelt intensities have not been more evenly distributed over the winter and spring. No change was either demonstrated in the maximum spring discharge. It could thus be hypothesized that the observed increases in winter and spring rainfall, and in spring rainfall intensity, were not sufficiently intense to trigger an increase in spring flooding or were offset by the decrease in SWE, which then contributed less to the spring flooding. This is in line with previous research hypothesizing that whereas most of the historical spring flooding were associated with cold and snow winters, long lasting snow cover and heavy rainfall (Nolin et al., 2021a), the warmer average spring temperature in the Upper Harricana River watershed since the last 40 years may have likely shifted the contribution of snow vs rain in the spring flooding processes (Nolin et al., 2022). In other locations of northeastern Canada and during the 20th century, increased frequency and intensity of rainfall on mid-winter and spring snow cover (Brown, 2010; Jeong et al., 2018; Vincent et al., 2018; Li et al., 2019) has generally augmented the number of freeze-thaw cycles (Yagouti et al., 2008), magnifying the spring peak discharge by a generally higher winter discharge (Whitfield & Cannon, 2000; Zhang et al., 2001a; Déry et al., 2011; Vincent et al., 2015). In this study and from 1915 to 2020 the increase in rainfall had likely offset the decrease in snowpack in the contribution to the mean A15J30 discharge of the Upper Harricana River which indicated no changes but a slightly increasing frequency of high mean A15J30 discharge in the last decade (2010–2020). An increase in both the magnitude and frequency of high mean A15J30 discharge has however been demonstrated at the scale of the last 250 years (Nolin et al., 2021a), and more broadly, similar trends in flood frequency and magnitude were observed in numerous paleorecords of the Little

Ice Age across eastern boreal and subarctic Canada having investigated the spring discharge (Tardif & Bergeron, 1997b; Bégin et al., 2000; Bégin, 2001; Lemay & Bégin, 2008; Boucher et al., 2011; Lemay & Bégin, 2012; Nicault et al., 2014; Nasri et al., 2020; Nolin et al., 2021b).

5.6.2 Projected hydroclimatic changes affecting the mean A15J30 discharge by 2100

Projected trajectories of hydroclimatic changes affecting the mean A15J30 discharge followed the hydroclimatic trends found in the 20th century and compared well with the DEH22 simulations, as well as with other regional and Québec-wide projections issued using various models and for various horizons (2050, 2080, 2100). Without daily projected hydroclimatic changes it still remains hazardous to distinguish a snowmelt-driven from a rainfall-driven high spring discharge. However, the decrease in the length of the snow season, the sharp decrease in spring snowfall, and the sharp increase in spring rainfall and heavy rainfall support the hypothesis of a projected higher contribution of rainfall storms in spring flooding dynamics in the future. Our results support the likely increase in total annual precipitation expected for northeastern Canada, with a sharp transition to more rain than snow in fall and spring (Cohen et al., 2015; Guay et al., 2015; Wang et al., 2015; Mudryk et al., 2018; Bush & Lemmen, 2019) associated to increases in both maximum and intensity of rainfall storms (Wang et al., 2015). As in the simulations issued by Guay et al., (2015) for northern Québec, increased maximum snowfall in mid-winter favored by average temperatures remaining below freezing is expected for the Upper Harricana River and under both climate scenarios. Modest changes were expected in the mean A15J30 discharge by 2100, which was projected to likely (8 out of 10 climate model) stay within the range of discharges observed during the 20th century, or below. Two climate models, however, projected an increasing magnitude and frequency of high discharge outside the range of historical variability reconstructed since the end of the Little Ice Age (1771–2020). These were associated with climate conditions like those known to have caused major

spring flooding across the region (Nolin et al., 2021a, Nolin et al., 2022). This concurs with other regional projections of spring flood magnitude and frequency, projecting both a decrease in southwestern Ontario (Cunderlik & Simonovic 2005), north central Ontario (Gaur et al., 2018), southwestern Quebec (Oubennaceur et al., 2021), and an increase in northeastern Quebec and south-central Ontario (Gaur et al., 2018), as well as a province-wide rise across Quebec (Clavet-Gaumont et al., 2013a). This result thus reemphasizes the importance of considering climate model ensembles and different hydrological modeling to assess changes in spring flooding at the watershed scale when considering the potential effects of climate change on discharge (Clavet-Gaumont et al. (2017). The two GCMs projecting increase *vs.* eight GCMs projecting similar variability in high discharge by 2100 likely reflect the uncertainty that exists in representations of future global climate and/or in the biases of using these models at the scale of small watersheds like the Upper Harricana River.

5.6.3 Uncertainties in climate change results

In climate change projections a major source of uncertainties is often inherent to the climate models and downscaling method used (Chen et al., 2011; Clavet-Gaumont et al., 2017; Lucas-Picher et al., 2021). Projections were computed using a 10-GCM subset of models runs from the CMIP5 ensemble designed by Ouranos to cover the global range of the full CMIP5 ensemble over Québec. Further studies involving ML models could benefit from the use of the newer CMIP6 simulations once they would have been bias-corrected and downscaled for Québec. Recent comparison between CMIP5 and CMIP6 climate projections over Canada indicated that CMIP6 projected warming was significantly higher than CMIP5 models under the same climate scenario, and that CMIP6 exhibited significant change in the variability of extreme precipitation (Sobie et al., 2021). While the SWE was successfully estimated using the TAP index, another improvement to our approach could be to benefit from a more detailed representation of the snow processes in climate model data. For

instance, it could help to understand how the decrease in seasonal snowpack and snow duration may affect the timing and duration of snowmelt in spring, or to account for the evaporation of water directly from the snowpack (sublimation) which is projected to increase under warmer snow-season temperatures (Burn et al., 2010). Of importance is that the maturity of the snowpack (*e.g.*, density; Brown, 2000) has a significant impact on whether heavy rainfall in spring may have a flood-generating potential or not (rain-on-snow events; Musselman et al., 2018; Li et al., 2019). In particular, the synergy between rain-snow events and freeze-thaw cycles is important for understanding how snowmelt can be mobilized for the spring freshet, or conversely, whether the formation of ice layers and/or surface crust will delay the mobilization of water from the snow. Finally, the future changes in watershed-scale climate were projected without taking into account changes in land use practices and changes in vegetation composition and structure induced by climate change that may impact hydrological processes. In particular, projections suggest significant increase in the loss of forest cover and densification of land by hardwood species with increased fire disturbance and tree mortality due to water and thermal stresses in the future (Chaste et al. 2019; Boulanger et al. 2022) that will certainly have impacts on boreal hydrology.

The hydrological modeling approach used in this study was similar to that of regionalization studies where data from river gauging networks are regressed against climatic and physiographic parameters in ungauged basins (*Worldwide*: Loáiciga, 1997; *Barbarossa* et al., 2017; *USA*: Vogel et al., 1999; McIntyre et al., 2005; Capesius and Stephens, 2009; Fouad et al., 2018). Multiple linear regressions were often used as traditional models in hydrological studies for long-term trend and scenarios projections (Krstanovic and Singh, 1991; Modini, 2000) or as a baseline for comparison with other data-driven techniques (Elshorbagy et al., 2010; Adamowski et al., 2012). There are however concerns that it may linearized the relationships between hydroclimatic and watershed variables and that annual low and high extreme discharge may generally be

underestimated (Krstanovic & Singh, 1991; McIntyre et al., 2005). Therefore, multiple linear models performed generally better when used with parameters derived from a large number of similar gauged watersheds (McIntyre et al., 2005) or a large number of climate predictors (Fouad et al., 2018). Compared to further advanced data-driven methods such as learning models or artificial neural networks, they were also demonstrated adequate for operational water management and land use planning when decisions can be made without detailed or daily hydrologic information or forecasts (Hrachowitz et al., 2013) which was the case for this study.

5.7 Conclusions

Future development and water resources management within the Upper Harricana River watershed will thus need to accommodate to the uncertainties in projected high mean A15J30 discharge changes. This study indicates that, climate change during the 20th century already have affected the proportion of precipitation falling as snow and rain, as well as the estimated timing of the river ice break-up. Future winter and spring warming was projected to favor rain instead of snowfall, which then contributed more to the discharge and compensated for the loss of snowmelt. Modest changes were expected in the mean A15J30 discharge of the Upper Harricana River by 2100, which was projected to likely (eight out of ten climate models) stay within the range of discharges observed during the 20th century, or below. Two out of ten climate models however projected increasing magnitude and frequency of high mean A15J30 discharge associated to climate conditions similar to those known to have led major historical spring flooding across the region. While this scenario remains unlikely it should be taken into consideration by stakeholders as a precautionary principle to plan for mitigating flood risks.

5.8 Acknowledgements

We thank the contribution and continuous support of Marco Braun, Travis Logan, David Huard and Trevor-J Smith (Ouranos) for their help retrieving CMIP5 dataset using PAVICS, and for their constructive comments and suggestions all along this study. David Huard wrote most of the PAVICS script to retrieve CMIP5 datasets over the study area. Richard Turcotte and Charles Malenfant (DEH) provided the DEH22 simulations and technical detail of the HYDROTEL modeling. This research is a contribution of the Canada Research Chairs (NSERC-CRC) held by Yves Bergeron and Jacques C. Tardif and was funded by a Natural Sciences and Engineering Research Council of Canada Collaborative research program including our partners Ouranos, Hydro-Québec, Ontario Power Generation (OPG) and The University of Winnipeg. This work was also supported by a scholarship from RIISQ – Intersectorial Flood Network of Québec (2nd Program 2020-2021) awarded to Alexandre F. Nolin.

5.9 Supplementary Materials

5.9.1 Adaptation of climate indexes for the Upper Harricana River watershed

5.9.1.1 Total accumulated precipitation

As SWE data were available as bias-corrected and downscaled climate change simulations, surrogates had to be calculated from the other CMIP5 climate parameters. Total accumulated precipitation (TAP) is the sum of the daily snowfall accumulated for November to December, and of the daily total precipitation accumulated from January to March (Romolo et al., 2006). This index was introduced as a surrogate of the peak seasonal SWE and was positively and significantly associated to April 1st SWE with high value of TAP corresponding to high values of April 1st SWE in western Canada (Romolo et al., 2006). It expresses the variability in the onset and melt of snowpack and indicate the amount of runoff that will be available in the spring. Climate data interpolated from the Upper Harricana River (1900–2021) showed that persistent snowpack, (as indicated by 5 days of consecutive SWE > 1; Table 2) established on average on November 07th \pm 11 days and was completely melted on average on April 15th \pm 11 days. Including the month of April in the TAP index increased the correlation between the mean spring discharge of the Harricana River from $r = 0.56$ to $r = 0.64$.

5.9.1.2 Accumulated melting degree days

A critical aspect of predicting the spring mean discharge was to estimate the timing of ice break-up. Exploratory analysis of the observed data showed that (1) Lake Duparquet breakup occurred on average when melting degree days (MDD) had accumulated $162.85 \pm 37.36^\circ\text{C}$ (1968–2018), (2) that the onset of spring freshet in the Harricana River, defined as the last inflexion point in the 10-day moving average of the daily discharge before flood peak, occurred on average when the MDD had

accumulated $4.62 \pm 6.98^{\circ}\text{C}$ (1915–2021), and (3) that the maximum annual discharge in the Harricana River occurred when the MDD had accumulated $146.03 \pm 49.85^{\circ}\text{C}$ (1915–2021). Highest correlation coefficient with the Harricana River mean spring discharge was found for a threshold of 99 accumulated MDD. An arbitrary threshold of 100 MDD accumulated from a mean daily temperature above 0°C was thus chosen to be representative of the ice break-up timing, instead of the initial value of 50 MDD presented by Williams, (1971). Lamontagne et al., (2021) also observed in Western Canada that 40 MDD (or degree-C-days of thaw) was enough to initiate a breakup on the Smoky River and that 150 MDD corresponded to the high freshet discharge on the Peace River. This correction from observed data increased the correlation between the mean spring discharge of the Harricana River and the MDD index from $r = 0.30$ to $r = 0.39$.

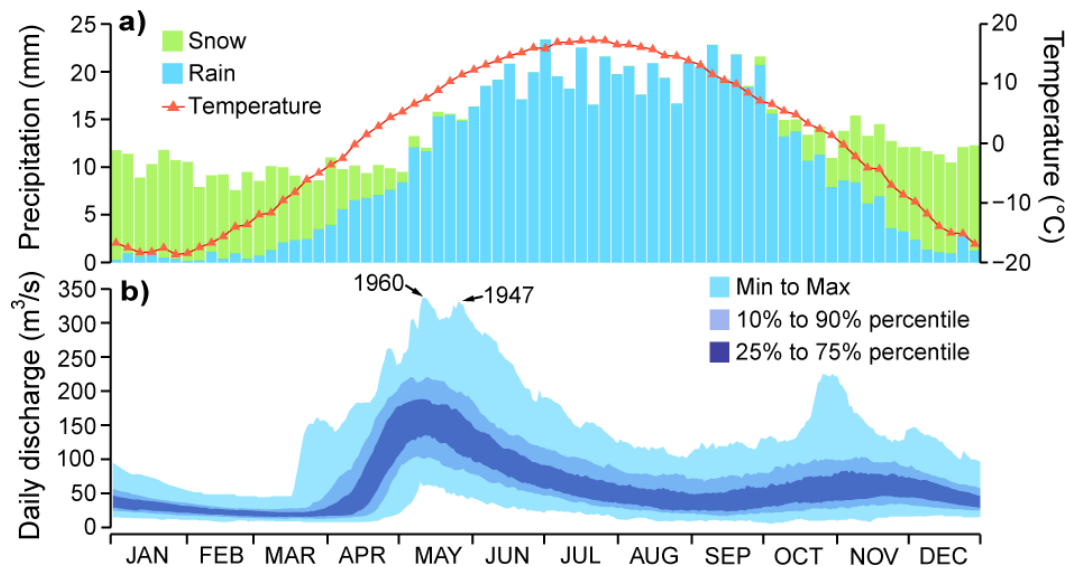


Figure 5.S1 Observed climate and discharge at Amos indicating the range of natural recorded variability. a) Mean 5-days average of temperature, rainfall, and snowfall from 1933 to 2000 for Amos meteorological station (7090120). b) Daily discharge of the Harricana River at Amos and from 1914 to 2021 (gage 04NA001-2). The two highest maximum spring discharge recorded were in 1960 ($337 \text{ m}^3/\text{s}$ on May 11 and 12) and in 1947 ($317 \text{ m}^3/\text{s}$ on May 26).

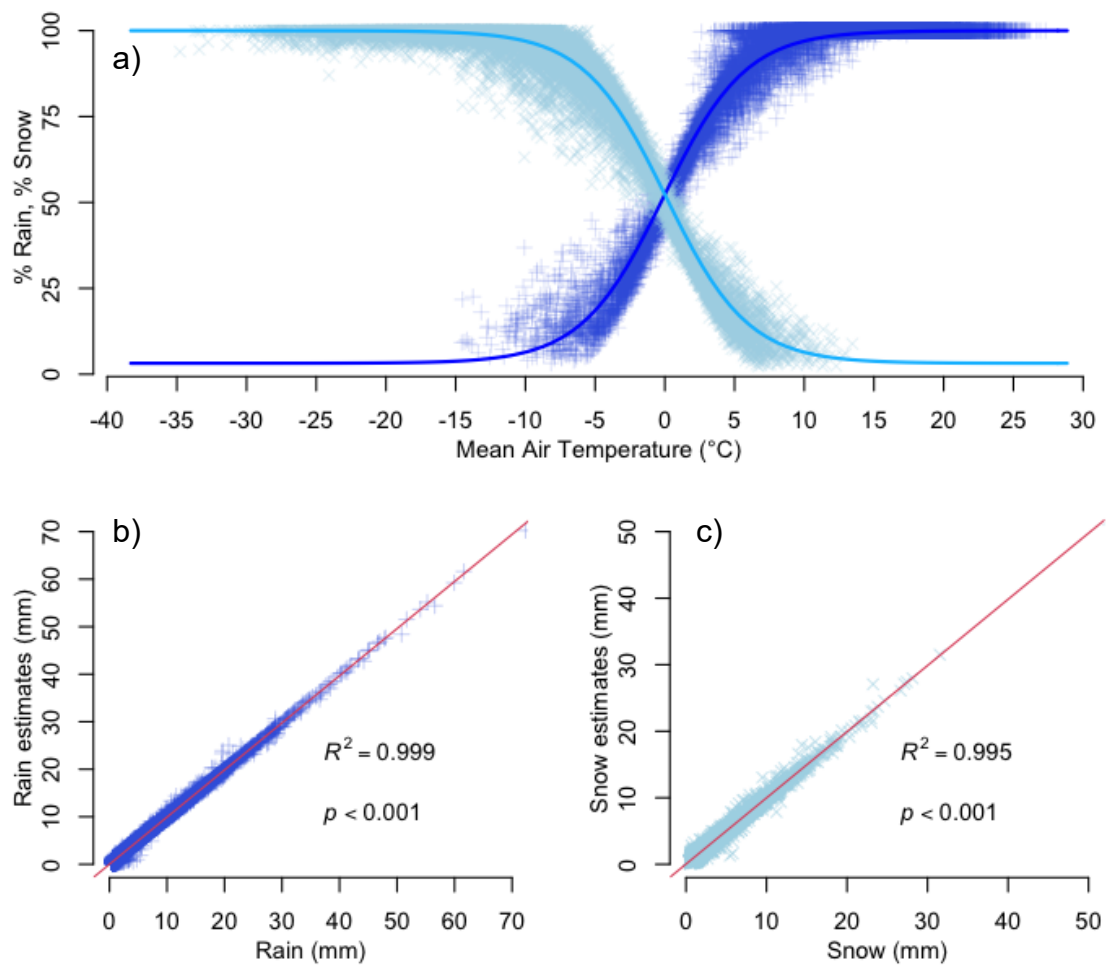


Figure 5.S2 Outputs from the logistic regression model calibrated on daily BioSIM data and applied to the CMIP5 data to produce estimates of rain and snow proportions of total precipitation as a function of mean air temperature. a) BioSIM daily snow (light blue) and rain (dark blue) daily values and their respective curvilinear fits. Model estimates compared to BioSIM interpolated values, respectively for b) rain ($n = 21,481$) and c) snow ($n = 16,079$).

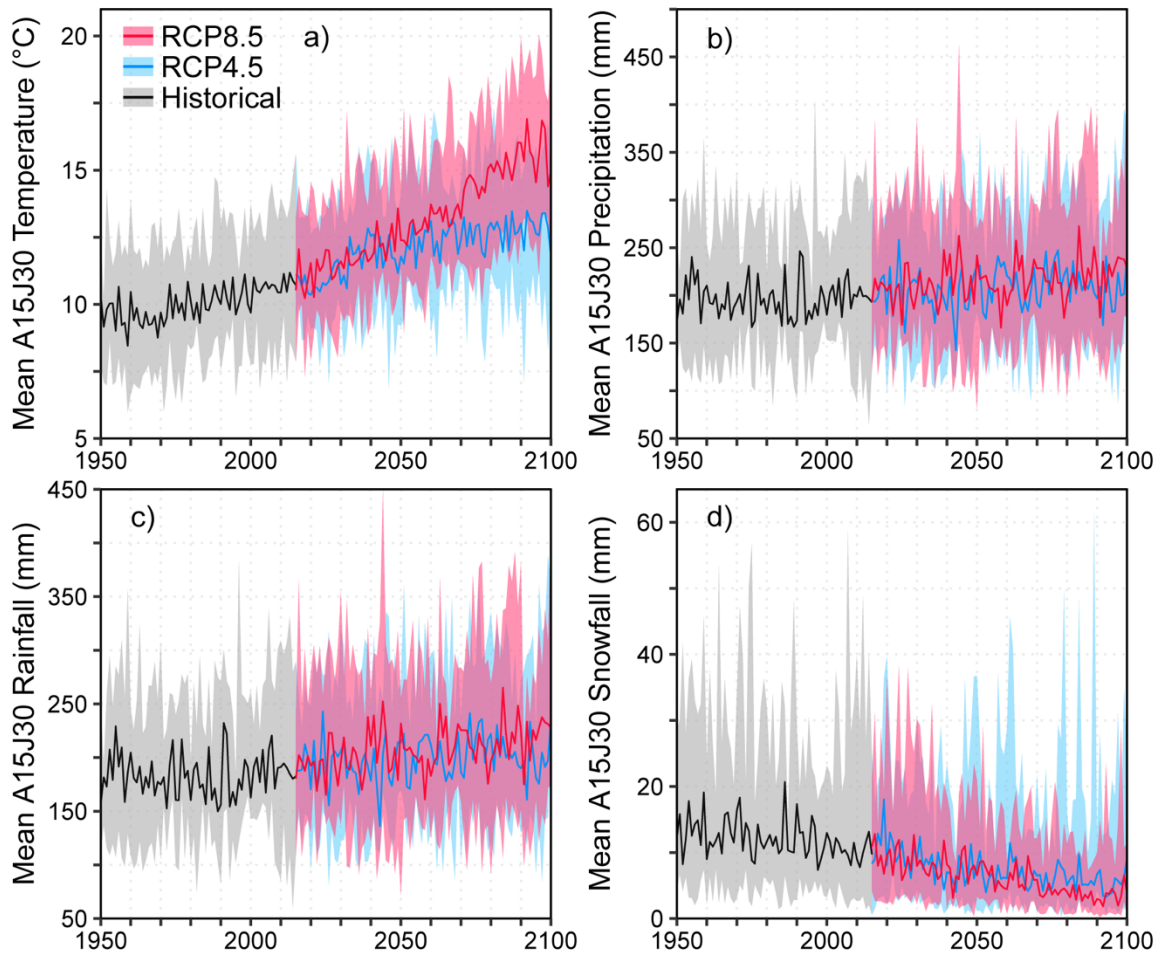


Figure 5.S3 April 15 to June 30 mean annual (a) temperature, (b) precipitation, (c) rainfall, and (d) snowfall averaged over the Upper Harricana River watershed for the period 1950–2100 and for the 10-GCM ensemble. Median values of historical (grey) and future projections under RCP4.5 (blue) and RCP8.5 (red) are presented with their minimum and maximums ranges (shades).

Table 5.S1 Annual climate index used as additional predictors to monthly and seasonal climate to develop machine learning model of the mean April 15 to June 30 discharge of the Harricana River. Each variable was calculated from 1900–2021 daily BioSIM climate series. Each variable calculated with SWE data are presented at the bottom and highlighted with a grey cell background.

Variable	Units	Description
CDD	°F	Cooling degree days, cumulative sum of daily temperature warmer than 65°F
DD0	days	Degree days above 0°C
ECD	days	Extreme cold days, daily minimum temperature inferior to –25°C, as in https://climatedata.ca/variable/
FDD	°C	Freezing degree days, sum of the departures of the mean daily temperature below 0°C, as in Assel, (1980)
FFF	julian day	First fall frost, first day in fall or late summer where daily minimum temperature is below 0°C, as in https://climatedata.ca/variable/
FSL	days	Frost-season length, duration between the first day with 0°C in autumn and the first day with 0°C in spring
FTC	days	Freeze-thaw cycles, daily maximum temperature higher than 0°C and daily Tmin inferior or equal to –1°C, as in https://climatedata.ca/variable/
HDD	°F	Heating degree days, cumulative sum of daily temperature colder than 65°F
IBU	julian day	Timing of lake ice-break up, the date when accumulated melting degree days reached 150 using a base of 32°F, adapted from Williams, (1971) (<i>c.f.</i> Suppl. Mat.)
LSF	julian day	Late spring frost, sometimes refer to as springtime warming, last day in spring or early summer where daily minimum temperature is below 0°C, as in https://climatedata.ca/variable/
ID	days	Ice days, number of days where maximum temperature is below 0°C, as in https://climatedata.ca/variable/
ISL	days	Ice season length, duration in days between the FFF and the LSF
% Rain	%	Mean percent precipitation as rain
HR10	days	Number of extreme single-day rainfall event of at least 10mm, adapted from Gleason et al., (2008)
Rainfall intensity	mm/day	Rainfall intensity
% Snow	%	Mean percent precipitation as snow
TAP	mm	Total Accumulated Precipitation, defined as the total daily snowfall accumulated for November and December, and the total daily precipitation accumulated from January to April, adapted from Romolo et al., (2006) (<i>c.f.</i> Suppl. Mat.)

Table 5.S1 (Suite)

Variable	Units	Description
MEL	days	Number melting events where $\Delta\text{SWE} < 0$ as in Barnhart et al., (2016) (see equation 1)
ROS	days	Number of rain-on-snow (ROS) events defined as "rainfall of at least 3 mm on a snowpack of at least 10 mm SWE and for which the sum of rainfall and snowmelt contains a minimum of 20% snowmelt", following criteria detailed in Freudiger et al. (2014), Musselman et al. (2018) and Li et al., (2019) to identify ROS days that have flood-generating potential. In this study, yearly ROS were calculated over a window spanning March 1 to June 30.
SMR	mm/day	Long-term average snowmelt rate from JAN to MAY as in Barnhart et al., (2016) (see their equation 1)
SMD	days	Snowmelt duration, duration of the snow ablation phase that extends from the day of maximum snow volume to the day of the last recorded positive SWE value, adapted from Dyer, (2008) (here, $\text{SMD} = \text{TMAXSWE} - \text{TMINSWE}$)
SSL	days	Snow season length, total number of days with at least 1mm of SWE for 5 consecutive days from previous winter to current spring
TMAXSWE	julian day	Timing of maximum snow water equivalent, estimate for the day of maximum snow volume before ablation phase, as in Dyer, (2008)
TMINSWE	julian day	Timing of minimum snow water equivalent, estimate for the last day with snow on the ground, adapted from Dyer, (2008)

CHAPITRE VI

CONCLUSION GÉNÉRALE

Dans l'est du Canada boréal, les crues printanières font partie intégrale du cycle hydrologique des rivières et constituent un risque naturel majeur. Les objectifs de cette thèse visaient à (1) reconstituer et étudier la variabilité historique des crues printanières par l'étude des cernes de crues, (2) reconstituer et étudier les mécanismes climatiques à l'origine du déclenchement des crues printanières historiques, et (3) projeter dans le futur les trajectoires prévisionnelles des crues printanières et de leurs facteurs climatiques dans l'est du Canada boréal. Ce dernier chapitre présente la contribution de ce travail à l'avancement des connaissances et les perspectives de recherches qui peuvent être envisagées pour la poursuite des travaux.

6.1 Variabilité printanière des débits moyens et des températures moyennes reconstituées depuis la fin du Petit Âge Glaciaire

L'ensemble des résultats obtenus démontre que la variabilité printanière des débits (chapitre I) et des températures (chapitre IV) au cours des 20^e et 21^e siècles s'est éloignée de la gamme de variabilité reconstituée pour la fin du Petit Âge Glaciaire, et ce de manière graduelle. De 1770 à 1870, la variabilité hydroclimatique régionale des débits moyens et des températures moyennes de printemps était caractérisée par des phases amples persistant plusieurs décennies. Les phases de printemps plus froids que la moyenne à long terme (1770–2021) semblent concorder avec des phases de débits printaniers de plus haute sévérité que la moyenne à long terme, et inversement. Durant cette période, la sévérité et la fréquence des hauts débits printaniers étaient les plus basses de la période 1770–2021. Après les années 1850–1870, qui marquent la transition du Petit Âge Glaciaire à l'époque contemporaine en Amérique du Nord (Matthews & Briffa, 2005), l'amplitude de ces phases a diminué vers des fluctuations décennales et ce jusqu'à 1930–1950. La fréquence et la sévérité des inondations printanières ont augmenté et restaient associées aux plus basses températures moyennes régionales reconstituées. La fréquence et la sévérité des hauts débits de la

période 1875–1890 (1876, 1880, 1885, 1888, 1890) contrastent notamment avec la période de faible activité des inondations printanières pendant la fin du Petit Âge Glaciaire (1770–1870) pendant laquelle seules trois années de hauts débits ont été reconstituées (1797, 1819, 1861). Après 1930–1950, la variabilité hydroclimatique des débits moyens et des températures moyennes de printemps a été caractérisée par une amplitude annuelle à interannuelle, et associée à une augmentation en fréquence et en sévérité, à la fois des printemps chauds et des hauts débits. Les plus hauts débits de la période 1771–2022 ont été 1947 et 1960. Toutefois, des débits de faible amplitude et survenant tôt au printemps ont dominé durant la période 1998–2012 avant les inondations printanières de 2013, 2014, 2017 et 2019 qui ont atteint une fréquence comparable aux années 1880.

Ces périodes de changements graduels (1870 et 1930–50) coïncident avec les périodes d’augmentations du niveau des lacs et des hauteurs et fréquences de cicatrices glacielles enregistrées dans la région du Lac Duparquet et du Québec subarctique (Tardif & Bergeron, 1997b; Bégin et al., 2000; Bégin, 2001; Lemay & Bégin, 2008; Boucher et al., 2011; Lemay & Bégin, 2012; Nicault et al., 2014; Nasri et al., 2020). Ces périodes de changements coïncident également avec une diminution de la fréquence et de la sévérité des sécheresses et incendies de forêts dans le centre du Québec et nord-est Ontario (Bergeron et al., 2001; Bergeron et Archambault, 1993; Drobyshev et al., 2017). Cohérents à large échelle spatiale ces changements hydroclimatiques semblent associés à une modification des circulations atmosphériques à plus large échelle et de leur contrôle sur la variabilité hydroclimatique interannuelle régionale.

6.2 Contrôles climatiques à large échelle et cohérence régionale des hauts débits moyens printaniers

L'ensemble des années de hauts débits printaniers reconstitués pour la rivière Harricana (chapitre I) a été observé dans les séries de cernes de crues échantillonnées dans les rivières naturelles, et dans une moindre mesure dans les rivières régulées, des bassins versants des Plaines de l'Abitibi (Mattagami, Abitibi, Harricana et Outaouais amont; chapitre II). Ces deux jeux de données ont été significativement associés à l'ensemble des débits instrumentaux disponibles pour les rivières naturelles à travers un territoire d'environ 70 000km², démontrant que l'historique régionale des inondations était commune entre ces rivières. Les plus hauts débits moyens printaniers du 20^e siècle dans la région des Plaines de l'Abitibi ont été générés par des hivers froids et neigeux, des printemps tardifs accompagnés de pluies intenses, et ce particulièrement depuis 1950. Les analyses de corrélations spatiales ont indiqué que ces associations seraient applicables à une large partie du centre-est nord canadien. Cependant, le réchauffement des températures moyennes printanières depuis environ 1940, l'absence d'inondations majeures entre 1996 et 2012, puis la dernière succession d'inondations majeures (2013, 2014, 2017, 2019) indiquent que les conditions climatiques à l'origine de leur déclenchement pourraient avoir changé. Les analyses de tendances hydroclimatiques (chapitre V) dans les données observées du bassin versant de la rivière Harricana ont démontré que depuis le début du 20^e siècle, le réchauffement des températures moyennes hivernales et printanières a réduit la proportion des précipitations nivales. Tout en augmentant les précipitations totales et particulièrement les pluies, ce changement a probablement limité le rôle de l'équivalent en eau de la neige dans la génération des débits moyens de printemps. Ce changement climatique centré sur 1950 pourrait aussi être une conséquence de l'augmentation de l'influence de l'indice de circulation atmosphérique à large échelle El-Niño oscillation australe (ENSO) constatée sur les débits de l'est du Canada (Nalley et al., 2012). Cet indice climatique

reflète des mécanismes de transport de masses d'air provenant de l'océan Pacifique-Sud. Les masses d'air chaud et humide des phases ENSO positives (El-Niño) étaient associées, dans l'est du Canada boréal, à des printemps hâtifs et de débits moyens printaniers de faibles amplitudes. Au contraire, des masses d'air froides et sèches des phases ENSO négatives (La-Niña) étaient plutôt corrélées à des dégels tardifs et à des débits moyens printaniers de plus haute amplitude.

6.3 Trajectoires hydroclimatiques prévisionnelles pour les débits moyens printaniers de la rivière Harricana

La variabilité des débits printaniers reconstitués fournit une nouvelle perspective historique (1771–2021) rare à l'échelle du Québec et nécessaire à l'évaluation des scénarios de changements hydroclimatiques probables. Huit modèles climatiques GCM sur 10 utilisés pour projeter le futur hydroclimatique de la rivière Harricana (chapitre V) suggèrent peu de changement dans la variabilité des débits moyens de printemps à l'horizon 2100 (par rapport à la variabilité observée pendant le 20^e siècle et la fin du Petit Âge Glaciaire). Les projections à l'horizon 2100 indiquent une nette diminution des couverts neigeux (–20 à –30% de chutes de neige sur l'année) compensée par une nette augmentation des pluies (+100 à +125mm annuel) principalement en automne, en hiver et au printemps. Les pluies intenses, qui présentent à l'échelle du Québec un potentiel à générer des inondations printanières, devraient augmenter avec l'augmentation la plus importante projetée sous un réchauffement plus prononcé (RCP8.5). L'augmentation projetée des cycles gel-dégel pourrait aussi contribuer à la formation de couches de glace dans les couverts neigeux. La modification de la fréquence et de l'intensité des précipitations et des dégels ne semble toutefois pas avoir d'effet sur l'évolution future des débits moyens printaniers. Le réchauffement des températures moyennes et l'intensification des pluies suggèrent aussi une débâcle printanière plus hâtive d'environ 15 à 25 jours en 2100.

Au contraire de ces projections, et toujours à l'échelle de l'ensemble multi-modèle 10-GCM utilisé (chapitre V), deux modèles climatiques projettent une augmentation de la sévérité, et dans une moindre mesure, de la fréquence des hauts débits moyens de printemps et selon des conditions climatiques comparables à celles ayant générées les inondations majeures historiques (hivers froids, neigeux, débâcle tardive et pluies intenses de printemps). Pour les deux modèles hydrologiques comparés et les deux scénarios climatiques envisagés, ce résultat semble surtout refléter l'incertitude qui existe à ce jour dans les représentations du climat planétaire futur et/ou dans les biais de l'utilisation de ces modèles à l'échelle de petits bassins versants comme celui de la rivière Harricana. Ces projections sont toutefois une contribution unique pour l'hydrologie régionale et viennent supporter les simulations effectuées, sur le même bassin versant et selon les mêmes modèles climatiques globaux, par la Direction de l'Expertise Hydrique du Québec. La perspective à long terme dans les débits (1771–2100) accentue aussi le fait que les crues majeures de la deuxième moitié du 20^e siècle sont sans équivalent depuis les derniers 250 ans. Bien que cela nécessite des recherches plus approfondies, ce phénomène pourrait avoir été une des premières conséquences du réchauffement climatique, lorsque l'augmentation des pluies printanières n'était pas encore compensée par la perte de couvert neigeux dans les débits.

6.4 Avantages, limites et perspectives de l'utilisation des cernes de crues comme indicateur des débits printaniers boréaux

En plus de contribuer à l'avancement des connaissances et de la compréhension du climat et des débits printaniers régionaux durant et après le Petit-Âge Glaciaire, les résultats de cette thèse constituent un apport théorique et appliqué important pour l'analyse des cernes de crues. Les analyses quantitatives (mesures anatomiques; chapitre I et II) et semi-quantitatives (classes visuelles F0, F1, F2; chapitre II et III) de cernes de crues ont démontré leur complémentarité et leur potentiel pour extraire de

l'information paléohydrologiques en milieu boréal à la fois en rivières naturelles et régulées par barrage, et ce, comparativement aux chronologies de largeurs de cernes annuels. Ces résultats appuient également l'utilisation des chronologies de nombres et de surface moyenne en coupe transversale des vaisseaux du bois initial pour reconstituer le signal d'inondations printanières, comme l'avait déjà suggéré Tardif et al., (2010) et Kames et al., (2016). En rivières naturelles, les analyses anatomiques ont permis de capturer un plus large spectre d'information hydrologique que l'étude des fréquences relatives de cernes de crues, mais l'étude des fréquences relatives a permis d'inclure un plus grand nombre d'échantillons sur une plus grande surface et a permis d'étudier la cohérence spatiale des inondations printanières régionales.

En rivières régulées, les fréquences relatives de cernes de crues ont aussi permis de documenter l'historique régional des inondations printanières avant l'installation des barrages, et de reconstituer les inondations printanières majeures après la création des barrages (chapitre II et III). L'étude des cernes de crues en contextes hydrologiques régulées (chapitre III) démontre qu'il est possible d'extraire de l'information encore plus largement, en adaptant la stratégie d'échantillonnage pour tenir compte des modifications hydrologiques apportées par le barrage. L'échantillonnage d'arbres riverains dans différents contextes hydrologiques (distance au barrage, distance à la berge) a permis de distinguer les crues majeures ayant inondé la totalité de la plaine alluviale des crues de plus petites amplitudes pouvant être le reflet de la gestion des niveaux d'eau par le barrage. Cependant, les résultats de Tardif et al. (2021a) précisent que des frênes noirs proches les uns des autres peuvent enregistrer des cernes de crues d'intensité différente (F1 et F2) démontrant que la microtopographie peut influencer l'exposition des arbres aux inondations. La hauteur de prise d'échantillon dendrochronologique semble aussi influencer la distinction des cernes de crues (intensité ou présence) puisqu'ils ne se forment que sous le niveau d'eau (St. George et al., 2002; St. George et Nielsen, 2002; Copini et al., 2016; Tardif et al., 2021a). Des

études supplémentaires sont nécessaires pour comprendre comment les variations d'intensité dans la verticalité de la tige (décroissance/disparition du signal au-dessus du niveau d'eau; St. George et al., 2002; St. George et Nielsen, 2002) affectent notre capacité à extraire de l'information paléohydrologique des fréquences relatives de cernes de crues à l'échelle de l'arbre, et à plus grande échelle.

Les comparaisons entre frênaies riveraines inondées et frênaies contrôles non inondées (chapitre II) confortent les résultats des études précédentes (Kames, 2009; Kames 2016). La signature anatomique des cernes de crues dans les frênes noirs des plaines inondables n'est pas confondable avec celles induites par d'autres facteurs paléoclimatiques que les inondations. Les observations de Yanosky (1983, 1984) suggéraient par exemple que les modifications anatomiques observées pendant les crues pouvaient être liée à la perte de canopée. Dans cette perspective, une défoliation prononcée, par attaque d'insecte, sécheresse, ou par un feu, qui peuvent aussi réduire la taille des vaisseaux du bois initial (*e.g.*, Kames 2009; Brauning et al., 2016), aurait donc pu conduire à la formation d'irrégularités anatomiques semblables à celles des cernes de crues. Tardif et al., (2021ab) démontrent également que les cernes de crues disparaissaient progressivement des plaines inondables riveraines aux peuplements de plus hautes terrasses non inondées. Le petit nombre de cernes de crues de faible intensité trouvée dans les peuplements contrôles non inondés au chapitre II semblent donc plus refléter les disparités d'identification de cernes F1 entre les deux observateurs, ceux-ci étant plus difficiles à déterminer que les cernes F2 (Tardif et al., 2021a).

Enfin, les résultats du chapitre I précisent que les chronologies de cernes de crues sont légèrement moins efficaces pour reconstituer les inondations printanières de faible intensité survenant tôt au printemps, c'est-à-dire, lorsque l'initiation de la crue printanière survient avant le début de la période de formation des vaisseaux du bois

initial (Copini et al., 2016). Dans l'hypothèse où les changements climatiques induisent des crues printanières plus hâtives et associées à des gel-dégel et des pluies plus fréquents et intenses, il reste à déterminer si l'efficacité des feuillus à zone poreuse à enregistrer les inondations printanières pourrait être influencée par ces changements (changements de phasage entre la phénologie des crues et la phénologie des arbres). Des suivis microcarottes en peuplements inondés, et en conditions expérimentales pourraient permettre de suivre et comparer la phénologie de formation des vaisseaux du bois initial en fonction des conditions climatiques et d'inondations printanières actuelles et futures envisagées.

6.5 Perspectives méthodologiques pour la caractérisation et la mesure des cernes de crues

Ces travaux de recherche ont également amélioré les techniques de prétraitement des images hautes résolutions pour la mesure continue d'éléments de vaisseaux du bois initial par rapport aux travaux précédents. L'étude des cernes de crues repose historiquement sur des indices de présence visuelle (St. George and Nielsen, 2003; Wertz et al., 2013; Therrel et Bialecki, 2015; Meko et Therrel, 2020), des mesures de surface moyenne des éléments de vaisseaux en coupe transversale sur un nombre restreint d'échantillons (St. George et al., 2002; Tardif et al., 2010; Kames et al., 2016; Tardif et al., 2021b), ou plus récemment sur des mesures de largeur de la première bande de vaisseaux dans le bois initial (Meko and Therrel, 2020). Il est désormais possible de mesurer plus rapidement un nombre plus important d'échantillons avec les procédés de préparation des images (réduction du bruit), d'automatisation de la délimitation des vaisseaux qui facilitent leur détection et leur mesure avec le logiciel WinCell (Fig. 3.2). Des améliorations semblables aux nôtres (Canny Edge; chapitre I) avaient déjà été proposées par Jevšenak et Levanič (2014), et par Land et al., 2017 avec CATS (Computer-Aided Tree-Ring Analysis Software) bien que le logiciel ait montré

des difficultés à délimiter les vaisseaux des frênes noirs dans nos analyses préliminaires (non présentés). L'expérimentation de méthodes émergentes comme la macrophotographie automatisée (Griffin et al., 2021), la tomographie à rayons X (*i.e.* De Mil et al., 2016; Buranská et al., 2021) pourrait aussi permettre d'accélérer ces procédures dans le futur (García-González et al., 2016; von Arx et al., 2016) et aider à développer un réseau de mesures anatomiques cohérent à grande échelle, comme il existe déjà pour les mesures de largeurs de cernes, de densité du bois, isotopes, etc. (*i.e.* International Tree-Ring Data Bank).

6.6 Perspectives de recherche et mot final

Pour poursuivre le développement des cernes de crues comme indicateur des crues printanières, il serait aussi nécessaire de comparer les approches existantes entre-elles (microtome / analyses d'image / rayons-X) et les différentes variables (notamment diamètre et nombre des vaisseaux, largeur de la première bande de vaisseaux proposée par Meko and Therrell, 2020; et variables proposées par Scholz et al., 2013) afin de statuer sur leur sensibilité respective aux inondations printanières et facteurs hydroclimatiques, mais aussi sur l'efficacité des analyses (temps, coûts, etc). Par ailleurs, l'étude des cernes de crues dans d'autres essences de feuillus à zone poreuse (*Fraxinus pensylvanica*, *Ulmus americana*, *Quercus* spp., *Acer* spp.) ou de manière plus limitée dans les feuillus à pores diffus (Dickson, 2020; Tardif et al., 2021a) permettrait d'élargir le champ d'application de la méthode développée dans cette thèse. On peut imaginer échantillonner un petit nombre d'arbres les plus anciens par bassin versant sur les rivières naturelles, et sur les rivières régulées, pour dresser un portrait global de l'historique des inondations dans le nord du Québec par exemple.

Cette thèse a apporté une base pour la compréhension à plus large échelle des conditions climatiques qui engendrent des hauts débits printaniers dans l'est du Canada

boréal. Ces travaux pourraient être poursuivis par une analyse plus détaillée des associations entre les débits et les indices de circulations climatiques à grandes échelles. Ces associations sont complexes spatialement et temporellement (Bonsal et al., 2008; Bonsal & Shabbar, 2011) et nécessitent souvent des décompositions temporelles et fréquentielles plus avancées que celles entreprises au chapitre I (*cf.*, Nalley et al., 2012). Cela améliorerait aussi nos capacités de prédiction du risque inondation puisque la réponse hydrologique des rivières dans l'est du Canada boréal est généralement décalée de plusieurs mois à plusieurs années par rapport aux fluctuations des indices climatiques à large échelle (Nalley et al., 2012; voir synthèse par Bonsal et Shabbar, 2008 sur les débits d'étiages). Dans un cadre plus appliqué, la reconstitution du chapitre I pourrait aussi participer à réduire l'incertitude associée aux calculs des débits de grandes fréquences de retour utilisés notamment, pour dimensionner les ouvrages hydrauliques (barrages, protections contre les crues, etc).

La reconstitution des températures printanières du chapitre IV a permis d'utiliser des méthodes jusqu'à ce jour peu utilisées en dendrochronologie (Girardin et al., 2016; Girardin et al., 2021). Le modèle de croissance GNE (Girardin et al., 2012) et l'utilisation de modèle GAMM, ont permis de réduire le bruit associé à la dynamique de recrutement post-feu dans les chronologies de largeurs de cernes saisonniers, de conserver un maximum de basses fréquences climatiques, et de prendre en compte des relations climat-croissance non linéaires (Suppl. Mat. du chapitre IV). L'ensemble a permis la reconstitution des températures moyennes de printemps en milieu boréal, ce qui reste encore peu accompli en dendroclimatologie (Guiot, 1987). Il serait intéressant de continuer ce travail en remesurant les chronologies existantes de *P. banksiana* pour la région (notamment celles de Hofgaard et al., 1999 datée à 1700 CE) pour consolider la partie la plus ancienne de la reconstitution, car l'incertitude était plus élevée à cause de la réduction du nombre d'échantillons. Une approche multi-indicateurs pourrait aussi être considérée en incluant des mesures d'intensité du bleu ('blue intensity');

Wilson et al., 2014) ou d'isotopes (Gennaretti et al., 2014, 2017) pour tenter de capturer un spectre plus large de variance dans les données observées de températures printanières et améliorer la force du signal climatique reconstruit (23% à 54% de variance capturée dans les observations). Le chapitre V présente également une méthode empirique consistante avec les résultats des simulations de modèles hydrologiques mécanistiques physiques. Les modèles mécanistiques fournissent en général projections hydrologiques détaillées et quotidiennes, uniquement après une longue phase de calibration des équations physiques utilisées pour générer le débit. Le modèle du chapitre V propose une alternative consistante, à partir de données publiques, pour calculer des projections des débits printaniers à long terme et supporter les prises de décisions dans l'aménagement futur du territoire et de sa gestion des risques inondations.

Enfin, l'ensemble de ce travail de recherche démontre le potentiel d'utiliser les cernes de crues pour les reconstitutions paléohydrologiques des débits boréaux printaniers à large échelle, et l'importance de continuer à développer des indicateurs du climat printanier en milieu boréal. Bien qu'il reste plusieurs améliorations à apporter, notamment aux projections hydroclimatiques, avant de pouvoir évaluer avec un niveau de confiance plus élevée l'effet des changements climatiques sur le futur des inondations printanières régionales, l'ensemble de ce travail apporte une nouvelle méthodologie et une nouvelle base de réflexion pour mettre en perspective les changements hydroclimatiques contemporains et futurs des inondations printanières à l'est du Canada boréal. Ces résultats réaffirment la nécessité de continuer à étudier les mécanismes climatiques à l'origine du déclenchement des inondations printanières pour mieux envisager les adaptations qui seront nécessaires à notre société pour évaluer et limiter les risques et effets du changement climatique.

RÉFÉRENCES

A

- Adam, J. C., Hamlet, A. F., & Lettenmaier, D. P. (2009). Implications of global climate change for snowmelt hydrology in the twenty-first century. *Hydrological Processes: An International Journal*, 23(7), 962-972.
- Adamowski, J., Fung Chan, H., Prasher, S. O., Ozga-Zielinski, B., & Sliusarieva, A. (2012). Comparison of multiple linear and nonlinear regression, autoregressive integrated moving average, artificial neural network, and wavelet artificial neural network methods for urban water demand forecasting in Montreal, Canada. *Water Resources Research*, 48(1), W01528.
- Agafonov, L. I., Meko, D. M., & Panyushkina, I. P. (2016). Reconstruction of Ob River, Russia, discharge from ring widths of floodplain trees. *Journal of Hydrology*, 543, 198-207.
- Anchukaitis, K. J., D'Arrigo, R. D., Andreu-Hayles, L., Frank, D., Verstege, A., Curtis, A., Buckley, B. M., Jacoby, G. C., & Cook, E. R. (2013). Tree-ring-reconstructed summer temperatures from northwestern North America during the last nine centuries. *Journal of Climate*, 26(10), 3001-3012.
- Angers, V. A., Drapeau, P., & Bergeron, Y. (2010). Snag degradation pathways of four North American boreal tree species. *Forest Ecology and Management*, 259(3), 246-256.
- Ashmore, P., & Church, M. (2001). "The impact of climate change on rivers and river processes in Canada". Geological Survey of Canada, Bulletin 555. Natural Resources Canada, 69p.
- Assel, R. A. (1980). Maximum freezing degree-days as a winter severity index for the Great Lakes, 1897-1977. *Monthly Weather Review*, 108(9), 1440-1445.
- Astrade, L., & Bégin, Y. (1997). Tree-ring response of *Populus tremula* L. and *Quercus robur* L. to recent spring floods of the Saône River, France. *ÉcoScience*, 4(2), 232-239.
- Aygün, O., Kinnard, C., & Campeau, S. (2019). Impacts of climate change on the hydrology of northern midlatitude cold regions. *Progress in Physical Geography: Earth and Environment*, 44(3), 338-375.

B

- Baena-Escudero, R., Guerrero-Amador, I.C., Rinaldi, M., & González-Sayago, A. (2021). Hydrological and geomorphic effects upstream of the Cantillana Dam along the Guadalquivir River (southern Spain). *Geomorphology*, 388, 107786.

- Baker, V. R. (2008). Paleoflood hydrology: Origin, progress, prospects. *Geomorphology*, 101(1-2), 1-13.
- Ballesteros-Cánovas, J. A., Stoffel, M., St. George, S., & Hirschboeck, K. (2015). A review of flood records from tree rings. *Progress in Physical Geography*, 39(6), 794-816.
- Ballesteros-Cánovas, J. A., Stoffel, M., Benito, G., Rohrer, M., Barriopedro, D., García-Herrera, R., & Brönnimann, S. (2019). On the extraordinary winter flood episode over the North Atlantic Basin in 1936. *Annals of the New York Academy of Sciences*, 1436, 206-216.
- Ballesteros-Cánovas, J. A., Bombino, G., D'Agostino, D., Denisi, P., Labate, A., Stoffel, M., Demetrio, A. Z., & Zimbone, S. M. (2020). Tree-ring based, regional-scale reconstruction of flash floods in Mediterranean mountain torrents. *Catena*, 189, 104481.
- Barbarossa, V., Huijbregts, M. A., Hendriks, A. J., Beusen, A. H., Clavreul, J., King, H., & Schipper, A. M. (2017). Developing and testing a global-scale regression model to quantify mean annual streamflow. *Journal of Hydrology*, 544, 479-487.
- Barber, V. A., Juday, G. P., Finney, B. P., & Wilmking, M. (2004). Reconstruction of summer temperatures in interior Alaska from tree-ring proxies: evidence for changing synoptic climate regimes. *Climatic Change*, 63(1), 91-120.
- Barnhart, T. B., Molotch, N. P., Livneh, B., Harpold, A. A., Knowles, J. F., & Schneider, D. (2016). Snowmelt rate dictates streamflow. *Geophysical Research Letters*, 43(15), 8006-8016.
- Bégin, Y. (2000). Ice-push disturbances in high-boreal and subarctic lakeshore ecosystems since AD 1830, northern Québec, Canada. *The Holocene*, 10(2), 179-189.
- Bégin, Y. (2001). Tree-ring dating of extreme lake levels at the subarctic-boreal interface. *Quaternary Research*, 55(2), 133-139.
- Bergeron, Y., & Archambault, S. (1993). Decreasing frequency of forest fires in the southern boreal zone of Quebec and its relation to global warming since the end of the 'Little Ice Age'. *The Holocene*, 3(3), 255-259.
- Bergeron, Y., & Dansereau, P. R. (1993). Predicting the composition of Canadian southern boreal forest in different fire cycles. *Journal of Vegetation Science*, 4(6), 827-832.
- Bergeron, Y. (2000). Species and stand dynamics in the mixed woods of Quebec's southern boreal forest. *Ecology*, 81(6), 1500-1516.
- Bergeron, Y., Gauthier, S., Kafka, V., Lefort, P., & Lesieur, D. (2001). Natural fire frequency for the eastern Canadian boreal forest: consequences for sustainable forestry. *Canadian Journal of Forest Research*, 31(3), 384-391.
- Berghuijs, W. R., Aalbers, E. E., Larsen, J. R., Trancoso, R., & Woods, R. A. (2017). Recent changes in extreme floods across multiple continents. *Environmental Research Letters*, 12(11), 114035.

- Bilefsky, D., & Austen, I. (2019). "Eastern Canada grapples with extreme flooding". The New-York Times, 19 April. <https://www.nytimes.com/2019/04/29/world/canada/canada-flooding.html> [Oct 01, 2022]
- Biondi, F., & Meko, D. M. (2019). Long-term hydroclimatic patterns in the Truckee-Carson basin of the eastern Sierra Nevada, USA. *Water Resources Research*, 55(7), 5559-5574.
- Boileau, G. (1999). L'annexion du territoire de l'Abitibi au Québec. *Histoire Québec*, 4 (2 bis), 30-33.
- Bonsal, B. R., Shabbar, A., & Higuchi, K. (2001). Impacts of low frequency variability modes on Canadian winter temperature. *International Journal of Climatology*, 21, 95-108.
- Bonsal, B. R., Prowse, T. D., Duguay, C. R., & Lacroix, M. P. (2006). Impacts of large-scale teleconnections on freshwater-ice break/freezing-up dates over Canada. *Journal of Hydrology*, 330, 340-353.
- Bonsal, B., & Shabbar, A. (2008). Impacts of large-scale circulation variability on low streamflows over Canada: a review. *Canadian Water Resources Journal*, 33(2), 137-154.
- Bonsal, B., & Shabbar, A. (2011). "Large-scale climate oscillations influencing Canada, 1900-2008". Canadian biodiversity: ecosystem status and trends 2010 - Technical thematic report No. 4. Ottawa, Ontario, Environment Canada. 20p.
- Boucher, É., Bégin, Y., & Arseneault, D. (2010). *Dendrohydrologie en milieu boréal*. Chapter 20 in Payette, S. & Filion, L. (Eds.) *Dendroécologie – Principes, Méthodes et Applications*, Presses de l'Université Laval, Québec, Québec. 573-592.
- Boucher, E., Ouarda, T. B. M. J., Bégin, Y., & Nicault, A. (2011). Spring flood reconstruction from continuous and discrete tree ring series. *Water Resources Research*, 47(7): W07516.
- Boucher, M.-A., & Leconte, R. (2013). Changements climatiques et production hydroélectrique canadienne: où en sommes-nous? *Canadian Water Resources Journal*, 38(3), 196-209.
- Boulanger, Y., Pascual, J., Bouchard, M., D'Orangeville, L., Périé, C., & Girardin, M. P. (2022). Multi-model projections of tree species performance in Quebec, Canada under future climate change. *Global Change Biology*, 28(5), 1884-1902.
- Boyer, C., Chaumont, D., Chartier, I., & Roy, A. G. (2010). Impact of climate change on the hydrology of St. Lawrence tributaries. *Journal of Hydrology*, 384(1-2), 65-83.
- Bräuning, A., De Ridder, M., Zafirov, N., García-González, I., Dimitrov, D. P., & Gärtner, H. (2016). Tree-ring features: indicators of extreme event impacts. *IAWA Journal*, 37(2), 206-231.
- Briffa, K. R., Jones, P. D., Pilcher, J. R., & Hughes, M. K. (1988). Reconstructing summer temperatures in northern Fennoscandia back to AD 1700 using tree-ring data from Scots pine. *Arctic & Alpine Research*, 20(4), 385-394.

- Briffa, K. R., Jones, P. D., & Schweingruber, F. H. (1994). Summer temperatures across northern North America: Regional reconstructions from 1760 using tree-ring densities. *Journal of Geophysical Research: Atmospheres*, 99(D12), 25835-25844.
- Briffa, K. R., Osborn, T. J., Schweingruber, F. H., Harris, I. C., Jones, P. D., Shiyatov, S. G., & Vaganov, E. A. (2001). Low-frequency temperature variations from a northern tree ring density network. *Journal of Geophysical Research: Atmospheres*, 106(D3), 2929-2941.
- Brigode, P., Brissette, F., Nicault, A., Perreault, L., Kuentz, A., Mathevet, T., & Gailhard, J. (2016). Streamflow variability over the 1881-2011 period in northern Québec: comparison of hydrological reconstructions based on tree rings and geopotential height field reanalysis. *Climate of the Past*, 12(9), 1785-1804.
- Brimley, B., Cantin, J.-F., Harvey, D., Kowalchuk, M., Marsh, P., Ouarda, T. B. M. J., Phinney, B., Pilon, B., Renouf, M., Tassone, B., Wedel, R., & Yuzik, T.R. (1999). "Establishment of the Reference Hydrometric Basin Network (RHBN) for Canada". Environment Canada Research Report, Ontario, Canada, 41 p.
- Brown, R. D., (2000). Northern Hemisphere snow cover variability and change, 1915-1997. *Journal of Climate*, 13, 2339-2355.
- Brown, R. D., Brasnett, B., & Robinson, D. (2003). Gridded North American monthly snow depth and snow water equivalent for GCM evaluation. *Atmosphere-Ocean*, 41(1), 1-14.
- Brown, R. D. (2010). Analysis of snow cover variability and change in Québec, 1948-2005. *Hydrological Processes*, 24(14), 1929-1954.
- Bunn, A. G. (2008). A dendrochronology program library in R (dplR). *Dendrochronologia*, 26(2), 115-124.
- Buranská, E., Rantuch, P., Buranský, I., & Kucmanová, A. (2021). Application of industrial computer tomography to determine wood porosity. *Vedecké Práce Materiálovotechnologickej Fakulty Slovenskej Technickej Univerzity v Bratislave so Sídrom v Trnave*, 29(49), 15-23.
- Burn, D. H., & Elnur, M. A. H. (2002). Detection of hydrologic trends and variability. *Journal of Hydrology*, 255(1-4), 107-122.
- Burn, D. H., Sharif, M., & Zhang, K. (2010). Detection of trends in hydrological extremes for Canadian watersheds. *Hydrological Processes*, 24(13), 1781-1790.
- Burn, D. H., & Whitfield, P. H. (2016). Changes in floods and flood regimes in Canada. *Canadian Water Resources Journal*, 41(1-2), 139-150.
- Burn, D. H., & Whitfield, P. H. (2017). Changes in cold region flood regimes inferred from long-record reference gauging stations. *Water Resources Research*, 53(4), 2643-2658.
- Burn, D. H., Whitfield, P. H., & Sharif, M. (2016). Identification of changes in floods and flood regimes in Canada using a peak over threshold approach. *Hydrological Processes*, 30(18), 3303-3314.

- Burn, D. H., & Whitfield, P. H. (2018). Changes in flood events inferred from centennial length streamflow data records. *Advances in Water Resources*, 121, 333-349.
- Burton, I. (2015). "Floods in Canada". The Canadian Encyclopedia, Historica Canada, Toronto, Ontario, Canada. <https://www.thecanadianencyclopedia.ca/en/article/floods-and-flood-control> [Oct 01, 2022]
- Bush, E., & Lemmen, D. S. (Eds.) (2019). "Canada's Changing Climate Report". Government of Canada, Ottawa, Ontario, Canada. 444p.
- Buttle, J. M., Allen, D. M., Caissie, D., Davison, B., Hayashi, M., Peters, D. L., Pomeroy, J. W., Simonovic, S., St-Hilaire, A., & Whitfield, P. H. (2016). Flood processes in Canada: Regional and special aspects. *Canadian Water Resources Journal*, 41(1-2), 7-30.

| C

- Cai, W., Wang, G., Santoso, A., McPhaden, M. J., Wu, L., Jin, F. F., Timmermann, A., Collins, M., Vecchi, G., Lengaigne, M., England, M. H., Dommenges, D., Takahashi, K., & Guilyardi, E. (2015). Increased frequency of extreme La Niña events under greenhouse warming. *Nature Climate Change*, 5(2), 132-137.
- Camarero, J. J., Collado, E., Martínez-de-Aragón, J., De-Miguel, S., Büntgen, U., Martínez-Peña, F., Martín-Pinto, P., Romppanen, T., Salo, K., Oria-de-Rueda, J. A., & Bonet, J. A. (2021). Associations between climate and earlywood and latewood width in boreal and Mediterranean Scots pine forests. *Trees*, 35(1), 155-169.
- Cannon, A. J., Sobie, S. R., & Murdock, T. Q. (2015). Bias correction of GCM precipitation by quantile mapping: how well do methods preserve changes in quantiles and extremes? *Journal of Climate*, 28(17), 6938-6959.
- Canny, J. (1986). A computational approach to edge detection. *IEEE Transactions on Pattern Analysis and Machine Intelligence*, PAMI-8(6), 679-698.
- Canty, A., & Ripley, B. (2021). "Boot: Functions and datasets for bootstrapping from the book "Bootstrap methods and their application" by A.C. Davison and D.V. Hinkley (1997, CUP)". R Package version 1.3-28
- Capesius, J. P., & Stephens, V. C. (2009). "Regional regression equations for estimation of natural streamflow statistics in Colorado (2009-5136)". US Department of the Interior, US Geological Survey.
- Castaneda-Gonzalez, M., Poulin, A., Romero-Lopez, R., Arsenault, R., Brissette, F., & Turcotte, R. (2019). Sensitivity of seasonal flood simulations to regional climate model spatial resolution. *Climate Dynamics*, 53, 4337-4354.
- Cayford, J. H., & McRae, D. J. (1983). "The ecological role of fire in jack pine forests". In R.W. Wein & D.A. MacLean (Eds.), The role of fire in northern circumpolar ecosystems, Scientific Committee on Problems of the Environment (SCOPE), 18(10), 183-199. John Wiley and Sons, New York.

- CEHQ - Centre d'Expertise Hydrique du Québec (2019). “*Répertoire des barrages*”. Ministère de l'Environnement et de la Lutte contre les Changements climatiques. Gouvernement du Québec, Québec, Canada. https://www.cehq.gouv.qc.ca/depot/Barrages/bd/repertoire_des_barrages.xls [Oct 01, 2022]
- Charron, I. (2016). “*A Guidebook on Climate Scenarios: Using Climate Information to Guide Adaptation Research and Decisions*”, 2016 Edition. Ouranos, 94p.
- Chaste, E., Girardin, M. P., Kaplan, J. O., Bergeron, Y., & Hély, C. (2019). Increases in heat-induced tree mortality could drive reductions of biomass resources in Canada's managed boreal forest. *Landscape Ecology*, 34(2), 403-426.
- Chen, J., Brissette, F. P., & Leconte, R. (2011). Uncertainty of downscaling method in quantifying the impact of climate change on hydrology. *Journal of Hydrology*, 401(3-4), 190-202.
- Chen, Y., & She, Y. (2020). Long-term variations of river ice breakup timing across Canada and its response to climate change. *Cold Regions Science and Technology*, 176, 103091.
- Cherry, J. E., Knapp, C., Trainor, S., Ray, A. J., Tedesche, M., & Walker, S. (2017). Planning for climate change impacts on hydropower in the Far North. *Hydrology and Earth System Sciences*, 21(1), 133-151.
- Clavet-Gaumont, J., Sushama, L., Khaliq, M. N., Huziy, O., & Roy, R. (2013a). Canadian RCM projected changes to high flows for Québec watersheds using regional frequency analysis. *International Journal of Climatology*, 33(14), 2940-2955.
- Clavet-Gaumont, J., Thiémonge, N., Merleau, J., Perreault, L., & Roy, R. (2013b, April). “*Climate change impact on spring flood volume in northeastern Canada watersheds using a climate ensemble*”. In EGU General Assembly Conference Abstracts (EGU2013-2082).
- Clavet-Gaumont, J., Huard, D., Frigon, A., Koenig, K., Slota, P., Rousseau, A., Klein, I., Thiémonge, N., Houdré, F., Perdikaris, J., Turcotte, R., Lafleur, J., & Larouche, B. (2017). Probable maximum flood in a changing climate: An overview for Canadian basins. *Journal of Hydrology: Regional Studies*, 13(July), 11-25.
- Coble, A. P., & Kolb, T. E. (2012). Riparian tree growth response to drought and altered streamflow along the Dolores River, Colorado. *Western Journal of Applied Forestry*, 27(4), 205-211.
- Cohen, J., Ye, H., & Jones, J. (2015). Trends and variability in rain-on-snow events. *Geophysical Research Letters*, 42(17), 7115-7122.
- Cook, E. R., & Kairiukstis, L. A. (1990). “*Methods of Dendrochronology - Applications in the Environmental Sciences*”. International Institute for Applied System Analysis. Dordrecht, Netherlands: Springer Netherlands. 351p.
- Cook, E.R., & Peters, K. (1997). Calculating unbiased tree-ring indices for the study of climatic and environmental change. *The Holocene*, 7(3), 361-370.

- Cook, E. R., Meko, D. M., Stahle, D. W., & Cleaveland, M. K. (1999). Drought reconstructions for the continental United States. *Journal of Climate*, 12(4), 1145-1162.
- Cook, E. R., Krusic, P. J., & Jones, P. D. (2003). Dendroclimatic signals in long tree-ring chronologies from the Himalayas of Nepal. *International Journal of Climatology*, 23(7), 707-732.
- Copini, P., Den Ouden, J., Robert, E. M. R., Tardif, J. C., Loesberg, W. A., Goudzwaard, L., & Sass-Klaassen, U. (2016). Flood-ring formation and root development in response to experimental flooding of young *Quercus robur* trees. *Frontiers in Plant Science*, 7(June), 1-14.
- Crochemore, L., Ramos, M. H., & Pappenberger, F. (2016). Bias correcting precipitation forecasts to improve the skill of seasonal streamflow forecasts. *Hydrology and Earth System Sciences*, 20(9), 3601-3618.
- Cunderlik, J. M., & Simonovic, S. P. (2005). Hydrological extremes in a southwestern Ontario river basin under future climate conditions. *Hydrological Sciences Journal*, 50(4), 631-654.
- Cunderlik, J. M., & Ouarda, T. B. (2009). Trends in the timing and magnitude of floods in Canada. *Journal of Hydrology*, 375(3-4), 471-480.

D

- Dansereau, P. R., & Bergeron, Y. (1993). Fire history in the southern boreal forest of northwestern Quebec. *Canadian Journal of Forest Research*, 23(1), 25-32.
- Daubois, V., Roy, M., Veillette, J. J., & Ménard, M. (2015). The drainage of Lake Ojibway in glaciolacustrine sediments of northern Ontario and Quebec, Canada. *Boreas*, 44(2), 305-318.
- Davi, N. K., Jacoby, G.C., & Wiles, G. C. (2003). Boreal temperature variability inferred from maximum latewood density and tree-ring width data, Wrangell Mountain region, Alaska. *Quaternary Research*, 60(3), 252-262.
- Davies., R. (2017). "Canada - Over 4,400 homes flooded in Quebec". Flood List, 12 May in Americas, News. <https://floodlist.com/america/canada-flood-quebec-may-2017> [Oct 01, 2022]
- Davis, R. E., Lowit, M. B., Knappenberger, P. C., & Legates, D. R. (1999). A climatology of snowfall-temperature relationships in Canada. *Journal of Geophysical Research: Atmospheres*, 104(D10), 11985-11994.
- De Mil, T., Vannoppen, A., Beeckman, H., Van Acker, J., & Van den Bulcke, J. (2016). A field-to-desktop toolchain for X-ray CT densitometry enables tree ring analysis. *Annals of Botany*, 117(7), 1187-1196.
- Denneler, B., Bergeron, Y., & Bégin, Y. (1999). An attempt to explain the distribution of the tree species composing the riparian forests of Lake Duparquet, southern boreal region of Quebec, Canada. *Canadian Journal of Botany*, 77(12), 1744-1755.

- Denneler, B., Asselin, H., Bergeron, Y., & Bégin, Y. (2008a). Decreased fire frequency and increased water levels affect riparian forest dynamics in southwestern boreal Quebec, Canada. *Canadian Journal of Forest Research*, 38(5), 1083-1094.
- Denneler, B., Bergeron, Y., Bégin, Y., & Asselin, H. (2008b). Growth responses of riparian *Thuja occidentalis* to the damming of a large boreal lake. *Botany*, 86(1), 53-62.
- Denneler, B., Bergeron, Y., & Bégin, Y. (2010). Flooding effects on tree-ring formation of riparian eastern white-cedar (*Thuja occidentalis* L.), Northwestern Quebec, Canada. *Tree-Ring Research*, 66(1), 3-17.
- Déry, S. J., Stahl, K., Moore, R. D., Whitfield, P. H., Menounos, B., & Burford, J. E. (2009). Detection of runoff timing changes in pluvial, nival, and glacial rivers of western Canada. *Water Resources Research*, 45(4), W04426.
- Déry, S. J., Mlynowski, T. J., Hernández-Henríquez, M. A., & Straneo, F. (2011). Interannual variability and interdecadal trends in Hudson Bay streamflow. *Journal of Marine Systems*, 88(3), 341-351.
- Déry, S. J., Stadnyk, T. A., MacDonald, M. K., & Gauli-Sharma, B. (2016). Recent trends and variability in river discharge across northern Canada. *Hydrology and Earth System Sciences*, 20(12), 4801-4818.
- Despots, M., & Payette, S. (1992). Recent dynamics of jack pine at its northern distribution limit in northern Quebec. *Canadian Journal of Botany*, 70(6), 1157-1167.
- DeWine, J. M., & Cooper, D. J. (2007). Effects of river regulation on riparian box elder (*Acer negundo*) forests in canyons of the Upper Colorado River Basin, USA. *Wetlands*, 27(2), 278-289.
- Dibike, Y. B., & Coulibaly, P. (2005). Hydrologic impact of climate change in the Saguenay watershed: comparison of downscaling methods and hydrologic models. *Journal of Hydrology*, 307(1-4), 145-163.
- Dickson, H. A. (2020). "Potential of diffuse-porous tree species in Dendrohydrology: Are periodic tangential bands of vessels the equivalent of flood rings in ring-porous tree species?". Honor's Thesis, University of Winnipeg, Manitoba, Canada. 80p.
- Drobyshev, I., Bergeron, Y., Girardin, M. P., Gauthier, S., Ols, C., & Ojal, J. (2017). Strong gradients in forest sensitivity to climate change revealed by dynamics of forest fire cycles in the post Little Ice Age era. *Journal of Geophysical Research: Biogeosciences*, 122(10), 2605-2616.
- Duguay, C. R., Prowse, T. D., Bonsal, B. R., Brown, R. D., Lacroix, M. P., & Ménard, P. (2006). Recent trends in Canadian lake ice cover. *Hydrological Processes: An International Journal*, 20(4), 781-801.
- Dyer, J. (2008). Snow depth and streamflow relationships in large North American watersheds. *Journal of Geophysical Research: Atmospheres*, 113(D18).

E

- ECCC - Environment and Climate Change Canada (2020). “Canada’s top 10 weather stories of 2019”. Government of Canada, Toronto, Canada. <https://www.canada.ca/en/environment-climate-change/services/top-ten-weather-stories/2019.html> [Oct 01, 2022]
- Efron, B. (1979). Bootstrap methods: another look at the jackknife. *Annals of Statistics*, 7, 1-26.
- Elshorbagy, A., Corzo, G., Srinivasulu, S., & Solomatine, D. P. (2010). Experimental investigation of the predictive capabilities of data driven modeling techniques in hydrology - Part 1: Concepts and methodology. *Hydrology and Earth System Sciences*, 14(10), 1931-1941.
- Estilow, T. W., Young, A. H., & Robinson, D. A. (2015). A long-term Northern Hemisphere snow cover extent data record for climate studies and monitoring. *Earth System Science Data*, 7(1), 137-142.
- Evans, J. E., Huxley, J. M., & Vincent, R. K. (2007). Upstream channel changes following dam construction and removal using a GIS / remote sensing approach. *JAWRA Journal of the American Water Resources Association*, 43(3), 683-697, J05029.

F

- Fonti, P., & García-González, I. G. (2004). Suitability of chestnut earlywood vessel chronologies for ecological studies. *New Phytologist*, 163(1), 77-86.
- Fonti, P., & García-González, I. (2008). Earlywood vessel size of oak as a potential proxy for spring precipitation in mesic sites. *Journal of Biogeography*, 35(12), 2249-2257.
- Fonti, P., Eilmann, B., García-González, I., & von Arx, G. (2009). Expeditious building of ring-porous earlywood vessel chronologies without losing signal information. *Trees*, 23(3), 665-671.
- Fonti, P., von Arx, G., García-González, I., Eilmann, B., Sass-Klaassen, U., Gärtner, H., & Eckstein, D. (2010). Studying global change through investigation of the plastic responses of xylem anatomy in tree rings. *New Phytologist*, 185(1), 42-53.
- Fortin, J. P., Turcotte, R., Massicotte, S., Moussa, R., Fitzback, J., & Villeneuve, J. P. (2001). Distributed watershed model compatible with remote sensing and GIS data. I: Description of model. *Journal of Hydrologic Engineering*, 6(2), 91-99.
- Fouad, G., Skupin, A., & Tague, C. L. (2018). Regional regression models of percentile flows for the contiguous United States: Expert versus data-driven independent variable selection. *Journal of Hydrology: Regional Studies*, 17, 64-82.
- Frank, D., & Esper, J. (2005). Temperature reconstructions and comparisons with instrumental data from a tree-ring network for the European Alps. *International Journal of Climatology*, 25(11), 1437-1454.

- Freudiger, D., Kohn, I., Stahl, K., & Weiler, M. (2014). Large-scale analysis of changing frequencies of rain-on-snow events with flood-generation potential. *Hydrology and Earth System Sciences*, 18(7), 2695-2709.
- Frigon, A., Music, B., & Slivitzky, M. (2010). Sensitivity of runoff and projected changes in runoff over Québec to the update interval of lateral boundary conditions in the Canadian RCM. *Meteorological Journal*, 19(3), 225-236.
- Fritts, H. C. (1976). *“Tree Rings and Climate”*. Academic Press, New York. 582p.
- Fu, C., & Yao, H. (2015). Trends of ice breakup date in south-central Ontario. *Journal of Geophysical Research*, 120(18), 9220-9236.

G

- Gädeke, A., Krysanova, V., Aryal, A., Chang, J., Grillakis, M., Hanasaki, N., Koutroulis, A., Pokhrel, Y., Satoh, Y., Schaphoff, S., Schmied, H. M., Stacke, T., Tang, Q., Wada, Y. & Thonicke, K. (2020). Performance evaluation of global hydrological models in six large Pan-Arctic watersheds. *Climatic Change*, 163(3), 1329-1351.
- García-González, I. G., & Fonti, P. (2006). Selecting earlywood vessels to maximize their environmental signal. *Tree Physiology*, 26(10), 1289-1296.
- García-Gonzalez, I., Souto-Herrero, M., & Campelo, F. (2016). Ring-porosity and earlywood vessels: a review on extracting environmental information through time. *IAWA Journal*, 37(2), 295-314.
- Gaur, A., Gaur, A., & Simonovic, S. P. (2018). Future changes in flood hazards across Canada under a changing climate. *Water*, 10(10), 1441.
- Gaur, A., Gaur, A., Yamazaki, D., & Simonovic, S. P. (2019). Flooding related consequences of climate change on Canadian cities and flow regulation infrastructure. *Water*, 11(1), 63.
- Gebre, S., Timalisina, N., & Alfredsen, K. (2014). Some aspects of ice-hydropower interaction in a changing climate. *Energies*, 7(3), 1641-1655.
- Gennaretti, F., Arseneault, D., Nicault, A., Perreault, L., & Bégin, Y. (2014). Volcano-induced regime shifts in millennial tree-ring chronologies from northeastern North America. *Proceedings of the National Academy of Sciences*, 111(28), 10077-10082.
- Gennaretti, F., Huard, D., Naulier, M., Savard, M., Bégin, C., Arseneault, D., & Guiot, J. (2017). Bayesian multiproxy temperature reconstruction with black spruce ring widths and stable isotopes from the northern Quebec taïga. *Climate Dynamics*, 49(11), 4107-4119.
- Genries, A., Drobyshv, I., & Bergeron, Y. (2012). Growth-climate response of jack pine on clay soils in northeastern Canada. *Dendrochronologia*, 30(2), 127-136.
- Geography of Monteith (n.d.). *“Geography of Monteith”* in handwritten journal entitled *“History of Monteith”*. Monteith Women Institute Tweedsmuir Community History, Volume 1: 1912-81, 1989, p. 4.

- Ghiggi, G., Humphrey, V., Seneviratne, S.I., & Gudmundsson, L. (2019). GRUN: an observation-based global gridded runoff dataset from 1902 to 2014. *Earth System Science Data*, 11(4), 1655-1674.
- Gingras, D., Adamowski, K., Pilon, P.J., (1994). Regional flood equations for the provinces of Ontario and Quebec. *Water Resources Bulletin*, 30(1), 55-67.
- Girardin, M. P., Tardif, J., & Bergeron, Y. (2001). Radial growth analysis of *Larix laricina* from the Lake Duparquet area, Quebec, in relation to climate and larch sawfly outbreaks. *Écoscience*, 8(1), 127-138.
- Girardin, M. P., & Tardif, J.C. (2005). Sensitivity of tree growth to the atmospheric vertical profile in the Boreal Plains of Manitoba, Canada. *Canadian Journal of Forest Research*, 35(1), 48-64.
- Girardin, M. P., Tardif, J. C., Flannigan, M. D., & Bergeron, Y. (2006). Synoptic-scale atmospheric circulation and boreal Canada summer drought variability of the past three centuries. *Journal of Climate*, 19(10), 1922-1947.
- Girardin, M. P., & Wotton, B. M. (2009). Summer moisture and wildfire risks across Canada. *Journal of Applied Meteorology and Climatology*, 48(3), 517-533.
- Girardin, M. P., Tardif, J.C., Epp, B., & Conciatori, F. (2009). Frequency of cool summers in interior North America over the past three centuries. *Geophysical Research Letters*, 36(7), L07705.
- Girardin, M. P., Bernier, P. Y., & Gauthier, S. (2011). Increasing potential NEP of eastern boreal North American forests constrained by decreasing wildfire activity. *Ecosphere*, 2(3), 1-23.
- Girardin, M. P., Guo, X. J., Bernier, P. Y., Raulier, F., & Gauthier, S. (2012). Changes in growth of pristine boreal North American forests from 1950 to 2005 driven by landscape demographics and species traits. *Biogeosciences*, 9(7), 2523-2536.
- Girardin, M. P., Isabel, N., Guo, X. J., Lamothe, M., Duchesne, I., & Lenz, P. (2021). Annual aboveground carbon uptake enhancements from assisted gene flow in boreal black spruce forests are not long-lasting. *Nature Communications*, 12(1), 1-15.
- Gleason, K. L., Lawrimore, J. H., Levinson, D. H., Karl, T. R., & Karoly, D. J. (2008). A revised US climate extremes index. *Journal of Climate*, 21(10), 2124-2137.
- Glenz, C., Schlaepfer, R., Iorgulescu, I., & Kienast, F. (2006). Flooding tolerance of Central European tree and shrub species. *Forest Ecology and Management*, 235(1-3), 1-13.
- González-González, B. D., Vázquez-Ruiz, R. A., & García-González, I. G. (2015). Effects of climate on earlywood vessel formation of *Quercus robur* and *Q. pyrenaica* at a site in the northwestern Iberian Peninsula. *Canadian Journal of Forest Research*, 45(6), 698-709.
- González, I. G., & Eckstein, D. (2003). Climatic signal of earlywood vessels of oak on a maritime site. *Tree Physiology*, 23(7), 497-504.

- Gouhier, T. C., Grinsted, A., & Simko, V. (2019). “*biwavelet: Conduct univariate and bivariate wavelet analyses*”. R-package version 0.20.19. <https://cran.r-project.org/package=biwavelet> [Oct 01, 2022]
- Graf, W. L. (2006). Downstream hydrologic and geomorphic effects of large dams on American rivers. *Geomorphology*, 79(3-4), 336-360.
- Griffin, D., Meko, D. M., Touchan, R., Leavitt, S. W., & Woodhouse, C. A. (2011). Latewood chronology development for summer-moisture reconstruction in the US Southwest. *Tree-Ring Research*, 67(2), 87-101.
- Griffin, D., Woodhouse, C. A., Meko, D. M., Stahle, D. W., Faulstich, H. L., Carrillo, C., Touchan, R., Castro, C. L., & Leavitt, S. W. (2013). North American monsoon precipitation reconstructed from tree-ring latewood. *Geophysical Research Letters*, 40(5), 954-958.
- Grillakis, M. G., Koutroulis, A. G., & Tsanis, I. K. (2011). Climate change impact on the hydrology of Spencer Creek watershed in Southern Ontario, Canada. *Journal of Hydrology*, 409(1-2), 1-19.
- Guay, C., Minville, M., & Braun, M. (2015). A global portrait of hydrological changes at the 2050 horizon for the province of Québec. *Canadian Water Resources Journal*, 40(3), 285-302.
- Gudmundsson, L., Bremnes, J. B., Haugen, J. E., & Engen-Skaugen, T. (2012) Technical Note: Downscaling RCM precipitation to the station scale using statistical transformations - a comparison of methods. *Hydrology & Earth System Sciences*, 16, 3383-3390.
- Guiot, J. (1987). Reconstruction of seasonal temperatures in central Canada since AD 1700 and detection of the 18.6-and 22-year signals. *Climatic Change*, 10(3), 249-268.
- Gurrapu, S., St-Jacques, J. M., Sauchyn, D. J., & Hodder, K. R. (2016). The influence of the Pacific Decadal Oscillation on annual floods in the rivers of western Canada. *Journal of the American Water Resources Association*, 52(5), 1031-1045.

H

- Hamed, K. H., & Rao, A. R. (1998). A modified Mann-Kendall trend test for autocorrelated data. *Journal of Hydrology*, 204(1-4), 182-196.
- Han, W., Xiao, C.D., Dou, T.F., & Ding, M.H. (2018). Changes in the proportion of precipitation occurring as rain in northern Canada during spring-summer from 1979-2015. *Advances in Atmospheric Sciences*, 35(9), 1129-1136.
- Harrell, F. E., (2020). “*Hmisc: Harrell Miscellaneous*”. R package version 4.4-0. <https://cran.r-project.org/package=Hmisc> [Oct 01, 2022]
- Harris, I., Osborn, T. J., Jones, P., & Lister, D. (2020). Version 4 of the CRU TS monthly high-resolution gridded multivariate climate dataset. *Scientific data*, 7(1), 1-18.
- Hebbali, A. (2020). “*Olsrr: Tools for building Ordinary Least Square Regression Models*”. R package version 0.5.3. <https://cran.r-project.org/package=Olsrr> [Oct 01, 2022]

- Hidalgo, H. G., Piechota, T. C., & Dracup, J. A. (2000). Alternative principal components regression procedures for dendrohydrologic reconstructions. *Water Resources Research*, 36(11), 3241-3249.
- Hirabayashi, Y., Mahendran, R., Koirala, S., Konoshima, L., Yamazaki, D., Watanabe, S., Hyungjun, K., & Kanae, S. (2013). Global flood risk under climate change. *Nature Climate Change*, 3(9), 816-821.
- Hoffer, M., & Tardif, J.C. (2009). False rings in jack pine and black spruce trees from eastern Manitoba as indicators of dry summers. *Canadian Journal of Forest Research*, 39(9), 1722-1736.
- Hofgaard, A., Tardif, J.C., & Bergeron, Y. (1999). Dendroclimatic response of *Picea mariana* and *Pinus banksiana* along a latitudinal gradient in the eastern Canadian boreal forest. *Canadian Journal of Forest Research*, 29(9), 1333-1346.
- Holmes, R. L. (1983). Computer-assisted quality control in tree-ring dating and measurement - COFECHA. *Tree-Ring Bulletin*, 43, 69-78.
- Hrachowitz, M., Savenije, H. H. G., Blöschl, G., McDonnell, J. J., Sivapalan, M., Pomeroy, J. W., Arheimer, B., Blume, T., Clark, M. P., Ehret, U., Fenicia, F., Freer, J. E., Gelfan, A., Gupta, H. V, Hughes, D. A., Hut, R. W., Montanari, A., Pande, S., Tetzlaff, D., Troch, P.A., Uhlenbrook, S., Wagener, T., Winsemius, H.C., Woods, R.A., Zehe, E., & Cudennec, C. (2013). A decade of predictions in ungauged basins (PUB) - a review. *Hydrological Sciences Journal*, 58(6), 1198-1255.
- Huang, J., Tardif, J. C., Bergeron, Y., Denneler, B., Berninger, F., & Girardin, M. P. (2010). Radial growth response of four dominant boreal tree species to climate along a latitudinal gradient in the eastern Canadian boreal forest. *Global Change Biology*, 16(2), 711-731.
- Huziy, O., Sushama, L., Khaliq, M. N., Laprise, R., Lehner, B., & Roy, R. (2013). Analysis of streamflow characteristics over Northeastern Canada in a changing climate. *Climate Dynamics*, 40(7-8), 1879-1901.
- Hydro-Québec (2019). Centrales électriques au 1er Janvier 2019. Statistiques de l'énergie. <https://www.hydroquebec.com/data/documents-donnees/pdf/rapport-annuel.pdf> [Oct 01, 2022]
- Hydro-Québec (2020). "Annual Report 2019". Report n° 2019G500A. Bibliothèque et Archives nationales du Québec. Montréal, Québec, Canada. 177p.
- I
- IBS - Insurance Bureau of Canada (2020). "Investing in Canada's Future; The Cost of Climate Adaptation at the Local Level". Final report (February 2020). Federation of the Canadian Municipalities, Ottawa, Ontario, Canada. 59 p. <https://data.fcm.ca/documents/reports/investing-in-canadas-future-the-cost-of-climate-adaptation.pdf> [Oct 01, 2022]

- IPCC - Intergovernmental Panel on Climate Change (2014). “AR5 Climate Change 2014: Impacts, Adaptation, and Vulnerability”. In Contribution of Working Group II to the Fifth Assessment Report of the Intergovernmental Panel on Climate Change [Barros, V. R., Field, C. B., Dokken, D. J., Mastrandrea, M. D., Mach, K. J., Bilir, T. E., Chatterjee, M., Ebi, K. L., Estrada, Y. O., Genova, R. C., Girma, B., Kissel, E. S., Levy, A. N. (Eds.)]. <https://www.ipcc.ch/report/ar5/wg2/> [Oct 01, 2022]
- IPCC - Intergovernmental Panel on Climate Change (2018). “Global Warming of 1.5°C. An IPCC Special Report on the impacts of global warming” [Masson-Delmotte, V., Zhai, P., Pörtner, H.-O., Roberts, D., Skea, J., Shukla, P. R., Pirani, A., Moufouma-Okia, W., Péan, C., Pidcock, R., Connors, S., Matthews, J. B. R., Chen, Y., Zhou, X., Gomis, M. I., Lonnoy, E., Maycock, T., Tignor, M., & Waterfield, T. (Eds.)]. 616p.
- IPCC – Intergovernmental Panel on Climate Change (2021). “Climate Change 2021: The Physical Science Basis. Contribution of Working Group I to the Sixth Assessment Report of the Intergovernmental Panel on Climate Change” [Masson-Delmotte, V., P. Zhai, A. Pirani, S. L. Connors, C. Péan, S. Berger, N. Caud, Y. Chen, L. Goldfarb, M. I. Gomis, M. Huang, K. Leitzell, E. Lonnoy, J. B. R. Matthews, T. K. Maycock, T. Waterfield, O. Yelekçi, R. Yu, and B. Zhou (Eds.)]. Cambridge University Press, Cambridge, United Kingdom and New York, NY, USA, 2391p.

J

- Jackson, M. B. (1985). Ethylene and responses of plants to soil waterlogging and submergence. *Annual Review of Plant Physiology*, 36(1), 145-174.
- Jacoby, G. C., Ivanciu, I. S., & Ulan, L. D. (1988). A 263-year record of summer temperature for northern Quebec reconstructed from tree-ring data and evidence of a major climatic shift in the early 1800s. *Palaeogeography, Palaeoclimatology, Palaeoecology*, 64(1-2), 69-78.
- Jacoby, G. C., & D'Arrigo, R. (1989). Reconstructed northern hemisphere annual temperature since 1671 based on high-latitude tree-ring data from North America. *Climatic Change*, 14(1), 39-59.
- Javelle, P., Ouarda, T. B. M. J. & Bobée, B. (2003). Spring flood analysis using the flood-duration-frequency approach: application to the provinces of Quebec and Ontario, Canada. *Hydrological Processes*, 17, 3717-3736.
- Jeong, D. I., & Sushama, L. (2018). Rain-on-snow events over North America based on two Canadian regional climate models. *Climate Dynamics*, 50(1), 303-316.
- Jennings, K. S., Winchell, T. S., Livneh, B., & Molotch, N. P. (2018). Spatial variation of the rain-snow temperature threshold across the Northern Hemisphere. *Nature Communications*, 9(1), 1-9.
- Jensen, O. P., Benson, B. J., Magnuson, J. J., Card, V. M., Futter, M. N., Soranno, P. A., & Stewart, K. M. (2007). Spatial analysis of ice phenology trends across the Laurentian

Great Lakes region during a recent warming period. *Limnology and Oceanography*, 52(5), 2013-2026.

Jerome, D., Westwood, M., Oldfield, S., Romero-Severson, J. (2017). “*Fraxinus nigra*”. The IUCN Red List of Threatened Species 2017. e.T61918683A61918721.

Jevšenak, J., & Levanič, T. (2014). Makro EWVA-učinkovito orodje za analizo prevodnih elementov ranega lesa venčastoporoznih listavcev. *Acta Silvae et Ligni*, (104), 15-24.

Jones, N. E., Petreman, I. C. & Schmidt, B. J. (2015). “*High flows and freshet timing in Canada: Observed trends*”. Climate Change Research Report CCRR-42, Ontario Ministry of Natural Resources and Forestry, Science and Research Branch, Peterborough, Ontario. 34p.

Junghans, U., Langenfeld-Heyser, R., Polle, A., & Teichmann, T. (2004). Effect of auxin transport inhibitors and ethylene on the wood anatomy of poplar. *Plant Biology*, 7(01), 22-29.

K

Kames, S. (2009). “*Sensitivity of vessels in black ash (Fraxinus nigra Marsh.) tree rings to fire and hydro-climatic variables*”. Master’s Thesis, University of Manitoba, Canada. 174p.

Kames, S., Tardif, J. C., & Bergeron, Y. (2016). Continuous earlywood vessels chronologies in floodplain ring-porous species can improve dendrohydrological reconstructions of spring high flows and flood levels. *Journal of Hydrology*, 534, 377-389.

Kendall, M. G. (1975). “*Rank Correlation Methods*”, Second Edition. New York, Hafner. 196 p.

Kienzle, S.W. (2008). A new temperature-based method to separate rain and snow. *Hydrological Processes*, 22(26), 5067-5085.

Koprowski, M., Okoński, B., Gričar, J., & Puchałka, R. (2018). Streamflow as an ecological factor influencing radial growth of European ash (*Fraxinus excelsior* (L.)). *Ecological Indicators*, 85, 390-399.

Koshida, G., Cohen, S., & Mortsch, L. (2015). Climate and water availability indicators in Canada: Challenges and a way forward. Part I - Indicators. *Canadian Water Resources Journal*, 40(2), 133-145.

Kozłowski, T. T. (Ed.). (1984). “*Flooding and plant growth*” (No. 581.5263 F631). Cambridge University Press, London. 356p.

Kozłowski, T. T., and Pallardy, S. G. (1997). “*Growth Control in Woody Plants*”. First edition. Academic Press. Elsevier. 1157p.

Krstanovic, P. F., & Singh, V. P. (1991). A univariate model for long-term streamflow forecasting 2. Application. *Stochastic Hydrology and Hydraulics*, 5(3), 189-205.

Kundzewicz, Z. W., Krysanova, V., Benestad, R. E., Hov, Ø., Piniewski, M., & Otto, I. M. (2018). Uncertainty in climate change impacts on water resources. *Environmental Science & Policy*, 79, 1-8.

- Kundzewicz, Z. W., Szwed, M., & Pińskwar, I. (2019). Climate variability and floods - A global review. *Water*, 11(7).
- Kursa, M. B., Jankowski, A., & Rudnicki, W. R. (2010). Boruta-a system for feature selection. *Fundamenta Informaticae*, 101(4), 271-285.
- Kursa, M. B. (2020). "Boruta: wrapper algorithm for all relevant feature selection". R package version 7.0.0. <https://cran.r-project.org/package=Boruta> [Oct 01, 2022]

L

- Lamontagne, J. R., Jasek, M., & Smith, J. D. (2021). Coupling physical understanding and statistical modeling to estimate ice jam flood frequency in the northern Peace-Athabasca Delta under climate change. *Cold Regions Science and Technology*, 192, 103383.
- Land, A., Wehr, M., Roelfs, K. U., Epkes, S., Reichle, D., & Kauer, G. (2017). A novel computer-aided tree-ring analysis software (CATS): oak earlywood vessel size reveals a clear spring heat sum response. *Trees*, 31(5), 1683-1695.
- Larsson, L. A. (2003a). CDendro: Cybis Dendro dating program v. 9.8.1. Cybis Elektronik & Data AB, Saltsjöbaden, Sweden.
- Larsson, L. A. (2003b). CooRecorder: image co-ordinate recording program v. 9.8.1. Cybis Elektronik & Data AB, Saltsjöbaden, Sweden.
- Legendre, P., & Legendre, L. (2012). "Numerical Ecology". Third Edition. Elsevier Scientific Publishing, New York. 1006p.
- Lemay, M., & Bégin, Y. (2008). Hydroclimatic analysis of an ice-scar tree-ring chronology of a high-boreal lake in Northern Québec, Canada. *Hydrology Research*, 39(5-6), 451-464.
- Lemay, M., & Bégin, Y. (2012). Using ice-scars as indicators of exposure to physical lakeshore disturbances, Corvette Lake, northern Québec, Canada. *Earth Surface Processes and Landforms*, 37(13), 1353-1361.
- Li, D., Lettenmaier, D. P., Margulis, S. A., & Andreadis, K. (2019). The role of rain-on-snow in flooding over the conterminous United States. *Water Resources Research*, 55(11), 8492-8513.
- Li, J., Xie, S. P., Cook, E. R., Morales, M. S., Christie, D. A., Johnson, N. C., Chen, F., D'Arrigo, R., Fowler, A. M., Gou, X & Fang, K. (2013). El-Niño modulations over the past seven centuries. *Nature Climate Change*, 3(9), 822-826.
- Lindenschmidt, K. E., Baulch, H. M., & Cavaliere, E. (2018). River and Lake Ice Processes - Impacts of Freshwater Ice on Aquatic Ecosystems in a Changing Globe. *Water*, 10(11), 1586.
- Ljungqvist, F. C., Krusic, P. J., Sundqvist, H. S., Zorita, E., Brattström, G., & Frank, D. (2016). Northern Hemisphere hydroclimate variability over the past twelve centuries. *Nature*, 532(7597), 94-98.
- Loáiciga, H. A., Haston, L., & Michaelsen, J. (1993). Dendrohydrology and long-term hydrologic phenomena. *Reviews of Geophysics*, 31(2), 151-171.

- Loáiciga H. A. (1997). Runoff Scaling in Large Rivers of the World. *Professional Geographer*, 49(3), 364-371.
- López, J., Del Valle, J. I., & Giraldo, J. A. (2014). Flood-promoted vessel formation in *Prioria copaifera* trees in the Darien Gap, Colombia. *Tree Physiology*, 34(10), 1079-1089.
- Lucas-Picher, P., Argüeso, D., Brisson, E., Trambly, Y., Berg, P., Lemonsu, A., Kotlarski, S., & Caillaud, C. (2021). Convection-permitting modeling with regional climate models: Latest developments and next steps. *Wiley Interdisciplinary Reviews: Climate Change*, 12(6), e731.

M

- Magilligan, F. J., & Nislow, K. H. (2005). Changes in hydrologic regime by dams. *Geomorphology*, 71(1-2), 61-78.
- Mann, H. B. (1945). Nonparametric tests against trend. *Econometrica* 13, 245-259.
- Martínez-Sifuentes, A. R., Villanueva-Díaz, J., & Estrada-ávalos, J. (2020). Runoff reconstruction and climatic influence with tree rings, in the mayo river basin, Sonora, Mexico. *IForest*, 13(2), 98-106.
- Masrur Ahmed, A. A., Deo, R. C., Feng, Q., Ghahramani, A., Raj, N., Yin, Z., & Yang, L. (2021). Deep learning hybrid model with Boruta-Random forest optimiser algorithm for streamflow forecasting with climate mode indices, rainfall, and periodicity. *Journal of Hydrology*, 599: 126350.
- Matteson, D. S., & James, N. A. (2014). A nonparametric approach for multiple change point analysis of multivariate data. *Journal of the American Statistical Association*, 109(505), 334-345.
- Matthews, J. A., & Briffa, K. R. (2005). The ‘Little Ice Age’: re-evaluation of an evolving concept. *Physical Geography*, 87(1), 17-36.
- McCarroll, D., Young, G. H., & Loader, N. J. (2015). Measuring the skill of variance-scaled climate reconstructions and a test for the capture of extremes. *The Holocene*, 25(4), 618-626.
- McIntyre, N., Lee, H., Wheeler, H., Young, A., & Wagener, T. (2005). Ensemble predictions of runoff in ungauged catchments. *Water Resources Research*, 41(12).
- McNeil, D.D. (2019). “An Independent Review of the 2019 Flood Events in Ontario”. Ontario’s Special Advisor on Flooding Report to Government, a Report to the Hon. John Yakabuski, Minister of Natural Resources and Forestry. (Report no. 100546746-01). 157p.
- Meko, D. M., & Graybill, D. A. (1995). Tree-ring reconstruction of Upper Gila River discharge. *Journal of the American Water Resources Association*, 31(4), 605-616.
- Meko, D. M., & Baisan, C.H. (2001). Pilot study of latewood width of conifers as an indicator of variability of summer rainfall in the North American monsoon region. *International Journal of Climatology*, 21, 697-708.

- Meko, D. M., Therrell, M. D., Baisan, C. H., & Hughes, M. K. (2001). Sacramento River flow reconstructed to AD 869 from tree rings. *Journal of the American Water Resources Association*, 37(4), 1029-1039.
- Meko, D. M., & Woodhouse, C. A. (2011). "Application of Streamflow Reconstruction to Water Resources Management". In *Dendroclimatology, Developments in Paleoenvironmental Research* (11), 231-261.
- Meko, D. M., Woodhouse, C. A., & Morino, K. (2012). Dendrochronology and links to streamflow. *Journal of Hydrology*, (412), 200-209.
- Meko, D. M., Panyushkina, I. P., Agafonov, L. A., & Edwards, J. A. (2020). Impact of high flows of an Arctic river on ring widths of floodplain trees. *The Holocene*, 30(6), 789-798.
- Meko, M. D., & Therrell, M. D. (2020). A record of flooding on the White River, Arkansas derived from tree-ring anatomical variability and vessel width. *Physical Geography*, 41(1), 83-98.
- MELCC - Ministère de l'environnement et de la lutte contre les changements climatiques (2018). "Atlas hydroclimatique du Québec méridional". Interface géomatique web, Gouvernement du Québec, Québec, Canada. <https://cehq.gouv.qc.ca/atlas-hydroclimatique/> [Oct 01, 2022]
- Merritt, D. M., & Wohl, E. E. (2002). Processes governing hydrochory along rivers: hydraulics, hydrology, and dispersal phenology. *Ecological Applications*, 12(4), 1071-1087.
- MFFP – Ministère des Forêts, de la Faune et des Parcs (2019). Écosystèmes forestiers exceptionnels classés depuis 2002. Gouvernement du Québec, Québec, Canada. <https://mffp.gouv.qc.ca/les-forets/connaissances/connaissances-forestieres-environnementales/ecosystemes-forestiers-exceptionnels-classes/> [Oct 01, 2022]
- Miina, J. (2000). Dependence of tree-ring, earlywood and latewood indices of scots pine and norway spruce on climatic factors in eastern Finland. *Ecological Modelling*, 132(3), 259-273.
- Minville, M., Brissette, F., & Leconte, R. (2008). Uncertainty of the impact of climate change on the hydrology of a nordic watershed. *Journal of Hydrology*, 358(1-2), 70-83.
- Minville, M., Brissette, F., Krau, S., & Leconte, R. (2009). Adaptation to climate change in the management of a Canadian water-resources system exploited for hydropower. *Water Resources Management*, 23(14), 2965-2986.
- Minville, M., Brissette, F., & Leconte, R. (2010). Impacts and uncertainty of climate change on water resource management of the Peribonka River System (Canada). *Journal of Water Resources Planning and Management*, 136(3), 376-385.
- Modini, G. C. (2000). "Long-lead precipitation outlook augmentation of multi-variate linear regression streamflow forecasts". In: Proceedings of the 68th annual Western Snow Conference, Port Angeles, Washington, 57-68.

- Mongrain, S. (2014). “*Dates de dégel du lac Duparquet*”. *Le Grand Héron: Le Journal de Duparquet*, 19 (1), 6.
- Monk, W. A., Peters, D. L., Allen Curry, R., & Baird, D. J. (2011). Quantifying trends in indicator hydroecological variables for regime-based groups of Canadian rivers. *Hydrological Processes*, 25(19), 3086-3100.
- Mood, B. J., Coulthard, B., & Smith, D. J. (2020). Three hundred years of snowpack variability in southwestern British Columbia reconstructed from tree-rings. *Hydrological Processes*, 34(25), 5123-5133.
- Moore, R. D., Sidle, R. C., Eaton, B., Takashi, G., & Wilford, D. (2017) “*Water and watersheds*”. Chapter 7 in Innes, J. L., & Tikina, A. V. (Eds.) *Sustainable Forest Management – From Concept to Practice*, Routledge, Taylor and Francis, New York, NY, USA. 396p.
- Moriasi, D. N., Arnold, J. G., Van Liew, M. W., Bingner, R. L., Harmel, R. D., & Veith, T. L. (2007). Model evaluation guidelines for systematic quantification of accuracy in watershed simulations. *Transactions of the American Society of Agricultural and Biological Engineers*, 50(3), 885-900.
- Mortsch, L., Cohen, S., & Koshida, G. (2015). Climate and water availability indicators in Canada: Challenges and a way forward. Part II - Historic trends. *Canadian Water Resources Journal*, 40(2), 146-159.
- Mudryk, L. R., Derksen, C., Howell, S., Laliberté, F., Thackeray, C., Sospedra-Alfonso, R., Vionnet, V., Kushner, P. J., & Brown, R. D. (2018). Canadian snow and sea ice: historical trends and projections. *The Cryosphere*, 12(4), 1157-1176.
- Mudryk, L. R., Santolaria-Otín, M., Krinner, G., Ménégos, M., Derksen, C., Brutel-Vuilmet, C., Brady, M., & Essery, R. (2020). Historical Northern Hemisphere snow cover trends and projected changes in the CMIP6 multi-model ensemble. *The Cryosphere*, 14(7), 2495-2514.
- Musselman, K. N., Lehner, F., Ikeda, K., Clark, M. P., Prein, A. F., Liu, C., Barlage, M., & Rasmussen, R. (2018). Projected increases and shifts in rain-on-snow flood risk over western North America. *Nature Climate Change*, 8(9), 808-812.
- Natural Resources Canada. (2015). “*Canada Landcover 2015*”. Canada Centre for Mapping and Earth Observation, Government of Canada, Ottawa, Ontario, Canada. [Data file]. <https://open.canada.ca/data/en/dataset/4e615eae-b90c-420b-adee-2ca35896caf6> [Oct 01, 2022]
- Nalley, D., Adamowski, J., & Khalil, B. (2012). Using discrete wavelet transforms to analyze trends in streamflow and precipitation in Quebec and Ontario (1954-2008). *Journal of Hydrology*, 475, 204-228.
- Nalley, D., Adamowski, J., Biswas, A., Gharabaghi, B., & Hu, W. (2019). A multiscale and multivariate analysis of precipitation and streamflow variability in relation to ENSO, NAO and PDO. *Journal of Hydrology*, 574, 288-307.

- Nash, J. E., & Sutcliffe, J. V. (1970). River flow forecasting through conceptual models part I - A discussion of principles. *Journal of Hydrology*, 10(3), 282-290.
- Nasri, B.R., Boucher, E., Perreault, L., Rémillard, B.N., Huard, D., Nicault, A., & Members of the ARCHIVES-PERSISTENCE projects (2020). Modeling hydrological inflow persistence using paleoclimate reconstructions on the Québec-Labrador (Canada) Peninsula. *Water Resources Research*, 56: e2019WR025122.
- Netsvetov, M., Prokopuk, Y., Puchalka, R., Koprowski, M., Klisz, M., & Romenskyy, M. (2019). River regulation causes rapid changes in relationships between floodplain oak growth and environmental variables. *Frontiers in Plant Science*, 10: 96.
- Nicault, A., Boucher, E., Bégin, C., Guiot, J., Marion, J., Perreault, L., Roy, R., Savard, M. M., & Bégin, Y. (2014). Hydrological reconstruction from tree-ring multi-proxies over the last two centuries at the Caniapiscou Reservoir, northern Québec, Canada. *Journal of Hydrology*, 513, 435-445.
- Nilsson, C., & Berggren, K. (2000). Alterations of riparian ecosystems caused by river regulation: Dam operations have caused global-scale ecological changes in riparian ecosystems. How to protect river environments and human needs of rivers remains one of the most important questions of our time. *BioScience*, 50(9), 783-792.
- Nolin, A. F., Tardif, J. C., Conciatori, F., Kames, S., Meko, D. M., & Bergeron, Y. (2021a). Multi-century tree-ring anatomical evidence reveals increasing frequency and magnitude of spring discharge and floods in eastern boreal Canada. *Global and Planetary Change*, 199: 103444.
- Nolin, A. F., Tardif, J. C., Conciatori, F., & Bergeron, Y. (2021b). Spatial coherency of the spring flood signal among major river basins of eastern boreal Canada inferred from flood rings. *Journal of Hydrology*, 596: 126084.
- O**
- OGS - Ontario Geological Survey (1920). “*Twenty-ninth annual report of the Ontario Department of Mines*”. Vol. XXIX, Part I to VI, (1920). Ryerson Press, Toronto, Ontario. 664p
- OMNR - Ontario Ministry of Natural Resources (2004). “*Abitibi River Management Plan*”. Government of Ontario, Toronto. 709p.
- OMNRF - Ontario Ministry of Natural Resources and Forestry (2019). “*Ontario Dam Inventory*”, Provincial Mapping Unit, Government of Ontario, Toronto. [Data File]. <https://geohub.lio.gov.on.ca/datasets/mnrf:ontario-dam-inventory/> [Oct 01, 2022]
- OPG - Ontario Power Generation (2019). “*River System Data*”. [Data File]. <https://www.opg.com/powering-ontario/our-generation/hydro/river-system-data/> [Oct 01, 2022]
- Oubennaceur, K., Chokmani, K., Gauthier, Y., Ratte-Fortin, C., Homayouni, S., & Toussaint, J. P. (2021). Flood risk assessment under climate change: the Petite Nation River watershed. *Climate*, 9(8), 125.

Ouellet, C., Saint-Laurent, D., & Normand, F. (2012). Flood events and flood risk assessment in relation to climate and land-use changes: Saint-François River, southern Québec, Canada. *Hydrological Sciences Journal*, 57(2), 313-325.

Ouranos (2022). PAVICS Power Analytics and Visualization for Climate Science. <https://pavics.ouranos.ca> [Oct 01, 2022]

P

Passow, C., & Donner, R. V. (2019). A rigorous statistical assessment of recent trends in intensity of heavy precipitation over Germany. *Frontiers in Environmental Science*, 143.

Payette, S. (1980). Major ice floods on the Leaf River (Nouveau-Québec): a dendrochronological analysis. *Naturaliste Canadien*, 107(4), 215-225.

Pellerin, J. E. (2019). "Updating the Canadian Reference Hydrometric Basin Network to detect climate-related trends in streamflow". Master's thesis, University of Waterloo. 130p.

Peters, D. L., Caissie, D., Monk, W. A., Rood, S. B., & St-Hilaire, A. (2016). An ecological perspective on floods in Canada. *Canadian Water Resources Journal*, 41(1-2), 288-306.

Petts, G. E. (1980). Long-term consequences of upstream impoundment. *Environmental Conservation*, 7(4), 325-332.

Phipps, R. L. (1985). "Collecting, preparing, crossdating, and measuring tree increment cores". U.S. Geological Survey. Water Resources Investigations Report 85-4148. 48p.

Prowse, T. D. & Bonsal, B. R. (2004). Historical trends in river-ice breakup: a review. *Hydrology Research*, 35 (4-5), 281-293.

Prowse, T. D., Bonsal, B. R., Duguay, C. R., & Lacroix, M. P. (2007). River-ice break-up / freeze-up: a review of climatic drivers, historical trends and future predictions. *Annals of Glaciology*, 46, 443-451.

Q

Quilbé, R., Rousseau, A. N., Moquet, J. S., Trinh, N. B., Dibike, Y., Gachon, P., & Chaumont, D. (2008). Assessing the effect of climate change on river flow using general circulation models and hydrological modelling - Application to the Chaudière River, Québec, Canada. *Canadian Water Resources Journal*, 33(1), 73-94.

R

R Core Team. (2020, 2021). "R: A language and environment for statistical computing". R Foundation for Statistical Computing, Vienna, Austria.

Régent Instruments Inc. (2018). "WinCell Pro Version 2018c user manual". Québec, Québec.

Régnière, J., Saint-Amant, R., Béchar, A., & Moutaoufik, A. (2014). "BioSIM 10: User's manual". Laurentian Forestry Centre. 74p.

Reily, P. W., & Johnson, W. C. (1982). The effects of altered hydrologic regime on tree growth along the Missouri River in North Dakota. *Canadian Journal of Botany*, 60(11), 2410-2423.

- Riboust, P., & Brissette, F. (2015). Climate change impacts and uncertainties on spring flooding of Lake Champlain and the Richelieu River. *Journal of the American Water Resources Association*, 51(3), 776-793.
- Rodionov, S., & Assel, R. A. (2003). Winter severity in the Great Lakes region: A tale of two oscillations. *Climate Research*, 24(1), 19-31.
- Roesch, A. & Schmidbauer, H. (2018). “*WaveletComp: Computational wavelet analysis*”. R package version 1.1. <https://CRAN.R-project.org/package=WaveletComp> [Oct 01, 2022]
- Rokaya, P., Budhathoki, S., & Lindenschmidt, K. E. (2018). Trends in the timing and magnitude of ice-jam floods in Canada. *Scientific Reports*, 8(1), 1-9.
- Rohde, R., Muller, R.A., Jacobsen, R., Muller, E., Perlmutter, S., Rosenfeld, A., Wurtele, J., Groom, D., & Wickham, C. (2013). A new estimate of the average Earth surface land temperature spanning 1753 to 2011, *Geoinformatics & Geostatistics: An Overview*, 1(1).
- Romolo, L., Prowse, T. D., Blair, D., Bonsal, B. R., & Martz, L. W. (2006). The synoptic climate controls on hydrology in the upper reaches of the Peace River Basin. Part I: snow accumulation. *Hydrological Processes*, 20(19), 4097-4111.
- Rossi, S., Anfodillo, T., Čufar, K., Cuny, H.E., Deslauriers, A., Fonti, P., Frank, D., Gričar, J., Gruber, A., King, G.M., Krause, C., Morin, H., Oberhuber, W., Prislán, P., & Rathgeber, C.B. (2013). A meta-analysis of cambium phenology and growth: linear and non-linear patterns in conifers of the northern hemisphere. *Annals of Botany*, 112(9), 1911-1920.
- Roy, L., Leconte, R., Brissette, F. P., & Marche, C. (2001). The impact of climate change on seasonal floods of a southern Quebec River Basin. *Hydrological Processes*, 15(16), 3167-3179.
- Rudolph, T. D., & Laidly, P. R. (1990). “*Jack pine*”. In Burns, R. M., & Honkala, B. H. (Eds.), *Sylvics of North America*, vol. 1, Conifers, 280-293. USDA Forest Service, Agriculture Handbook 654. Washington, DC.
- Rueden, C. T., Schindelin, J., Hiner, M. C., DeZonia, B. E., Walter, A. E., Arena, E. T., & Eliceiri, K. W. (2017). ImageJ2: ImageJ for the next generation of scientific image data. *BMC Bioinformatics*, 18(529), 1-26.
- Saint-Laurent, D. (2004). Palaeoflood hydrology: An emerging science. *Progress in Physical Geography*, 28(4), 531-543.
- Salzer M. W., McCord V. A. S., Stevens L. E., & Webb R. H. (1996). “*The dendrochronology of *Celtis reticulata* in the Grand Canyon: assessing the impact of regulated river flow on tree growth*”, in: *Tree Rings, Environment, and Humanity*. Department of Geosciences, University of Arizona, Tucson, AZ, 273-281.
- Sass-Klaassen, U., Sabajo, C., Belien, E., & den Ouden, J., (2010). “*Effect of experimental flooding on vessel area of pedunculate oak and common ash - a matter of timing*”. In Mielikäinen, K., Mäkinen, H., Timonen, M. (Eds.) *WorldDendro 2010: the 8th international conference on dendrochronology*. Rovaniemi, Finland, p. 155.

- Sass-Klaassen, U., Sabajo, C. R., & den Ouden, J. (2011). Vessel formation in relation to leaf phenology in pedunculate oak and European ash. *Dendrochronologia*, 29(3), 171-175.
- Schmiedel, D., & Tackenberg, O. (2013). Hydrochory and water induced germination enhance invasion of *Fraxinus pennsylvanica*. *Forest Ecology and Management*, 304, 437-443.
- Scholz, A., Klepsch, M., Karimi, Z., & Jansen, S. (2013). How to quantify conduits in wood? *Frontiers in Plant Science*, 4(MAR), 1-11.
- Schook, D. M., Friedman, J. M., & Rathburn, S. L. (2016a). Flow reconstructions in the Upper Missouri River Basin using riparian tree rings. *Water Resources Research*, 52(10), 8159-8173.
- Schook, D. M., Carlson, E. A., Sholtes, J. S., & Cooper, D. J. (2016b). Effects of moderate and extreme flow regulation on *Populus* growth along the Green and Yampa Rivers, Colorado, and Utah. *River Research and Applications*, 32(8), 1698-1708.
- Schweingruber, F. H. (1996). *Tree Rings and Environment: Dendroecology*. Paul Haupt, Berne, Switzerland. 609p.
- Sen, P. K. (1968). Estimates of the regression coefficient based on Kendall's tau. *Journal of the American Statistical Association*, 63, 1379-1389.
- Shamir, E., Meko, D., Touchan, R., Lopley, K. S., Campbell, R., Kaliff, R. N., & Georgakakos, K. P. (2020). Snowpack-and soil water content-related hydrologic indices and their association with radial growth of conifers in the Sierra Nevada, California. *Journal of Geophysical Research: Biogeosciences*, 125(1), e2019JG005331.
- Sigafoos, R. S. (1964). *Botanical evidence of floods and flood-plain deposition* (Vol. 485A). US Government Printing Office. 35p.
- Sims, R. A., Kershaw, H. M., & Wickware, G. M. (1990). *The autecology of major tree species in the north central region of Ontario*. Forestry Canada, Ontario Region, Sault Ste. Marie, Ontario. COFRDA Report 3302 - NWOFTDU Technical Report 48. 126 p.
- Slater, L. J., & Villarini, G. (2016). Recent trends in US flood risk. *Geophysical Research Letters*, 43(24), 12-428.
- Slivinski, L. C., Compo, G. P., Whitaker, J. S., Sardeshmukh, P. D., Giese, B. S., McColl, C., Allan, R., Yin, X., Vose, R., Titchner, H., Kennedy, J., Spencer, L. J., Ashcroft, L., Brönnimann, S., Brunet, M., Camuffo, D., Cornes, R., Cram, T. A., Crouthamel, R., Domínguez-Castro, F., Freeman, J. E., Gergis, K., Hawkins, E., Jones, P. D., Jourdain, S., Kaplan, A., Kubota, H., Le Blancq, F., Lee, T-C., Lorrey, A., Luterbacher, J., Maugeri, M., Mock, C. J., Moore, G. W. K., Przybylak, R., Pudmenzky, C., Reason, C., Slonosky, V. C., Smith, C. A., Tinz, B., Trewin, B., Valente, M. A., Wang, X. L., Wilkinson, C., Wood, K., & Wyszyński, P. (2019). Towards a more reliable historical reanalysis: Improvements for version 3 of the Twentieth Century Reanalysis system. *Quarterly Journal of the Royal Meteorological Society*, 145(724), 2876-2908.

- Slivinski, L.C., Compo, G.P., Sardeshmukh, P.D., Whitaker, J.S., McColl, C., Allan, R.J., Brohan, P., Yin, X., Smith, C.A., Spencer, L.J., Vose, R.S., Rohrer, M., Conroy, R.P., Schuster, D.C., Kennedy, J.J., Ashcroft, L., Brönnimann, S., Brunet, M., Camuffo, D., Cornes, R., Cram, T.A., Domínguez-Castro, F., Freeman, J.E., Gergis, J., Hawkins, E., Jones, P.D., Kubota, H., Lee, T.C., Lorrey, A.M., Luterbacher, J., Mock, C.J., Przybylak, R.K., Pudmenzky, C., Slonosky, V.C., Tinz, B., Trewin, B., Wang, X.L., Wilkinson, C., Wood, K., & Wyszyński, P. (2021). An evaluation of the performance of the twentieth century reanalysis version 3. *Journal of Climate*, 34(4), 1417-1438.
- Smith, M. C., Anthony Stallins, J., Maxwell, J. T., & Van Dyke, C. (2013). Hydrological shifts and tree growth responses to river modification along the Apalachicola River, Florida. *Physical Geography*, 34(6), 491-511.
- Snee, R. D. (1977). Validation of regression models: Methods and examples. *Technometrics*, 19(4), 415-428.
- Sobie, S. R., Zwiers, F. W., & Curry, C. L. (2021). Climate Model Projections for Canada: A Comparison of CMIP5 and CMIP6. *Atmosphere-Ocean*, 59(4-5), 269-284.
- St. George, S., & Nielsen, E. (2000). Signatures of high-magnitude 19th-Century floods in *Quercus macrocarpa* tree rings along the Red River, Manitoba, Canada. *Geology*, 28(10), 899-902.
- St. George, S., & Nielsen, E. (2002). Flood ring evidence and its application to paleoflood hydrology of the Red River and Assiniboine River in Manitoba. *Géographie Physique et Quaternaire*, 56(2-3), 181.
- St. George, S., Nielsen, E., Conciatori, F., & Tardif, J. (2002). Trends in *Quercus macrocarpa* vessel areas and their implications for tree-ring paleoflood studies. *Tree-Ring Research*, 58, 3-10.
- St. George, S., & Nielsen, E. (2003). Palaeoflood records for the Red River, Manitoba, Canada, derived from anatomical tree-ring signatures. *The Holocene*, 13(4), 547-555.
- Stahle, D. W., Cleaveland, M. K., Grissino-Mayer, H. D., Griffin, R. D., Fye, F. K., Therrell, M. D., Burnett, D. J., Meko, D., & Villanueva Diaz, J. (2009). Cool-and warm-season precipitation reconstructions over western New Mexico. *Journal of Climate*, 22(13), 3729-3750.
- Stallins, J. A., Nesius, M., Smith, M., & Watson, K. (2010). Biogeomorphic characterization of floodplain forest change in response to reduced flows along the Apalachicola River, Florida. *River Research and Applications*, 26(3), 242-260.
- Stella, J. C., & Bendix, J. (2019). "Multiple stressors in riparian ecosystems, in *Multiple Stressors in River Ecosystems. Status, impacts and prospects for the future*". In Sabater, S., Elosegi, A., & Ludwig R., (Eds.), New York, Elsevier, 81-110.
- Stromberg J. C., Patten D. T. (1990). Riparian vegetation instream flow requirements: a case study from a diverted stream in the Eastern Sierra Nevada, California, USA. *Environmental Management*, 14, 185-194.

T

- Tardif, J., & Bergeron, Y. (1992). Analyse écologique des peuplements de frêne noir (*Fraxinus nigra*) des rives du lac Duparquet, nord-ouest du Québec. *Canadian Journal of Botany*, 70(11), 2294-2302.
- Tardif, J., & Bergeron, Y. (1993). Radial growth of *Fraxinus nigra* in a Canadian boreal floodplain in response to climatic and hydrological fluctuations. *Journal of Vegetation Science*, 4(6), 751-758.
- Tardif, J., Déry, S., & Bergeron, Y. (1994). Sexual regeneration of black ash (*Fraxinus nigra* Marsh.) in a boreal floodplain. *American Midland Naturalist*, 124-135.
- Tardif, J., (1996). "Earlywood, latewood and total ring width of a ring-porous species (*Fraxinus nigra* Marsh.) in relation to climate and hydrologic factors". In Tree rings, environment and humanities. Dean, J. S., Meko, D. M., Swetnam, T. W. (Eds.). Radiocarbon. University of Arizona, Tucson, 315-324.
- Tardif, J., & Bergeron, Y. (1997a). Comparative dendroclimatological analysis of two black ash and two white cedar populations from contrasting sites in the Lake Duparquet region, northwestern Quebec. *Canadian Journal of Forest Research*, 27, 108-116.
- Tardif, J., & Bergeron, Y. (1997b). Ice-flood history reconstructed with tree-rings from the southern boreal forest limit, western Quebec. *The Holocene*, 7(3), 291-300.
- Tardif, J., Dutilleul, P., & Bergeron, Y. (1998). Variations in periodicities of the ring width of black ash (*Fraxinus nigra* Marsh.) in relation to flooding and ecological site factors at Lake Duparquet in northwestern Quebec. *Biological Rhythm Research*, 29(1), 1-29.
- Tardif, J., & Bergeron, Y. (1999). Population dynamics of *Fraxinus nigra* in response to flood-level variations, in northwestern Québec. *Ecological Monographs*, 69(1), 107-125.
- Tardif, J.C., Conciatori, F., & Bergeron, Y. (2001). Comparative analysis of the climatic response of seven boreal tree species from northwestern Québec, Canada. *Tree-Ring Research*, 57(2), 169-181.
- Tardif, J. C., & Conciatori, F. (2006a). A comparison of ring-width and event-year chronologies derived from white oak (*Quercus alba*) and northern red oak (*Quercus rubra*), southwestern Quebec, Canada. *Dendrochronologia*, 23(3), 133-138.
- Tardif, J. C., & Conciatori, F. (2006b). Influence of climate on tree rings and vessel features in red oak and white oak growing near their northern distribution limit, southwestern Quebec, Canada. *Canadian Journal of Forest Research*, 36(9), 2317-2330.
- Tardif, J. C., Kames, S., & Bergeron, Y. (2010). "Spring water levels reconstructed from ice-scarred trees and cross-sectional area of the earlywood vessels in tree-rings from eastern boreal Canada". In Stoffel, M., Bollschweiler, M., Butler, D.R., Luckman, B.H. (Eds.), *Tree-Rings and Natural Hazards: A State-of-Art. Advances in Global Change Research*. Vol. 41. Springer Dordrecht, 257-261.
- Tardif, J. C., Girardin, M.P., & Conciatori, F. (2011). Light rings as bioindicators of climate change in interior North America. *Global and Planetary Change*, 79(1-2), 134-144.

- Tardif, J. C., Kames, S., Conciatori, F., & Bergeron, Y. (2016). "Developing continuous earlywood vessels chronologies in ring-porous species can improve dendrohydrological reconstructions of spring high flows and flood levels". Third American Dendrochronology Conference - Dendrohydrology Session, 50-51.
- Tardif, J. C., Dickson, H., Conciatori, F., Nolin, A.F., & Bergeron, Y. (2021a). Are periodical (intra-annual) tangential bands of vessels in diffuse-porous tree species the equivalent of flood rings in ring-porous species: reproducibility and cause? *Dendrochronologia*, 70, 125889.
- Tardif, J. C., Kames, S., Nolin, A., & Bergeron, Y. (2021b). Earlywood vessels in black ash (*Fraxinus nigra* Marsh.) trees show contrasting sensitivity to hydroclimate variables according to flood exposure. *Frontiers in Plant Science*, 12:754596.
- Taylor, K. E., Stouffer, R. J., & Meehl, G. A. (2012). An overview of CMIP5 and the experiment design. *Bulletin of the American Meteorological Society*, 93(4), 485-498.
- The old and the new on Driftwood River. (1953). Unknown Newspaper Archive of 1953, May 6. Monteith Women Institute Tweedsmuir Community History, Volume 2: 1913-76, p.109.
- Therrell, M. D., Stahle, D. W., Cleaveland, M. K., and Villanueva-Diaz, J. (2002). Warm season tree growth and precipitation over Mexico. *Journal of Geophysical Research: Atmospheres*, 107(D14), ACL-6.
- Therrell, M. D., & Bialecki, M. B. (2015). A multi-century tree-ring record of spring flooding on the Mississippi River. *Journal of Hydrology*, 529(P2), 490-498.
- Thorntwaite, C. W., & Mather, J. R. (1955). The water balance. *Publications in Climatology*, 8(1), 104.
- Tiner, R. W. (2016). "Plant Indicators of Wetlands and Their Characteristics". Chapter 3 In *Wetlands Incators - A Guide to Wetlands Formation, Identification, Delineation, Classification, and Mapping*. Second Edition, CRC Press, Taylor & Francis. 157-240.
- Torrence, C., & Compo, G. P. (1998). A practical guide to wavelet analysis. *Bulletin of the American Meteorological Society*, 79(1), 61-78.
- Touchan, R., Black, B., Shamir, E., Hughes, M. K., & Meko, D. M. (2021). A multimillennial snow water equivalent reconstruction from giant sequoia tree rings. *Climate Dynamics*, 56(5), 1507-1518.
- Trouet, V., & Van Oldenborgh, G. J. (2013). KNMI Climate Explorer: a web-based research tool for high-resolution paleoclimatology. *Tree-Ring Research*, 69(1), 3-13.
- Turcotte, B., Burrell, B. C., & Beltaos, S. (2019). "The impact of climate change on breakup ice jams in Canada: state of knowledge and research approaches. CGU HS Committee on river ice processes and the environment". 20th Workshop on the hydraulics of ice-covered rivers, Ottawa, Ontario, Canada, May 14-16, 2019.
- Tyree, M. T., & Zimmermann, M. H. (2003). "Xylem Structure and the Ascent of Sap". Second edition. Springer - Verlag, Berlin, Germany. 284p.

V

- Varnell, L. M. (1998). The relationship between inundation history and baldcypress stem form in a Virginia floodplain swamp. *Wetlands*, 18(2), 176-183.
- Viau, A. E., & Gajewski, K. (2009). Reconstructing millennial-scale, regional paleoclimates of boreal Canada during the Holocene. *Journal of Climate*, 22(2), 316-330.
- Vincent, L. A., Zhang, X., Brown, R. D., Feng, Y., Mekis, E., Milewska, E. J., Wang, X., & Wang, X. L. (2015). Observed trends in Canada's climate and influence of low-frequency variability modes. *Journal of Climate*, 28(11), 4545-4560.
- Vincent, L. A., Zhang, X., Mekis, É., Wan, H., & Bush, E. J. (2018). Changes in Canada's climate: trends in indices based on daily temperature and precipitation data. *Atmosphere-Ocean*, 56(5), 332-349.
- Vogel, R. M., Wilson, I., & Daly, C. (1999). Regional regression models of annual streamflow for the United States. *Journal of Irrigation and Drainage Engineering*, 125(3), 148-157.
- Von Arx, G., Crivellaro, A., Prendin, A. L., Čufar, K., & Carrer, M. (2016). Quantitative wood anatomy—practical guidelines. *Frontiers in Plant Science*, 7: 781.

W

- Wan, H., Zhang, X., & Zwiers, F. (2019). Human influence on Canadian temperatures. *Climate Dynamics*, 52(1), 479-494.
- Wang, F., Huang, G. H., Cheng, G. H., & Li, Y. P. (2021). Impacts of climate variations on non-stationarity of streamflow over Canada. *Environmental Research*, 197: 111118.
- Wang, X., Huang, G., Liu, J., Li, Z., & Zhao, S. (2015). Ensemble projections of regional climatic changes over Ontario, Canada. *Journal of Climate*, 28(18), 7327-7346.
- WSC - Water Survey of Canada (2021). "Daily water levels at Driftwood River at Monteith (04MB002)", Ontario - Online Hydrometric Report. https://wateroffice.ec.gc.ca/search/historical_results_e.html?search_type=station_number&station_number=04MB002 [Oct 01, 2022]
- Wertz, E. L., St. George, S., & Zeleznik, J. D. (2013). Vessel anomalies in *Quercus macrocarpa* tree rings associated with recent floods along the Red River of the North, United States. *Water Resources Research*, 49(1), 630-634.
- Whitfield, P. H., & Cannon, A. J. (2000). Recent variations in climate and hydrology in Canada. *Canadian Water Resources Journal*, 25(1), 19-65.
- Whitfield, P. H., Burn, D. H., Hannaford, J., Higgins, H., Hodgkins, G. A., Marsh, T., & Looser, U. (2012). Reference hydrologic networks I. The status and potential future directions of national reference hydrologic networks for detecting trends. *Hydrological Sciences Journal*, 57(8), 1562-1579.
- Wigley, T. M. L., Briffa, K. R., & Jones, P. D. (1984). On the average value of correlated time series with applications in dendroclimatology and hydrometeorology. *Journal of Climate & Applied Meteorology*, 23(2), 201-213.

- Wilhelm, B., Ballesteros-Cánovas, J. A., Macdonald, N., Toonen, W. H. J., Baker, V., Barriandos, M., Benito, G., Brauer, A., Corella, J. P., Denniston, R., Glaser, R., Ionita, M., Kahle, M., Liu, T., Luetscher, M., Macklin, M., Mudelsee, M., Munoz, S., Schulte, L., St. George, S., Stoffel, M., & Wetter, O. (2019). Interpreting historical, botanical, and geological evidence to aid preparations for future floods. *Wiley Interdisciplinary Reviews: Water*, 6(1), e1318.
- Williams, G. P. (1971). Predicting the date of lake ice breakup. *Water Resources Research*, 7(2), 323-333.
- Williams, G. P., & Wolman, M.G. (1984). “Downstream effects of dams on alluvial rivers”. US Geological Survey Professional Paper Vol. 1286. United States Government Printing Office, Washington. 83p.
- Wilson, R., Rao, R., Rydval, M., Wood, C., Larsson, L.Å., & Luckman, B. H. (2014). Blue intensity for dendroclimatology: The BC blues: a case study from British Columbia, Canada. *The Holocene*, 24(11), 1428-1438.
- Winsemius, H. C., Aerts, J. C., van Beek, L. P., Bierkens, M. F., Bouwman, A., Jongman, B., Kwadijk, J. C. J., Ligtoet, W., Lucas, P. L., van Vuuren, D. P., & Ward, P. J. (2016). Global drivers of future river flood risk. *Nature Climate Change*, 6(4), 381-385.
- Wood, S. N. (2003). Thin plate regression splines. *Journal of the Royal Statistical Society: Series B (Statistical Methodology)*, 65(1), 95-114.
- Wood, S. N. (2017). “Generalized Additive Models: an Introduction with R”. Second edition. Chapman and Hall / CRC press. 496p.
- Wood, S. N. (2021). “mgcv: mixed GAM computation vehicle with automatic smoothness estimation”. R package version 1.8-36. <https://CRAN.R-project.org/package=mgcv> [Oct 01, 2022]
- Woodhouse, C. A., Gray, S. T., & Meko, D. M. (2006). Updated streamflow reconstructions for the Upper Colorado River Basin. *Water Resources Research*, 42(5), 1-16.
- X**
- Xu, Y., (2020). “hyfo: Hydrology and Climate Forecasting”. R package version 1.4.3. <https://CRAN.R-project.org/package=hyfo> [Oct 01, 2022]
- Y**
- Yagouti, A., Boulet, G., Vincent, L., Vescovi, L., & Mekis, E. (2008). Observed changes in daily temperature and precipitation indices for southern Québec, 1960-2005. *Atmosphere-Ocean*, 46(2), 243-256.
- Yamamoto, F., Sakata, T., and Terazawa, K. (1995). Physiological, morphological and anatomical responses of *Fraxinus mandshurica* seedlings to flooding. *Tree Physiology*, 15(11), 713-9.
- Yanosky, T. M. (1983). “Evidence of floods on the Potomac River from anatomical abnormalities in the wood of flood-plain trees” (Professional Paper Vol. 1296). US Geological Survey, Department of the Interior, Washington. 42p.

- Yanosky, T. M. (1984). Documentation of high summer flows on the Potomac River from the wood anatomy of ash trees. *Journal of the American Water Resources Association*, 20(2), 241-250.
- Youngblut, D., & Luckman, B. (2008). Maximum June-July temperatures in the southwest Yukon over the last 300 years reconstructed from tree rings. *Dendrochronologia*, 25(3), 153-166.
- Yue, S., Pilon, P., Phinney, B., & Cavadias, G. (2002). The influence of autocorrelation on the ability to detect trend in hydrological series. *Hydrological Processes*, 16(9), 1807-1829.

Z

- Zadeh, S. M., Burn, D. H., & O'Brien, N. (2020). Detection of trends in flood magnitude and frequency in Canada. *Journal of Hydrology: Regional Studies*, 28: 100673.
- Zang, C., & Biondi, F. (2015). treeclim: an R package for the numerical calibration of proxy-climate relationships. *Ecography*, 38(4), 431-436.
- Zhang, L., Zhao, Y., Hein-Griggs, D., & Ciborowski, J. J. (2018). Projected monthly temperature changes of the Great Lakes Basin. *Environmental Research*, 167, 453-467.
- Zhang, W., Mei, X., Geng, X., Turner, A. G., & Jin, F. F. (2019). A nonstationary ENSO-NAO relationship due to AMO modulation. *Journal of Climate*, 32(1), 33-43.
- Zhang, X., Vincent, L. A., Hogg, W. D., & Niitsoo, A. (2000). Temperature and precipitation trends in Canada during the 20th century. *Atmosphere-Ocean*, 38 (3): 395-429.
- Zhang, X., Harvey, K.D., Hogg, W. D., & Yuzyk, T. R. (2001a). Trends in Canadian streamflow. *Water Resources Research*, 37(4), 987-998.
- Zhang, X., Hogg, W.D., & Mekis, É. (2001b). Spatial and temporal characteristics of heavy precipitation events over Canada. *Journal of Climate*, 14(9), 1923-1936.
- Zhao, H., Higuchi, K., Waller, J., Auld, H., & Mote, T. (2013). The impacts of the PNA and NAO on annual maximum snowpack over southern Canada during 1979-2009. *International Journal of Climatology*, 33(2), 388-395.